Volume 1, Number 2
July-August, 1960

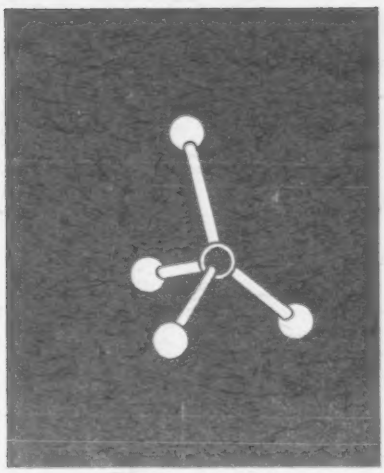

JOURNAL OF
STRUCTURAL CHEMISTRY

ЖУРНАЛ СТРУКТУРНОЙ ХИМИИ / ZHURNAL STRUKTURNOI KHIMII

TRANSLATED FROM RUSSIAN (c/b) CONSULTANTS BUREAU

THE STRUCTURE OF GLASS

Volume 2

Proceedings of the Third All-Union Conference on the Glassy State, held in Leningrad, November 16-20, 1959.

This notable volume contains papers presented at the conference convened by the Institute of Silicate Chemistry of the Academy of Sciences, USSR, the D. I. Mendeleev All-Union Chemical Society, and the S. I. Vavilov (Order of Lenin) State Optical Institute for discussion of recent experimental studies of various properties of glass, the principal methods for investigating glass structure, and the problem of glass formation.

A complete account is given of research work on the glassy state since the previous conference. The most modern optical, spectroscopic, and electrical techniques were used in studying the structure of glass in all its aspects, and the results are interpreted in the light of contemporary physical theories of the solid state.

Volume 2: $25.00

CONTENTS include

Investigation of Glass Structures by the Methods of Optical Spectroscopy. *A. A. Lebedev*
Diffraction Methods for the Study of Glassy Substances. *E. A. Porai-Koshits*
The Cellular Structure of Glass. *W. Vogel*
Characteristic Vibrations of the Glass Network and Glass Structure. *A. G. Vlasov*
General Problems of the Structure and Properties of Glasses. *K. S. Evstrop'ev*
Additivity of the Properties of Silicate Glasses in Relation to their Structure. *L. I. Demkina*
Glassy Systems and the Problem of Glass Structure. *M. A. Bezborodov*
Chemical Characteristics of Polymeric Glass-Forming Substances and the Nature of Glass Formation. *R. L. Myuller*
Characteristics of Glass Formation in Chalcogenide Glasses *N. A. Goryunova and B. T. Kolomiets*
Glass as a Polymer. *V. V. Tarasov*
Formation of a Crystalline Phase from a Silicate Melt. *A. I. Avgustinik*
The Vitrification Process and Structure of Glass. *O. K. Botvinkin*
Formation of Glass Structure during the Melting Process. *L. G. Mel'nichenko*
The Structure of Glass in the Light of the Crystal Chemistry of Silicates. *N. V. Belov*

492 pages **illustrated**

Volume 1

Proceedings of the Second All-Union Conference on the Glassy State.

". . . The Glass Division of the American Ceramic Society and the National Science Foundation are to be congratulated for making this inspiring collection available . . ." — *Journal of Chemical Education*

"The book should be of great interest to scientific and technical personnel interested in glass technology, ceramics, the states of matter, and any work involving the vitreous state. They should all have the experience of reading this book." — *Chemistry in Canada*

". . . a stimulating experience . . ." — *Trans. British Ceramic Society*

". . . lively discussions which show the diversity of opinions on every experimental report." — *The Glass Industry*

". . . the volume is excellent . . . the translation was well worth while . . ." — *R. W. Douglas, Nature*

Volume 1: $20.00

Volumes 1 and 2: $40.00 per set

CONTENTS include

The Crystallite Theory of Glass Structure. *K. S. Evstropyev*
Structure and Properties of Organic Glasses. *P. P. Kobeko*
The Structure of Glass. *O. K. Botvinkin*
The Possibilities and Results of X-Ray Methods for Investigation of Glassy Substances. *E. A. Porai-Koshits*
Structural Peculiarities of Vitreous and Liquid Silicates. *O. A. Esin and P. V. Geld*
Raman Spectra and Structure of Glassy Substances. *E. F. Gross and V. A. Kolesova*
The Quantum Theory of Heat Capacity and the Structure of Silicate Glasses. *V. V. Tarasov*
The Infrared Spectra of Simple Glasses and Their Relationship to Glass Structure. *V. A. Florinskaya and R. S. Pechenkina*
The Coordination Principle of Ion Distribution in Silicate Glasses. *A. A. Appen*
Concepts of the Internal Structure of Silicate Glasses Which Follow from the Results of Studies of the Properties of Glasses in Certain Simple Systems. *L. I. Demkina*
Measurement of the Expansion of Glass as a Method for Investigating its Structure. *A. I. Stozharov*
The Theoretical Views of D. I. Mendeleev on the Structure of Silicates and Glasses, and Their Significance for Modern Science. *L. G. Melnichenko*
The Views of D. I. Mendeleev on the Chemical Nature of Silicates. *V. P. Barzakovsky*

296 pages **illustrated**

Complete contents available upon request

CONSULTANTS BUREAU
227 W. 17 ST., NEW YORK 11, N. Y.

ZHURNAL STRUKTURNOI KHIMII
EDITORIAL BOARD:

S. S. Batsanov *(Secretary)*
G. B. Bokii *(Editor)*
A. V. Nikolaev *(Acting Editor)*
B. V. Ptitsyn
O. Ya. Samoilov
Yu. T. Struchkov
Ya. K. Syrkin
V. V. Voevodskii
M. V. Vol'kenshtein

JOURNAL OF

STRUCTURAL CHEMISTRY

A translation of ZHURNAL STRUKTURNOI KHIMII,

a publication of the Academy of Sciences of the USSR

© 1961 CONSULTANTS BUREAU ENTERPRISES, INC.
227 West 17th Street, New York 11, N. Y.

Volume 1, Number 2 July-August, 1960

CONTENTS

	PAGE ENG.	PAGE RUSS.
Interaction of the HSO_4^- Anion with Nearest Water Molecules in Water Solutions. O. Ya. Samoilov, Hu K'o-yüan, and T. A. Nosova.	121	131
Spectrophotometric Study of the Complex Formation Processes of Tetravalent Plutonium in Nitric Acid Solutions. L. V. Lipis, B. G. Pozharskii, and V. V. Fomin	125	135
Polymorphism in the Higher Normal Fatty Acids: Differential Thermal Analysis and Infrared Absorption Spectra. L. B. Arutyunova	134	145
Structure of Potassium Nitroso-Pentachlororuthenate. T. S. Khodashova and G. B. Bokii	138	151
The Crystal Structure of Triphenyldichlorostybine. T. N. Polynova and M. A. Porai-Koshits	146	159
The Relationship Between the Structure of Minerals and Their Flotation Properties. V. V. Bakakin.	149	162
The Crystal Structure and Chemical Character of Lower Oxides of Titanium $TiO_{0-0.48}$. E. S. Makarov and L. M. Kuznetsov	156	170
An X-Ray Diffraction Study of the Kinetics of Formation of Barium-Calcium Aluminates and Tungstates. A. A. Maklakov and E. P. Ostapchenko	163	178
Vibrational Spectra of the Water of Crystallization in Monocrystals of $NiSO_4 \cdot 7H_2O$, $NiSO_4 \cdot 6H_2O$, $CaSO_4 \cdot 2H_2O$ near the Fundamental of the O–H Valence Vibration. S. N. Andreev, S. A. Shchukarev, and T. G. Balicheva	168	183
The Formation of Three-Center Bonds in Chemisorption. Ya. K. Syrkin	173	189
Determination of the Effective Charges of Atoms in Complexes from the X-Ray Absorption Spectra. R. L. Barinskii	183	200
Radii of the Ions in Molecules of Gaseous Inorganic Compounds of Elements of the Principal Groups of the Periodic System. K. S. Krasnov	191	209
The Drop Model of Atomic Structure. A. F. Kapustinskii	198	217
Determination of the Minimum Effective Radii of the Atoms. Minimum Effective Radii of the Atoms of Elements of the First Three Principal Groups of the Periodic System. G. Dimov and Ml. Genchev	211	233
REVIEWS		
Some Results from Electron-Diffraction Studies of the Structures of Semiconductors. Z. G. Pinsker	215	238
Use of Nuclear Quadrupole Resonance in Chemical Crystallography. G. K. Semin and É. I. Fedin	232	252

Annual Subscription: $80 **Single Issue: $20** **Single Article: $12.50**

Note: The sale of photostatic copies of any portion of this copyright translation is expressly prohibited by the copyright owners.

CONTENTS (continued)

	PAGE ENG.	PAGE RUSS.
BRIEF COMMUNICATIONS		
Proton Relaxation in Aqueous Solutions of Diamagnetic Salts. III. Effects of Polarization Paramagnetism. V. M. Vdovenko and V. A. Shcherbakov	247	268
List of Papers on Radiofrequency and Microwave Spectroscopy Published or Accepted for Publication During 1959-1960	249	270

INTERACTION OF THE HSO_4^- ANION WITH NEAREST WATER MOLECULES IN WATER SOLUTIONS

O. Ya. Samoilov, Hu K'o-yüan, and T. A. Nosova
N. S. Kurnakov Institute of General and Inorganic Chemistry,
Academy of Sciences of the USSR
Translated from Zhurnal Strukturnoi Khimii, Vol. 1, No. 2, pp. 131-134,
July-August, 1960
Original article submitted January 30, 1960

Using the equation which connects the structural characteristics of water solutions of electrolytes with the characteristics of the thermal motion of water molecules, provides the possibility that the results of the thermochemical method for determining the coordination numbers of ions in water solutions may be applied to analysis of the character of the bonds of sn ions, with neighboring molecules of the solution water. A qualitative characteristic of the covalency of the HSO_4^- anion with neighboring molecules is obtained. The coordination number of the HSO_4^- anion in water solutions and its temperature dependence are determined.

Previously [1], an equation was obtained which permitted connection of the structural characteristics of water solutions of electrolytes with the characteristics of the thermal motion of the molecules of the solution water:

$$\frac{n_i}{4\pi R_i^2} = \frac{n}{4\pi R_0^2} \frac{j_0}{j_{0i}} e^{\Delta E_i/RT}, \qquad (1)$$

where n_i and R_i are the coordination number and the radius of the first coordination sphere of the anion in the solution; $\underline{n}$ and R_0 are the corresponding values for water molecules in water; j_0 and j_{0i} are factors before exponentials in expressions for averages (over 1 sec) of numbers of activated jumps, of water molecules in water and of water molecules of the first coordination sphere of the ions; and ΔE_i is the change produced by the effect of the ion of the potential barrier separating neighboring positions of equilibrium of the water molecules of the solution, with respect to the corresponding value (E) for pure water.

The quantity j_{0i} is connected with the slope of the curve of dependence of the interaction energy $\underline{h}$ of the ion with a neighboring water molecule upon the distance $\underline{r}$ between them, i.e., with the quantity $\partial h/\partial r$. It was shown [2] that the higher $\partial h/\partial r$, the higher j_{0i} and, respectively, the lower the ratio j_0/j_{0i}. But, an increase of $\partial h/\partial r$ for a constant charge and radius of the ion means an increase of the degree of covalency of the bonds of the ion with the neighboring water molecules: as the degree of covalency of the bonds increases, the interaction energy of the particles decreases, more and more rapidly with an increase of distance between them (the minimum value of $\partial h/\partial r$ corresponds, for a constant charge and radius of the ion, to a pure electrostatic interaction of the ion with the water molecules).

Equation 1 relates the quantities j_{0i} to the quantities n_i, R_i, and ΔE_i. The quantities $\underline{n}$, R_0, and j_0 are known [3]. Therefore if ΔE_i is known, Eq. 1 permits use of the values found in some way for n_i and R_i, for finding j_{0i} (or the ratio j_0/j_{0i}), and, consequently, for judging the character of the bond of the ion with the neighboring water molecules. The present paper reports an attempt to determine the degree of covalency of the HSO_4^- ion with the neighboring water molecules.

The value of ΔE_i for the HSO_4^- anion may be found by the method previously elaborated [3] on the basis of Kerker's data [4]; he determined the equivalent electrical conductivity of HSO_4^- for a number of different

temperatures at infinite dilution (mobility). According to these data $\Delta E_{HSO_4^-} = -0.05$ kcal/mole (t = 21.5°).

As the "radius" of the HSO_4^- anion one can use the value of the thermochemical radius reported by Yatsimirskii [5]. This value is 2.06 A, which gives for the radius of the first coordination sphere of the $R_{HSO_4^-} = 2.06A + 1.38A = 3.44$ A.

In order to determine the coordination number of the HSO_4^- anion in water solution, we used the thermochemical method of [3]. We determined the integral heats of solution of $KHSO_4$ in water and in water solutions of HCl of different concentrations. The measurements were carried out in a calorimeter with an isothermal enclosure at temperatures t = 15, 25, and 35°. The method was not different from that described previously in [6]. The weights of the salt were taken so that the final concentration of $KHSO_4$ in solution was ~ 0.06 moles of $KHSO_4$ in 50 moles of water. The material used contained 97.27% $KHSO_4$, 1.22% free H_2SO_4, and 1.51% H_2O (titration by 0.1 N alkali and determination of SO_4^{2-} in the form of $BaSO_4$).

Due to the fact that the potassium bisulfate used contained free sulfuric acid, the integral heats of solution of H_2SO_4 in water and in water solutions of HCl were also determined. The experiments were carried out at 25°. Chemically pure H_2SO_4 having a concentration of 96.04% was used. The weight was chosen so that the final concentrations of sulfuric acid in the solution were ~ 0.03 moles of H_2SO_4 in 50 moles of water. The results of the measurements are reported in the table. The heats of solution L are expressed in kcal/mole of solute (the thermochemical sign convention has been used) and the concentration of hydrocloric acid m is expressed in moles of HCl in 50 moles of water.

TABLE 1

Integral Heats of Solution of $KHSO_4$ and H_2SO_4 in Water Solutions of HCl

Substance	t	m	L	Substance	t	m	L
$KHSO_4$	15	0,00	—3,15	$KHSO_4$	35	0,00	—2,64
	»	1,50	—5,33		»	0,91	—5,21
	»	2,05	—5,33		»	1,44	—5,30
	»	2,34	—5,35		»	1,84	—5,36
	»	3,13	—5,35		»	2,34	—5,39
	25	0,00	—2,82				
	»	0,69	—5,10	H_2SO_4	25	0,00	17,30
	»	1,35	—5,27		»	0,46	15,68
	»	1,78	—5,36		»	0,94	15,08
	»	2,21	—5,38		»	1,36	14,83
	»	2,90	—5,44		»	1,73	14,63
	»	3,49	—5,52		»	2,12	14,34

Figure 1 shows the dependence of L (m) for $KHSO_4$ at 25°. As in the case of the solution of sulfates, the part of the curve L (m) with m < 1 is connected to the equilibrium $SO_4^{2-} + H^+ \rightleftharpoons HSO_4^-$ [3]. The dissolution of $KHSO_4$ with m < 1 is accompanied by the dissociation of anion HSO_4^-. Therefore, in order to determine the quantity $\beta = -\Delta L/\Delta m$ the parts of the curves L (m) corresponding to m > 1 were used; they were taken as approximately linear. The values of β were calculated from the experimental data by the least square method. For H_2SO_4 at 25° β = 619 cal/(mole [m]). The value of β used below for $KHSO_4$ at 25° was corrected for the sulfuric acid contained in the material used. For the above mentioned content of H_2SO_4, the correction was 9 cal/(mole [m]). It could also be used approximately for temperatures of 15 and 35°. The water contained in the material obviously did not affect to any practical degree the values of β. The corrected values of β for $KHSO_4$ are the following:

β_{15}	$\beta_{25} - \beta_{15}$	β_{25}	$\beta_{35} - \beta_{25}$	β_{35}	$\Delta\beta$
14	82	96	20	116	51

(A)

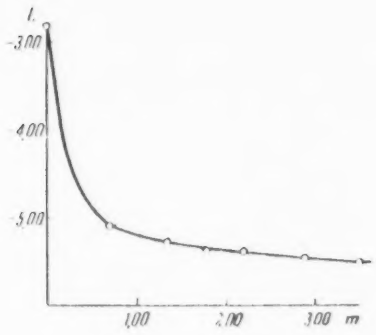

Fig. 1. Integral heats of solution of $KHSO_4$ in water solutions of HCl at 25°.

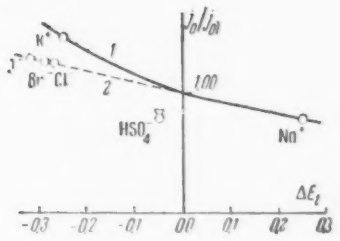

Fig. 2. Dependence of j_0/j_{0i} upon ΔE_i for a number of ions; ▽ denotes the upper limit of the value of $j_0/j^0_{HSO_4^-}$.

Here, the values of β are expressed in cal/(mole [m]). The subscript of β denotes the temperature, and

$$\Delta_1\beta = (\beta_{35} - \beta_{15})/2 \quad [7]. \tag{B}$$

Let us write the relationship previously obtained [3] for the quantity β to the case of the dissolution of $KHSO_4$ (for m > 1):

$$\beta = K\left(\frac{n_{K^+}}{R_{K^+}} - \frac{n_{HSO_4^-}}{R_{HSO_4^-}}\right), \tag{2}$$

where n_{K^+} and R_{K^+} are the coordination number and the radius of the first coordination sphere of the K^+ cation in a water solution, $n_{HSO_4^-}$ and $R_{HSO_4^-}$ are the corresponding quantities for the HSO_4^-, and K is some essentially positive coefficient, whose numerical value was taken equal to $1.17 \cdot 10^9$ [3]. Equation 1, written for the case of the HSO_4^- anion, gives

$$\frac{n_{HSO_4^-}}{R_{HSO_4^-}} = R_{HSO_4^-}\frac{n}{R_0^2}\cdot\frac{j_0}{j^0_{HSO_4^-}}e^{\Delta E_{HSO_4^-}/RT} \tag{C}$$

and, substituting the values $R_{HSO_4^-} = 3.44$ A and $\Delta E_{HSO_4^-} = 0.05$ kcal/mole, we get

$$\frac{n_{HSO_4^-}}{R_{HSO_4^-}} = 1{,}67\,\frac{j_0}{j^0_{HSO_4^-}}. \tag{D}$$

This equality holds for a temperature close to 25°. The relationship (2) for the quantity β_{25} is written now in the form

$$\beta_{25} = K\left(\frac{n_{K^+}}{R_{K^+}} - 1{,}67\,\frac{j_0}{j^0_{HSO_4^-}}\right). \tag{3}$$

As the coefficient K is an essentially positive quantity, and $\beta_{25} > 0$, the quantity in parentheses is positive, and, for any numerical value of K,

$$\frac{j_0}{j^0_{HSO_4^-}} < 0{,}60\,\frac{n_{K^+}}{R_{K^+}}. \qquad (E)$$

Substituting in this inequality the values $n_{K^+} = 3.8$, and $R_{K^+} = 2.71$A [3,8], we get

$$j_0 / j^0_{HSO_4^-} < 0{,}84. \qquad (4)$$

Taking K numerically equal to $1.17 \cdot 10^3$ [3], equation (3) gives

$$j_0 / j^0_{HSO_4^-} = 0{,}79. \qquad (F)$$

Figure 2 shows the values of j_0 / j_{0i} for Na^+ and K^+ as a function of ΔE_i [2]. For $\Delta E_i = 0$, j_0 / j_{0i} is obviously equal to 1. Curve 1 shows the dependence of j_0/j_{0i} upon ΔE_i in the case of the interaction of anion with the neighboring water molecules; this case has essentially a ion-dipole character. The lowering of the point $j_0 / j^0_{HSO_4^-}$ with respect to the curve 1 is a measure of the covalency of the bond of the HSO_4^- anion with the neighboring water molecules.

The circumstance that the value of $j_0 / j^0_{HSO_4^-}$ lies below the curve 1 (Fig. 2) is related, first, to the difference of the predominant orientations of the water molecules with respect to cations and anions (with respect to the cations, the neighboring water molecules are preferably directed with their electrically negative parts, and toward the anions they point their positive ends) and, second, with the presence of the oxygen atoms of the HSO_4^- anion, which ensures the possibility of formation of comparatively stable hydrogen bonds with the neighboring water molecules. For the sake of comparison Fig. 2 includes values of j_0 / j_{0i} for the Cl^-, Br^- and I^- anions. The dotted curve relates to the interaction of halogen anions with the neighboring water molecules of a solution (curve 2); the value of j_0/j_{0i} for HSO_4^- lies below the curve 2. The latter circumstance is in agreement with the results obtained by Vodvenko and Shcherbakova [9], who found by the nuclear magnetic resonance method that the values of the ratio τ_i / τ for oxygen anions are greater than those for the anions Cl^-, Br^-, and I^- (τ_i is the average duration of the permanence of water molecules in equilibrium positions in the structure of the solution close to the ion, τ is the corresponding quantity for water molecules in water).

The values of β and $\Delta\beta$ found for $KHSO_4$ provide the possibility of determining $n_{HSO_4^-}$ and $\Delta n_{HSO_4^-}$ [7]. These values are equal to 4.5 and -0.42, respectively. The surface density of the distribution of water molecules in the first coordination layer of the HSO_4^- anion in a water solution is $\rho_{HSO_4^-} = 0.030A^{-2}$ at 25°. We note that the experimental value of $\Delta^2\beta$ for $KHSO_4$ is negative and is -62 cal/(deg^2 · mole [m]).

LITERATURE CITED

1. O. Ya. Samoilov, Doklady Akad. Nauk SSSR 126, 2, 330 (1959); Zhur. Fiz. Khim. 33, 11, 2631 (1959).
2. O. Ya. Samoilov, Zhur. Strukt. Khim. 1,1, 36 (1960).•
3. O. Ya. Samoilov, Structure of Water Solutions of Electrolytes and Hydration of Ions [in Russian] (Izd. AN SSSR, Moscow, 1957).
4. M. Kerker, J. Am. Chem. Soc. 79, 14, 3664 (1957).
5. K. B. Yatsimirskii, Thermochemistry of Complex Compounds [in Russian] (Izd. AN SSSR, Moscow, 1951).
6. M. N. Rodnikova (Buslaeva), Zhur. Neorg. Khim. 3, 10, 2417 (1958).
7. O. Ya. Samoilov and M. N. Buslaeva, Collection: Structure of Matter and Spectroscopy [in Russian] (Izd. AN SSSR, Moscow, 1960).
8. G. W. Brady and J. T. Krause, J. Chem. Phys. 27, 1, 304 (1957).
9. V. M. Vdovenko and V. A. Shcherbakov, Zhur. Strukt. Khim. 1, 1, 122 (1960).•

• Original Russian pagination. See C. B. translation.

SPECTROPHOTOMETRIC STUDY OF THE COMPLEX FORMATION PROCESSES OF TETRAVALENT PLUTONIUM IN NITRIC ACID SOLUTIONS*

L. V. Lipis, B. G. Pozharskii, and V. V. Fomin

Translated from Zhurnal Strukturnoi Khimii, Vol. 1, No. 2, pp. 135-144
July-August, 1960
Original article submitted April 8, 1959

The processes of complex formation of tetravalent plutonium in nitric acid solutions are investigated. An increase of the concentration of hydrogen ions and of cations enjoying an appreciable hydration energy favors the formation of complex ions containing a large number of nitrate groups. The composition of the complex ions is represented by the formula $[Pu(NO_3)_n(H_2O)_{8-n}]^{+4-n}$, where n may take all values from 1 to 6.

Hindman [1] carried out a spectrophotometric study of tetravalent plutonium in nitric acid solutions and found that in solutions with an HNO_3 concentration lower than 4.6 M, the complex ion $PuNO_3^{3+}$ is present, and came to the conclusion that ions intermediate between $PuNO_3^{3+}$ and $Pu(NO_3)_6^{2-}$ may exist. The experimental results of Hindman were confirmed by Rabideau and Lemons [2].

A study of the electromigration of tetravalent plutonium in HNO_3 by McLane, Dixon, and Hindman [3] showed that the formation of the complex anion proceeds in the concentration limits for HNO_3 from four to 10 M. The formation of $Pu(NO_3)_6^{2-}$ was proved by the isolation of the double ammonium and plutonium nitrate $(NH_4)_2Pu(NO_3)_6$, isomorphic with $(NH_4)_2$ $Ce(NO_3)_6$ and $(NH_4)_2$ $Th(NO_3)_6$, and also by the isolation of double nitrates of plutonium with potassium, rubidium, cesium, tallium, quinoline, and pyridine having the general formula $R_2Pu(NO_3)_6$ [4].

We studied the absorption spectra of solutions of tetravalent plutonium in HNO_3, whose concentration changed from 0.5 to 10 M, in order to detect the changes in the absorption spectra due to complex formation processes.

EXPERIMENTAL METHODS

The measurement of the absorption spectra of the solutions was carried out by the quartz nonrecording spectrophotometer SF-11. Coupled glass cells of a photoelectro colorimeter, which permitted a change of the length of absorbing liquid from 0.30 to 5.00 cm, were used. The absorption spectra were measured in the region from 385 to 1000-1200 mμ. The width of the slit was 0.015 mm.

In order to avoid losses from the solution due to the action of capillary forces, and also the loss of the liquid during changes of the spectrophotometer cell container, the upper part of the walls of the cells were covered by a layer of purified paraffin, which served at the same time also to hold the cover of the cell (the internal and external walls were covered by a paraffin layer not more than 2-3 mm from the upper edge). After the cell had been filled with the solution, the glass cover was heated and then applied to the cell. The paraffin covering the top of the cell melted and flowed uniformly on the whole surface of contact of the cover with the cell. After the paraffin had solidified it was possible to carry out on the cell all operations, without risking a loss of solution.

Preparation of the Solutions

The starting solutions of tetravalent plutonium was prepared by dissolving trivalent plutonium hydroxide

* The work was completed in 1953.

Molar extinction coefficients ϵ in the maxima λ of the absorption bands of nitric acid solutions of tetravalent plutonium.

0.004 M solution of Pu in 0.5 M HNO_3		0.006 M solution of Pu in 0.75 M HNO_3		0.012 M solution of Pu in 1.5 M HNO_3		0.0114 M solution of Pu in 2.08 M HNO_3		0.004 M solution of Pu in 3.8 M HNO_3		0.005 M solution of Pu in 5.7 M HNO_3		0.0116 M solution of Pu in 6.67 M HNO_3		0.0114 M solution of Pu in 7.8 M HNO_3		0.00173 M solution of Pu in 8.4 M HNO_3		0.0693 M solution of Pu in 10 M HNO_3	
λ, mμ	ϵ	λ, mμ	ϵ	λ, mμ	ϵ	λ, mμ	ϵ	λ, mμ	ϵ	λ, mμ	ϵ	λ, mμ	ϵ	λ, mμ	ϵ	λ, mμ	ϵ	λ, mμ	ϵ
863	16,9	865	17,3	863	18,2	862	19,1	860	18,8	863	16,1	857,5	13,3	857	11,3				
808	23,8	808	23,8	810	24,4	805	25,0	800	23,3	804	22,3	800	22,1	798	21,1	795	18,9	795	16,8
												750	14,9	750	18,4	750	22,7	753	26,9
715	17,5	715	17,6	715	18,6	712,5	18,9	710	19,1	712,5	19,2			690	20,7	688	22,6	690	24,8
665	35,1	665	36,7	665	37,2	662,5	37,8	662,5	36,3	662,5	34,4	660	31,2	657,5	30,7	655	27,5	655	25,0
																612,5	23,1	612,5	27,4
																555	9,9	556	8,5
552	18,5	550	18,3	549	20,0	548	18,1	546	20,4	544	19,5	538	19,8	539	20,3	538	21,7	538	23,3
504	11,0			500	13,8	500	13,8	500	13,8										
477,5	67,8	478	73,8	478	79,7	478	80,0	478	74,6	479,5	62,7	479,5	49,2	480	43,4	491	48,6	493	57,0
																		475	19,3
450	20,8	448	22,3	447	24,4	446	24,8	446	23,0	444	26,4	444	29,4	443	32,0	444	36,9	445	38,5
425	27,2	422	27,7	423	32,8	423	34,7	423	34,3	425	33,1	423,5	29,0			423	23,2		
																		416	20,7
404,5	31,7	404	35,8	404	40,7	404	42,1	404	38,5	405	40,1	403	40,6	404	42,7	404	44,4	404	42,1

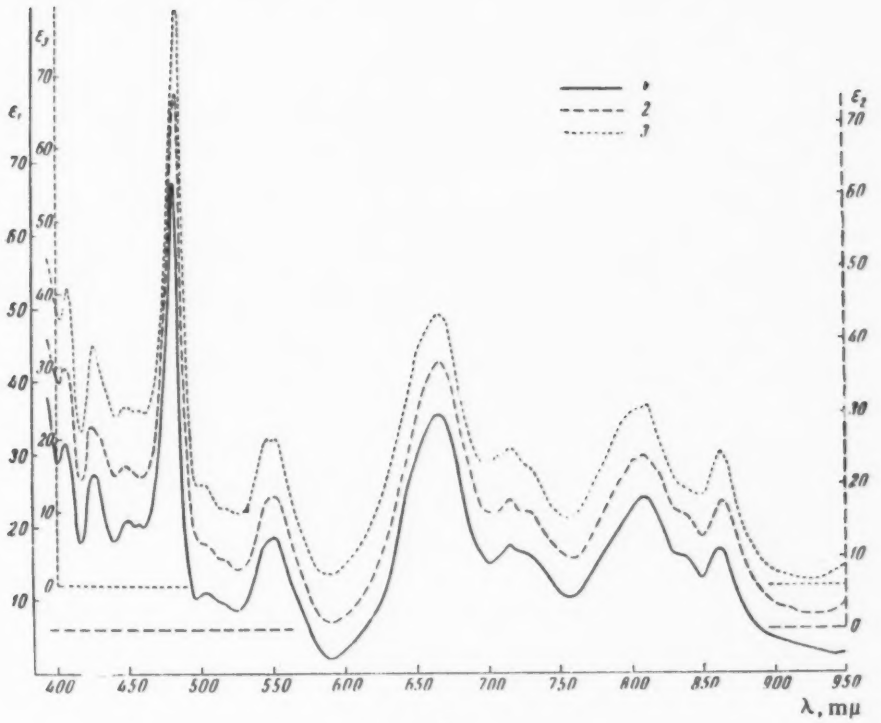

a

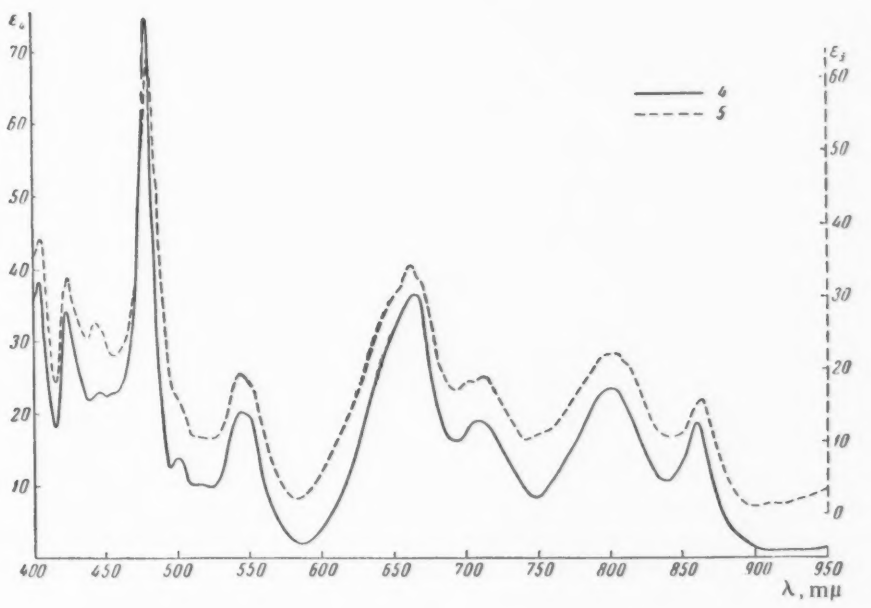

b

Fig. 1, a, b. Absorption spectra of solutions of tetravalent plutonium in HNO_3; 1) 0.004 M solution of Pu in 0.5 M HNO_3; 2) 0.006 M solution of Pu in 0.75 M HNO_3; 3) 0.012 M solution of Pu in 1.5 M HNO_3; 4) 0.004 M solution of Pu in 3.8 M HNO_3; 5) 0.005 M solution of Pu in 5.7 M HNO_3.

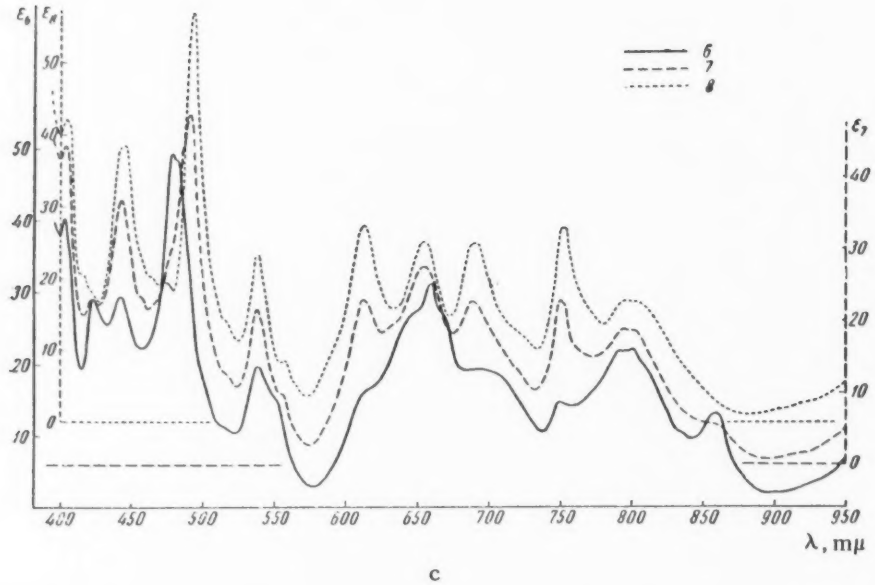

c

Fig. 1, c. Absorption spectra of solutions of tetravalent plutonium in HNO_3: 6) 0.0114 M solution of Pu in 6.67 M HNO_3; 7) 0.00173 M solution of Pu in 8.4 M HNO_3; 8) 0.0693 M solution of Pu in 10 M HNO_3.

in a small quantity of concentrated distilled nitric acid. In order to prevent the formation of the plutonium compound in a colloidal form, the solution was made under heating on a steam bath below 70°.

The solutions to be studied were prepared by diluting the starting solution with water and nitric acid of different concentrations. Solutions of tetravalent plutonium in 0.5, 0.75, 1.5, 2.08, 3.8, 5.7, 6.67, 7.08, 8.4, and 10.0 M HNO_3.

Study of the Absorption Spectra of Tetravalent Plutonium with Different Nitric Acid Concentrations

The main changes of the absorption spectra of nitric acid solutions of tetravalent plutonium when the concentration of HNO_3 is increased consist in changes of the values of the molar extinction coefficients ϵ and in a shift of the absorption bands (Fig. 1 a, b, and c, and Table).

The comparison of the values of ϵ of the absorption bands of tetravalent plutonium for different HNO_3 concentrations showed that, in the majority of the bands, the curve representing the dependence of ϵ upon the HNO_3 concentration shows a series of maxima and minima. Figure 2 shows that the ϵ of the principal band in the region 480 mμ (λ varies from 477.5 to 493 mμ) increases as the HNO_3 concentration increases from 0.5 to 1.5 M; in the concentration region from 1.5 to 2 M it stays practically the same, and for a further increase of the HNO_3 concentration up to ~ 7 M it decreases and then increases again. On the curves representing the dependence of ϵ of the other bands upon the concentration of HNO_3 a series of maxima and minima is also present. It is interesting to note that the position of all these extremes corresponds to the same values of the HNO_3 concentration. Consequently, as the HNO_3 concentration increases, perturbations of the energy levels of the electrons of the 5f shell of Pu(IV) take place, which indicates the presence of radical changes in the ion structure.

The extremes of the curves of ϵ vs. the HNO_3 concentration correspond to the following HNO_3 concentrations; 2.5, 2.1, 3.8, 5.6, and 7.1 M. If the presence of extremes of the curves is attributed to the successive formation of complex ions, then the increase of the HNO_3 concentration to 1.5 M should lead to the formation of the first nitrate complex ion $PuNO_3^{3+}$; a further increase of the HNO_3 concentration to 2.1 M should lead to

the formation of the second nitrate complex ion $Pu(NO_3)_2^{2+}$; for an increase of the HNO_3 concentration to 3.8 M, the ion $Pu(NO_3)_3^{+}$ would be formed; and, finally, an increase of the HNO_3 concentration to 5.6 M should lead to the formation of neutral $Pu(NO_3)_4$ molecules. A further increase of the concentration of HNO_3 to 7.1 M would lead to the formation of the $Pu(NO_3)_5^{-}$ anion, and an increase of acidity beyond 7.1 M is accompanied by the formation of $Pu(NO_3)_6^{2-}$.

The regions found to correspond to the beginning of formation of complex ions of tetravalent plutonium with different numbers of nitrate groups, agree well with the results of migration experiments [3]. Therefore, the stepwise formation of nitrate complex ions for tetravalent plutonium from $PuNO_3^{3+}$ to $Pu(NO_3)_6^{2-}$, including the neutral $Pu(NO_3)_4$ molecule, can be considered as an established fact.

A comparison of the absorption spectra of nitric acid solutions of tetravalent plutonium shows that an increase of HNO_3 concentration, producing a shift of the reaction of complex formation toward an increase of the concentration of certain complex ions and a decrease of the concentration of others, leads to a change of the quantity ϵ and to a shift of the positions of the maxima of the existing absorption bands towards the long-wave or the short-wave region of spectrum. However, due to the fact that the absorption bands for different complex ions have different wavelengths when in the solution under study, there is an equilibrium between the various complex ions and hydrated plutonium ions, one gets a series of absorption bands with different molar extinction coefficients and with maxima in different positions. In view of the fact that the absorption bands have finite and quite appreciable widths, the resolution of these bands was impossible in the working conditions on the SF-11 spectrophotometer; therefore, only the relative shifts of the resulting absorption bands towards the long-wave or the short-wave part of the spectrum could be observed, in addition to changes of the measured values of ϵ. In some cases, when the wavelengths of the maxima of the absorption bands corresponding to the different complex ions in equilibrium were very different, it became possible to resolve these bands by means of the spectrophotometer. This, for instance, took place for the band in the region 480 m μ for 6.7 M and 7.08 M concentrations of HNO_3.

The recording of the absorption spectra of 0.0116 M solution of plutonium in 2.08, 4.00, 5.67, 6.67, 7.08, and 11.67 M nitric acid on the ISP-51 spectrograph by a camera with F = 270 mm (the spectrograph dispersion in the 480 mμ region was almost 6 times greater than the dispersion of the spectrophotometer) showed immediately; thus, when the HNO_3 concentration was increased to 7.08 M, the band in the 480 mμ region was resolved into two and then into three bands (in 6.67 and 7.08 M nitric acid solutions), due to the existence in the solution of an equilibrium among different complex ions. For an 11.67 M concentration of HNO_3, this band again became ordinary, and was appreciably shifted towards the long-wave part of the spectrum. This circumstance indicates that, in this range of concentrations of HNO_3, practically all the plutonium was in the form of the complex ion $Pu(NO_3)_6^{2-}$.

Influence of Nitrate Ions and Hydrogen Ions, and Also of Cations on the Complex Formation Processes in Nitric Acid Solutions of Tetravalent Plutonium

In order to clarify the dependence of the degree of complex formation of tetravalent plutonium upon the acidity of the medium and the nitrate ion concentration, the absorption spectra of plutonium solutions in 2 M HNO_3 containing 6.7 M/1 liter NH_4NO_3 and in 8 M HNO_3 containing 3.35 M/1 liter NH_4NO_3 were measured.

The introduction of ammonium nitrate in a solution of tetravalent plutonium in 2 M HNO_3 led to a significant change of the absorption spectrum compared with the spectrum of the solution in 2 M HNO_3. Figure 3 reports the absorption spectra of these two solutions, and also the absorption spectrum of a plutonium solution in 5.7 M HNO_3, which is close in shape to absorption spectrum of a plutonium solution in 2 M HNO_3 containing 6.7 M/1 liter ammonium nitrate.

The main difference of the absorption spectrum of a solution of tetravalent plutonium in 2 M HNO_3, containing ammonium nitrate from the absorption spectrum of plutonium in 5.7 M HNO_3, consists in a lower intensity of the absorption bands in the 480, 665, and 870 mμ regions. A study of the curves reported in Fig. 2 shows that an increase of the HNO_3 concentration above 2 M causes the beginning of the formation of the third nitrate complex ion $Pu(NO_3)_3^{+}$, which is accompanied by a decrease of the values of ϵ of the bands at 404, 450, 480, and 650 mμ. As to the formation of the fourth nitrate complex — the neutral molecule $Pu(NO_3)_4$ — in 5.7 M HNO_3; it is accom-

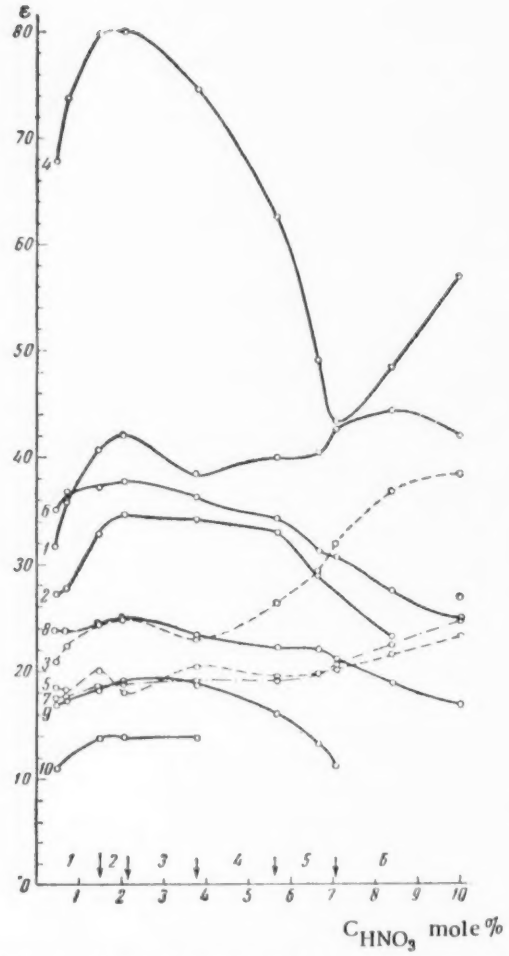

Fig. 2. Diagram representing the dependence of ϵ of the absorption bands of tetravalent plutonium upon the HNO_3 concentration. The absorption bands are the regions: 1) 404; 2) 425; 3) 450; 4) 480; 5) 552; 6) 665; 7) 715; 8) 808; 9) 863; 10) 504 mμ.

panied by a decrease of the values of ϵ for the bands at 425, 480, and 665 mμ, and by an increase of the values of ϵ of the bands at 404 and 450 mμ. Therefore, if the introduction of ammonium nitrate in a plutonium solution in 2 M HNO_3 led to the formation of the same complexes as in a solution of plutonium in 5.7 M HNO_3, the lower optical density of the band at 665 mμ – which can be explained by an increase of the degree of γ complex formation, due to the higher concentration of nitrate ions – should be accompanied by an increase of the optical density of the absorption bands at 404 and 450 mμ. Figure 3 shows that no increase of the optical density of the two bands in question takes place. Thus, the addition of ammonium nitrate to a 2 M nitric acid solution of tetravalent plutonium would lead only to an increase of the complex ion concentration, whose formation starts at the given concentration of the acid, i.e., in this case to an increase of the concentration of the third nitrate complex ion $Pu(NO_3)_3^+$.

A comparison of the absorption spectra of plutonium in 8 M HNO_3 containing 3.35 M/liter of ammonium nitrate with the absorption spectra of plutonium solutions in 8.4 and 10 M HNO_3 (Fig. 4) leads to a similar conclusion.

The main conclusion that can be derived on the basis of the experimental results consists in the fact that, for the formation of complex ions of tetravalent plutonium with a high nitrate-group content, an increase of the solution acidity is necessary in addition to a high nitrate ion concentration. An explanation of the role of an increase of the acidity of the solution in the formation of complex ions of tetravalent plutonium with a high number of nitrate groups lies, apparently, in the following: It is well known that all the ions including Pu^{4+} in water solutions are surrounded by a more or less strongly bound hydrate sphere, and the hydrogen ion, interacting with a water molecule, forms an oxonium ion H_3O^+. Thus, the introduction in a solution of large quantities of ions, whose bonding energy to the surrounding hydrate sphere is high, may lead to a decrease of the total number of water molecules apt to form a hydrate sphere around the Pu^{4+} ions, and, consequently, to a weakening of the bonds of the latter with the solvated water molecules. It is entirely evident that an increase of the concentration of such a strong mineral acid as nitric acid would lead to a significant decrease of the concentration of water molecules apt to form a hydrate sphere around Pu^{4+}. The increase of the nitrate ion concentration with the increase of the HNO_3 concentration would enhance the probability of replacement of the water molecules in the hydrate sphere by nitrate ions.

This discussion, of the processes taking place in a solution when the HNO_3 concentration increases, provides the possibility of establishing the causes which are responsible for the fact that the absorption spectrum of a solution of tetravalent plutonium in 0.1 M HNO_3 + 9.1 M/liters calcium nitrate, according to Hindman [1], was identical with the absorption spectrum of a plutonium solution in 10-13 M HNO_3. Evidently, the difference in effect of $Ca(NO_3)_2$ and of NH_4NO_3 on the absorption spectrum of a tetravalent plutonium solution in nitric acid does not lie in the different "effective" concentration of nitrate ions in these solutions, as Hindman suggested [1], but in the difference of the hydration energy of the corresponding cation.

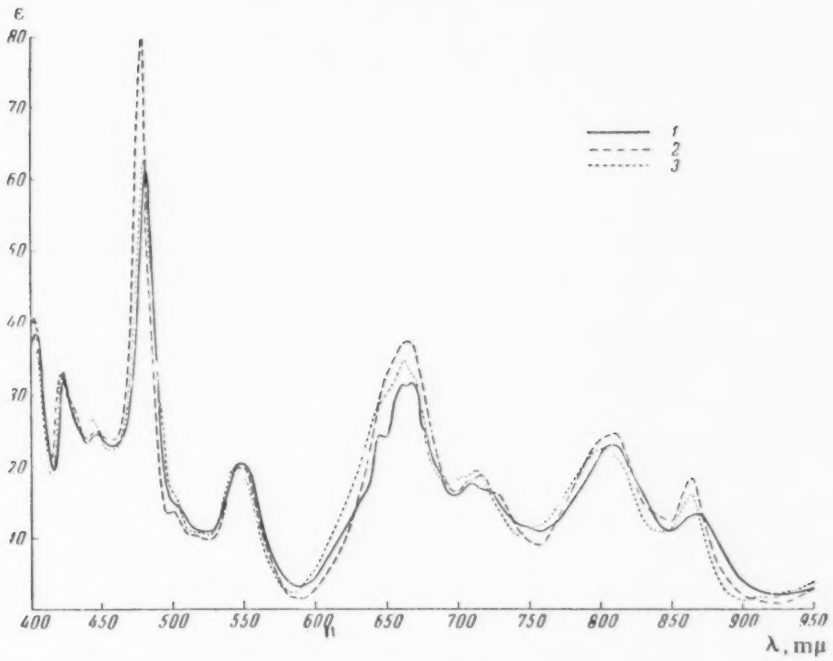

Fig. 3. Effect of NH_4NO_3 on the absorption spectra of nitric acid solutions of tetravalent plutonium: 1) 0.0153 M solution of Pu in 2 M HNO_3 + 6.7 M/liter NH_4NO_3; 2) 0.012 M solution of Pu in 2 M HNO_3; 3) 0.0059 M solution of Pu in 5.7 M HNO_3.

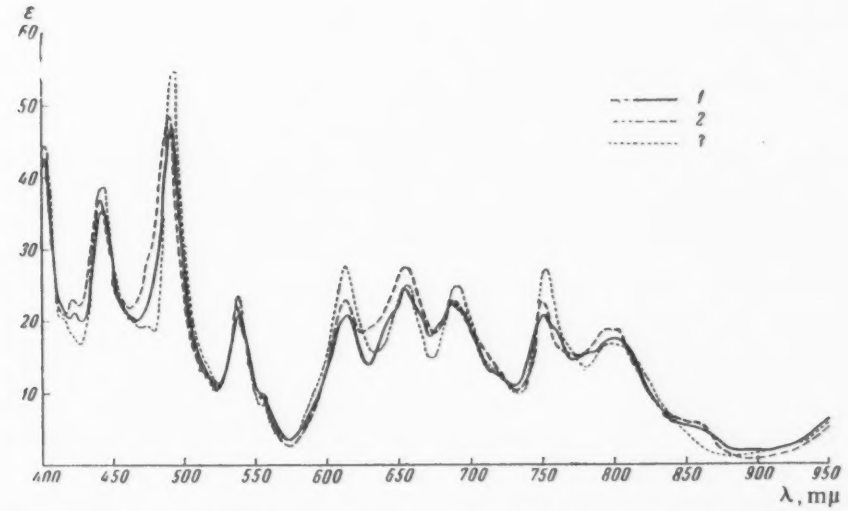

Fig. 4. Effect of NH_4NO_3 on the absorption spectra of nitric acid solutions of tetravalent plutonium: 1) 0.0076 M solution of Pu in 8 M HNO_3 + 3.35 M/liter NH_4NO_3; 2) 0.00173 M solution of Pu in 8.4 M HNO_3; 3) 0.0693 M solution of Pu in 10 M HNO_3.

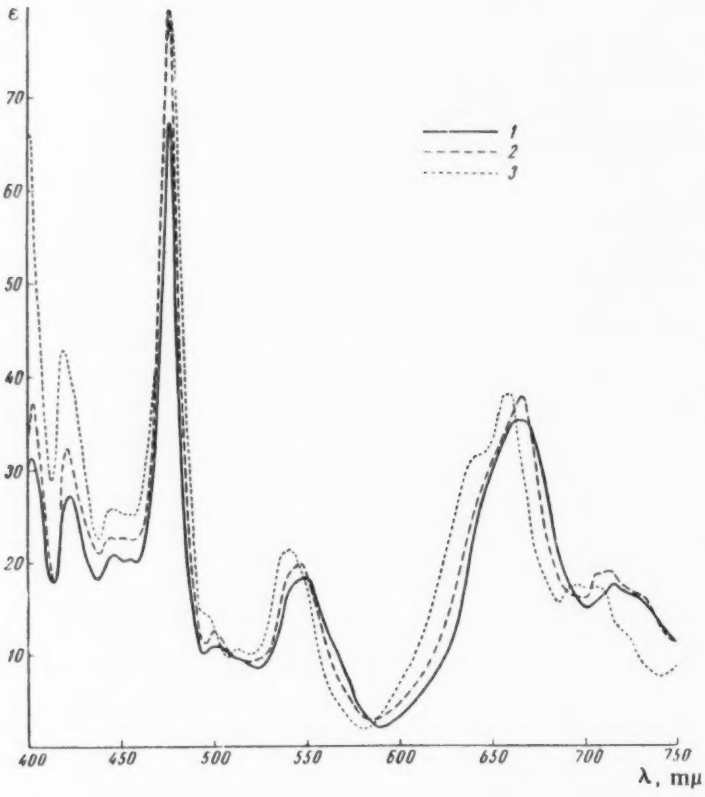

Fig. 5. Absorption spectra of 0.0023 M solutions of plutonium for different concentrations of hydrogen and nitrate ions: 1) solution of Pu in 0.5 M HNO_3; 2) solution of Pu in 0.5 M + 6.67 M/liter NH_4NO_3; 3) solution of Pu in 6 M $HClO_4$ + 0.33 M/liter HNO_3.

In order to verify the idea that the formation of the higher nitrate complex ions of tetravalent plutonium is favored by the high concentration of hydrogen ions, and the increase of the nitrate ion concentration for a fixed acidity and in the absence of cations with a high hydration energy leads only to an increase of the concentration of the complex ions already present, the following experiment was carried out. The absorption spectra of 0.0023 M solutions of plutonium in 6 M chloric acid containing 0.33 M/liter HNO_3, and in 0.5 M nitric acid containing 6.67 M/liter ammonium nitrate were measured (Fig. 5). As expected, the absorption spectrum of a plutonium solution in 0.5 M HNO_3 + 6.67 M/liter NH_4NO_3 is very similar to the absorption spectrum of plutonium in 1.5 M HNO_3. This permits us to think that in the solution under study, plutonium is mainly in the form of the second nitrate complex ion $Pu(NO_3)_2^{2+}$. The absorption spectrum of a plutonium solution in 6 M chloric acid containing only 0.33 M/liter HNO_3 is similar to the absorption spectrum of a plutonium solution in 5.7 M HNO_3. This indicates that regardless of the relatively small nitrate ion concentration, a high concentration of hydrogen ions leads to the formation of appreciable quantities of higher nitrate complex ions of tetravalent plutonium.

SUMMARY

1. The formation of nitrate complex compound of Pu^{4+} when the HNO_3 concentration is increased carries a stepwise character. The formation of mainly one or another complex ion takes place in a definite region of HNO_3 concentration. This does not exclude the possibility of coexistence in the given HNO_3 concentration range of some complex ions; a proof of this is given by the doubling and even tripling of the absorption band in the 480 mμ region.

2. A high concentration of hydrogen ions or of cations having a significant hydration energy enhances the formation of complex ions with a high content of nitrate groups.

3. The formation of nitrate complex ions of tetravalent plutonium leads to a significant shift of the absorption band. At the same time there takes place a change of the values of the molar extinction coefficients which either increase or decrease, due to the perturbations of the 5f energy levels produced by the nitrate groups replacing the water molecules in the hydrate sphere of the ion.

4. The coordination number of plutonium in the formation of nitrate complex ions remains the same and equal to the number of water molecules forming the hydrate sphere of a hydrated Pu^{4+} ion. Since the literature data [5] give for tetravalent plutonium a coordination number equal to 8, the reaction of successive formations of nitrate complexes of plutonium may be written in the following form

$$[Pu(H_2O)_{8-n}(NO_3)_n]^{+4-n} + NO_3^- \rightleftarrows [Pu(H_2O)_{8-(n+1)}(NO_3)]_{n+1}^{+4-(n+1)} + H_2O$$

The composition of the complex ions which are formed for HNO_3 concentrations from 0.5 to 10-11 M is expressed by the formula $[Pu(NO_3)_n(H_2O)_{8-n}]^{+4-n}$, where n = 1,2,... 6.

LITERATURE CITED

1. J. C. Hindman, Nat. Nucl. Energ. Ser., Div. IV, The Transuranium Elements (New York, 1949), Vol. 14B, Paper 4, p. 5.
2. S. W. Rabideau and J. F. Lemons, J. Am. Chem. Soc. 73, 6, 2895 (1951).
3. C. K. McLane, J. S. Dixon, and J. C. Hindman, Nat. Nucl. Energ. Ser., Div. IV, The Transuranium Elements (New York, 1949), Vol. 14B, Paper 3, p. 4.
4. H. H. Anderson, Nat. Nucl. Energ. Ser., Div. IV, The Transuranium Elements (New York, 1949), Vol. 14B, Paper 6, p. 220.
5. J. C. Hindman, Nat. Nucl. Energ. Ser., Div. IV, The Transuranium Elements (New York, 1949), Vol. 14B, Paper 4, p. 7.

POLYMORPHISM IN THE HIGHER NORMAL FATTY ACIDS: DIFFERENTIAL THERMAL ANALYSIS AND INFRARED ABSORPTION SPECTRA

L. B. Arutyunova

N. S. Kurnakov Institute of General and Inorganic Chemistry, Academy of Sciences of the USSR; Institute of Crystallography, Academy of Sciences of the USSR

Translated from Zhurnal Strukturnoi Khimii, Vol. 1, No. 2, pp. 145-150, July-August, 1960
Original article submitted November 29, 1959

Results from differential thermal analysis and from infrared absorption studies are compared. It is found that differences in the various infrared spectra occur for modifications of stearic, palmitic, and oleic acids, that the polymorphic transitions of stearic and palmitic acids are not reversible, and that there is a modification of oleic acid having a transition temperature of 20.5°C.

X-ray methods [1-4] and differential thermal analysis (d.t.a.) are the main sources of information on polymorphism in the higher fatty acids.

The even-numbered acids are polymorphic and exist in forms A, B, and C (or α, β'', and β'), the large lattice parameters decreasing in that sequence. The form that is produced depends on the conditions (temperature, purity, crystallization rate, and solvent).

Ravich, et al. [5] have made a systematic study of these forms, in particular by means of d.t.a. They have shown that the labile α form of stearic acid goes over to the stable β' form at 49°C; Ravich, et al. [6], have examined oleic acid as well, which also has three forms; they claim a transition temperature of 19-20°C for the high-melting form but these results have not been confirmed by x-ray analysis.

Sydow [7], and, earlier, Stenhagen [8] (both at the University of Uppsala), have examined the forms of the higher fatty acids since 1950. They have checked earlier results and have extended the x-ray studies to forms hitherto unexamined. Sydow considers that orthorhombic and triclinic subcells are the most typical of the fatty acids; the first type has been studied by Bunn [9] and by Vainshtein and Pinsker [10], the second by Vand and Bell [11].

The stable β' (C) form of the even-numbered acids is monoclinic, but its subcell is orthorhombic; whereas the labile α form is triclinic, and so is its subcell [7].

Differences in the infrared spectra have been reported [12-14] for the various forms of the fatty acids and for the ethyl esters and mono-and triglycerides thereof. The deductions from the spectra usually agree with the results from x-ray analysis.

I have not been able to find any papers relating infrared absorption spectra to d.t.a. curves, and it may be that this paper represents the first step in that direction.

I have recorded infrared spectra and d.t.a. curves for stearic, palmitic, and oleic acids. The spectra were recorded on an IKS-14 spectrometer fitted with a device for keeping the specimen at a fixed temperature. The d.t.a. curves were recorded from thin sections of the material, which could be observed simultaneously under the microscope [15]. A modified EPP-09 pen recorder was used to trace the curves.

Fig. 1. Crystals of the α phase of stearic acid (x 80).

The spectroscopic and thermal studies were made under identical conditions of heating and cooling. The materials were extremely pure (Kahlbaum) and were additionally recrystallized; their iodine numbers were 0 (stearic and palmitic acids) and 89.8 (oleic acid).

The first two acids crystallize from benzene as their labile α forms, the plates having good (001) faces and being rhombic in shape (Fig. 1). A film of this type was placed with a thermocouple on the heated stage of the microscope (rate of rise of temperature 0.3° per min) and the d.t.a. curve was recorded. Spectra were recorded for the α phase and after the transition.

The d.t.a. curve for stearic acid showed a marked exothermic effect at 49° C; the transition is undoubtedly not reversible (Fig. 2). This result does not conflict with Ravich and Vol'nova's (an endothermic effect in the same range), because their rate of heating was very high and they used a monocrystal. In this case fusion may occur before the transition can start, so the latter is not observed. The melting must occur near the maximum transition temperature. We are dealing here with the kinetics of an irreversible transition, not with an equilibrium state, and the rate of heating is extremely important. The same applies for palmitic acid, which shows a similar exothermic effect at 42°C.

Oleic acid (Fig. 3) shows an endothermic effect at 20-20.5°C, which agrees with the result given in [6].

The infrared absorption spectra of stearic acid were recorded with a NaCl prism at 25 and 52°C; the two differ in the following respects:

1) The β' form shows in the 1400-1460 cm^{-1} region a triplet whose bands are 1460 cm^{-1} — δ (—CH_2—); 1445 cm^{-1} — $\delta_{as}(CH_3)$; 1418 cm^{-1} — δ(—C(=O)O). The α (labile) form does not give these bands.

2) The β' form shows in the range 1200-1300 cm^{-1} five distinct weak bands whose spacing is 16-17 cm^{-1}; the labile form does not give these, but has a broad band centered on 1087 cm^{-1}.

3) The δ(OH) (deformation) band lies at 870 cm^{-1} for the α form but at 954 cm^{-1} for the β form; the CH_2-torsion band at 724 cm^{-1} is single for the α form but is split into two (738 and 724 cm^{-1}) for the β' form (Fig. 4). The C-H, C=O, and C-O valence bands show no appreciable differences. The same is true for palmitic acid.

The infrared spectra agree with the d.t.a. results in showing that the transitions are irreversible, because the films still show the spectrum of the β' form when they have cooled. The α form could not be induced to appear no matter what cooling rate was used.

The various forms of oleic acid have different spectra, particularly the two forms related by the transition at 20.5°C (Fig. 5); this result is in agreement with the d.t.a. data. It seems probable that here we have liquid-crystal phases, which are typical of long-chain aliphatic compounds, e.g., oleate soaps.

The infrared spectrum of a crystal is governed by the symmetry of the molecule and by the symmetry of the microstructure, which also controls the interaction between the molecules. Polymorphic transitions must affect the infrared spectra, because they result in changes in the disposition of the molecules (here, of the chains).

The polymorphic forms of any aliphatic hydrocarbon show differences in their spectra in the 1500-500 cm^{-1} range, i.e., in the region of the CH and CH_2 deformation frequencies and of the -C-C- skeletal valence vibrations. The effects often appear as band splitting, shifts in peak positions, intensity changes, and complete loss of certain bands. There are three factors principally responsible for these effects, namely, changes in the hydrogen bonds, changes in the molecular configuration (themselves a result of rotational isomerism), and changes in the symmetry of the crystal. The normal fatty acids form dimers in the liquid and solid states, so no very extensive changes in the spectra are to be expected; any changes that do occur must be caused either by changes in molecular configuration or by changes in the symmetry of the crystal, or perhaps by both together.

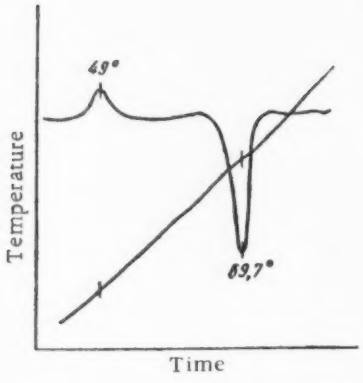

Fig. 2. Direct and d.t.a. curves for stearic acid.

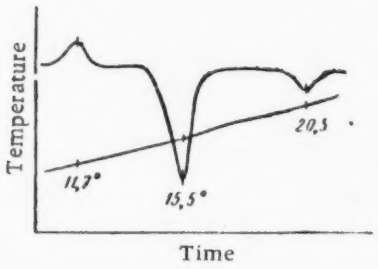

Fig. 3. Direct and d.t.a. curves for oleic acid.

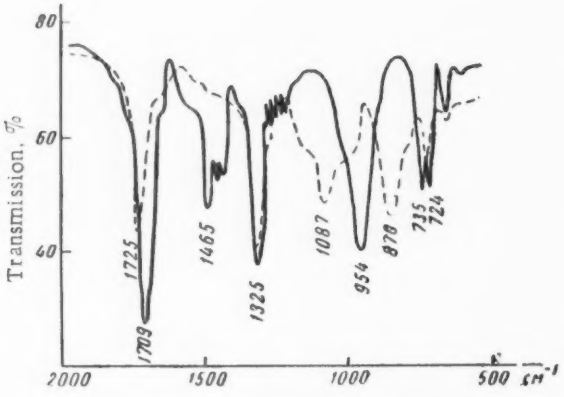

Fig. 4. Infrared absorption spectra of stearic acid: full line, stable β' form; broken line, labile α form.

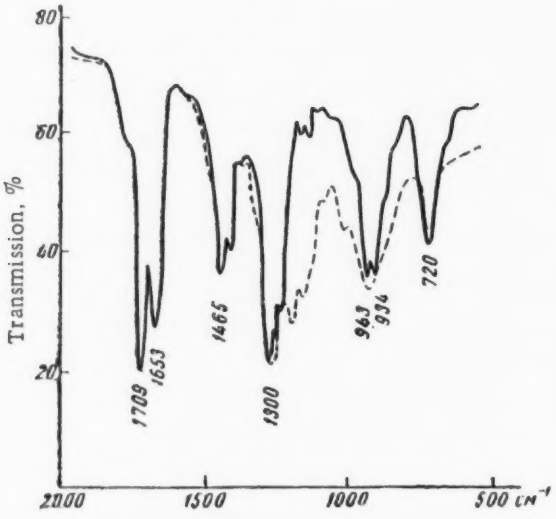

Fig. 5. Infrared absorption spectrum of oleic acid: full line, form of m.p. 5°C; broken line, form of m.p. 20.5°C.

Davison and Corisch [16-18] have used the infrared absorption spectra of crystalline films of polyesters and of monocarboxylic acids to show that the configuration taken up by the molecule in the crystal is one of the configurations most favored by energy considerations. Chapman [12,13] has made a systematic study of the infrared spectra of the normal fatty acids (and of the triglycerides, etc., thereof); he concludes that the position and splitting of the CH_2-torsion band near 720 cm^{-1} are related to the type of packing adopted by the chain. He has extended Davison and Corisch's and Stein's [19] ideas to show that double bands near 720 cm^{-1} are typical of orthorhombic packing (i.e., of orthorhombic subcells).

The $\alpha \rightarrow \beta'$ transitions are exothermic and irreversible, as we have shown, so we may conclude that the configuration taken up in the β' form is more favorable. This configuration is the trans (zigzag) form for the flat hydrocarbon chain. Davison and Corisch's results show that the presence of a band at 720 cm^{-1} points to the occurrence of the trans configuration. The splitting of the 724 cm^{-1} observed for the β' forms of stearic and palamitic acids (which have orthorhombic subcells) is in agreement with Chapman's evidence that splitting of the band near 720 cm^{-1} is proof of the existence of an orthorhombic subcell.

Our d.t.a. and infrared-absorption results show that the $\alpha \rightarrow \beta'$ transitions are irreversible in stearic and palmitic acids. Further, the results demonstrate that oleic acid has forms whose transition temperature is 20.5°C.

In conclusion, I note that infrared spectra are being used ever more extensively (in conjunction with methods such as d.t.a., x-ray analysis, etc) to solve important problems. It is clear from the literature that many features of the crystalline forms of long-chain hydrocarbons can be elucidated by means of infrared spectra used in conjunction with x-ray analysis. I think that the combination of infrared spectroscopy with d.t.a. and with other methods is likely to be of great value in studies of many effects other than polymorphism, expecially for organic systems, which are often difficult to examine by x-ray methods.

I wish to thank G. I. Distler, leader of the optical textures group at the Institute of Crystallography, for making available an IKS-14 spectrometer, and to thank M. I. Ivanova, a member of that group, for assistance in this work.

LITERATURE CITED

1. A. Müller, Proc. Roy. Soc. A114, 542 (1927).
2. S. H. Piper, T. Malkin, and H. E. Austin, J. Chem. Soc., 2310 (1926).
3. F. Francis, S. H. Piper, and T. Malkin, Proc. Roy. Soc. A128, 214 (1930).
4. V. Vand, W. M. Morley, and T. R. Lomer, Acta Cryst. 4, 324 (1951).
5. G. Ravich, V. Vol'nova, and T.Kuz'mina, Acta Physicochim USSR, 14, 3, 403 (1941); G. B. Ravich, V. A. Vol'nova, and G. G. Tsurinov, Izv. Sekt. Fiz.-Khim. Anal. IONKh AN SSSR 19, 220 (1949); G. B. Ravich and V. A. Vol'nova, Doklady Akad. Nauk SSSR 86, 2, 325 (1952); G. B. Ravich, Uspekhi Khim. 21, 9, 1117 (1952).
6. G. B. Ravich, V. A. Vol'nova, and T. N. Kuz'mina, Doklady Akad. Nauk SSSR 29, 2, 90 (1940).
7. E. von Sydow, Arkiv Kemi 9,3, 231 (1956).
8. E. Stenhagen, Acta Chem. Scand. 5, 805 (1951).
9. C. W. Bunn, Trans. Farad. Soc. 35, 482 (1939).
10. B. K. Vainshtein and Z. G. Pinsker, Doklady Akad. Nauk SSSR 72, 53 (1950).
11. V. Vand and G. P. Bell, Acta Cryst. 4, 465 (1951).
12. D. Chapman, Proc. Colloquium Spectroscopicum Internat. VI (London, Pergamon Press, 1957), p. 609.
13. D. Chapman, Nature 176, 216 (1955).
14. E. von Sydow, Acta Chem. Scand. 9,7, 1119 (1955).
15. G. B. Ravich, V. A. Vol'nova, and G. G. Tsurinov, Izv. Sekt. Fiz.-Khim. Anal. IONKh AN SSSR 25, 41 (1954); L.B. Arutyunova and L. G. Mindadze, Trudy Gruz. Politekh, Inst. im. V. I. Lenina 4, 29 (1959).
16. P. J. Corisch and D. Chapman, J. Chem. Soc., 1746 (1957).
17. W. H. T. Davison and P. J. Corisch, J. Chem. Soc., 2428 (1955).
18. P. J. Corisch and W. H. T. Davison, J. Chem. Soc., 2434 (1955).
19. R. S. Stein, J. Chem. Phys. 23, 734 (1955).

STRUCTURE OF POTASSIUM NITROSO-PENTACHLORORUTHENATE

T. S. Khodashova and G. B. Bokii

N. S. Kurnakov Institute for General and Inorganic Chemistry,
Academy of Sciences of the USSR
Translated from Zhurnal Strukturnoi Khimii, Vol. 1, No. 2,
pp. 151-158, July-August, 1960
Original article submitted November 25, 1959

The structure of $K_2[RuNOCl_5]$ has been determined by means of x-ray analysis. The space group is D_{2h}^{16} - Pnma, N = 4; a = 13.31, b = 10.25, c = 6.84 A. The analysis of the structure was carried out by Patterson's projections and by the electron density. The atom coordinates were refined on the basis of "weighted" and of difference projections of the electron density. $K_2[RuNOCl_5]$ is isomorphic with a number of complex aquo compounds of the type $K_2MeCl_5H_2O$. The coordination number of ruthenium is 6, the octahedron being formed by five chlorine atoms and by the nitrogen atom of the NO group; Ru-Cl = 2.35 A. The Ru-N-O group is linear: Ru-N = 1.70 A, N-O = 1.25 A, in agreement with a representation of the bonds by the formula Ru ≡ N-O.

In a previous paper [1] we examined the problem of the character of metal-nitrogen bonds in nitroso compounds, and carried out a comparison between structural types of the NO group theoretically possible, and the available structural data, which were so far in a very small number. The present paper reports the results of an x-ray investigation of potassium nitroso-pentachlororuthenate. The purpose of the investigation in question was to determine the configuration and type of bond of the nitroso group, when a chlorine atom lay in a trans position with respect to it.

CRYSTALLOGRAPHIC CHARACTERISTICS AND BASIC STRUCTURAL PARAMETERS

The $K_2[RuNOCl_5]$ crystals are dark red in color, and almost black in thick layers. Their habitus depends upon the conditions of crystallization: usually needle-shaped crystals are obtained, different crystallographic directions coinciding with their longitudinal axes in different cases; more rarely, crystals having shapes of rectangular plates are obtained.

The results of goniometric measurements on crystals of different habitus coincide with each other and with Dufet's data [2]. The refraction indices are $N_1 = 1.745$, $N_2 \geq 1.780$. The density is $d_{picn} = 2.707$ g/cm^3, $d_{x\text{-rays}} = 2.741$ g/cm^3. No piezoelectric effect takes place. The compound is diamagnetic [3]. The parameters of the cell were determined in a KFOR camera with an NaCl standard: a = 13.31 ± 0.05 A, b = 10.25 ± 0.05 A, c = 6.84 ± 0.03 A. Space group D_{2h}^{16} - Pnma, N = 4.

The structural analysis was carried out on the data of x-ray photographs (camera KFOR, Mo $K\alpha$ radiation). There were 123 h0l reflections 76 hk0, 103 h1l, and 82 h2l reflections used. The corresponding F^2_{max}:F^2_{min} ratios were: 1665:1, 194:1, 309:1, 554:1. In calculating the structural factors, the polarization and kinematic factors were taken into account. The intensities were evaluated visually. The crystals were almost cylindrical in shape.

STRUCTURE ANALYSIS

The comparison of the basic structural parameters with the data for the structures of compounds similar in composition, of the type $Me^I_2[Me^{III}Cl_5H_2O]$, where $Me^I = NH_4$, K, Me^{III} = Fe, In [4,5] gives grounds for thinking that nitroso and aquo compounds have similar structures.

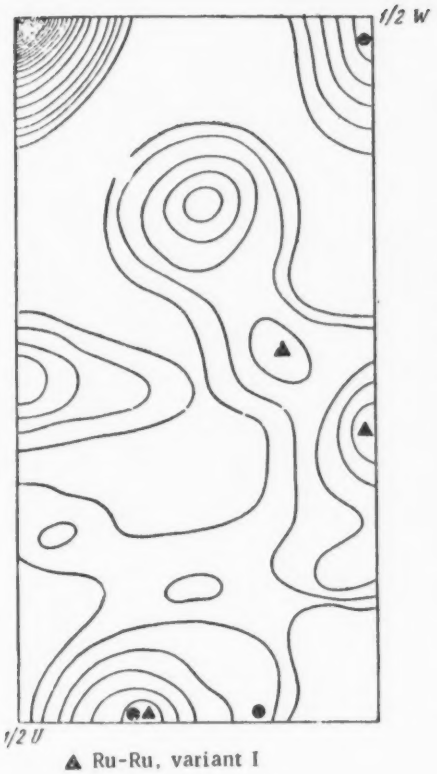

▲ Ru-Ru, variant I
● Ru-Ru, variant II

Fig. 1. Patterson projection along [010].

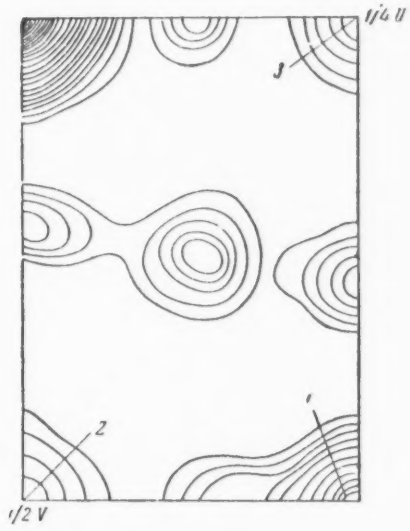

Fig. 2. Patterson projection along [001].

From a Patterson analysis (Figs. 1 and 2) we found that 4 ruthenium atoms occupy the partial position 4 (c) on the mirror symmetry planes m (y = 1/4 and 3/4), and the potassium ions lie in the general position 8(d); 4N and 4O also must occupy the 4 (c) position. The projection along the direction [010] may be interpreted in two ways: in one case $x_{Ru} \approx 0.1$, $z_{Ru} \approx 0.2$, which correspond to the positions of Me^{III} in the structures of aquo compounds. In the second variant $x_{Ru} \approx 0.25$, $z_{Ru} \approx 0.2$. For both cases, the minimum Patterson projection was carried out. The analysis of the obtained minimized projections did not give any preference to either of the variants, but led to a precise determination of the orientation of the complexes themselves (the same in both cases) relative to the m plane; the four addends in the projection along [010] were located at the vertices of a square around the central atom. This means that if one takes into account the symmetry characteristic of the octahedron $RuNCl_5$, in the symmetry planes of the position 4 (c) there are, in addition to the NO groups, three chlorine atoms (in the following we shall call them Cl_I, Cl_{II}, Cl_{III}). The chlorine atoms occupying the fifth and the sixth vertices of the octahedron must lie in the general position 8 (d) above and below this plane (Cl_{IV}). Moreover, from the minimized projections were determined the approximate coordinates of the potassium atoms. It was found that the two variants differ for the relative positions of the complex ions and of the potassium ions, the first one being analogous to that of the aquo compounds.

The choice of the variant was finally made on the basis of a Patterson projection along [001]. The distribution of the maxima in this projection in both cases should be the same, but the ratio of their heights was expected to be different: in the first variant, the first maximum ($u \approx 1/4$, $v \approx 1/2$) would be higher, and the maxima 2 and 3 (0, 1/2, and 1/4, 0) would be the same. In the case of the second variant, all three maxima would have different intensities, with $2 \gg 3 > 1$. The analysis permitted calculation of the coordinates of the chlorine and potassium atoms, obtained from the minimized projections along [010].

As can be seen from Fig. 2, the projection coincides with the first variant, i.e., the structure is actually similar to the structures of aquo compounds.

The coordinates xz of the Ru, K, and Cl_{IV} atoms, obtained from Patterson projections, were used for calculating the signs of the structural amplitudes F (h0l) in constructing the projection of the electron density along [010]. The distribution σ_0 (x z) confirmed the correctness of the assumed structural distribution and clarified the positions occupied in the octahedral complex by the nitrogen atom of the nitroso group: $x_N \approx 0$, $z_N \approx 0$. This corresponds to the positions of the water molecule in aquo compounds. A precise determination of the xz coordinates of the Cl_I, Cl_{II}, Cl_{III}, N, and O was impossible starting from the projections because of the overlapping of the maxima of electron densities corresponding to atoms of different complexes.

The refinement was carried out by the weighted projection method.

In structure, all atoms are distributed in four layers perpendicular to the y axis: Ru, Cl_I, Cl_{II}, Cl_{III}, N, and O in partial positions 4 (c) at heights y = 1/4 and y = 3/4; Cl_{IV} and K are in the general positions 8 (d) at heights $y \approx 0$ and $y \approx 1/2$. The closeness to 0 of the y coordinates of the latter two atoms follows from the analogy with the above mentioned structures.

TABLE 1

Values of the Experimental F_e (h0l) and of the Calculated F_c (h0l) of Structural Amplitudes

h0l	F_e	F_c	h0l	F_e	F_c	h0l	F_e	F_c	h0l	F_e	F_c
400	31,6	—39,83	17.03	7,6	—7,44	309	3,6	—2,61	15.04	4,1	—3,62
600	13,3	—15,87	19.03	5,2	—5,08	509	9,4	7,45	17.04	5,0	—5,55
800	51,4	46,52	004	36,4	—34,70	909	4,2	—4,09	205	8,8	9,27
10.00	11,9	12,96	204	17,1	12,66	13.09	4,4	3,75	405	10,9	12,17
14.00	7,1	—5,10	404	12,8	13,60	10.11	4,3	3,19	605	7,0	—4,90
18.00	7,7	6,82	604	8,0	9,62	201	31,9	—32,77	805	15,4	—18,71
20.00	4,9	5,83	804	11,2	—10,36	401	37,9	—39,44	10.05	4,7	4,38
101	10,7	13,86	10.04	6,8	5,31	601	22,9	22,03	12.05	9,9	12,13
301	7,0	—8,25	14.04	1,9	2,09	801	28,5	31,20	16.05	7,9	—7,46
501	20,5	—21,80	105	13,7	12,26	10.01	6,4	—6,38	106	3,8	—3,98
701	20,9	—23,12	305	4,4	—2,97	12.01	25,4	—24,75	506	5,6	—5,43
901	15,2	15,79	505	13,5	—16,08	14.01	4,2	3,41	706	8,7	7,65
13.01	9,3	—10,96	705	6,0	4,89	16.01	11,0	12,29	13.06	4,2	—3,55
15.01	6,9	—6,29	905	9,1	9,94	20.01	4,8	—4,01	207	13,9	—12,00
17.01	2,8	2,79	11.05	6,5	6,74	102	25,8	—30,25	607	6,5	7,02
002	20,3	—21,82	13.05	5,6	—6,38	302	60,8	—71,45	807	9,0	10,78
202	4,1	4,76	15.05	2,1	—3,30	502	44,9	37,81	10.07	6,6	—5,12
402	48,9	47,40	006	21,1	21,32	702	14,6	17,06	12.07	8,6	—7,98
602	15,5	14,13	206	6,3	5,17	11.02	15,2	—12,87	16.07	5,1	4,38
802	6,1	—7,58	406	31,8	—26,98	15.02	2,4	2,42	108	10,7	—10,81
10.02	3,5	—3,65	806	9,8	10,71	17.02	5,8	5,81	308	3,5	—5,06
12.02	6,7	5,65	10.06	7,7	5,34	203	13,1	10,67	708	8,0	6,13
14.02	9,2	9,08	12.06	3,8	—2,37	403	7,4	—8,44	209	3,3	3,93
103	28,3	—26,62	14.06	6,5	—5,88	603	3,2	—3,28	609	4,0	—4,18
503	32,8	31,80	307	5,1	7,45	803	5,1	—5,72	10.10	4,4	3,82
703	7,2	11,61	907	4,6	4,20	10.03	2,2	5,60	30.10	4,5	3,91
903	33,7	—28,86	11.07	4,2	5,34	104	39,3	35,18	70.10	5,6	—4,80
11.03	8,6	—14,30	008	5,9	—7,10	304	28,3	25,57			
13.03	15,8	15,43	208	5,9	—4,62	504	10,3	—12,03			
15.03	7,5	7,82	408	6,8	6,49	704	28,4	—24,50			
			808	3,0	—3,60	904	4,0	2,61			
			10.08	8,0	—7,31	11.04	14,5	10,17			
			109	1,5	—1,91	13.04	1,9	3,67			

TABLE 2

Values of the Experimental F_e (hk0) and of the Calculated F_c (hk0) of the Structural Amplitudes

hk0	F_e	F_c	hk0	F_e	F_c	hk0	F_e	F_c
020	25,2	—35,32	8.10.0	6,7	—6,45	630	8,2	—7,34
040	56,0	110,38	8.12.0	6,7	7,68	650	18,9	17,75
060	22,6	—22,94	8.14.0	5,7	—3,49	690	12,5	11,69
080	49,0	50,22	10.00	10,1	11,89	6.13.0	8,2	5,63
0.10.0	13,9	—13,80	10.20	18,3	—16,39	810	23,3	22,58
0.12.0	19,1	19,15	10.40	9,1	9,22	830	17,0	—17,17
0.14.0	10,4	—7,81	10.60	12,7	—12,65	850	21,6	19,15
220	6,7	—8,00	10.80	5,1	4,49	870	8,2	—9,40
260	4,5	—4,64	10.10.0	7,7	—8,44	890	12,4	11,64
400	26,8	—50,97	12.20	4,6	—2,83	8.13.0	6,7	4,99
420	38,4	—33,94	14.00	6,1	—4,88	10.10	16,7	—15,48
440	26,7	—36,31	14.20	8,3	5,10	10.30	12,7	11,65
460	19,5	—15,27	14.40	5,2	—3,73	10.50	16,2	—13,32
480	14,1	—14,95	14.60	6,1	4,57	10.70	4,8	6,14
4.12.0	4,6	—4,86	18.00	6,2	5,82	10.90	9,0	—8,89
600	14,6	—15,34	18.20	6,0	—4,53	12.10	10,3	—9,73
620	23,1	22,97	18.40	6,8	4,64	12.30	7,7	6,51
640	9,4	—11,36	210	31,3	—47,28	12.50	11,4	—9,66
660	16,3	16,29	230	22,1	22,69	12.70	4,0	3,17
680	5,6	—5,32	250	33,7	—39,10	12.90	9,1	—6,23
6.10.0	9,4	9,45	270	7,7	6,81	16.10	5,5	5,84
800	44,4	44,26	290	24,7	—23,11	16.30	4,2	—3,93
820	11,2	—10,20	2.13.0	12,3	—10,64	16.50	6,6	5,61
840	38,5	34,22	450	4,5	—4,25	16.90	6,2	3,20
860	9,4	—8,72	490	4,5	—3,02			
880	21,6	18,75	610	17,5	17,31			

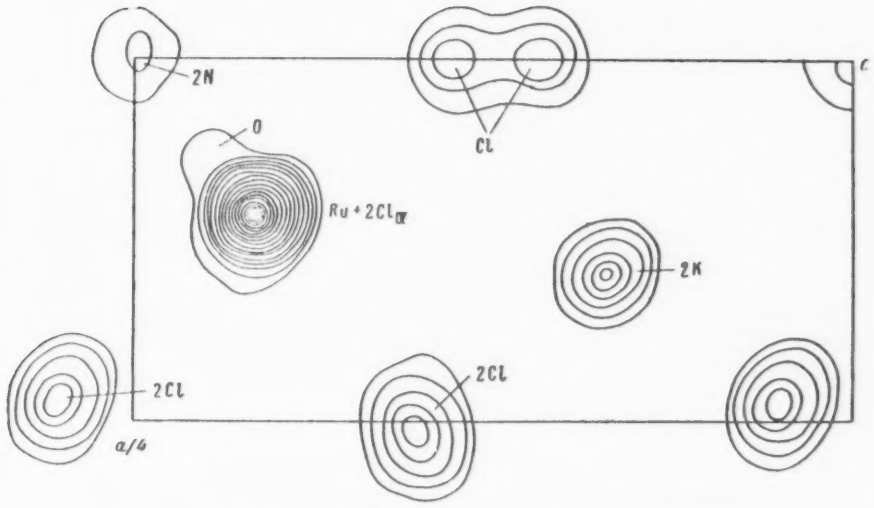

Fig. 3. Distributions of the electron density σ_0 (xz).

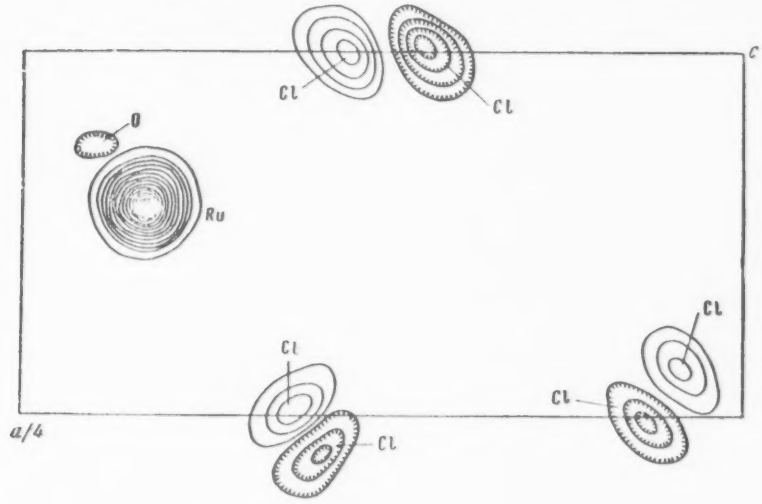

Fig. 4. Weighted projection σ_1 (xz).

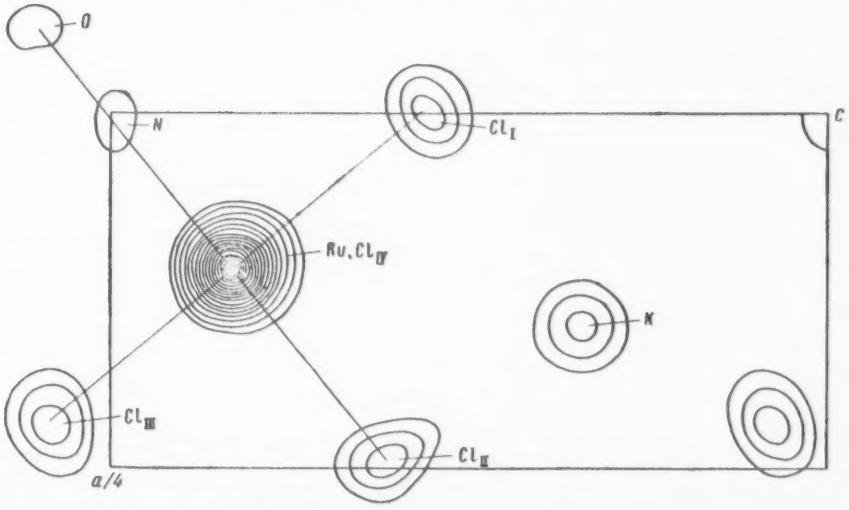

Fig. 5. Distribution σ_0 (xz) + $\frac{1}{\aleph_1}$ σ_1 (xz).

TABLE 3

Coordinates of the Atoms

Atom	Position	In fractions of the cell edges			In A		
		x	y	z	x	y	z
Ru	4(c)	0,108	0,250	0,173	1,437	2,561	1,183
K	8 d)	0,146	0,005	0,654	1,943	0,051	4,473
Cl_I	4(c)	0,001	0,250	0,447	0,013	2,561	3,057
Cl_{II}	4(c)	0,248	0,250	0,381	3,300	2,561	2,606
Cl_{III}	4(c)	0,221	0,250	—0,089	2,941	2,561	—0,609
Cl_{IV}	8(d)	0,108	0,021	0,173	1,437	0,215	1,183
N	4(c)	0,011	0,250	0,016	0,146	2,561	0,109
O	4(c)	—0,058	0,250	—0,108	—0,772	2,561	—0,739

TABLE 4

Interatomic Distances and Valence Angles in the Complex

Atoms	A	Atoms	A	Atoms	A	Atoms	Angle, degrees
$Ru — Cl_I$	2,35	N — O	1,25	$Cl_I — Cl_{IV}$	3,33	Ru — N — O	177 ± 3
$Ru — Cl_{II}$	2,34	$Cl_I — Cl_{II}$	3,32	$Cl_{II} — Cl_{IV}$	3,32	Cl_I — Ru — Cl_{II}	90
$Ru — Cl_{III}$	2,34	$Cl_{II} — Cl_{III}$	3,23	$Cl_{III} — Cl_{IV}$	3,32	Cl_{II} — Ru — Cl_{III}	88
$Ru — Cl_{IV}$	2,35	Cl_I — N	2,95	N — Cl_{IV}	2,89	Cl_{III} — Ru — N	90
Ru — N	1,70	Cl_{III} — N	2,89			Cl_I — Ru — N	92

TABLE 5

Interatomic Distances K-Cl and O-Cl

Atoms	A	Atoms	A	Atoms	A	Atoms	A
$K — Cl^*_{I\,(1)}$	3,47	$K — Cl_{II\,(3)}$	3,35	$K — Cl_{IV\,(3)'}$	3,29	$O_2 — Cl_{II\,(1)}$	3,01
$K — Cl_{II\,(1)}$	3,40	$K — Cl_{III\,(3)}$	3,57	$K — Cl_{IV\,(3)''}$	3,99	$O_2 — Cl_{I\,(2)'}$	3,14
$K — Cl_{II\,(1)'}$	3,23	$K — N_{(4)'}$	4,03	$K — Cl_{I\,(4)'}$	3,33	$O_2 — Cl_{III\,(1)'}$	3,43
$K — N_{(1)'}$	3,96	$K — Cl_{IV\,(1)'}$	3,32	$K — Cl_{IV\,(1)''}$	3,59	$2(O_{(2)} — Cl_{IV(3)'})$	2,89

* K(x, 1/2 - y, z); the subscript in parentheses indicates the number of the complex molecule (Fig. 7a).

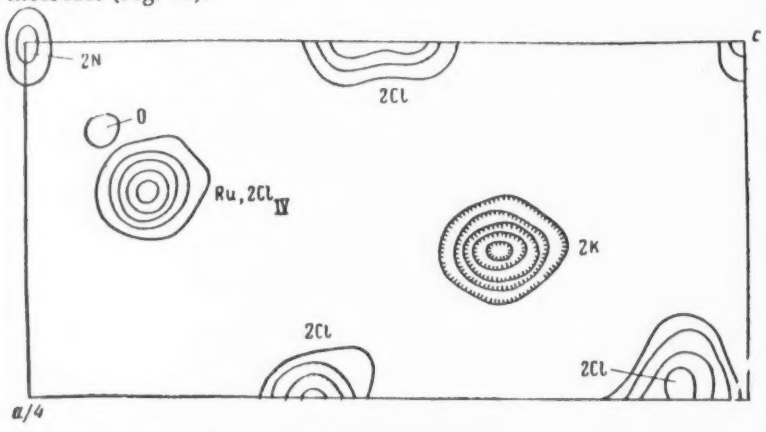

Fig. 6. Weighted projection σ_2 (xz).

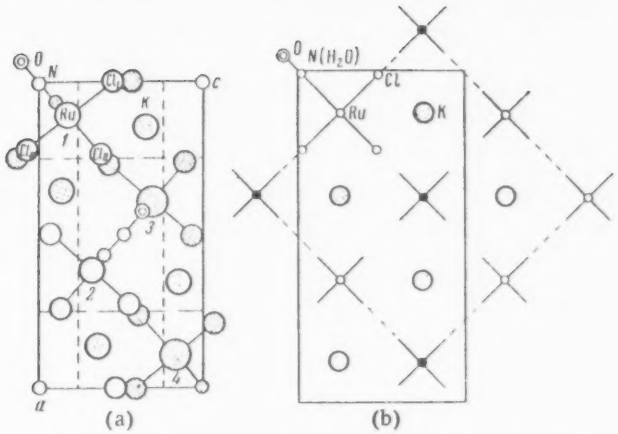

Fig. 7. a) Projection of the structure along the y axis; b) projection of the idealized structure. The dotted line shows the cell of K_2PtCl_6.

A proof of this is given by the identity of the developments of the layer lines along the y axis, which are different for the four orders of k (i.e., $F^2_{h01} \approx F^2_{h41}$, etc.). This peculiarity of the structures makes convenient the use of the method of combination of the weighted projections, since the "weight factors" of all atoms in this case have only three values: +1.0, and -1 [6]. On the weighted projections $\sigma_1(xz)$, the highest positive maxima are given by the atoms lying at the height $y = 1/4$; the most intense negative maxima are given by atoms with $y = 3/4$; the atoms lying at the heights $y = 0$ and $y = 1/2$ (Cl_{IV} and K) do not give any maxima.

The distribution $\sigma_0(xz) + (1/8)\sigma_1(xz)$ representing the superposition of the section $y = 0$ and $y = 1/4$ gives the possibility of distinguishing the atoms lying just in these layers from those lying at the height $y = 3/4$. The experimental material was provided by the h01 and h11 reflections. Three cycles of successive approximations were carried out.

After each cycle, the values of the structural amplitudes F (h0l) were reduced to an absolute scale. Table 1 gives a comparison of F_e (h0l) and F_c (h0l). The values of F_e (h0l) and F_e (h1l) were reduced to one scale in such a way that the equality $\sum_h \sum_l F_e(h0l) = \sum_h \sum_l F_e(h1l)$ would be satisfied for the summation over identical indices [6].

The calculation of the structural amplitudes F (h0l) in the first refinement stages was carried out taking into account Ru, K, and all the Cl atoms; similarly, the calculation of the coordinates of Ru, Cl_I Cl_{II}, and Cl_{III}.

The N and O atoms were included in the final stage of the calculation of F_c (Table I). Figures 3,4, and 5 report the final pictures of the electron density distributions: $\sigma_0(xz)$, $\sigma_1(xz)$, and their combinations. The projections $\sigma_0(xz)$ and $\sigma_1(xz)$, obtained from independent experimental data, are in complete agreement with each other. The pairs of chlorine atoms of the layers $y = 1/4$ and $y = 3/4$ are projected very close to each other. This holds, in particular, for Cl_{II} and Cl_{III}. In the distribution of $\sigma_0(xz)$, general maxima coming together correspond to them, whereas in the distribution of $\sigma_1(xz)$ the corresponding maxima and minima appear. The maximum at the origin of the coordinates in the diagram of $\sigma_0(xz)$ corresponds to a value close to zero of the electron density on the diagram of $\sigma_1(xz)$, since the nitrogen atoms of the various complexes lie almost exactly one above the other. The oxygen atom of a complex at the height $y = 3/4$ gives a small maximum in the distribution of $\sigma_0(xz)$ near the maximum of Ru ($y_{Ru} = 1/4$); in the distribution of $\sigma_1(xz)$ it corresponds to a minimum.

An additional check of the coordinates of the oxygen atom was provided by the weighted projection $\sigma_2(xz)$ constructed on the h21 reflections. (The atoms with coordinates $y = 1/4$ and $y = 3/4$ give maxima, those with $y = 0$ and $y = 1/2$ gave minima.) As can be seen from Fig. 6, also in this case, near the Ru maximum, there is a small maximum whose coordinates coincide with those of the oxygen atom obtained from $\sigma_0(xz)$ and $\sigma_1(xz)$.

In order to determine the final values of xz coordinates of all the atoms, we used the distribution $\sigma_0(xz) + \sigma_1(xz)/R$. The y coordinates of the K and Cl_{IV} atoms were at first roughly evaluated from the projections of the electron density along [001]. As in this projection there is a superposition of the maxima of K and Cl_{IV}, the refinement of the y coordinates was carried out on the difference projections $\sigma_0(xz)$, where the quantities $\Phi_1(hk0) = F_e - F_c(Cl_{IV})$ were used as expansion coefficients. The values of $F_e(hk0)$ and $F_c(hk0)$ are reported in Table 2.

The localization of the maxima was carried out according to the method proposed by Megaw [7], changing the exponential approximation into a hyperbolic approximation [8]. The accuracy of the localization was equal in the average to:Ru, 0.003; k,0.013; Cl, 0.006; N,0.006; O, 0.011 A.

Table 3 gives the coordinates of the atoms. The value of the probable error was calculated according to Vainshtein's formula [9] with constants refined by Porai-Koshits [10]: $\epsilon(x)_{Ru} = 0.004$; $\epsilon(x)_K = 0.012$; $\epsilon(x)_{Cl} = 0.013$; $\epsilon(x)_N = 0.038$; $\epsilon(x)_O = 0.033$ A.

The values of the deviation coefficients R(h0l) and R(hk0) were equal to 0.16 and 0.17 if the zero reflections were taken into account, and 0.13 and 0.15 if they were not taken into account. The sharpest reflections (040) were strongly weakened because of the extinction and were not taken into account in the calculation of R(hk0). The temperature correction constant was B = 3.7 A.

Table 4 shows the interatomic distances and the valence angles in the complex under consideration.

DESCRIPTION OF THE STRUCTURE

$K_2[RuNOCl_5]$ belongs to the rhombically distorted structural type of K_2PtCl_6. Figure 7 shows the relationship between the structure of the complex in question and those of K_2PtCl_6 and $K_2MeCl_5H_2O$. Figure 7a, shows the projection of the structure of $K_2RuNOCl_5$ along the y axis; Fig. 7b shows the same projection, but for an idealized structure, where the Ru and K atoms are placed exactly in the places of Pt and K. An exchange of one of the chlorine atoms of K_2PtCl_6 with a molecule of water in structures of the type $K_2MeCl_5H_2O$ or with a nitrogen atoms in $K_2RuNOCl_5$ leads to a decrease of the symmetry.

The replacement of water molecules by NO groups without changes of the structural frame as a whole is possible because the oxygen atoms of the nitroso group occupy octahedral holes not occupied in the structures K_2PtCl_6 and $K_2MeCl_5H_2O$. Formally, the structure of $K_2RuNOCl_5$ may be referred to the rhombically distorted type of $(NH_4)_3FeF_6$, where all the octahedral holes are filled. However, in the present case, the oxygen atom does not lie exactly in the center of an octahedron, but is displaced quite appreciably toward one of its vertices — the nitrogen atom forming the Ru-N-O chain. The remaining five vertices of the deformed octahedron are occupied by chlorine atoms of different molecules of the complex. The K ions are surrounded by Cl forming a distorted cube-octahedron.

The complex $RuNCl_5$ appears to be an almost perfect octahedron, with angles either equal or close to 90°. All the Ru-Cl distances are the same (2.35 A) within the limits of experimental accuracy. The Ru-N-O group, situated in our case trans to α chlorine atom, appears to be almost linear. The closeness of the valence angle of nitrogen to 180° (Table 4) provides some grounds for believing that in our case the configuration $Ru \equiv N^+ - O^-$ or $^-Ru = N^+ = O$ is present [1,3]. An analysis of the interatomic distances permits giving a preference to the first of these two theoretically possible structures. The Ru-N distance (1.70 A) is significantly lower than the sum of the assumed covalent radii even for the case Ru≡N (1.35 + 0.55). However, the N-O distance is equal to 1.25 A, and, hence, is intermediate between that of a double and of a single bond. A contraction of the metal-ligand bond was observed also for other Ru and Os complexes [1].

The authors take the opportunity for expressing their gratitude to S. M. Starostin, who prepared the crystals for the structure analysis, and to M. A. Porai-Koshits, for a number of valuable suggestions regarding the work.

LITERATURE CITED

1. G. B. Bokii, L. O. Atovmyan, and T. S. Khodashova, Doklady Akad. Nauk SSSR 128, 1, 78 (1958).
2. H. Dufet,Bull. Soc. Mineral 14, 206 (1891).
3. Ya. K. Syrkin, V. I. Belova, Izvest Akad. Nauk SSSR, Otdel Khim. Nauk 12, 1492 (1958). •
4. I. Lindqvist, Arkiv Kemi, Mineralogi och Geologi 24A, 1, 11 (1947).

•Original Russian pagination. See C.B. translation.

5. H. P. Klug, E. Kummer, and A. Lerov, J. Am. Chem. Soc. 70, 3064 (1948).
6. M. A. Porai-Koshits, Tr. Instituta Kristallogr. Akad. Nauk SSSR 12, 31 (1956).
7. H. D. Megaw, Acta Cryst. 7, 771 (1952).
8. A. D. Booth, Fourier Technique in X-ray Organic Structure Analysis (Cambridge, 1948).
9. B. K. Vainshtein, Zhur. Eksp. i Teoret. Fiz 27, 1, 44 (1954).
10. M. A. Porai-Koshits, Practical Course of X-ray Analysis [in Russian] (Izd. MGU, 1960). Vol. 2.

*Original Russian pagination. See C. B. translation.

THE CRYSTAL STRUCTURE OF TRIPHENYLDICHLOROSTIBINE

T. N. Polynova and M. A. Porai-Koshits

M. V. Lomonosov State University, Moscow
Translated from Zhurnal Strukturnoi Khimii, Vol. 1, No. 2, pp. 159-161
July-August, 1960
Original article submitted October 28, 1959

Crystals of $(C_6H_5)_3SbCl_2$ were studied by the x-ray method. The parameters of the lattice are: a = 19.74, b = 10.92, c = 12.26 A. The space group is $P2_12_12_1$, N = 4. The coordinates of the Sb atoms were established by the Patterson projection method, the coordinates of the Cl atoms were obtained by the superposition and minimization method. The positions of the C atoms were determined by geometrical analysis. The molecule has the configuration of a trigonal bipyramid, in whose center lies the Sb atom, and in whose vertices lie the Cl atom; the C_6H_5 groups are located in the equatorial plane. The investigation is in contrast with the conclusion by E. V. Stroganov that the compound $(C_6H_5)_3SbCl_2$ is built from associated cations $[Sb_2(C_6H_5)_6]^{4+}$ tetrahedrically surrounded by Cl^- ions.

The structure of $(C_6H_5)_3SbCl_2$ was previously studied by Stroganov [1], who came to the conclusion that the structure scheme is based on "associated cations" $[Sb_2(C_6H_5)_6]^{4+}$ tetrahedrically surrounded by Cl^- ions. Apart from the question of the chemical plausibility of the formation of associated ions of such compositions, it must be noted that the atom coordinates and interatomic distances given in [1] are not in agreement with the structure scheme suggested by its author. The shortest Sb-Sb distance is 6.601 A, in contrast with the possibility of a direct chemical bond between the metal atoms; on the other hand, the $Sb-Cl_I$ and $Sb-Cl_{II}$ distances, which are respectively equal to 2.43 and 2.39 A, indicated that the chlorine "ions" lie in direct contact with the antimony atoms (and not with the phenyl radicals, which should form the "shells" of the "associated cations"). Sb-Cl distances close in value to the distances in question were found in the structures of $(CH_3)_3SbX_2$ (X = Cl, Br, I) [2] and $(ClCH{=}CH)_3SbX_2$ [3], which are formed by five coordinated trigonal-bipyramidal R_3SbCl_2 molecules. Therefore, on the basis of the coordinates of the Sb, Cl_I, and Cl_{II} atoms, as given [1], it could be supposed that actually the crystals have the usual molecular structure: the two $(C_6H_5)_3SbCl_2$ molecules which Stroganov had taken as the "structure unit" $[Sb_2(C_6H_5)_6]^{4+}Cl_4^-$ should be contacted by the phenyl groups (at the usual intermolecular distances). Since the angle between the straight lines $Sb-Cl_I$ and $Sb-Cl_{II}$ calculated from the data of [1] is equal to 119°40', it would have been reasonable to suppose that both the Cl atoms and one of the phenyl groups lay in the equatorial plane of a bipyramidal molecule, and the other two groups lay at the vertices of the bipyramid.

Such a model required an accurate reexamination of the coordinates of the atoms of all the three phenyl groups given in [1].

The $(C_6H_5)_3SbCl_2$ crystals, obtained by us from the double salt of phenyldiazonium chloride and antimony trichloride [4], had the form of small plates and belong to the symmetry type of the rhombotetrahedron. Simple forms were developed: the prism $\{110\}$, and the tetrahedra $\{111\}$ and $\{11\bar{1}\}$. The cell parameters were established from oscillation x-ray photographs: a = 13.44, b = 10.92, c = 12.26 A (±0.05 A) (according to Stroganov's data a = 13.10, b = 10.95, c = 12.18 kX), N = 4, ρ_{peak} = 1.55 g/cm³, $\rho_{x\text{-ray}}$ = 1.53 g/cm³. The space group $D^4_2 = P2_12_12_1$ was uniquely determined from the extinctions. The presence of a piezoeffect (data by

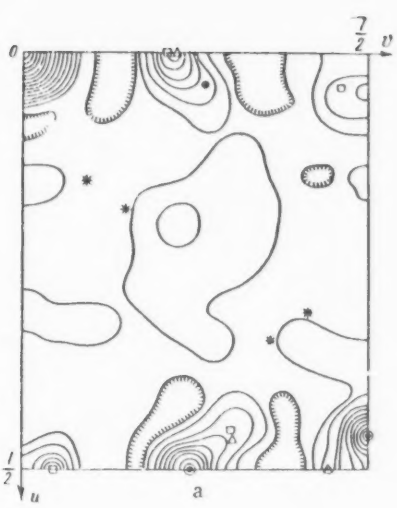

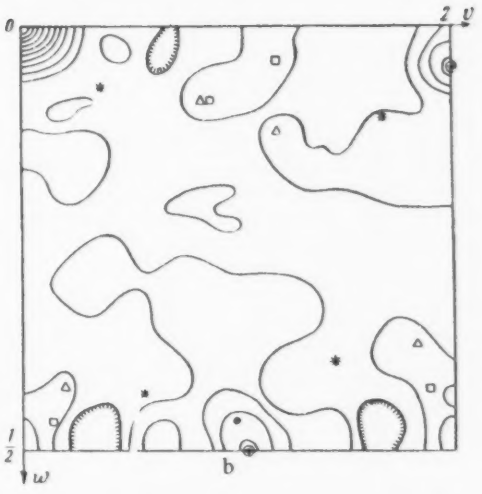

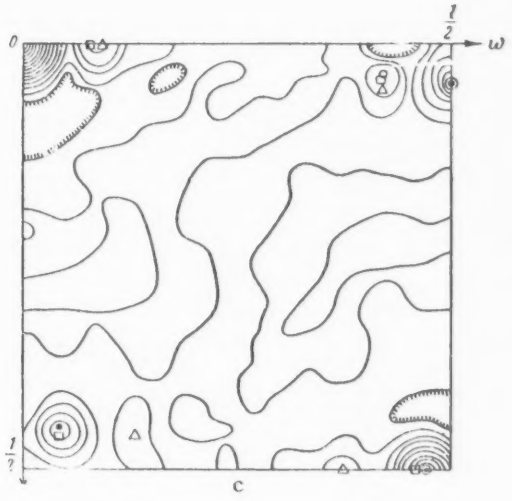

Patterson projections on the coordinate planes. The ends of the vectors, according to the atom coordinates as found by us, are denoted by: • ◉ Sb-Sb, □ Sb-Cl_I, △ Sb-Cl_{II}. Asterisks indicate the ends of the Sb-Cl_{II} vectors according to [1].

Koptsik, Moscow State Univ.) is in agreement with the fact that the space group found is not centrosymmetric. The investigation was carried out with the Mo-radiation.

According to Stroganov [1], the coordinates of the Sb and Cl atoms have the values

	x	y	z
Sb	0,234	0,383	0,733
Cl_I	0,233	0,166	0,774
Cl_{II}	0,079	0,473	0,658

(A)

In [1], the basis was provided by the coordinates x', y', z', related in the following way to

$$x' = x,\ y' = \frac{1}{2} - y,\ z' = \frac{1}{2} + z. \qquad \text{(B)}$$

However, an analysis of the projections of the interatomic function did not support the correctness of the determination of the coordinates of the Cl_{II} atom. On the (001) and (100) projections, the majority of the Sb-Cl_{II} vectors fall in regions with low values of the density of the interatomic function (in Figs.a and b, it is denoted by asterisks). The application of the superposition of the minimization method permitted us to determine new values of the coordinates of the Cl_{II} atoms. The projections of the electron density in the first approximation (with the signs of the coefficients determined according to the coordinates of the Sb, Cl_I, and Cl_{II} atoms), and in particular the difference projections ρ_e-ρ_c (Sb) confirmed the correctness of the new distribution found for the antimony and chlorine atoms. At this stage of the investigation, the following values were obtained for the coordinates of these atoms:

	x	y	z
Sb	0,229	0,372	0,729
Cl_I	0,225	0,162	0,811
Cl_{II}	0,220	0,580	0,644

The Sb-Cl_I distance is equal to 2.50 A, the Sb-Cl_{II} distance is equal to 2.53 A. The Cl_I and Cl_{II} atoms are located on one straight line on the two sides of Sb, i.e., just as in the $(CH_3)_3SbX_2$ and $(ClCH{=}CH)_3SbCl_2$ molecules. This permitted us to take the model of the $(C_6H_5)_3SbCl_2$ molecule in the form of a trigonal bipyramid, with the C_6H_5 groups in the equatorial plane. The slopes of the planes characteristic of the phenyl groups and the orientations of the molecules as a whole were found by geometric analysis (with the structure analyzed by Kitaigorodskii [5]): the molecules are packed in the cell without important stresses.

We expect to carry out a further refinement of the coordinates of the carbon atoms by the iterative method on the difference projections of the electron density.

LITERATURE CITED

1. E. V. Stroganov, "Application of the harmonic series in x-ray analysis in the example of the study of the structure of triphenyldichlorostibine crystals," Thesis [in Russian] (Leningrad Gos. Univ., 1953).
2. A. F. Wells, Z. Krist. 99, 367 (1938).
3. Yu. T. Struchkov and T. L. Khotsyanova, Doklady Akad. Nauk SSSR 91, 3, 565 (1953).
4. O. A. Reutov, Doklady Akad. Nauk SSSR 37,6, 991 (1952).
5. A. I. Kitaigorodskii, Izvest. Akad. Nauk SSSR, Otdel. Khim. Nauk, 6, 587 (1946).

THE RELATIONSHIP BETWEEN THE STRUCTURE OF MINERALS AND THEIR FLOTATION PROPERTIES

V. V. Bakakin
Inorganic Chemistry Institute, Siberian Section, Academy of Sciences of the USSR
Translated from Zhurnal Strukturnoi Khimii, Vol. 1, No. 2, pp. 162-169,
July-August, 1960
Original article submitted December 9, 1959

The part played by structural theories in the solution of certain problems connected with flotation properties has been shown for the case of a number of oxidized lead minerals, for which the tendency of the surface to be hydrated and the behavior towards sodium sulfide and xanthate are related to the magnitude of the noncompensated electrostatic charge of the surface and to the nature of the distribution of ions in the surface layer.

The flotation method for enriching mineral deposits is based on the use of differences in the physicochemical properties of the surfaces of the mineral particles. These differences obviously result from the specific character of the composition of the minerals and the structure of their surface layers. Since the latter depends essentially on the composition and crystal structure of the given substance as a whole, it must be concluded that a knowledge of the fine crystalline structure of a mineral and of the main features of the breakdown of the crystals during mechanical grinding should make it possible to obtain a picture of the nature of the distribution of the structural units in the surface layer of the mineral and to relate this to the particular features of the flotation behavior of the latter.

This formulation of the problem may of course appear too direct and simplified, when account is taken of the fact that the flotation conditions are determined by many factors, and that the classical theory of ideal crystals cannot at present be applied to all of the many properties of real crystals. Nevertheless it may prove practicable to approach the interpretation of the separate features of the flotation process by introducing structural ideas. Without claiming to provide a unique or exhaustive explanation of the action of a complex combination of different factors, these ideas can make a definite contribution to the construction of a final theory of the process. Proof that work in this direction is timely is provided by the ever-increasing interest in it being taken by research workers in the field of flotation, who, when explaining certain interesting experimental data, are still often forced to confine themselves simply to quoting the notorious phrase "the nature of the mineral surface". At the same time the number of works dealing directly with the problem of the relationship between the floatability of a mineral and the nature of its surface is very small. We shall refer to the most important of these.

In 1951, Bachmann [1], who made a study of the flotation of cubic mineral salts with alkylamine hydrohalides as collectors and examined the crystal structure of both, put forward a theory, according to which the familiar analogy (on the surface) between the crystal lattice of the mineral undergoing flotation and the lattice of the collector is the essential prerequisite for the attachment of the latter. The attachment of the collector was regarded as a process similar to the orientated growth of crystals on a carrier-crystal of a different type.

It was later established that the data for the lattice parameters of the alkylamine hydrohalides, used by Bachmann, should be corrected. The problem of the attachment of the collector received a corresponding new interpretation; it was now more convenient to relate it to the purely geometrical problem concerning the ratio

of the area of the collector ions to the "landing areas" around the oppositely-charged ions on the mineral surface. This was done in a paper by Schubert [2] on the flotation of a whole series of minerals by alkylpyridinium bromides. Even here, however, the author restricted the structural part of the work to a schematic solution of the problem of the possible geometrical distribution of the valencies on the surface of the mineral particles.

One of the first works to deal with the problem of the relationship between the internal structure of minerals and certain of their flotation properties appears to be the interesting paper by Strel'tsyn entitled "The natural flotability of minerals from the point of view of their structural characteristics" [3], which suggests, in particular, that a structural systematization of crystals according to the nature of the external bond forces should be carried out for flotation purposes.

A number of theories (and assumptions) regarding the part played by the crystal structure of minerals in flotation processes are contained in papers published in 1957-1958 on the influence of gases on the floatability of certain nonsulfide minerals [4, 5, 6]. Starting from the familiar theory that the breakdown of minerals on grinding takes place chiefly along planes which have a definite crystallographic and crystallochemical significance and which are determined exclusively by the structure of the minerals [7], the authors of these works point out the necessity for a strictly individual approach in the examination of the processes involved in the interaction between the reagents and minerals, and also mention the importance of a knowledge of the specific distribution of the structural units of the mineral on definite surfaces.

Starting from the same theories, and developing essentially the same theme, we shall make a comparison of the flotation and structural data for a number of secondary lead minerals: cerussite $PbCO_3$, anglesite $PbSO_4$, wulfenite $PbMoO_4$, pyromorphite $Pb_5[Cl(PO_4)_3]$, mimetite $Pb_5[Cl(AsO_4)_3]$, vanadinite $Pb_5[Cl(VO_4)_3]$, beudantite $PbFe_3^{3+}[(OH)_6(SO_4)(AsO_4)]$, and plumbojarosite $PbFe_6^{3+}[(OH)_6(SO_4)_2]_2$. All the experimental data on the flotation behavior of these minerals and on their tendency to react with the various reagents are taken from [8], which gives the results of the study of a whole series of flotation properties of these minerals.

At the same time we are of the opinion that the most fundamental of these properties, directly dependent on the structural features of the mineral, are the tendency of the surface to undergo hydration and its activity towards the flotation reagents. We relate the first property to the nature of the distribution of the ions in the surface layers of the mineral and to the extent to which their electrostatic charges are not compensated (in the first instance, to the total charge of the surface, which may be charged or electrically neutral). As far as the tendency to undergo hydration is concerned, the minerals studied can be divided into two categories: in the case of cerussite, anglesite, wulfenite, and pyromorphite, the surface is relatively hydrophobic (compared with other minerals), while for mimetite, beudantite, and plumbojarosite, the surface is extremely hydrophilic. The second property depends on the structural characteristics of both mineral and reagent. The reagents used in [8] were sodium sulfide and xanthate. Without going into the details of the mechanism of their interaction with the mineral surface, we would point out that here it is necessary to take account of the steric factor. In this case the regulator-reagent Na_2S influences the floatability chiefly as a result of the attachment to the mineral surface of large hydrosulfide and sulfide ions [9], whose area, for ionic radius S^{2-} equal to 1.82 A, exceeds 10 A^2. The solid-attracting group of the xanthate $ROC(=S)SMe$ contains two divalent sulfur atoms and the corresponding area of the anion, arranged at right angles to the surface, exceeds 20 A^2.

When the large size of these anions is taken into account, it must be assumed that the reagents in question are able to attach themselves to the mineral only if the Pb^{2+} cations which serve as centers for their attachment are situated in relatively accessible positions, for example directly on the surface of the mineral particles. In order to confirm this assumption, it is sufficient to establish the nature of the distribution of the lead cations in the surface layer of each of the minerals and compare this with the following experimental data (we quote from paragraphs 4 and 5 of the Summary in [8]): "The efficiency of the action of sodium sulfide and xanthate on oxidized lead minerals decreases in the following order: cerussite, anglesite, wulfenite, vanadinite, pyromorphite, mimetite, and beudantite. The surface of plumbojarosite does not undergo sulfidization".

In order to find an explanation for both these flotation properties, we proceeded as follows.

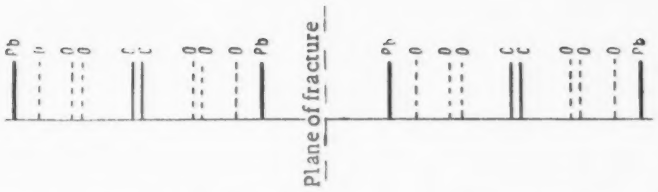

Fig. 1. Diagram illustrating the sequence of planar (110) networks in the cerrusite structure.

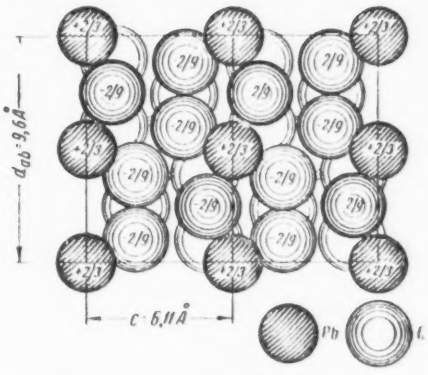

Fig. 2. Cerussite surface with fracture along the (110) cleavage plane.

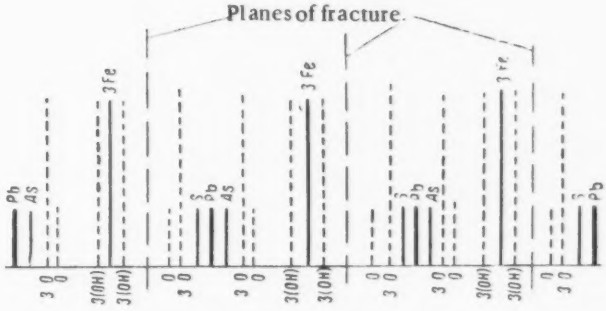

Fig. 3. Diagram illustrating the planar pinacoidal networks in the beudantite structure.

By analyzing the crystal structure of each mineral, we first of all found the directions of the most probable planes of fracture and constructed a diagram showing the sequence of the planar ionic networks parallel to these. For this purpose we have as far as possible used accurate structural data (the coordinates of all the atoms in the structure). We then constructed figures showing the corresponding surfaces and indicating the distribution of the ions and the magnitudes of their noncompensated electrostatic charges, which were calculated according to Pauling's electrostatic valence rule [10]. In addition, for convenience in using these diagrams, we constructed, for each surface, a table showing the ions present in the surface layer, the magnitudes of their noncompensated charges, the depth in Angstrom units of the arrangement from the upper level, and finally the total charge of the surface. The combination of the figures, diagrams and tables provided a sufficiently clear characterization of each mineral from the point of view in which we were interested.*

We give below the principal results of the study, including some general data borrowed from [12, 13, 14, 15]. Only the most characteristic examples are illustrated graphically. In all the figures, the intensity of shading decreases with increase in the distance of the ions from the surface.

Cerussite $PbCO_3$, orthorhombic system, lattice periods a = 5.15, b = 8.47, and c = 6.11 A; forms crystals with the aragonite-type structure. Distinct cleavage is observed along (110) and (021), with traces along (010) and (012). Analysis of the surfaces formed by fracture along these directions shows that they are comparatively

*The authors of [8] also posed the problem of the relationship between the flotation properties and the structural and crystallochemical features of the minerals; this was even reflected in the title of the article. While welcoming the fact, gratifying in itself, that workers in the field of ore-concentrating should pose such a question, we must nevertheless point out the unsatisfactory nature of the crystallochemical part of the work, since the authors reached conclusions which did not follow from their fragmentary, often naive and factually erroneous discussion. The effort to relate the floatability to the strength of the crystal lattice of the mineral was unfounded, and the authors' classification of minerals on the basis of the values of the specific energies of the crystal lattice seems to us to be unjustifiable, either in essence or formally (see [11]).

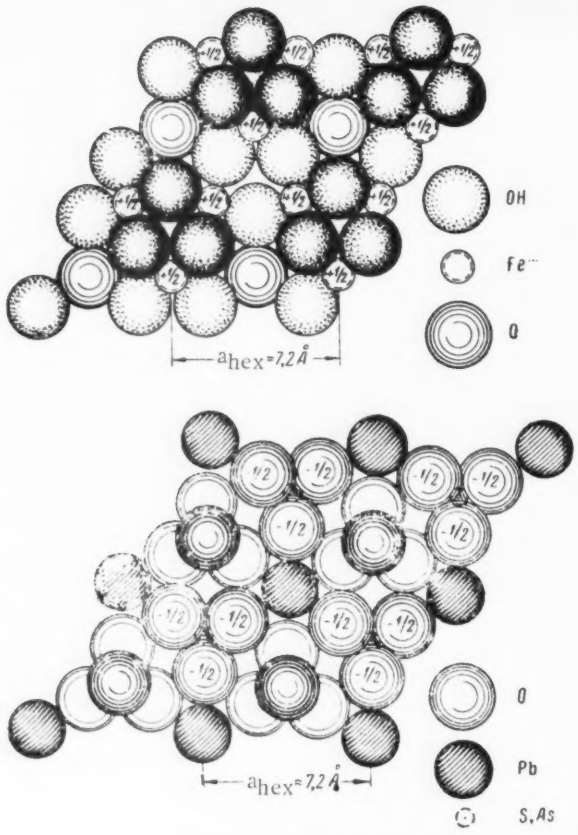

Fig. 4 The two nonequivalent surfaces of beudantite, formed during fracture along the (0001) cleavage plane.

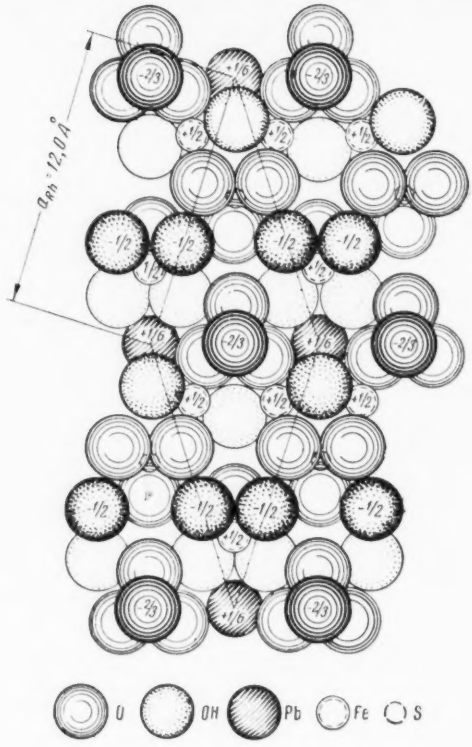

Fig. 6. Surface of plumbojarosite after fracture along the $(10\bar{1}1)$ cleavage plane.

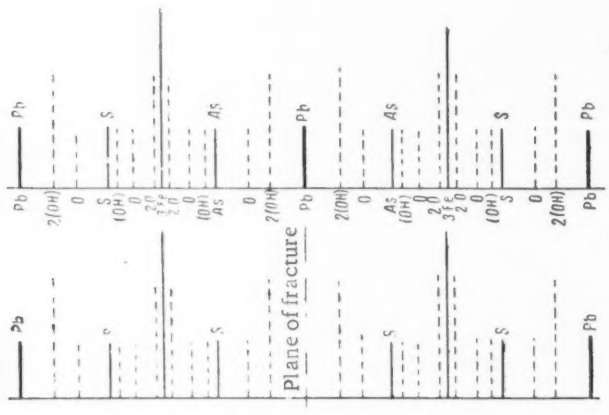

Fig. 5. Diagram illustrating the sequence of planar rhombohedral networks in the structures of: a) beudantite, b) plumbojarosite.

even (the height of the centers of the noncompensated charges in the surface layer is not more than 0.8 A) and electrically neutral (the total charge is equal to zero). The lead cations with noncompensated charges + 4/9 and + 2/3 are situated on approximately the same level as the oxygen anions of the CO_3 group, or even slightly above them, i.e., directly on the surface (Figs. 1 and 2).

Anglesite $PbSO_4$, orthorhombic system, lattice periods a = 8.47, b = 5.39, and c = 6.94 A; crystallizes with the barytes-type structure. Cleavage is excellent along (001), distinct along (210), and hardly noticeable along (010). The surface of fracture is electrically neutral, although it is characterized by a high relief and irregular distribution of the noncompensated charges within the limits of the unit cell. The lead cations with charges + 1/3, + 1/2, and + 2/3 are situated at a distance of 1.0-1.3 A below the level of the anions, but are not screened by them.

Wulfenite $PbMoO_4$, tetragonal system, lattice periods a = 5.42 and c = 12.10 A; crystallizes with the scheelite-type structure. Analysis of the probable planes of fracture (112), (101), and (001) shows that the surfaces of fracture are electrically neutral; lead cations with charges + 1/2 and + 3/4 are situated partly on the surface and partly on a level 1.1-1.7 A below the surface.

Comparison of Structural and Flotation Data for Certain Oxidized Lead Minerals

Mineral	Flotation data	Structural data
	Behavior towards flotation reagents	
Cerussite, anglesite, wulfenite	Readily sulfidized, floated efficiently by xanthates	Lead cations situated directly on the surface or at a short distance from it; surface neutral
Vanadinite, pyromorphite, mimetite	Sulfidized, floated slightly by xanthates	Lead cations situated deep in the surface layer or partly on the charged surface
Beudantite	Slightly sulfidized, floated slightly by xanthates	No lead cations on the greater part of the surface area
Plumbojarosite	Not sulfidized, not floated by xanthates	No lead cations detected on the surface
	Tendency to undergo hydration	
Cerussite, anglesite, wulfenite, pyromorphite	Comparatively hydrophobic surface	Surface electrically neutral overall
Mimetite, Beudantite, plumbojarosite	No hydrophobic properties	Surfaces charged

Pyromorphite $Pb_5[Cl(PO_4)_3]$, hexagonal system, lattice periods a = 9.97 and c = 7.33 A; crystallizes with the apatite-type structure. Traces of cleavage are observed along $(10\bar{1}0)$ and $(10\bar{1}1)$. Of these two directions, we have as yet examined only one -- along the $(10\bar{1}0)$ prism. The surface has a high relief (the difference in the heights of the noncompensated charges is 3.1 A) and is electrically neutral overall. The exposed lead cations with charges 0, + 3/ 10, and + 2/ 3 are situated on the lowest levels, but are only slightly screened by the anions lying above them and are in general accessible for interaction with reagents.

Mimetite $Pb_5[Cl(AsO_4)_3]$, hexagonal system, lattice periods a = 10.38 and c = 7.54 A. The structure is analogous to that of pyromorphite. Replacement of the $(PO_4)^{3-}$ ion by the larger $(AsO_4)^{3-}$ anion, however, brings about an increase in the lattice period and a change in the coordinates of the atoms and in the interatomic As-O distances, compared with the P-O distances. The relative arrangement of the planar networks of the structure is also altered. As a result of this, fracture, for example, in the $[10\bar{1}0]$ direction, for which traces of cleavage are observed, will with a high probability take place involving quite different pairs of planar networks from those in pyromorphite. The surface naturally acquires different properties. Thus fracture along the $(10\bar{1}0)$ plane in this case leads to the formation of two nonequivalent surfaces which are relatively flat but are electrically charged (the total noncompensated charge within the limits of the unit cell is ± 2.0).

This type of surface is evidently not the only one for mimetite, although it is possibly the determining one; other cases, such as those examined above for pyromorphite and undoubtedly present here, may play a subordinate role.

Vanadinite $Pb_5[Cl(VO_4)_3]$, hexagonal system, lattice periods a = 10.49 and c = 7.44 A. The structure is analogous to that of pyromorphite and mimetite, but there are no complete structural data for vanadinite in the literature (particularly for the coordinates of the oxygen atoms). It is thus impossible to establish exact relationships in this series of minerals. We intend to return to this problem later, when new structural data have been obtained. At present we can only point out that there are no reports of cleavage of vanadinite in the mineralogical literature.

Beudantite $PbFe_3^{3+}[(OH)_6(SO_4)(AsO_4)]$, trigonal system, lattice periods $a \approx 7.2$ and $c \approx 17.0$ A, structurally similar to alunite. The Fe^{3+} cation is surrounded by an octahedron of four OH^- anions and two O^{2-} ions from the $(S,As)O_4$ groups. The lead atom has six oxygen atoms as nearest neighbors and six hydroxide groups at a slightly greater distance. Cleavage is distinct along the (0001) pinacoid.

Fracture along the cleavage plane leads to the formation of two nonequivalent surfaces (Figs. 3 and 4). On one of these, Fe^{3+}, $(OH)^-$ and O^{2-} ions are exposed, the charge being noncompensated only in the case of the Fe^{3+} cations, so that the surface is positively charged. Lead ions are absent. The second surface contains oxygen ions, either neutralized or with noncompensated charge, and neutralized lead ions (at a depth of 1.2 A). The fact that the lead has no noncompensated charge and is situated below oxygen anions with charge - 1/ 2, which surround it closely, practically excludes the possibility of its interaction with reagents. This beudantite surface is negatively charged.

Thus the surfaces formed when beudantite is fractured along the pinacoidal cleavage are electrically charged and contain no active lead ions. On the finely-ground mineral particles, these surfaces will obviously predominate (in view of the excellent cleavage and the absence of other cleavage directions), but they are not the only surfaces, since the pinacoid is an open form and can exist only in combination with other surfaces. These surfaces, which are formed in arbitrary directions on fracture, will obviously contain lead ions with noncompensated charges. As mentioned above, however, these surfaces will play a subordinate role quantitatively.

Plumbojarosite $PbFe_6^{3+}[(OH)_6(SO_4)_2]_2$, trigonal system, lattice periods a = 7.21 and c = 33.67 A. The structure of plumbojarosite, as can be seen from a comparison of the formulae and lattice periods, should be similar to that of beudantite. In fact it can be derived from the latter as follows. If we take the unit cell of beudantite, doubled along the c axis (with composition $Pb_2Fe_6^{3+}[(OH)_6(SO_4)(AsO_4)]_2$), replace the $(AsO_4)^{3-}$ ions by $(SO_4)^{2-}$ ions, and remove one Pb^{2+} ion to compensate for the valence change, we obtain the plumbojarosite structure. At the same time, as can be seen clearly from Fig. 5, the cleavage along the $(10\bar{1}1)$ rhombohedron, characteristic of plumbojarosite, is produced. The rhombohedron is a closed form, so that the presence in the plumbojarosite of excellent cleavage along the rhombohedron and the apparent absence of pinacoidal cleavage (analogous to that of beudantite) on the second plan, mean that practically the entire bulk of the ground particles can be represented by two types of surface. One of these, along (0001), is similar to that dealt with above for the case of beaudantite (Fig. 4). The characteristics of the other type are given in Fig. 6. The surface is distinguished by an exceptionally high relief; the following ions, with the noncompensated charges indicated, are exposed: O with - 2/ 3, (OH) with -1/ 2, Fe with + 1/ 2, and Pb with + 1/ 6. The distribution of the charges is extremely irregular; the surface is electrically neutral overall, the cations are situated considerably lower than the anions and are effectively screened by them, and this should undoubtedly be reflected in the electrical properties of the surface. The lead cations (with minimum noncompensated charge of one-twentieth) are situated at the 3.7 A level, where they are screened by anions and practically completely inacessible for interaction with reagents. A considerable quantity of noncompensated iron cations, surrounded by hydroxide anions, are exposed on the plumbojarosite surface. Effective collectors for plumbojarosite should thus be collectors of the anionic type, with the hydroxide group functioning as the solid-attracting group. This is in accordance with experimental data [8] which show that phosphotene, cresol $HOC_6H_4CH_3$, and xylenol $C_6H_3(CH_3)_2OH$ have a favorable influence on the flotation properties of plumbojarosite although the majority of other collectors are inert.

The results obtained are given in the Table. Comparison of these data with flotation data leads to the conclusion that specific structural data, considered on a definite plan, can throw light on the reasons for the different flotation behavior of minerals.

Thus the suggestion made at the start of this paper, regarding the possible part played by structural ideas in the solution of certain flotation problems, appears to us to have been fairly convincingly confirmed.

LITERATURE CITED

1. R. Bachmann, Erzmetall 4, 316 (1951).
2. H. Schubert, Freiberger Forschungshefte A77 (Berlin, 1957).
3. G. S. Strel'tsyn, Proceedings of the Second Scientific and Technological Session of the Mechanical Treatment Institute [in Russian] (Metallurgizdat, Moscow, 1952).
4. V. V. Bakakin, I. N. Plaksin, and E. M. Chaplygina, Doklady Akad. Nauk SSSR 116, 4, 625 (1957).*
5. V. V. Bakakin, I. N Plaksin, and E. M. Chaplygina, Izvest. Akad Nauk SSSR, Otdel Tekh. Nauk, 9, 96 (1957).
6. V. V. Bakakin, I. N Plaksin, and E. M. Chaplygina, Izvest. Akad. Nauk SSSR, Otdel. Tekh. Nauk, 6, 84 (1958).
7. N. V. Belov and M. V. Klassen-Neklyudova, Zhur. Tekh. Fiz. 18, 3, 265 (1948).
8. E. A. Anfimova, V. A. Glembotskii, I. N. Plaksin, and A. S. Shcheveleva, Izvest. Akad. Nauk SSSR, Otdel.

*Original Russian pagination. See C.B. translation.

Tekh. Nauk SSSR, 4, 16 (1958).
9. V. I. Klassen and V. A. Mokrousov, Introduction to the Theory of Flotation [in Russian] (Metallurgizdat, Moscow, 1959).
10. L. Pauling, The Nature of the Chemical Bond [Russian translation] (Goskhimizdat, Moscow, 1947).
11 I. N Shorsher, Tsvetnye Metally 6, 93 (1959).
12. A. G. Betekhtin, Mineralogy [in Russian] (Gosgeologizdat, Moscow, 1950).
13. Dana's System of Mineralogy [Russian translation] (Moscow, IL, 1953).
14. H. Strunz, Mineralogische Tabellen (Leipzig, 1957).
15. W. G. Wyckoff, Crystal Structures (New York–London, 1951), Vols. I and II.

THE CRYSTAL STRUCTURE AND CHEMICAL CHARACTER OF LOWER OXIDES OF TITANIUM $TiO_0 \rightarrow 0.48$

E. S. Makarov and L. M. Kuznetsov

V. I. Vernadskii Geochemistry and Analytical Chemistry Institute,
Academy of Sciences of the USSR
Translated from Zhurnal Strukturnoi Khimii, Vol. 1, No. 2,
pp. 170-177, July-August, 1960
Original article submitted November 25, 1959

An x-ray diffraction study of lower oxides of titanium in the composition range $TiO_{0 \rightarrow 0.48}$ has been carried out. Accurate measurements have been made of the lattice parameters, densities, and intensities of the diffraction maxima on the diffraction diagrams for specimens of the lower oxides of titanium. The theoretically-calculated and experimentally-determined values of the intensities of the reflections and the number of atoms in the unit cell of the lower oxides of titanium have been used to gain information regarding their crystal structure and chemical character.

INTRODUCTION

As part of a crystallochemical study of compounds of variable composition, we have carried out an x-ray diffraction study of lower oxides of titanium, which can also be regarded as solid solutions of oxygen in α titanium.

The first detailed study of the crystal structure of lower oxides of titanium was made in 1941 by Ehrlich [1], who used titanium prepared by the Kroll method and found that the homogeneity range boundary for the solid solution of oxygen in α titanium corresponds to the composition $TiO_{0.42}$. The nature of the change in the lattice constants, density, and intensity of the reflections on the x-ray diffraction patterns indicated a statistical distribution of oxygen atoms in the octahedral holes of the hexagonal lattice of the α phase in the titanium-oxygen system.

With the appearance of the highly pure titanium prepared by the iodide method,* scientific and technical interest in titanium and its compounds increased considerably, and a large number of studies of the titanium-oxygen system have now been carried out. The most interesting of these is the work by Hansen and coworkers [2] on the determination of the phase diagram for this system in the temperature range 600-2000°. According to this diagram, the α phase melts congruently with a broad maximum at 1900°, corresponding approximately to a concentration of 25 at.% oxygen; this indicates its high thermal stability. The limit of saturation of the α phase by oxygen corresponds approximately to 33 at.% oxygen.

In 1956, data on the technology, chemistry, and metallurgy of titanium were collected in a monograph by A. D. McQuillan and M. K. McQuillan [3] According to the detailed studies of Andersson, Collen, Kuylenstierna, and Magneli [4], the range of homogeneity of the α phase extends approximately to the composition $TiO_{0.5}$ (Ti_2O) for specimens annealed at 400° for 6 weeks. The curves giving the change in the lattice constants with change in the α phase composition showed extreme points corresponding approximately to the composition $TiO_{0.35}$, which is close to the simple stoichiometric composition $TiO_{0.33}$ (Ti_3O).

*High-purity titanium is obtained by thermal decomposition of the iodide.

TABLE 1

Chemical composition	a, Å	c, Å	c/a	Chemical composition	a, Å	c, Å	c/a
α-Ti	2,9510	4,6850	1,5875	$TiO_{0,299}$	2,9703	4,7789	1,6089
$TiO_{0,012}$	2,9515	4,7054	1,5942	$TiO_{0,337}$	2,9702	4,7901	1,6127
$TiO_{0,053}$	2,9556	4,7225	1,5978	$TiO_{0,401}$	2,9685	4,7950	1,6153
$TiO_{0,102}$	2,9610	4,7370	1,5998	$TiO_{0,451}$	2,9705	4,7992	1,6156
$TiO_{0,154}$	2,9640	4,7510	1,6029	$TiO_{0,513}$	2,9710	4,8105	1,6192
$TiO_{0,193}$	3,9670	4,7616	1,6049	$TiO_{0,560}$	2,9704	4,8101	1,6193
$TiO_{0,248}$	2,9695	4,7701	1,6064	$TiO_{0,600}$	2,9701	4,8097	1,6194

TABLE 2

Chemical composition TiO_x	Average atomic weight (A)	Volume of unit cell (V, A^3)	Density ($d, g/cm^3$)	Total no. of atoms in unit cell (N)	No. of Ti atoms in unit cell (N_{Ti})	O atoms in unit cell $(N_O)_{exp.}$	O atoms in unit cell, from chemical comp. $(N_O)_{calc}$
α-Ti	47,90	35,334	4,500	2,01	2,00	0,00	0,00
$TiO_{0,053}$	46,30	35,728	4,547	2,13	2,00	0,13	0,11
$TiO_{0,102}$	44,96	35,969	4,610	2,24	2,00	0,24	0,20
$TiO_{0,154}$	43,68	36,148	4,644	2,33	2,00	0,33	0,31
$TiO_{0,193}$	42,76	36,302	4,698	2,42	2,00	0,42	0,39
$TiO_{0,248}$	41,59	36,428	4,762	2,53	2,00	0,53	0,50
$TiO_{0,299}$	40,58	36,515	4,808	2,62	2,00	0,62	0,60
$TiO_{0,337}$	39,23	36,598	4,841	2,74	2,00	0,74	0,67
$TiO_{0,401}$	38,80	36,594	4,908	2,81	2,00	0,81	0,80
$TiO_{0,451}$	38,03	36,675	4,996	2,92	2,00	0,92	0,90
$TiO_{0,513}$	—	—	4,969	—	—	—	—
$TiO_{0,560}$	—	—	4,879	—	—	—	—

TABLE 3

TiO_x	Ti — 12O, Å	Ti — Ti, Å		O — O, Å		TiO_x	Ti — 12O, Å	Ti — Ti, Å		— O, Å	
		Ti — 6Ti b*	Ti — 6Ti	O — 2O h*	O — 6O			Ti — 6Ti b*	Ti — 6Ti	O — 2O h*	O — 6O
α-Ti	2,067	2,951	2,897	2,342	2,951	$TiO_{0,248}$	2,089	2,970	2,937	2,385	2,970
$TiO_{0,012}$	2,071	2,952	2,905	2,353	2,952	$TiO_{0,299}$	2,090	2,970	2,941	2,389	2,970
$TiO_{0,053}$	2,075	2,956	2,914	2,361	2,956	$TiO_{0,337}$	2,091	2,970	2,946	2,396	2,970
$TiO_{0,102}$	2,080	2,961	2,921	2,369	2,961	$TiO_{0,401}$	2,092	2,969	2,947	2,398	2,969
$TiO_{0,154}$	2,083	2,964	2,928	2,376	2,964	$TiO_{0,451}$	2,093	2,971	2,950	2,400	2,971
$TiO_{0,193}$	2,086	2,967	2,933	2,381	2,967	$TiO_{0,513}$	2,095	2,971	2,954	2,405	2,971

* b = basal; h = hexagonal.

According to the authors cited, the appearance of these extreme points, together with the observed superstructure lines (001) and (003), is due to the ordered arrangement of the oxygen atoms at the composition Ti_3O.

Ariya and coworkers [5, 6, 7] made an experimental thermodynamic and magnetochemical study of chemical compounds of variable composition, including phases in the titanium – oxygen system. The main conclusion reached by these authors, regarding the "islet," submicroheterogeneous structure of crystals of compounds of variable composition, is not in accordance with modern crystallochemical data. The thermodynamic data for the α phase of the titanium – oxygen system allow a statistical distribution of oxygen in α titanium [6].

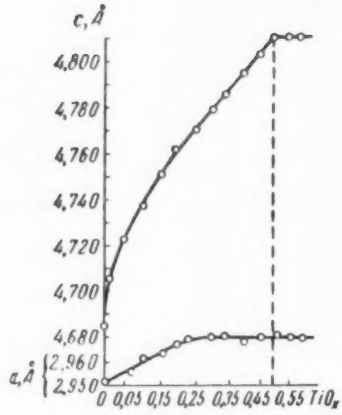

Fig. 1. Curves showing the relationship between the lattice constants c and a and the oxygen concentration in α titanium.

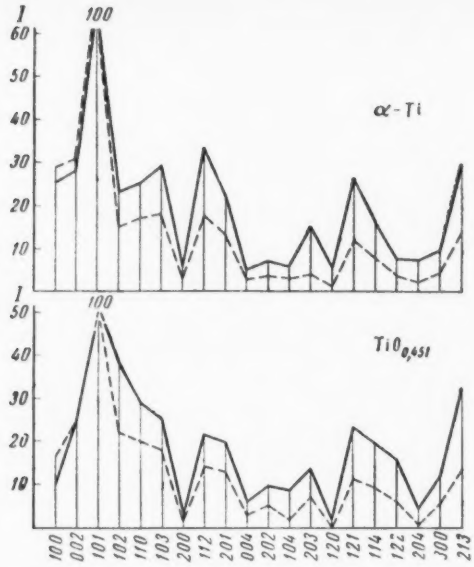

Fig. 3. Theoretical (broken lines) and experimental (solid lines) intensities for α titanium and $TiO_{0.451}$.

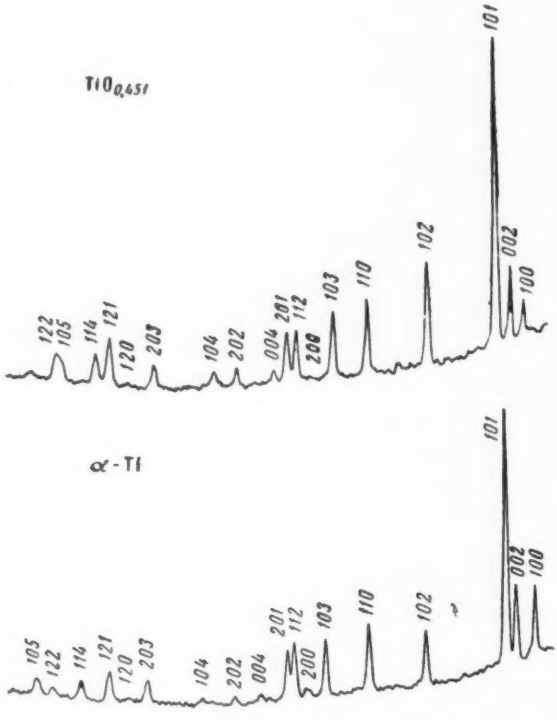

Fig. 2. Diffractometric curves for specimens of α Ti and $TiO_{0.451}$

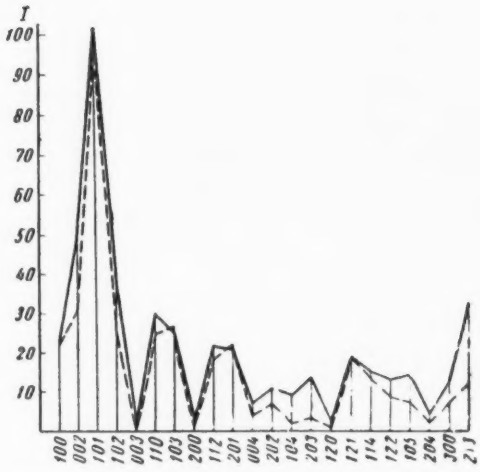

Fig. 4. Theoretical (broken line) and experimental (solid line) intensities for $TiO_{0.451}$ with an ordered arrangement of oxygen atoms.

The aim of the present work was to obtain accurate data on the crystal structure of lower oxides of titanium and to discuss their chemical character.

EXPERIMENTAL

a) The test specimens. In the present study we used the specimens of lower oxides of titanium which were prepared in earlier work [8]. Titanium prepared by the iodide method was used as starting material. The oxides were prepared by saturating the titanium with the required quantity of gaseous oxygen in a special vacuum system at 500-550°. Details of the preparation of the specimens have been given earlier [8]. Studies were made of specimens of lower oxides of titanium with the following compositions:

$TiO_{0.053}$; $TiO_{0.102}$; $TiO_{0.154}$; $TiO_{0.193}$; $TiO_{0.248}$; $TiO_{0.299}$; $TiO_{0.337}$; $TiO_{0.401}$; $TiO_{0.451}$; $TiO_{0.513}$; $TiO_{0.560}$; $TiO_{0.600}$.

The exact composition of the specimens was checked by the vacuum fusion method, which permits direct determination of the oxygen [9]. The specimens were annealed in the vacuum system under different conditions:

1) at a temperature of 1000° for 15 hours with subsequent rapid cooling of the vacuum system to room temperature;

2) at 300° for 1 month.

b) The range of homogeneity and the values of the lattice constants. The values for the lattice constants of the specimens of the lower oxides of titanium were obtained from x-ray powder diagrams. The technique of asymmetric film mounting was used, so that the error was ±0.0004 A. The results for specimens annealed at 1000° are given in Table 1.

The x-ray diffraction patterns of all the specimens up to the composition $TiO_{0.513}$ contain only lines corresponding to the hexagonal structure of the α phase. Lines corresponding to traces of a cubic phase based on TiO appear after the $TiO_{0.513}$ specimen and gradually increase in intensity. Thus the results of the x-ray phase analysis indicate that the boundary of the α phase on the oxygen side lies close to the composition $TiO_{0.5}$. This boundary can be established more accurately from the curve showing the relationship between the lattice constant c and the oxygen concentration. Fig. 1 shows that the boundary of the homogeneity range of the α phase corresponds to the composition $TiO_{0.48}$.

c) Determination of the density of the specimens. The density of powdered specimens of the lower oxides of titanium was determined by the ordinary pycnometric method [10]. Methylene iodide, with density equal to 3.324 g/ cm^3 at 20°, was used as working liquid. The error in the determination of the density was ± 0.002 g/ cm^3, and the values obtained are given in Table 2.

An interesting feature is that the point of intersection of the branches of the density–composition curves, corresponding to the single-phase and two-phase regions, can be used to establish the boundary of the range of homogeneity of the α phase; the result shows good agreement with the composition $TiO_{0.48}$ found above.

d) The number of atoms in the unit cell and the nature of the structure of the α phase. By comparing the values of the unit cell volume, density, and chemical composition, it is possible to calculate the experimental values of the numbers of atoms in the unit cell of the lower oxides of titanium. The results obtained, together with the initial data necessary for the calculation, are given in Table 2.

Table 2 shows that the total number of atoms in the unit cell increases with increase in the oxygen content of the oxides and reaches the value 2.92 for the oxide of composition $TiO_{0.451}$. It can thus be assumed that the total number of atoms for the composition Ti_2O, which is close to the boundary of the α phase, will be equal to 3. The number of titanium atoms in the unit cell does not change and in all specimens is equal to 2, as in the original titanium. This is indicated by the generally good agreement between the values of the number of oxygen atoms in the unit cell, found experimentally or calculated from the composition; this can be seen by comparing the last two columns in Table 2. Examination of Table 2 indicates that the unit cell contains the doubled formula of a given titanium oxide.

Thus, the α phase of the titanium – oxygen system is produced by the introduction of oxygen atoms in the holes in the α-titanium lattice.

e) The intensities of the reflections on the powder diagrams. The intensities were determined experimentally by the ionization method on a URS-50 x-ray apparatus with Cu radiation and a nickel filter in front of the Geiger counter for recording the β and fluorescent radiation. The specimens were prepared by depositing a thin layer of the test powder on the surface of plexiglas plates with nondrying adhesive. The thickness of the layer of test powder was the same for all specimens, so that for constant tube conditions it was possible to make a direct comparison of the intensities of the reflections for all the specimens. The particle size of the powder was approximately 25 μ. The integral intensities were determined from the areas of the peaks on the diffractometric curves. The accuracy of the determination of the intensities amounted to 4-6% for the strong and moderate lines, and to

10-15% for the weak lines. Characteristic diffractometric curves for specimens of α Ti and $TiO_{0.451}$ are given in Fig. 2.

As already pointed out by Ehrlich [1], the oxygen atoms have a marked influence on the intensities of the x-ray interferences of the lower oxides of titanium. The statistical introduction of oxygen atoms into the holes in the hexagonal structure of α titanium does not produce new reflections but brings about the redistribution of the intensities of a number of lines on the x-ray diagrams of the lower oxides of titanium. We have confirmed Ehrlich's conclusion that the octahedral holes in the α-titanium lattice are filled by oxygen atoms during the formation of the lower oxides of titanium. The theoretical values of the intensities were caluclated for all the test specimens ignited at 1000°, from data for their compositions, on the assumption that the oxygen atoms are introduced statistically into the octahedral holes. In the calculation of the relative intensities, account was taken of the Lorentz polarization factor and the repeatability factor. We used the method involving recording from a planar specimen, so that the absorption factor was not taken into account, since it is a constant quantity, independent of the magnitude of the angle of reflection [11].

The theoretically calculated and experimentally observed intensities for the original α titanium and a $TiO_{0.451}$ specimen are compared in Fig. 3. All the specimens of intermediate composition from $TiO_{0.053}$ to $TiO_{0.401}$ gave intensity pictures corresponding to a gradual transition from α-titanium to $TiO_{0.451}$.

Figure 3 shows that the agreement between the theoretical and experimental intensities is satisfactory, both for α titanium and for $TiO_{0.451}$. The influence of the oxygen is particularly marked in the case of the intensities of the (102) and (110) reflections. Together with the (103) reflection, these two reflections form a characteristic triad on the x-ray diagram and this can conveniently be used to compare the intensities of α titanium and its lower oxides. Figure 3 shows that the course of the change in intensities for this triad in the case of α titanium is the reverse of that for $TiO_{0.451}$. Another characteristic feature is the lower intensities of the (100) and (112) lines for $TiO_{0.451}$, compared with those for α titanium. Thus the good agreement between the experimental and theoretical intensities confirms the conclusion that the oxygen atoms are statistically distributed in the octahedral holes of the "titanium part" of the α-phase lattice of specimens annealed at 1000°.

All other possible modifications of the α-phase structure (for example, replacement of the titanium atoms by oxygen atoms, introduction of oxygen atoms into tetrahedral or doubled tetrahedral holes, combination with oxygen atoms to form submicroscopic grains of some higher oxide of titanium, interspersed in the α-titanium structure) do not show agreement with the observed intensities and must therefore be rejected.

f) Degree of order in the arrangement of oxygen atoms at low temperatures. Both the photographic and ionization "x-ray diagrams" for specimens of $TiO_{0.401}$, $TiO_{0.451}$, $TiO_{0.513}$, $TiO_{0.560}$, and $TiO_{0.600}$ show a very weak (003) reflection which, according to the literature data [4], indicates an ordered arrangement of oxygen atoms.

The (001) reflection could not be observed because of the background present at low angles of reflection.

The simplest version of an ordered arrangement of oxygen atoms corresponds to their distribution through one layer of octahedral holes (these layers are arranged perpendicularly to the z axis of the hexagonal lattice of the α phase). We have calculated the theoretical intensities of the reflections for a $TiO_{0.451}$ specimen assumed to have this structure and have compared the results with the experimental intensities; satisfactory agreement was observed (Fig. 4).

The existence of reflections of the (00l) type, where l is odd, is incompatible with the $D^4_{6h} - P6_3/mmc$ space group, to which the hexagonal close-packed α titanium belongs. The ordered arrangement of oxygen atoms assumed above therefore requires conversion to the space group $D^3_{3d} - P\bar{3}m1$, in which the distribution of atoms will be as follows:

2 Ti in 2 : (d); $z \approx 0.25$;
1 O in 1 (a)*

* This low-temperature structure (which could be called the α'-phase) is of the same structural type as $Mg(OH)_2$, with the Ti atoms in the positions of the OH groups and the O atoms arranged statistically in the Mg positions.

g) Interatomic distances. Change in the composition of the lower oxides of titanium leads to a marked change in the unit cell dimensions. It is therefore of interest to examine the changes undergone by the shortest interatomic distances and the coordination of the atoms with change in the oxygen contentof the lower oxides of titanium. Table 3 gives values of the interatomic distances for all the lower oxides of titanium annealed at 1000°.

Examination of Table 3 leads to the following conclusions: with increase in the oxygen content of the oxide, the Ti–Ti distances increase and the packing of the titanium atoms approaches more closely to the ideal hexagonal packing; the Ti–O and O–O distances increase smoothly.

DISCUSSION OF RESULTS

If we examine the chemical elements in order of increasing atomic number, we find that the titanium is the first element which is able to form α phases of extremely wide composition ranges with nonmetals, particularly oxygen. This property of titanium, which is also the first transition element (after scandium) is apparently related to the peculiar properties of d electrons in chemical bond formation between atoms. None of the elements before titanium are able to form extensive α phases with nonmetals, and form only typical compounds of constant composition, with simple stoichoimetric formulas satisfying thè normal valences. On the other hand, however, a large number of elements beyond titanium, and not only those in the transition series but also heavy elements in the b subgroups, have a marked tendency to form extensive phases of variable composition with nonmetals. In this connection, titanium is of particular interest in the study of the chemistry of compounds of variable composition, and the quantitative development of this field of chemistry should start from a detailed study of the chemical composition and crystal structure of titanium compounds.

The α phase has a clearly defined maximum melting point on the phase diagram [2] and is undoubtedly a chemical compound of titanium and oxygen. The nonsingular nature of this maximum, in accordance with Kurnakov's teaching regarding Daltonide and Berthollide compounds [12], indicates that the α phase in the titanium–oxygen system is Berthollide. From the viewpoint of modern crystallochemical theories [13], there is every justification for regarding phases such as the α phase in the titanium–oxygen system as chemical compounds of variable composition.

In fact, the experimental results given above for the crystal structure, i.e., for the distribution of the oxygen and titanium atoms in the α-phase structure, indicates that the change in the structure of this phase with change in composition is continuous. At high temperatures the oxygen atoms gradually, continuously, and statistically fill the octahedral holes of the titanium lattice, leading to a continuous increase in the unit cell dimensions, as can be seen from Tables 1 and 2.

At lower annealing temperatures, the oxygen atoms are introduced predominantly into holes in the lattice corresponding to 000 coordinates, which corresponds to the formation of an ordered α phase, in the sense that long-range order is present.

It may be assumed that the continuous nature of the change in the crystal structure of a chemical compound of variable composition of the same types as the α phase in the titanium–oxygen system corresponds to a continuous chemical addition reaction:

$$Ti + xO \rightarrow TiO_x + Q_{cal},$$

where x can vary continuously from 0 to a value corresponding to the limit of homogeneity of the phase. From the crystallographic viewpoint, the oxygen atoms are in fact added on to the atomic lattice of the α phase, continuously filling a new regular systems of points (a) in D^4_{6h}–$P6_3/mmc$ space group. It is known that the magnitude of the thermal effect Q of the reaction is of the same order of magnitude for α phases as for ordinary chemical compounds.

It is undoubtedly the case that the continuous nature of the change in crystal results from the continuous change in the chemical structure of the compounds of variable composition. In view of the lack of a reliable experimental criterion for estimating the effective number of electrons taking part in the formation of a given chemical bond, however, the problems of the detailed chemical structure of the α phase of the titanium–oxygen system cannot at present be resolved.

SUMMARY

1. The densities of specimens of lower oxides of titanium in the composition range $TiO_{0-0.560}$ were determined by a pycnometric method.

2. Data on the densities and unit cell dimensions have been used to calculate the total number of atoms in the unit cell of the lower oxides of titanium and also the individual numbers of titanium and oxygen atoms.

3. The α phase of the titanium – oxygen system is produced by the introduction of oxygen atoms (ions) into the holes in the α-titanium lattice.

4. The intensities of the reflections in the powder diagrams of lower oxides of titanium have been studied and satisfactory agreement has been found between the theoretical and experimental intensities both for the α phase and for the oxide $TiO_{0.451}$, assuming a statistical distribution of oxygen atoms (ions) in the octahedral holes of the α-phase.

5. Analysis of the theoretical and experimental intensities of the reflections for specimens of titanium oxides $TiO_{0.401-0.600}$ annealed for a prolonged period at 300° has shown that the oxygen atoms are arranged in ordered fashion in every second layer of octahedral holes, lying perpendicular to the z axis.

6. With increase in the oxygen content of the oxides, the interatomic Ti–Ti, Ti–O, and O–O distances in the lower oxides of titanium increase smoothly and the packing of the titanium atoms approaches ideal hexagonal packing.

7. The chemical character of the lower oxides of titanium has been discussed and it has been concluded that the α phase of the titanium–oxygen system is a chemical compound of variable composition.

LITERATURE CITED

1. P. Ehrlich, Z. anorgan. and allgem. Chem. 247, 53 (1941).
2. E. S. Bumps, H. D. Kessler, and M. Hansen, Trans. Am. Soc. Metals 45, 1008 (1953).
3. A. D. McQuillan and M. K. McQuillan, Titanium (London, 1956).
4. S. Andersson, B. Collén, U. Kuylenstierna, and A. Magnéli. Acta Chem. Scand. 11, 1641 (1957).
5. S. M. Ariya, M. P. Morozova, and E. Vol'f, Zhur. Neorg. Khim. 2, 1, 13 (1957).
6. M. P. Morozova, E. Vol'f, and T. P. Balova, Vestnik Leningradsk. Univ., 4; Ser. Fiz. i Khim. 1, 78 (1959).
7. G. Grossman, Thesis [in Russian] (Izd. LGU, 1959).
8. L. M. Kuznetsov, E. S. Makarov, and Z. M. Turovtseva, Zhur. Anal. Khim. 14, 4, 463 (1959).*
9. Z. M. Turovtseva and R. Sh. Khalitov, Zhur. Anal. Khim, 7, 6, 720 (1957). *
10. E. M. Bonshtedt-Kupletskaya, The Determination of the Specific Gravity of Minerals [in Russian] (Izd. AN SSR, Moscow, 1951).
11. H. P. Klug and L. E. Alexander, X-ray Diffraction Procedures for Polycrystalline and Amorphous Materials (New York–London, 1954), p. 376.
12. N. S. Kurnakov, Introduction to Physicochemical Analysis [in Russian] (Izd. AN SSSR, Moscow–Leningrad, 1940).
13. E. S. Makarov, Zhur. Neorg. Khim. 1, 9, 2032 (1956).
14. F. Weibke and O. Kubaschewski, Thermochemie der Legierungen (Berlin, 1943).

*Original Russian pagination. See C. B. translation.

AN X-RAY DIFFRACTION STUDY OF THE KINETICS OF FORMATION OF BARIUM-CALCIUM ALUMINATES AND TUNGSTATES

A. A. Maklakov and E. P. Ostapchenko

Translated from Zhurnal Strukturnoi Khimii, Vol. 1, No. 2,
pp. 178-182, July-August, 1960
Original article submitted February 28, 1959

An x-ray diffraction study has been made of the conditions for the formation of barium–calcium aluminates ($2.5BaO \cdot 0.5CaO \cdot Al_2O_3$) and tungstates ($2.5BaO \cdot 0.5CaO \cdot WO_3$) obtained both by sintering together the original oxides and by combined precipitation of substances which produce the aluminates or tungstates on subsequent ignition of the product of the combined precipitation. The second method not only ensures a high purity and uniformity of composition for the aluminates and tungstates, but also, in the case of the aluminates, leads to a considerable decrease in the temperature and duration of the ignition necessary to obtain the required product. In the preparation of the tungstates by combined precipitation, however, no significant decrease in the temperature or duration of the ignition was obtained.

In recent years in electrical vacuum apparatus, extensive use has been made of metal-film cathodes, which are resistant to poisoning and to ion bombardment, and are comparatively simple to prepare; they also make it possible to take off high emission current densities, and have a number of other advantages over other types of cathode. The emission properties of metal-film cathodes are determined primarily by so-called active substances, of which the most widely used are barium–calcium aluminate ($2.5\ BaO \cdot 0.5CaO.Al_2O_3$) and tungstate ($2.5BaO \cdot 0.5\ CaO \cdot WO_3$).

These substances are prepared chiefly by sintering together appropriate mixtures of barium and calcium carbonates with aluminum or tungsten oxides at temperatures of the order of 1350-1400°. During sintering the following reactions take place:

$$2{,}5\ BaCO_3 + 0{,}5\ CaCO_3 + Al_2O_3 \rightarrow 2{,}5\ BaO \cdot 0{,}5\ CaO \cdot Al_2O_3 + 3CO_2;$$

$$2{,}5\ BaCO_3 + 0{,}5\ CaCO_3 + WO_3 \rightarrow 2{,}5\ BaO \cdot 0{,}5\ CaO \cdot WO_3 + 3CO_2.$$

The reactions involved in the formation of the active substances take place in the solid phase, so that for success in carrying out these reactions, the degree of subdivision and intermixing of the reacting components is of considerable importance. Carbonates and oxides prepared industrially, however, have an indefinite grain size varying from 2-10 μ. Analysis of the grain size has shown that the particle size of the grains is almost unchanged after grinding in ball mills. Another serious disadvantage of the preparation of barium aluminates and tungstates by this method is the contamination of the final product by undesirable impurities introduced during the prolonged mixing of the starting components. Control of the product formed as a result of the above reaction is carried out chiefly by x-ray phase analysis. Values of the interplanar spacings and relative intensities of the lines for barium–calcium aluminate are given in Table 1.

TABLE 1

Interplanar Spacings and Relative Intensities of the Lines for Barium-Calcium Aluminate

d, A	I	d, A	I
4,10	40	2,03	23
3,75	9	1,92	6
3,49	9	1,81	14
3,04	12	1,71	6
2,88	100	1,66	22
2,43	8	$1,43_6$	9
2,35	34	$1,35_2$	12
2,12	6		

TABLE 2

Interplanar Spacings and Relative Intensities of the Lines for Barium-Calcium Tungstate

d, A	I	d, A	I
4,90	22	1,76	14
3,07	60	1,72	42
2,99	100	1,62	5
2,60	5	1,52	3
2,54	11	1,48	15
2,43	7	1,42	4
2,16	11	1,32	15
2,11	37	1,21	5
1,93	5	1,12	15

TABLE 3

Interplanar Spacings and Relative Intensities of the Lines for the Product of the Combined Precipitation of $BaCO_3$, $CaCO_3$, and $Al(OH)_3$

d, A	I	d, A	I
4,13	36	1,57	30
3,69	30	$1,44_2$	24
3,62	18	$1,37_6$	12
3,11	12	$1,35_5$	3
2,90	48	$1,28_4$	4
2,47	100	$1,23_9$	4
2,36	100	$1,21_8$	4
2,04	30	$1,16_9$	6
1,87	24	$1,13_6$	4
1,82	24	$1,08_4$	8
1,67	24	$1,05_3$	4

TABLE 4

Interplanar Spacings and Relative Intensities of the Lines for the Product of the Combined precipitation, which Forms Barium–Calcium Tungstate on Subsequent Ignition

d, A	I	d, A	I
4,10	14		
3,71	56	2,02	24
3,40	100	1,99	18
3,20	33	1,93	10
2,82	30	1,87	24
2,46	30	1,71	30
2,35	38	1,63	16
2,25	10	1,38	10
2,11	40	1,36	14

A study was made of the kinetics of the formation of barium–calcium aluminate, in order to determine the necessary conditions for its preparation. Figure 1 gives diffractometric diagrams* illustrating the process of barium–calcium aluminate formation at an ignition temperature of 1350°. Aluminate starts to be formed in the mixture after ignition for 3 min. After ignition of the mixture for 10 min, none of the original components remain in the reaction products, but the x-ray diagrams for these products are very poor, even after ignition for 20 or 30 min; this probably indicates that the reaction is not complete. Complete formation of barium–calcium aluminate is observed only after ignition for one and a half hours. Decrease in the ignition temperature to 1200° leads to an increase in the time required for the complete formation of the aluminate to two hours, and at 1000° the formation of aluminate is not complete even after ignition for 5 hr, and unreacted starting material remains in the reaction product.

The formation of barium–calcium tungstate (Table 2) at an ignition temperature of 1350° is complete in 70-80 min (Fig. 2). At 1200° this time increases to 2 hours, and no tungstate is formed when the temperature of ignition is decreased to 1000°.

* All the diffraction diagrams given in this work were obtained with a URS-50i apparatus. Cu K α radiation was used. In Figs. 1-4 the angle of scattering 2 ϑ is plotted on the x axis and the relative intensity is plotted on the y axis.

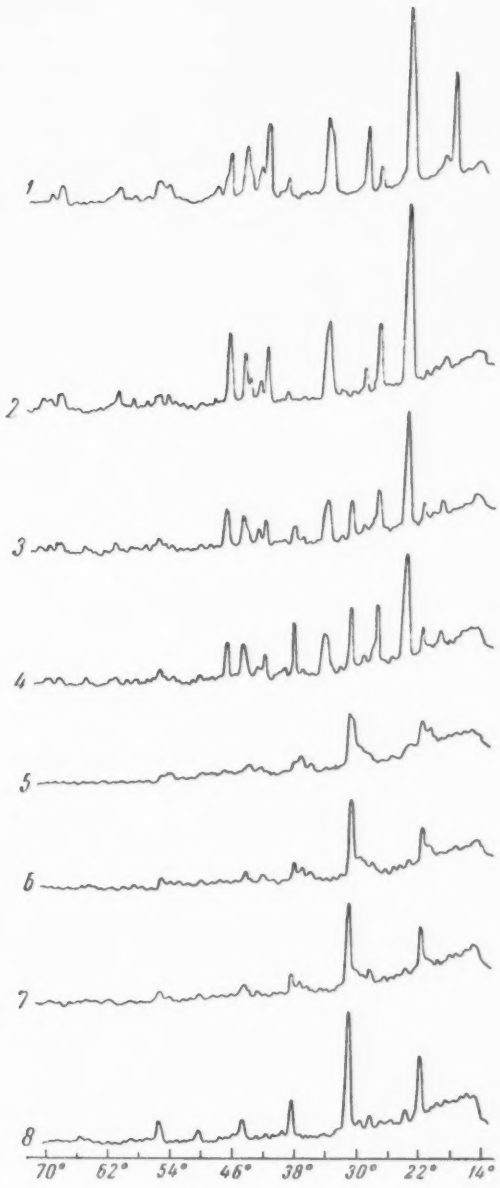

Fig. 1.

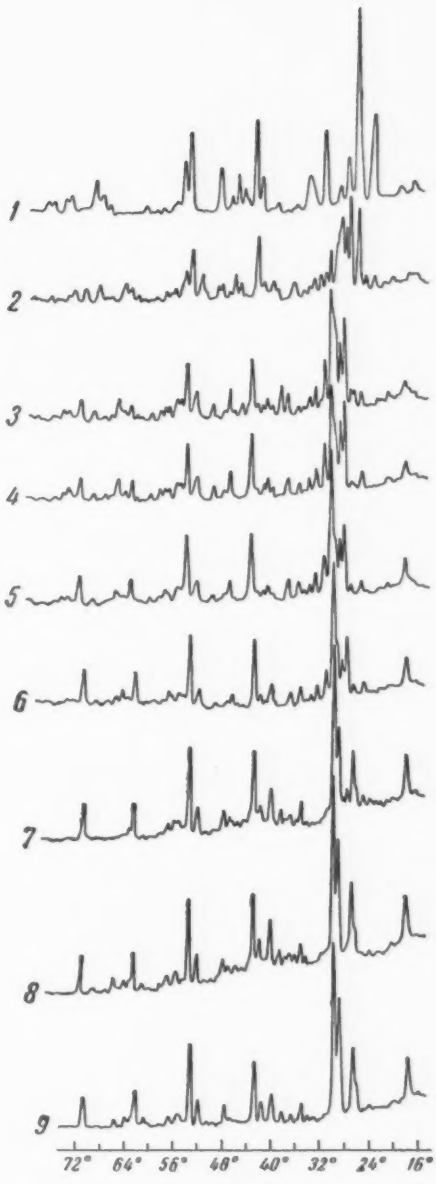

Fig. 2.

Fig. 1. Diffraction patterns for aluminates obtained by igniting mixtures of the oxides at 1350°: 1) original mixture of barium and calcium carbonates with aluminum oxide; 2) after ignition for 1 min; 3) 3 min; 4) 5 min; 5) 10 min; 6) 20 min; 7) 30 min; 8) 120 min.

Fig. 2. Diffraction patterns for tungstates obtained by igniting a mixture of the oxides at 1350°: 1) original mixture of barium and calcium carbonates with tungsten trioxide; 2) after ignition for 1 min; 3) 2 min; 4) 3 min; 5) 9 min; 6) 10 min; 7) 20 min; 8) 40 min; 9) 70 min.

In view of the above disadvantages associated with the method described for the preparation of barium–calcium aluminates and tungstates, we developed a method based on the combined precipitation of substances which form aluminates or tungstates on subsequent ignition.

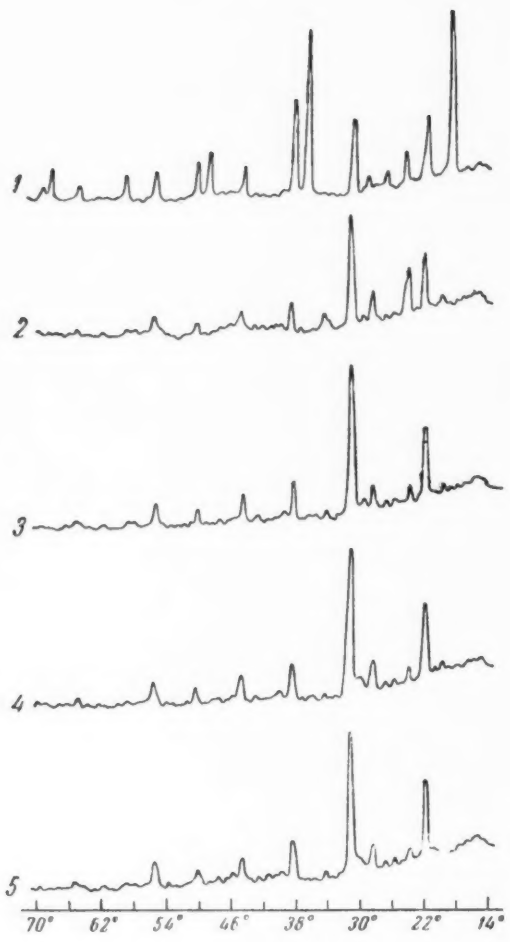

Fig.3.

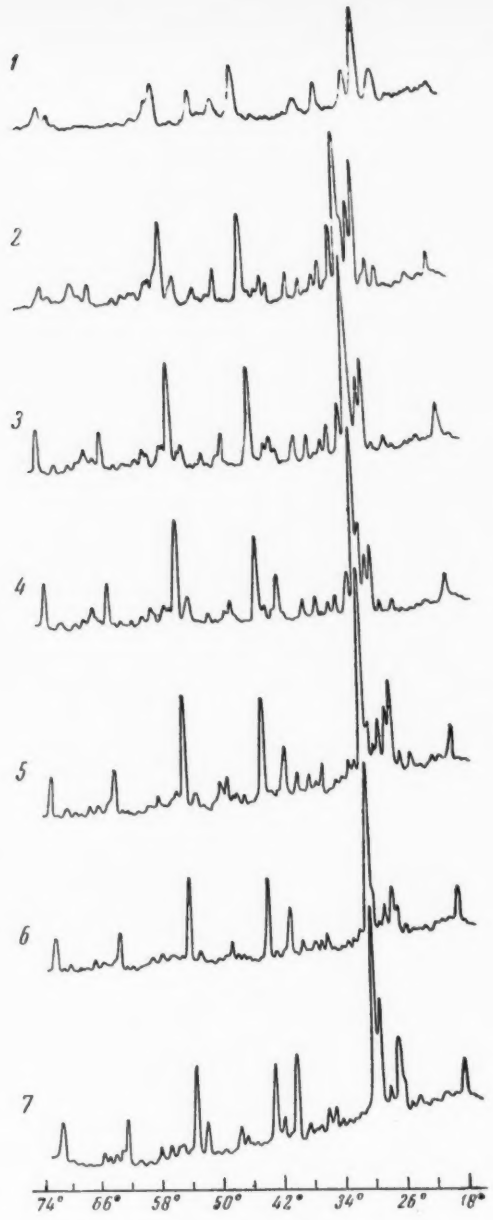

Fig.4.

Fig. 3. Diffraction patterns for aluminates obtained by combined precipitation: 1) the product of the combined precipitation; 2) after ignition at 1350° for 1 min; 3) 2 min; 4) 30 min; 5) 120 min.

Fig. 4. Diffraction patterns for tungstates obtained by combined precipitation: 1) the product of the combined precipitation; 2) after ignition at 1350° for 2 min; 3) 9 min; 4) 10 min; 5) 20 min; 6) 50 min; 7) 70 min.

In the preparation of barium–calcium aluminates by this method, the starting materials were $Ba(NO_3)_2$, $Ca(NO_3)_2$, $Al(NO_3)_3$, $(NH_4)_2CO_3$ and NH_4OH A solution of $(NH_4)_2CO_3$ and NH_4OH was heated to 60° and poured into a solution of $Ba(NO_3)_2$, $Ca(NO_3)_2$, and $Al(NO_3)_3$ in the required proportions at the same temperature The quantity of ammonia solution was that found by previous experiment to give a pH of 6.5-7 5 in the solution after cooling. The products of the combined precipitation were dried, compressed, and ignited.

X-ray phase analysis showed that barium–calcium aluminate is formed when the product of the combined precipitation is ignited (the calculation for the x-ray diagram of the product of the combined precipitation is given in Table 3) The study of the kinetics of the formationof the aluminate during the ignition of the product of the combined precipitation showed (Fig. 3) that at 1350°, extensive formation of aluminate is observed after ignition for only one minute, and ignition for two minutes leads to complete conversion to the aluminate At an ignition temperature of 1200°, complete conversion to the aluminate requires 5 min, and at 1000° it requires 15 min.

In the preparation of tungstates by the combined precipitation method, the starting materials were $Ba(NO_3)_2$, $Ca(NO_3)_2$, $(NH_4)_2WO_4$, and $(NH_4)_2CO_3$. The precipitation was carried out as described for the preparation of the aluminates Ignition of the product of the combined precipitation (the calculation for the x-ray diagrams of this product are given in Table 4) leads to the formation of barium–calcium tungstate.

SUMMARY

By making use of x-ray phase analysis it is possible to determine the technological conditions for preparing barium–calcium tungstates and aluminates. It has been shown that the preparation of barium–calcium aluminates by combined precipitation of substances which form the aluminates on subsequent ignition makes it possible to increase the purity of the product obtained and to decrease the temperature and shorten the duration of the ignition. This is probably related to the fact that during the combined precipitation, thorough mixing of the original components takes place, facilitating the course of the reaction in the solid phase. In the preparation of tungstates by the combined precipitation method, however, no significant decrease in the temperature or duration of ignition were obtained.

VIBRATIONAL SPECTRA OF THE WATER OF CRYSTALLIZATION IN MONOCRYSTALS OF $NiSO_4 \cdot 7H_2O$, $NiSO_4 \cdot 6H_2O$, $CaSO_4 \cdot 2H_2O$ NEAR THE FUNDAMENTAL OF THE O–H VALENCE VIBRATION

S. N. Andreev, S. A. Shchukarev, and T. G. Balicheva

A. A Zhdanov State University, Leningrad
Translated from Zhurnal Strukturnoi Khimii, Vol. 1, No. 2,
pp. 183-188, July-August, 1960
Original article submitted December 10, 1959

Unpolarized radiation has been used to measure the absorption spectra in the 3700-2500 cm^{-1} range for plates 15 to 50 μ thick cut from $NiSO_4 \cdot 6H_2O$, $NiSO_4 \cdot 7H_2O$, $CaSO_4 \cdot 2H_2O$ monocrystals. The frequencies found for $CaSO_4 \cdot 2H_2O$ are in good agreement with published values. The O–H frequencies found for $NiSO_4 \cdot 6H_2O$ are close to the values deduced from reflection spectra. The results obtained for $NiSO_4 \cdot 7H_2O$ disagree with results given by others.

The O–H bands of the last two compounds are very much broader than the corresponding bands for $CaSO_4 \cdot 2H_2O$ and are shifted some 300 cm^{-1} to the long-wave side; hydrated $NiSO_4$ has stronger $OH_2 \ldots OSO_3^{2-}$ bonds than $CaSO_4 \cdot 2H_2O$ does. The results do not agree with the finding that the O . . . O distance in hydrates of $NiSO_4$ is larger than that distance in $CaSO_4 \cdot 2H_2O$. The conflict can be eliminated by treating the hydrogen bond in terms of Sokolov's theory of molecular interactions and by making allowance for the donor-acceptor bond between the cation and the H_2O molecules (the bond can affect the residual charge of the hydrogen atoms).

The state of the water molecules forming the innermost shell around an ion is just as important as the hydration number itself, although there are very few papers on the subject

It is very difficult to solve the problem by examining solutions, because the theory of hydration and of structure for solutions is at present only in an early stage of development. Grinberg [1] gives the most complete review on the states of molecules coordinated to ions in solution; his arguments lead us to conclude that the H_2O molecules in the innermost shell of an aquocomplex are capable of protolytic dissociation. He relates the proton-donor function to the polarity of the molecule and to the charge on the central cation.

It is simpler, although it involves approximations, to use crystals of hydrated salts in order to study these H_2O molecules. X-ray analysis gives a reliable indication of the structure of the shells and enables us to elucidate the dispositions of the anions, cations, and water molecules.

Mikhailenko and Mushinskii [2], and later Semishin [3] and Alekseeva [4] have used the reactions of Mg, Zn, and Be (as powders) with hydrated salts to demonstrate that the water is capable of protolytic dissociation. In some cases the metal displaces the hydrogen from the water of crystallization as rapidly as if the water were a strong acid. However, it is scarcely possible to use the reaction rate of a heterogeneous system of this kind to evaluate the strength or otherwise of the O–H bonds in water of crystallization.

Sokolov's theory of molecular interactions and of proton transitions [5-9] can be used to explain this behavior of the water.

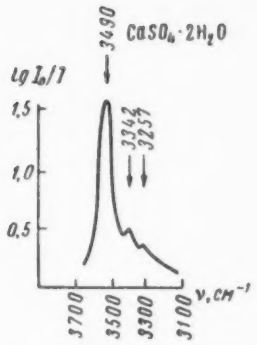

Fig. 1. Absorption spectrum of a $CaSO_4 \cdot 2H_2O$ crystal 20 μ thick. I_0 is the incident intensity, I is the transmitted intensity.

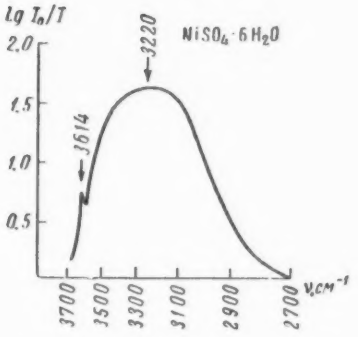

Fig. 2. Absorption spectrum of a $NiSO_4 \cdot 6H_2O$ crystal 15 μ thick.

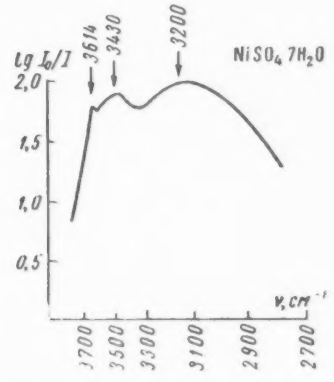

Fig. 3. Absorption spectrum of a $NiSO_4 \cdot 7H_2O$ crystal 50μ thick.

The exact Madelung potential ought to be used in such studies on O—H bonds, but, as a first approximation, we may suppose that the state of the H_2O molecules will be determined on the one hand by the donor-acceptor bonds to the anion and on the other by the interaction with the cation if all of the water molecules are coordinated to the cation (form the cation's nearest neighbors).

The first stage in the transfer of a proton from a water molecule to an anion is the formation of a hydrogen bond between the molecule and the anion [7], i.e., is the first stage in the protolytic dissociation of water. The probability of that dissociation is the greater the larger the energy of the hydrogen bond, which depends on the residual charge on the hydrogen atom in H_2O as well as on the distance and on the structure of the anion [7].

The O—H bonds of the water molecules are polarized by the field of the cation to which the molecules are bound; the interaction between the cation and the oxygen can be of typical donor-acceptor type if the cation derives from a subgroup of a long period. That interaction increases the residual charge on the hydrogen atoms and strengthens the hydrogen bonds to the anions, i.e., increases the probability of the protolytic dissociation.

Sokolov [6-8] has shown that the M—H frequency is reduced by the formation of an M—H....B hydrogen bond (in which MH is a hydride and B is an atom having a nonbonding electron pair). The shift to longer wavelengths (lower frequencies) may be taken to be roughly proportional to ϵ / D, in which ϵ is the dissociation energy of the hydrogen bond and D is that energy for the unperturbed M—H bond.

Sokolov's theory can be applied to crystals of hydrated salts to explain why the bound water behaves as an acid and also to indicate methods of examining the behavior of the water, e.g. measurement of the O—H frequency.

The frequency varies in the same sense as the force constant of the O—H bond, so the vibrational spectra can give us valuable information about the effects of cations and anions on that constant for the bound water and on the tendency of that water to dissociate.

Here we give the infrared absorption spectra for $NiSO_4 \cdot 7H_2O$, $NiSO_4 \cdot 6H_2O$, $CaSO_4 \cdot 2H_2O$, which we have recorded for the region of the fundamental O—H valence vibration.

Published information on the first two compounds is restricted to Schaefer and Schubert's paper [10] on the reflection spectrum of $NiSO_4 \cdot 6H_2O$ and to Lecomte's [11] and Matsumura's [12] papers on the absorption spectrum of $NiSO_4 \cdot 7H_2O$. Lecomte's results were obtained on polycrystalline powders; Matsumura's on a monocrystal 690 μ thick, whose optical density must have been at least 20-30. The frequencies quoted by those two for $NiSO_4 \cdot 7H_2O$ are completely different.

The spectrum of $CaSO_4 \cdot 2H_2O$ has been examined repeatedly, but the results given in the table make it clear that the results depend on the state of the material and on the method used.

X-ray studies on $NiSO_4 \cdot 6H_2O$ [18], $NiSO_4 \cdot 7H_2O$ [19], $CaSO_4 \cdot 2H_2O$ [20] indicate that all of the water molecules in the first and last lie very close to their respective cations (Ni^{2+} and Ca^{2+}); the cation-oxygen distances are almost equal to the respective sums of the radii of cation and H_2O.

Spectrum	State	Authors listed in this paper	Observed frequencies cm^{-1}										
Absorption	Monocrystal	[13]			3580	3496		3334	3244		2238	2199	2122
	The same	[14]			3560	3495		3350	3248		2235	2198	2130 2112
	"	[15]			3600			3300			2220		2130
	"	[12]		3610		3490	3410		3260				
	"	Own results			3584	3490		3342	3257		2231	2210	2124
	Powder	[13]			3542		3405	3340	3240		2245	2203	2113
	The same	[16]	3711		3554	3513	3408	3324	3247	3189	3067		
					3640								
					3605								
	"	[17]					3410					2200	
Reflection	Monocrystal	[14]			3537	3490	3430						
							3410						
	The same	[15]				3510	3400						

Six of the water molecules in $NiSO_4 \cdot 7H_2O$ are close to the cation; the seventh is 4.1 A away.

In every case the coordinated water can form hydrogen bonds to oxygen in the anions. The H_2O... ...OSO^{2-}_3 distance in $NiSO_4 \cdot 6H_2O$, $NiSO_4 \cdot 7H_2O$, $CaSO_4 \cdot 2H_2O$ is respectively 2.74, 2.79, and 2.71 A. The minimum distance from the seventh H_2O molecule to oxygen in SO^{2-}_4 in $NiSO_4 \cdot 7H_2O$ is 3.7 A; it is unlikely that this molecule could form a hydrogen bond to the anion, but it could form one to the coordinated water, because the H_2O .....OH_2 distance is 2.8A.

If we ignore the effect of the cation on the hydrogen bond, whose energy we assume to depend only on the H_2O...OSO^{2-}_3 distance, we have that the change in the O–H frequency (relative to the frequency for the unperturbed bond) for $CaSO_4 \cdot 2H_2O$ will be larger than the changes for the other two salts; the absorption band for the first should be much broader than the bands for the other two. Moreover, we would expect to find in the spectrum for $NiSO_4 \cdot 7H_2O$ a frequency similar to the frequency for liquid water, because there is one water molecule outside the coordinated group.

We grew large monocrystals of $NiSO_4 \cdot 7H_2O$ and $NiSO_4 \cdot 6H_2O$ from aqueous $NiSO_4$ by means of the planetary rotation method [21] at 27-28°C and 39-40°C. We cut from a crystal of $NiSO_4 \cdot 6H_2O$ plates 10 × 10 mm parallel to the plane of perfect cleavage, (001); from $NiSO_4 \cdot 7H_2O$, ones parallel to a; in both cases the plates were ground with emery mixed with mineral oil, carefully dried over sodium metal, and were polished with rouge in the same oil. The thicknesses were measured to 1 μ with an IKV vertical optimeter. The plates of $CaSO_4 \cdot 2H_2O$ were cut parallel to the cleavage plane from a natural crystal of gypsum and were treated in the same way. The thicknesses varied from 50 μ ($NiSO_4 \cdot 7H_2O$) to 15 μ ($NiSO_4 \cdot 6H_2O$) or 20 μ ($CaSO_4 \cdot 2H_2O$).

The absorption spectra were recorded with an IKS-6 spectrometer fitted with an LiF prism.

Scattered light and absorption by atmospheric water vapor can distort the absorption curve [22], as in our measurements on liquid water [23]. Special care was taken to eliminate water vapor from the air. The monochromator and light source were sealed, and the apparatus was flushed with nitrogen dried first over KOH and then over P_2O_5 for 70 hr before the measurements started. Moreover, beakers containing P_2O_5 were placed in the monochromator.

Scattered-light effects were eliminated by placing between the light source and slit a glass plate 9 mm thick, which was opaque to radiation having $\nu < 3500$ cm^{-1} [22].

The apparatus was calibrated to ±2 cm^{-1} over the range from 2000 to 4000 cm^{-1} by reference to the spectra of NH_3, HCl, HBr, CH_4, CO, $CHCl_3$, C_6H_6. The pen recorder usually used at the output was replaced by a Hilger galvanometer having a 500 mm scale in order to provide sufficient accuracy in the optical-density measurements. The spectral width of the slit was about 3 cm^{-1} in the range from 4000 to 3100 cm^{-1} and was about 1.5 cm^{-1} in the range from 2300 to 2100 cm^{-1}.

Figures 1 - 3 give the result obtained with unpolarized radiation.

Our results for $CaSO_4 \cdot 2H_2O$ agree well with those given by Hass and Sutherland and by Pain, Duval, and Lecomte. The spectrum we find for $NiSO_4 \cdot 6H_2O$ is similar to that given (for reflection) by Schaefer and Schubert [10].

The spectrum of $NiSO_4 \cdot 7H_2O$ shows very strong bands at 3200 and 3430 cm^{-1}; the curve for this crystal may be treated as the sum of the curve for $NiSO_4 \cdot 6H_2O$ and the curve for liquid water given by Chulanovskii [24]. The latter band corresponds to the O—H frequency of liquid water and is caused by the seventh (uncoordinated) H_2O molecule.

The frequencies we find for this compound agree only in part with the ones given by Matsumura (3510 and 3458 cm^{-1}) and by Lecomte (3091, 3208, and 3279 cm^{-1}).

We have established the cause of the weak maximum at 3614 cm^{-1} found in the spectra of the hydrates of $NiSO_4$.

Estimates of the O—H frequency and of the width of the band from the O...O distance alone indicate that the frequency for gypsum should be much lower than the frequencies for the two hydrates of nickel sulfate; moreover, the band for gypsum should be much broader than the bands for the other two compounds.

Figures 1-3 show that these predictions are not confirmed; the bands for the two hydrates of nickel sulfate lie 300 cm^{-1} to the long-wave side of the band for gypsum and are much broader than that band.

This unexpected result is explained if we suppose that the O—H frequency and the energy of a hydrogen bond depend on the cation as well as on the distance from the water molecule to the anion. The $H_2O...OSO^{2-}_3$ distances in the two hydrates of nickel sulfate are much larger than that distance in gypsum, but the Ni^{2+} ion has a much larger effect than the Ca^{2+} ion does on the O—H frequency; the result is that the residual charge on a hydrogen atom is larger in those two hydrates than it is in gypsum, so the hydrogen bond to the anion is stronger in the hydrates of nickel sulfate, although the O...O distances are larger.

SUMMARY

1. The infrared absorption spectra in the region of the fundamental O—H frequency are reported for crystals of $NiSO_4 \cdot 7H_2O$, $NiSO_4 \cdot 6H_2O$, $CaSO_4 \cdot 2H_2O$ from 50 to 15 μ thick.

2. The peaks for $NiSO_4 \cdot 6H_2O$ and $NiSO_4 \cdot 7H_2O$ are displaced about 300 cm^{-1} to the long-wave side of the peak for $CaSO_4 \cdot 2H_2O$. The hydrates of $NiSO_4$ gives bands much broader than the band given by gypsum.

3. The relation between the O—H frequencies and between the bands widths are explained on the assumption that the energies of the $OH_2...OSO^{2-}_3$ hydrogen bonds depend not only on the $H_2O...OSO^{2-}_3$, distance but also on the Me^{2+} cation.

LITERATURE CITED

1. A. A. Grinberg, Introduction to the Chemistry of Coordination Compounds [in Russian] (Goskhimizdat, 1957).
2. Ya. I. Mikhailenko and P. G. Mushinskii, Transactions of the 1st Mendeleev Congress [in Russian], p. 317.
3. V. I. Semishin, Zhur. Org. Khim. 10, 319, 328, 339 (1940).
4. O. P. Alekseeva, Zhur. Org. Khim. 22, 1906 (1952).
5. N. D. Sokolov, Doklady Akad. Nauk SSSR 58, 611 (1947).
6. N. D. Sokolov, Doklady Akad. Nauk SSSR 82, 369 (1952).
7. N. D. Sokolov, Dissertation, Institute of Chemical Physics [in Russian] (Izd. AN SSSR, 1953).
8. N. D. Sokolov, Uspekhi Fiz. Nauk 57, 205 (1955).
9. N. D. Sokolov, Ukrain. Khim. Zhur. 22, 19 (1956).

10. C. Schaefer and M. Schubert, Ann. Phys. 50, 339 (1916).
11. J. P. Lecomte, J. chim. phys. et phys.-chim.biol. 50, 53 (1953).
12. On. Matsumura, Mem. Fac. Sci., Kyushu. Univ. 13, 1 (1951).
13. G. Pain, G. Duval, and J. Lecomte, Compt. rend., 237, 238 (1953).
14. M. Hass and G. H. Sutherland, Proc. Roy. Soc. 236, 427 (1956).
15. G. A. Zaitsev and B. S. Neporent, Zhur. Éksp. Teoret. Fiz. 29, 857 (1955).
16. A. N. Lazarev. Izvesti Akad. Nauk SSSR, Ser. Fiz. 21, 322 (1957).
17. A. Miller and C. Wilkins, Anal. Chem. 24, 1253 (1952).
18. Strukturberichte 2, 95 (1935).
19. C. A. Beevers and C. M. Schwartz,Z. Krist., 91, 157 (1935).
20. W. A. Wooster, Z. Krist. 94, 375 (1936).
21. O. M. Ansheles, V. B. Tatarskii, and A. A. Shternberg, Rate of Growth of Homogeneous Crystals from Solutions [in Russian] (Lenizdat, 1945).
22. M. O. Bulanin, Candidate's Dissertation, [in Russian] (Leningrad Gos. Univ., 1958).
23. S. N. Andreev and T. G. Balicheva, Doklady Akad. Nauk SSSR 90, 149 (1953).
24. V. M. Chulanovskii, Doklady Akad. Nauk SSSR 93, 25 (1953).

THE FORMATION OF THREE-CENTER BONDS IN CHEMISORPTION

Ya. K. Syrkin

Translated from Zhurnal Strukturnoi Khimii, Vol. 1, No. 2,
pp. 189-199, July-August, 1960

The chemisorption of the diatomic molecules H_2, O_2, N_2, CO and so on and unsaturated organic molecules of the ethylene type, which proceeds with a small activation energy, is explained by the formation of three-center bonds having, on the one hand, donor-acceptor properties originating from the electron pair of the π-bond (or the σ-bond in H_2) and the unoccupied p-orbitals of the metal and, on the other hand, a dative character resulting from the d-electron pairs of the metal and the antibonding orbitals of the adsorbed molecule. For this reason the chemisorption turns out to be a rapid reversible adsorption proceeding at low temperatures.

The aim of this paper is to pay attention to the possibility that three-center bonds are formed in chemisorption. Bonds of this type are known in various cases. So, in the first stage of ethylene bromination there is formed a complex in which bromine interacts with the ethylene π-bond as a whole. Three-center bond exist also in compounds as, for instance, Zeise's salt $K[PtCl_3C_2H_4]$. The structure of the complex $[PtCl_3C_2H_4]$ ion has been investigated by Bokii and Kukina [1] and they have found that the C_2H_4 group is placed perpendicular to the $PtCl_3$ plain and that both C atoms have equal distances to the Pt atom. Chatt and Duncanson [2] have proposed that in this ion the Pt atom is not bonded to a single carbon atom but to the double bond in the ethylene molecule as a whole. By means of group theory Dyatkina has given a theoretical discussion of this problem [3]. The ethylene molecule has two molecular π-orbitals, namely, the bonding one $\Psi_1 + \Psi_2$, which is occupied by an electron pair and the unoccupied antibonding orbital $\Psi_1 - \Psi_2$. The Pt atom has an unoccupied p_z orbital, which has the same symmetry as the $\Psi_1 + \Psi_2$ orbital so that a three-center $\Psi_1 + \Psi_2 + \alpha p_z$ orbital can be formed for which the electron pair is provided by ethylene (donor-acceptor bond). Moreover, the d_{xz} orbital of the Pt atom, which is occupied by an electron pair, can interact with the unoccupied $\Psi_1 - \Psi_2$ orbital of ethylene and form another three-center orbital $\Psi_1 - \Psi_2 + \beta d_{xz}$ for which Pt furnishes the electron pair (dative bond). In this way two three-center bonds are realized in Zeise's salt. For certain, Zeise's salt is not the sole representative of compounds having such bonds. There is known a great number of complexes between transition metals and olefins, acetylenes and so on, which have this structure.

It may be supposed that in the system consisting of "an atom on a metal(Ni,Fe,Pd,Pt) surface together with a molecule with a multiple bond" an analogous three-center bond may be formed too. The system of three atoms

has the same symmetry as the PtC_2H_4 group in the anion of Zeise's salt so that for a molecule interacting in chemisorption with an atom in the metal surface the same considerations can be applied. This means that a donor-acceptor bond is formed from an unoccupied adsorbent orbital and the electron pair in the $\Psi_1 + \Psi_2$ orbital of the adsorbate and a second dative bond from the antibonding unoccupied $\Psi_1 - \Psi_2$ orbital of the adsorbed molecule and an orbital of the metal atom containing an electron pair. Here the presence of a great number of

d-electrons provides both the bonds in the metal and the bond with the chemisorbed molecule.

The effective charge of the surface atom and the direction of the metal-molecule bond depends upon which of the two parts (donor-acceptor or dative bond) dominates in the electron shift. We will show that, if the system Me $\rightleftharpoons N_2$ is discussed along these lines by the molecular orbital method, ionic states are already included.

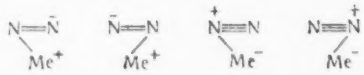

The fact that the surface atom interacts with other metal atoms, probably , has no influence upon the formation of the said bonds, if this atom has a sufficient number of d-electrons and at least one unoccupied orbit, which is the case for Fe,Co, Ni,Pt,Pd and others.

The chemisorption of a molecule on a single surface atom by the formation of three-center bonds can take place with an activation energy which is small or practically zero, that is, the chemisorption will proceed rapidly. Many cases are known where the chemisorption rate on metals at low temperatures is very high and, consequently, proceeds with a very small activation energy. Here it is natural to suppose that the molecule as a whole is chemisorbed by the formation of three-center bonds and not in the form of atoms, since in the latter case a thorough rearrangement of the bonds would be required, which must be accompanied by a considerable activation energy, as is characteristic for activated adsorption. Meanwhile, the formation of donor-acceptor bonds, for instance, at the reaction between NH_3 and BF_3 requires, as is well known, an activation energy of at most about 2 kcal [4]. The heat effect of such reactions, however, can be very considerable and attain many times ten kcal.

A rapid adsorption is not of necessity a physical one. It is impossible to identify chemisorption with activated adsorption. The conception of chemisorption comprises more, since chemisorption may proceed with a negligible activation energy. It is characteristic that a weak unactivated chemisorption at low temperatures is decreased, when the temperature is raised to a value at which a strongly activated adsorption proceeds. Meanwhile the heat of chemisorption increases with temperature. The heat effect is a criterion to test the chemical character of a low temperature adsorption. It is natural to infer that under these conditions (at low temperature) adsorption is not accompanied by dissociation into atoms. But for few exceptions, transition metals, which, because of their d-electrons, are able to form dative as well as normal donor-acceptor bonds, show a high activity.

The formation of covalent bonds with atomic d-orbitals at the chemisorption of ethylene has been supposed by Beek [5]. But he assumed here that the adsorption meant a "polarization" of a physically adsorbed molecule. This point of view has no ground. Chemisorption is a chemical reaction involving lone pairs and unoccupied orbitals and, obviously, the formation of three-center bonds. In this reaction a redistribution of charges takes place which entails the appearance of a dipole moment.

When the chemisorbed molecule forms three-center bonds it may become more reactive and react with a lower activation energy. Moreover, the polar character of the three-center bonds may promote the catalytic reaction. It is generally pointed out that a weak and rapid chemisorption of the reacting substance is a requirement for catalysis. When the molecules are adsorbed very strongly, they run the risk of being relatively unreactive. A slow adsorption, of course, retards the reaction. When chemisorption is not an activated one then, probably, it will be weaker than an activated adsorption, that is, it will be accompanied by a heat effect smaller than that corresponding with the formation of atomic bonds with the surface. In any case, it is uncertain whether a high heat of chemisorption is advantageous for a catalytic reaction. Decreasing the heat of chemisorption and raising the amount adsorbed so considerably that the degrees of surface coverage which are generally used in catalysis are reached facilitates the catalytic reaction and implies already small values for the heat of chemisorption. This has been pointed out by de Boer [6] and others. In fact, the chemisorption of an atom under the formation of a strong bond as, for instance, Me≡N may have the result that the nitrogen atom to a considerable extent is unfit to react; in any case, it will require a high activation energy in order to react. So it is far from obvious that this atom can take part in a catalytic reaction. It is, therefore, possible that in many cases the

reaction is preceded by the formation of a molecular compound from the adsorbed molecule and a surface atom. If this path of minimum structural change results in raising the reactivity of the adsorbed molecule, then it will be used in preference to other mechanisms. In this connection it is interesting to mention that a catalytic poison, that is, a molecule which, obviously, is adsorbed on just the site where the reaction should take place, reacts with the metal, as has been pointed out by Maxted [7], forming a donor bond donated by its lone electron pair so it makes the profitable reaction impossible. The fact that pyridine, NH_3, AsH_3, PH_3, R_2S, thiophenol are poisons (while NH^+_4, $C_2H_5NH^+$, AsO^{3-}_4 do not poison the surface) points out clearly that the lone pairs of the poison molecule play a role and that the metal atom in the surface has unoccupied s- or p-orbitals. When poisoning with pyridine, ammonia and the like, a semipolar bond is formed with a dipole moment the positive charge of which is directed outwards from the surface and gets a negative charge, which lowers the work function. We will show that also in nonpolar molecules when adsorbed on the surface by means of "physical" forces dipoles are induced, as can be seen from the change in contact potentials. The positive terminal of the dipole is directed away from the surface, that is, the metal plays the role of acceptor. So on the surface a Xe atom gets a dipole of $0.42 \cdot 10^{-18}$. When nitrogen is adsorbed atomically on iron, a donor-acceptor bond cannot be formed; when, on the contrary, nitrogen molecules are adsorbed, only such bonds can be formed. The question arises whether it is just the chemisorbed atom that takes part in the catalytic reaction. Oxygen adsorbed on platinum can be present in the form of Pt=O, but that part of the oxygen which has oxidizing properties, probably, will be present in the form

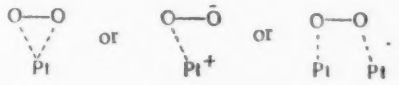

With other words, various types of bonds can be formed in chemisorption, but only one of them is of decisive importance for a given catalytic reaction.

The ability of CO and N_2 molecules to move freely over the metal surface can also be understood easily in the case of molecular adsorption [8].

The existence of adsorption assisted by three-center orbitals indicates that a continuous transition between physical adsorption and chemisorption is possible, since donor-acceptor bonds can be formed with energies ranging from several times ten to a few kcal.

The energy of a dative bond can be estimated from data on the energy required to dissociate in the gas phase the diatomic molecules Cu_2, Ag_2 and Au_2 into atoms. These energies are 46, 37.5 and 50 kcal, respectively [9]. Since the part of the bond energy originating from the s-electrons in all these molecules is equal to about 10 kcal (derived from data on K_2, Rb_2 and Cs_2) and there are two dative bonds in each molecule, because each Cu, Ag or Au atom donates two d-electrons from its lone pairs and accepts two foreign d-electrons in its unoccupied p-orbitals, the energy of one dative bond for Cu is 18, for Ag 13.7 and for Au 20 kcal. The dative bonds in metallic Cu, Ag and Au cause the sublimation energy to be high: 81 kcal for Cu, 65 for Ag and 85 for Au. The part of the sublimation energy originating from the s-electrons does not exceed 19 kcal (as follows from the data for K, Rb and Cs). This means that the delocalized dative bonds in these metals cause an energy gain of 62, 46 and 66 kcal, respectively. Each atom in the metal cannot accept more than three lone d-electron pairs from neighboring atoms, since it has no more than three unoccupied p-orbitals. This enables the energy of one delocalized dative bond to be estimated as 20.7 kcal for Cu, 15.2 for Ag and 22 for Au. These values are close to those evaluated for gaseous molecules. So the experiment confirms that atoms of transition metals may form rather strong donor-acceptor and dative bonds. The fact that zerovalent diamagnetic compounds of chromium do exist shows that such bonds may even be formed at the cost of forcedly uncoupling the electrons, which for chromium requires an energy of the order of 180 kcal [10]. All this gives evidence that atoms with d-electrons and unoccupied s- or p-orbitals may form strong donor-acceptor and dative bonds with entire molecules such as N_2, CO and others, which are acceptors of d-electrons because of their unoccupied antibonding orbitals and electron donors because of the their π-bonds.

It is known that gold and copper chemisorb CO, C_2H_4 and C_2H_2. It will be noticed that the atoms of these elements have filled d-shells. But just because they have many coupled d-electrons, they may form dative bonds and precisely because they have empty p-orbitals, they may give acceptor bonds. As regards aluminum,

here the presence of empty p-orbitals is essential for the formation of stable donor-acceptor bonds. In this case a dative bond is impossible.

It is convenient to compare the ability to form bonds of the type considered with the position of the highest occupied electron level in the molecule. In the case of H_2,N_2 and CO the highest occupied level of the molecule lies lower than that of the atom. This is clear from the ionization potentials: H 13.59;H_2 15.8; N 14.54;N_2 15.8; O 13.62;C 12.26;CO 14.01. For the molecules O_2, NO, C_2H_2 and C_2H_4 the picture is reversed: their upper occupied level lies higher than that of the atoms. The corresponding ionization potentials are: NO 9.5;O_2 12.2; C_2H_2 11.41; C_2H_4 10.51 ev. Under equal conditions the latter four molecules tend to form dative bonds. This is well known for the interaction between ethylene and Pt or Pd. Obviously, the same is valid also for acetylene. Dyatkina [11] has pointed out the possibility that carbon monoxide can be bonded to transition metals by the type of bond which ethylene has in Zeise's salt. We add that this supposition can be extended to the chemisorption of such molecules as N_2,CO,C_2H_4 and so on

Further we denote that when arranging the metals according to decreasing heats of chemisorption the sequence not always but often coincides with the arrangement according to increasing work function. This is connected with the depth of the donor levels in the metals.

HYDROGEN CHEMISORPTION

On singly promoted iron at 200° C hydrogen is chemisorbed with a heat of 20-15 kcal At 0°C the heat of adsorption is 16.5-8 kcal. Recently [12] it has been found that at -195°C there exists a third type of chemisorption with a heat of 5,4 kcal or less. This is a chemisorption and not a physical adsorption, since in the latter case the heat effect for hydrogen could be hardly higher than 1.5-2 kcal. At the same time the adsorption at the temperature of liquid air differs considerably from that at 0 or 200°C. Experiments by Kummer and Emmett have shown that singly promoted iron, in contrast with the doubly promoted substance, catalyzes the exchange with deuterium at -195°C. There are also reported observations of chemisorption with a heat of 3 kcal. On iron and zinc oxide an adsorption with an activation energy of 3 kcal has been observed. It might be thought that in these cases a Me-H bond is not formed. For the adsorption at high temperature (~180°C) the activation energy increases to 15 kcal A process implying the dissociation of H_2 into atoms could hardly proceed with an activation energy of a few kcal. It is natural to suppose that just the high temperature chemisorption with raised activation energy is the atomic one. Therefore, possibly, the rapid chemisorption at low temperature pertains to the type

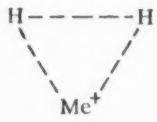

where H_2 is engaged in a three-center bond with a positive metal ion.

There is an indication that on industrial catalysts for ammonia synthesis hydrogen is adsorbed in the positive form, that is, the electron cloud of the hydrogen molecule is shifted partly to a positive metal ion. As is well known, hydrogen can adsorb reversibly on metal ions and irreversibly on oxygen ions. We further mention that the activation of H_2 by Cu^{++} or Ag^+ ions in solution has been established with certainty. In solution the activation energy is considerably higher (up to 24 kcal) which is explained by the fact that copper is present in the form of a complex ion. At room temperature dry hydrogen does not interact with metallic potassium. This points out that the formation of a Me-H bond requires a high activation energy. Molecular hydrogen has no influence on the spectral distribution of photosensitivity of a potassium surface. This too is an indirect indication that on the surface the hydrogen molecule does not dissociate into atoms.

We do not know exactly the energy of the three-center bond between a metal and hydrogen. From the heat of formation of H^+_3, which is equal to ~170 kcal, it follows that the heat of the reaction between H^+ and H_2 amounts to about 65. From data on the CH^+_5 ion one derives 36 kcal for the heat effect of the reaction $CH^+_3 + H_2$. It is possible that for surface ions this energy is smaller, but , in any case, such a three-center bond is completely actual. The fact that exchange with deuterium is possible at low temperatures in the neighborhood of -195°C indicates that in molecular adsorption the H-H bond is weakened and that its reactivity is

enhanced. On several transition metals as Ni,Fe,W or on Cr_2O_3 exchange with deuterium proceeds already at -183°C. If it is assumed that here hydrogen is chemisorbed in the form of molecules, the latter must be very active. Langmuir has supposed that the exchange proceeds via the recombination of hydrogen atoms adsorbed on different sites. But the transition from Me-H and Me-D bonds to a H-D bond will require an activation energy and occur only at higher temperatures. According to Rideal, the exchange takes place via a reaction between a chemisorbed hydrogen atom and a physically adsorbed D_2 molecule, which gives a chemisorbed deuterium atom and a physically adsorbed HD molecule. Both Langmuir and Rideal suppose that for the exchange one or two hydrogen atoms are required, which for certain have to be adsorbed in the form of atoms [13], but, anyhow, from neither of these mechanisms does it follow that the activation energy for exchange would be negligible small. In our opinion it is possible to do a further step and suppose that in molecular chemisorption the bonds are loosened because H_2 takes part in a two-electron three-center bond

and that, therefore, an exchange between two chemisorbed molecules can occur (possibly, with a change of sites):

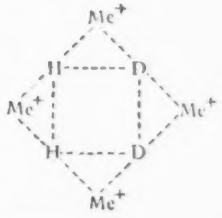

It has been supposed that a high heat of atomic hydrogen adsorption impedes the recombination to H_2 molecules. When examining the mechanism of ortho-parahydrogen conversion it turned out that hydrogen chemisorption is irreversible. Subsequently it has been established that at high hydrogen pressures the chemisorption proceeds reversibly.

At the chemisorption of hydrogen on other metals a complicated picture is observed. On tungsten films the heat of reversible H_2 chemisorption drops from 15 kcal at about 80% surface coverage to 3 kcal in a complete layer. This value too is somewhat high for physical adsorption. Hydrogen chemisorption on W is reversible at -183°C and obviously, has a molecular character. On copper a rapid initial H_2 adsorption with a heat of 9 kcal has been observed. On coal exchange with deuterium takes place at 90° K and does not require an activation energy [14]. At this temperature it is hardly possible that hydrogen or deuterium is adsorbed in the form of atoms, that is, under the formation of C-H and C-D bonds with the surface. It is strange that the dissociation of H_2 into atoms and the consecutive recombination reaction would not require an activation energy. H and D atoms in C-H and C-D bonds generally do not exchange even at considerably higher temperatures.

On cobalt [15] the hydrogen adsorption at 20°C has a heat of 25 kcal at zero coverage. The heat drops to 13 kcal at $\theta = 0.3$. At -183°C the initial stage of the adsorption is rapid and is completed in 20 min. After this rapid stage one observes a slow adsorption with a high activation energy and a high heat effect.

The initial heat of adsorption on nickel at 20° K is 1.2 kcal. At the temperature of liquid air hydrogen is chemisorbed, if the surface is not contaminated by oxygen or other gases. The activation energy for chemisorption on a free surface is close to zero and the heat is about 30 kcal. According to other data the heat of adsorption at small surface coverages varies between 15 and 20 kcal and attains 31 kcal on films deposited by evaporation. In general one has to keep in mind that the reproducibility of the data is insufficient and that the heat values of the various authors are scattered. At energies of about ten kcal the adsorption may be completely molecular. Many transition metals are active in hydrogenation at room temperature or below where molecular adsorption is very probable.

From the data on chemisorption on oxides we mention those on chromic oxide. Here two different kinds of adsorption are observed, namely, a rapid, weak and reversible adsorption at low temperatures and a strong one at high temperatures. At the temperature of liquid air hydrogen is chemisorbed on chromic oxide with a heat of 5 kcal, while exchange with deuterium will take place. In the reversible chemisorption desorption gives H_2. If a strong bond (obviously, with oxygen) is formed, desorption gives water. One may think that the rapid, weak and reversible chemisorption takes place on chromic ions under the formation of three-center bonds. At high temperature one observes a chemisorption with a heat of 72 kcal. In this case oxygen ions are the adsorption sites and hydrogen, obviously, is taken up in the form of atoms.

NITROGEN CHEMISORPTION

On iron films at low temperatures nitrogen is adsorbed instantaneously forming a complete monolayer. The heat of adsorption drops from 10 to 5 kcal as the coverage increases. One must expect that this is not an atomic adsorption. The question is only whether nitrogen occupies two (I) or one (II) sites on the surface

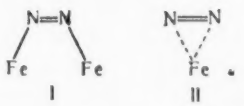

In the first case one π-bond of nitrogen has to be broken, which will be accompanied by an activation energy and may cause the reaction to be slow at low temperatures. In the second case the activation energy will be close to zero. The adsorption at high temperature differs considerably from that at low temperature and has a heat of 40 kcal. As dependent upon the degree of coverage, for the heat of chemisorption values ranging from 55 to 35 kcal have been found [16]. The activation energy of the adsorption at high temperature is 24 kcal. If the chemisorption was atomic, then taking the dissociation energy of N_2 to be 225 kcal we obtain 140 kcal for the energy of the bond between nitrogen and the metal atom. This value is only possible, when a chemical bond of the type Me ≡N is formed. It is interesting that in nitrides the mean energy of the metal-nitrogen bond is 44 kcal for VN, 48 for MoN, 50 for ZrN and 38 for CrN. The question arises whether such a strong bond with an energy of 140 kcal is needed for ammonia synthesis or nitrogen in the following form would be more effective for the reaction

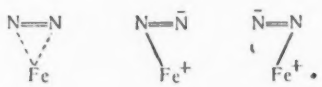

Also on nickel two types of nitrogen adsorption are observed [17]. The gas adsorbed at -185°C "comes off" easily at room temperature. We are inclined to believe that this is molecular adsorption. At 250-300°C nitrogen is adsorbed in a small amount When adsorbing on Ni at low temperatures a 0.21 ev change in contact potential is observed. This points out that electrons are shifted to the metal. In this case the donor bond shifts the electrons more to the metal than the dative bond shifts them to the empty nitrogen orbital [18]. On a platinum surface the electrons are displaced from the metal to the nitrogen molecule. This is connected with the fact that the 5 d-electrons of platinum give more easily dative bonds than do the 3 d-electrons of nickel.

There have been described experiments in which nitrogen was adsorbed on W at room temperature with a high rate and a small activation energy. If it is true that the heat of nitrogen adsorption can attain 115 kcal, then the corresponding energy of a bond between a nitrogen atom and a surface atom is 170 kcal. It would seem that the consecutive reaction with hydrogen will require a high activation energy. The question arises whether this is the nitrogen with which hydrogen reacts or whether nitrogen must go over to another chemisorbed state to make the reaction proceed more easily.

On chromic oxide there has also been observed a rapid nitrogen chemisorption at the temperature of liquid air with a heat of 9 kcal. In physical adsorption the heat would be much smaller. These data are in accordance with the supposition that it is molecular adsorption. There are indications that nitrogen is adsorbed the best by the metals which have the lowest work function, that is, by the metals which are the best electron donors.

CARBON MONOXIDE CHEMISORPTION

The CO molecule is isoelectronic with that of N_2. They have much in common in those cases where both are adsorbed in the form of molecules. But since in CO the strongly electronegative oxygen atom is present, the carbonylic type of adsorption via carbon has its special pecularities. On a cobalt catalyst carbon monoxide is chemisorbed already at the temperature of liquid air. The CO adsorbed comes off at -78°C [19]. There exist two types of chemisorption, since gas adsorbed at -78° C, cannot be removed from the surface. It may be supposed that the adsorption at low temperature is a molecular one with three-center bonds and the chemisorption at high temperature, probably, is accompanied by the formation of a carbonylic CO-metal bond. There is no evidence that at the low temperature adsorption CO occupies two sites, since, if two covalent bonds were formed with two adsorbent atoms, then it would be difficult to take off CO. The heat of chemisorption is about 15-20 kcal.

On copper films deposited by evaporation there is found a chemisorption with an initial heat of 9 kcal. The poisoning of an ammonia synthesis catalyst might be ascribed to the formation of a carbonyl bond. However, carbon dioxide, which cannot form a carbonyl bond, also poisons the surface and this indicates that CO is adsorbed in the same way as nitrogen.

The adsorption of carbon monoxide on oxides at room temperature is reversible. On $ZnO \cdot Cr_2O_3$ there is found a chemisorption with a dual character: partly reversible and partly irreversible. When both processes proceed simultaneously, the fraction reversibly adsorbed increases when the temperature is lowered. Therefore it is possible that the reversible chemisorption is a three-center one:

The rapid initial adsorption (90% within 5 min) has a heat of ~ 15 kcal.

On pure chromic oxide the reversible chemisorption proceeds rapidly at the temperature of liquid air and the heat is 12.7 kcal. In physical adsorption the heat would not exceed 5-6 kcal. In this case too the adsorption at low temperature is weak and rapid and that at high temperature strong and slow. CO adsorbed at low temperature on cuprous oxide comes off unchanged. On the contrary, when desorbing the gas which has been adsorbed at 100° it is liberated to a considerable extent as CO_2. On zinc oxide reversible adsorption also takes place at room temperature. We note that from a mixture of CO and O_2 mainly the former is adsorbed and carbonate is not formed. In general it is characteristic that carbon monoxide when adsorbed at low temperature can be liberated unchanged. Quite so it should be when the adsorption is a molecular three-center one.

OXYGEN CHEMISORPTION

When compared with nitrogen an oxygen molecule has two more electrons in an antibonding orbital. The upper filled level of oxygen lies 3.6 ev higher than that of nitrogen. An oxygen molecule can accept only into an antibonding orbital lying very high. For a long time the electron affinity of oxygen has been taken equal to 20±2 kcal. Recently, however, Mulliken[20] has come to the conclusion that it is much smaller, namely about 0.15 ev. The high heat of oxygen chemisorption on tungsten, nickel and iron (155,130 and 75 kcal) indicates that it is an atomic adsorption with Me=O bonds (energies 136, 124 and 96 kcal). These values are close to the bond energies (heats of formation) in $Me_{gas}+O_{gas}=MeO_{gas}$, which are: 104 kcal for CuO; 101 for MnO;97 for NiO and 110 for FeO. Besides this there is possible an adsorption with bonds of the following type, which have lower energies

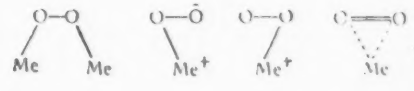

The first case corresponds with a peroxidic state of the oxygen molecule with a lowered O-O bond energy. The

second case, which is the most probable, corresponds to an adsorbed molecule having a dipole with its negative terminal directed away from the metal.

It is known that on W at ϑ=1 the dipole moment is equal to 0.76 D and on Pt it is 0.5 D. It should be noted that the magnetic criterion is unable to discriminate the character of oxygen adsorption, since in molecular chemisorption of the type

both oxygen atoms are diamagnetic. In oxidation reactions the oxygen adsorption must be rapid and weak. But, when the adsorption energy on a metal is of the order of 100 kcal, atomic oxygen on the surface becomes inactive, as is, for instance, oxygen in the PtO lattice, which does not catalyze oxydations. Therefore it is natural to suppose that from the oxygen only the molecularly adsorbed part is active and not that which is present on the surface in the form of Pt=O. In that case the reaction with a substance B can proceed according to the equation

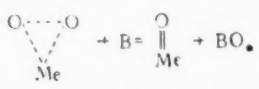

A low work function does not imply with certainty that atomic adsorption takes place. When discussing the reduction of oxygen on a mercury electrode Frumkin [21] has come to the conclusion that on the surface oxygen is present not in the atomic but in the molecular form. Just the same holds also for the initial stage of adsorption on coal. Here the bond between oxygen and the surface has a low stability. These facts may be explained, if the formation of three-center bonds is assumed.

Molecular oxygen adsorption easily explains that organic hydroperoxides are formed when oxidizing on silver or copper. If the adsorption was an atomic one, the formation of hydroperoxides would require a high activation energy. For the rapid chemisorption of O_2 on MnO the heat is equal to 24 kcal, while the chemisorption heat would be much higher if a stable Mn-O bond was formed. On coal at the temperature of liquid air Dewar observed adsorption with a heat of 3.75 kcal. At higher temperatures the heat is much greater attaining 70-90 kcal in the initial stage. But even at room temperature coal powder rapidly chemisorbs oxygen in 10-30 sec. with a small activation energy. Oxygen sorbed on coal at low temperatures does not accelerate ortho-parahydrogen conversion. Oxygen adsorbed at higher temperatures poisons that reaction. It is known that oxygen adsorption on silver at -78° is quite different from that at 0°. Recently it has been found [22] that two stages can be distinguished in oxygen adsorption on germanium, namely a rapid and a slow one. We suppose that the rapid stage will be molecular.

On chromic oxide oxygen is adsorbed at low temperatures with a heat of 27 kcal. All this fits the picture that there are two types of oxygen adsorption: an atomic with a high heat and a molecular one with three-center bonds and a lower heat.

When oxygen is adsorbed on iron at -120°C, the work function increases by 0.19 ev. Upon adsorbing on nickel the work function is raised by 0.1 and on platinum by 0.2 ev [23]. In polar metal-oxygen bonds the negative terminal of the dipole is directed away from the surface. In connection with these data we remind that the electron affinity of oxygen is about 0.15 ev. At higher temperatures adsorption results in a decreased work function. Frumkin and Burshtein explain this by the fact that oxygen penetrates to below the metal surface, which causes the negative part of the dipole layer to reverse its direction. In any case it is obvious that there exist two different ways for the interaction between oxygen and metals one of which is molecular chemisorption in which a polar bond is formed together with an excess negative charge on oxygen. In conclusion we note that atomic oxygen adsorption has been proposed more often than atomic nitrogen adsorption.

ETHYLENE CHEMISORPTION

On metals with atoms having enough d-electrons (for instance, Ni) ethylene can be adsorbed giving three-center bonds as occur in Zeise's salt. It is known that on metals on which the chemisorption of methane requires an activation energy the chemisorption of ethylene and acetylene requires none. This is connected with the fact that methane cannot give three-center bonds with the surface, while this is quite possible for ethylene and acetylene. On rhodium, nickel, iron and chromium the adsorption heat of ethylene is higher than that of hydrogen. Under such conditions that the adsorption of hydrogen can be accompanied by rupture of the H-H bond, the adsorption of ethylene can only take place by the formation of new bonds. Here it is also important that the upper filled molecular level of hydrogen lies 5.3 ev lower than that of ethylene, which causes the donor properties of ethylene with respect to the metal to be much more pronounced. In ethylene hydrogenation a considerable part of the surface is covered, which in many cases results in a reaction of zero order with respect to ethylene and of first order to hydrogen. On several oxides (Cu_2O, ZnO, $ZnO{\cdot}Cr_2O_3$) ethylene is adsorbed rapidly with an initial heat of 20,25.2 and 19.9 kcal. On copper and gold the initial heat of ethylene chemisorption is 18 and 21 kcal. Such values can be attained by the formation of three-center bonds.

There are data, which indicate that the heat of acetylene chemisorption on nickel is 67 kcal and that of ethylene 58 kcal. Obviously, in the case of high heats of adsorption metalorganic bonds can be formed. Further, it is known that, when ethylene is adsorbed on nickel at room temperature, ethane is found in the gas phase. Upon adsorbing C_2H_4 on Ni dissociation under formation of acetylene is observed too [24]. The disproportionation of ethylene into ethane and acetylene in the gas phase requires 9 kcal (ΔS—2 eu). The energy consumed can be compensated by the high heat of C_2H_2 adsorption. Obviously, C_2H_4 is adsorbed on one surface atom under formation of a three-center orbital. In the consecutive reaction on the surface hydrogen atoms are transferred from the ethylene molecule to neighboring nickel atoms. These atoms react with another ethylene molecule striking from the gas or located on another surface site.

SUMMARY

It is proposed that molecular adsorption may be brought about by the formation of three-center bonds. In this two donor-acceptor bonds are formed between the molecule to be adsorbed and an atom in the adsorbent surface. The molecule to be adsorbed, for instance, ethylene, acts as a donor because of its π-electron pair and the adsorbent atom because of its p-orbital. At the same time the adsorbent atom is a donor on account of its electron pair in a d_{xz}-orbital and the molecule an acceptor on account of its antibonding Ψ_1-Ψ_2 orbital; by this a dative bond is formed. In the case of a metal without d-electrons (for instance, Al) a dative bond is impossible, but the metal can give an acceptor bond because of its empty p-orbital.

Such a three-center chemisorption must proceed with a small activation energy, that is, be reversible, unactivated and rapid. Most often chemisorption at low temperature has these properties. The heat of such a chemisorption may vary between a few times ten or a few kcal.

Three-center chemisorption may be of considerable importance in catalytic reactions and also in exchange processes on the surface.

Only a considerable activation energy and a very high heat of adsorption is a reliable proof that the adsorbed substance occurs on the surface as atoms or in a state in which one adsorbent atom forms a stable chemical bond with only one adsorbate atom.

LITERATURE CITED

1. G. B. Bokii and G. A. Kukina, Kristallografiya 2, 400 (1957).
2. J. Chatt and L. A. Duncanson, J. Chem. Soc., 2939 (1953).
3. M. E. Dyatkina, Zhur. Neorg. Khim. 3, 2039 (1958).
4. G. Kistiakowsky, J. Chem. Phys. 23, 334 (1955).
5. O. Beek, Disc. Faraday Soc. 8, 118 (1950).
6. J. H. de Boer, Advances in Catalysis [Russian translation] (IL,Moscow,1959),p. 167.
7. E. Maxted, Advances in Catalysis [Russian translation](IL, Moscow, 1955),p. 100.
8. J. H. de Boer and S. Kruyer, Kon. Ned. Akad. Wet., Proc. Ser. B 55, 451 (1952) and more recent papers, e.g., Kon. Ned.Akad. Wet., Proc. Ser. B 58 ,61 (1955).

9. I. Drowart and R. Honing, Mem. Soc. Rov. Liege 18, 536 (1957).
10. E. M. Shustorovich and M. E. Dyatkina, Zhur. Neorg. Khim. 3, 2721 (1958).
11. M. E. Dyatkina, Zhur. Neorg. Khim. 4, 402, 553 (1959).
12. R. A. Beebe and E. Camplin, J. Phys. Chem. 63, 480 (1959).
13. B. Trapnell, Chemisorption [Russian translation] (IL, Moscow, 1958).
14. R. Burshtein, Zhur. Fiz. Khim. 14, 1195 (1940).
15. R. Rudham and F. S. Stone, Trans. Faraday Soc. 54, 420 (1958).
16. I. I. Scholten and Zwietering, Trans. Faraday Soc. 53, 1363 (1957).
17. R. Kokes and P. Emmett, J. Am. Chem. Soc. 80, 2082 (1958).
18 I. Mignolet, Disc. Faraday Soc. 8, 326 (1950).
19. M. V. Sartry, T. S. Viswana, and T. S. Nagarjunan, J. Phys. Chem. 63, 518 (1959).
20. R. F. Mulliken, Phys. Rev. 115, 1225 (1959).
21. A. N. Frumkin, Adsorption and Oxidation Processes. IV Bakh Lectures [in Russian] (Izd. AN SSSR, Moscow, 1957).
22. R. Kh. Burshtein, L. A. Larin and G. F. Voronina, Doklady Akad. Nauk SSSR 130, 801 (1960).*
23. R. Bourstein, J. Chim. Phys., 106 (1957).
24. G. I. Jenkins and E. K. Rideal, J. Chem. Soc., 2490,2496 (1955).

*Original Russian pagination. See C. B. translation.

DETERMINATION OF THE EFFECTIVE CHARGES OF ATOMS IN COMPLEXES FROM THE X-RAY ABSORPTION SPECTRA

R. L. Barinskii

Rare Earths Institute, Academy of Sciences of the USSR
Translated from Zhurnal Strukturnoi Khimii, Vol. 1, No. 2, pp 200-208,
July-August, 1960
Original article submitted December 12, 1959

A method is proposed for calculating the x-ray K-absorption spectra of atoms in molecules and complexes with an approximate central symmetry of the field around the absorbing atom. The method provides the possibility of determining the charge of the atom and of evaluating approximately its radius in the compound under study. The method is used for the calculation of the charges of transition metal atoms in complicated complexes with different types of chemical bonds. It is shown, in particular, that the type of bonds in aromatic complexes of metals is mainly covalent, with the exception of $(C_5H_5)_2Mn$, which has bonds of the ionic type.

The description of the chemical structure of a molecule or of a complex is not complete when the effective charge of each atom (or group of atoms)entering the composition of the compound under study is unknown. Just the effective charge characterizes, after all, the nature of the chemical bond forces, stabilities, degree of localization, etc. The value of the effective charge, together with the formal covalency of an atom makes it possible to draw conclusions, to some degree of plausibility, concerning the configuration of the valence electrons of the atom under consideration and the extent of its participation in the formation of bonds with the other atoms of the compound. A knowledge of the effective charge of atoms also provides the possibility of judging the distribution of the electron density to within a molecule.

The most used methods available at present for determining the charges of atoms, among which are the electronegativity method, the measurement of dipole moments, and nuclear quadrupole resonance spectra, have a number of serious defects. Being by their nature artificial, these methods are applicable for the evaluation of atomic charges only in the most simple systems, for instance, in molecular gaseous, or crystals consisting of two types of atoms. Even in this case the results thus obtained depend to a high degree upon the assumptions (in particular the character of hybridization) made in calculating the charge.

In view of this, it is interesting to try to study other physical methods of investigation apt, first, to measure directly the charge of an atom, and, second, to determine the region of the molecule where it is concentrated. Evidently, one of such methods may be the method proposed recently[1, 2] by the author together with Nadzhakov for measuring the charges of atoms from their x-ray absorption spectra. In order to judge the validity of this method for the solution of the problem mentioned above, it is appropriate to examine more accurately the physical ideas lying at the basis of it.

PHYSICAL BASIS OF THE METHOD FOR THE CALCULATION OF THE CHARGE

The value of an electric charge is measured, as is well known, from the force acting on a unit probe charge placed in the field of the charge under consideration. Consequently, in order to find the distribution of electrons within a molecule it would be necessary to place a probe charge in various points of the molecule and to measure the forces acting on this charge, or its potential energy. In the nuclear quadrupole resonance method, the problem of determining the charge of an atom in a molecule is reduced to the measurement of the gradient

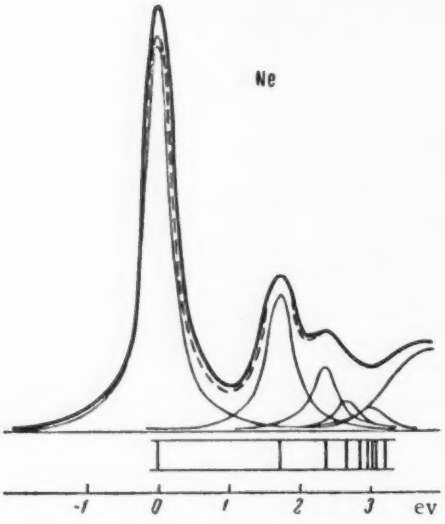

Figure 1. K-absorption spectrum of neon. Here and below - thick full line: experiment; thin curves: absorption lines and continuous spectrum; dotted line: sum of the absorption lines and of the continuous spectra. The accuracy of the calculation is confirmed by the coincidence of the total dotted line with the experimental line. The vertical lines show the locations of the absorption lines and of the limit of the absorption spectrum. On the vertical axis is reported a quantity proportional to the absorption coefficient; on the horizontal axis is reported the energy in electron volts. The experimental curve is taken from [8].

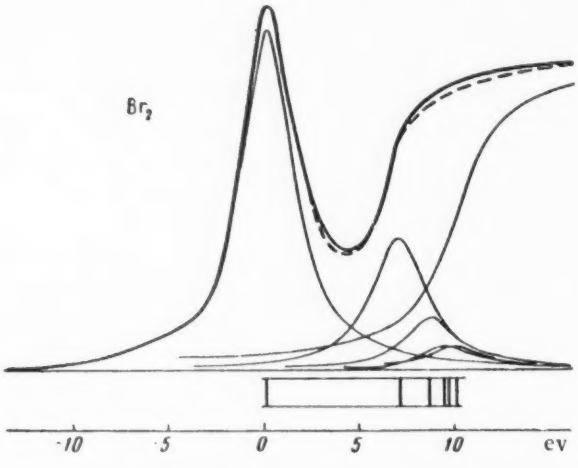

Fig. 2. K-absorption spectrum of bromine in the Br_2 molecule. The experimental curve is taken from [9]

of the charge field, and the nuclei of the atoms forming the molecules act as probe charges: their positions are fixed and determined by the molecular structure. In this lies one of the defects of the method, since the indications obtained by it concern the electron density only in one point [3]. In using x-ray spectra investigations the position appears to be much more favorable. As will be seen later, the probe charge in this case lies in that part of the molecule which forms the periphery of the atom under investigation, in its immediate neighborhood; therefore, the effective charge is measured just in this part of the molecule.

In order to make this remark more convincing, let us consider the K spectrum of absorption of a free atom. As a result of the absorption of x-rays, an electron is extracted from the K shell of the atom, and remains at the periphery of the atom (beyond the limits of its filled shells) and moves in the field of the unit charge remaining in the K shell of the atom after its K ionization. The other electrons of the atom, as we shall see later, have no important shielding effect on this charge. The system formed in this way is similar to a hydrogen atom, and its stationary energy levels form a Rydberg series converging to a limit which corresponds to the case of complete separation of the electron of the K shell (for the sake of conciseness we shall call it a K electron) from the atom. The transition of the excited electron to the successive energy levels of such a system gives in the spectrum absorption lines, and its transition beyond the limit of the series gives a continuous absorption.

A typical K-absorption spectrum of such an atom is reported in Fig. 1 (thick full line): it clearly shows the presence of at least three absorption lines, converging to the limit of the continuous spectrum. Calculation of such a spectrum can be performed with sufficient accuracy. The theory of the method and the calculation procedure are described in detail [1,2]. The calculation is based on the two formulas

$$\varepsilon_n = \varepsilon_\infty - \frac{\eta^2}{n^2} Ry, \qquad (1)$$

$$\frac{\tau_n}{\tau_\infty} = \frac{4\eta^2}{\pi\Gamma} \frac{n^2-1}{n^5}, \qquad (2)$$

describing the location of the successive absorption lines and of the limit of the series [Eq. (1)] and the ratio of the intensity of the first absorption line to the intensity of the limit of the continuous spectrum [Eq. (2)]. Equation (2) also gives the law governing the decrease of the intensities of the successive absorption lines. In these formulas ε_m is the energy of the tran-

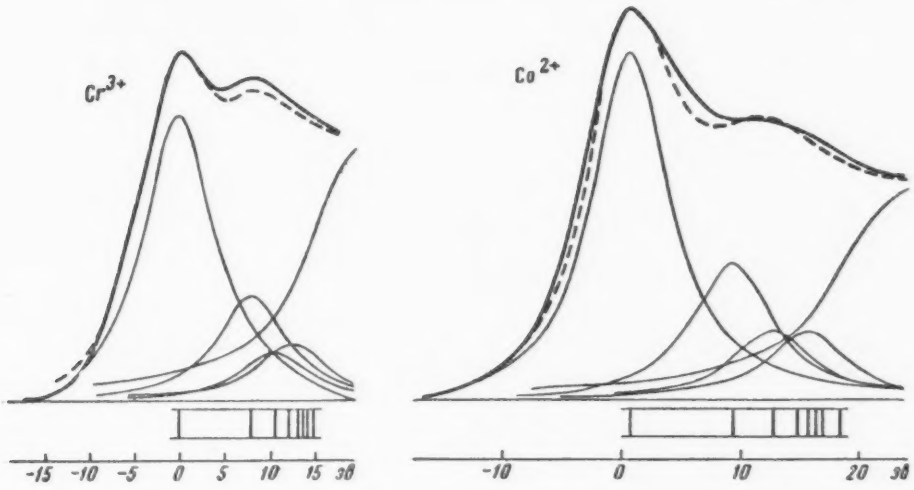

Fig. 3. K absorption spectra of cobalt and chromium as ions in water solution. The spectra of cobalt in Co^{2+} and $Co(C_5H_7O_2)_2$ are practically identical.

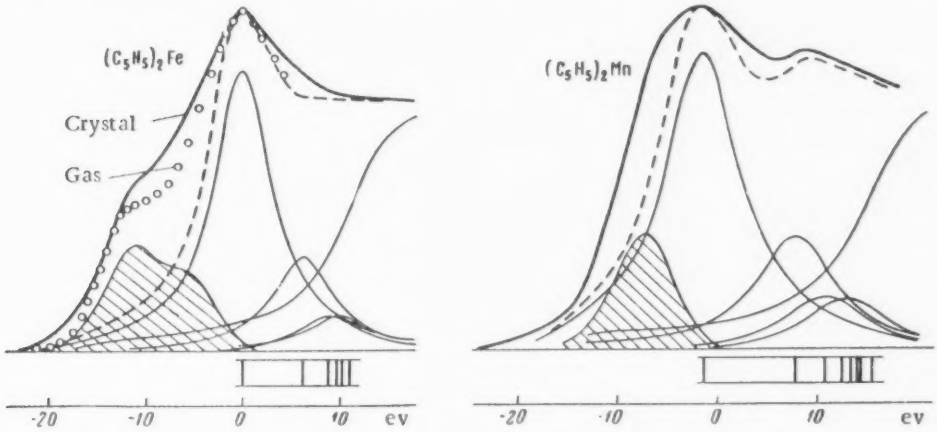

Fig. 4. K absorption spectra of iron and manganese in ferrocene and bis-cyclopentadienyl manganese.

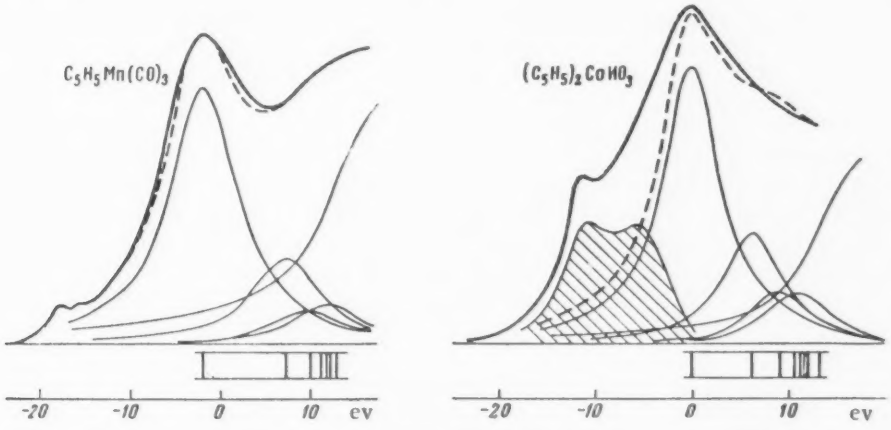

Fig. 5. K-absorption spectra of manganese and cobalt in cyclopentadienyl carbonyl and in the cobalticinium ion.

TABLE 1

Molecule	H_2S	CS_2	HCl	Cl_2	Br_2	IBr	$GeBr_4$		$ZnBr_2$	
Absorbing atom	S		Cl		Br		Ge	Br	Zn	Br
Charge $\eta' = \eta - 1$	−0,1	−0,03	−0,2	+0,01	+0,01	−0,1	+0,75	−0,15	+0,5	−0,21

TABLE 2

Molecule or ion	Absorbing atom	Charge, η'	Molecule or ion	Absorbing atom	Charge, η'
Co^{2+}		+1,8	$(NH_4)_2FeSO_4 \cdot 6H_2O$		+1,9
$Co(NO_3)_2 \cdot xH_2O$		+1,8	$K_3Fe(CN)_6$	Fe	+1,0
Co^{3+}	Co	+1,2	$Fe(CO)_5$		+0,4
$Co(C_5H_7O_2)_2$		+1,8	$Fe(C_9H_{11})_2$		+0,6
$(C_5H_5)_2CoNO_3$		+1,2	$(C_5H_5)_2Fe$		+0,4
$Co_2(C_5H_5)_5$		+0,4	Mn^{2+}		+1,8
Cr^{2+}		+1,9	$Mn(NO_3)_2 \cdot 4H_2O$		+1,8
$Cr(SO_4) \cdot 7H_2O$		+1,9	$K_3Mn(CN)_6$	Mn	+0,9
Cr^{3+}		+1,2	$(C_5H_5)_2Mn$		+1,5
$Cr(NO_3)_3 \cdot xH_2O$	Cr	+1,2	$C_5H_5Mn(CO)_3$		+0,6
K_2CrO_4		+0,1	$KOsO_3N$		+1,0
$Cr(CO)_6$		+0,5	K_2OsO_4		+0,8
$Cr(C_6H_6)_2$		+1,1	$K_2OsNOCl_5$	Os	+0,7
Zn^{2+}		+2	K_2OsCl_6		+0,8
$ZnSO_4$	Zn	+2	OsO_2		+0,8
$Zn(C_5H_7O_2)_2$		+1,8	$[Os(NH_3)_6]Br_3$		+1,0
$Zn(C_6H_5)_2$		+0,2	$K_4Os(CN)_6$		+1,5

sition of the K electron to the np level of the system (dipole selection rule, $\Delta l = 1$), e_∞ is the energy of the transition of the K electron to the limit of the continuous spectrum, τ_n is the intensity of the nth absorption line, τ_∞ is the intensity of the continuous spectrum, Γ is the width of the absorption lines and of the limit of the continuous spectrum,* R_y is Rydberg's constant (13.6 ev), η is the effective charge of the K ionized atom, in whose field moves the electron extracted from the K shell of the atom; $\underline{n}$ is the effective principal quantum number of the nth energy level.

Equations (1) and (2) contain only the two unknowns η and $\underline{n}$. All the other parameters may be taken from the experimental K-absorption curve. This gives the possibility on one side of calculating completely the entire absorption spectrum, on the other side it permits finding the values of the effective charge and the quantum number in which we are interested. The results of such a calculation(expansion of the spectrum into a Rydberg series and continuous absorption) are also reported in Fig. 1. It is important that the effective charge of the system (η) was found in this case to be exactly equal to 1; this proves the absence of a shielding effect of the other electrons on the charge remaining in the K shell of the atom after the separation from it of the K electron.

*The shapes of the absorption lines in x-ray spectra are usually close to those of dispersion lines. The shape of the limit of the continuous spectrum is described by a curve of the type of an arctangentoid.

Knowing the effective charge of an atom, η, and the effective quantum number n, it is possible to evaluate approximately the effective radius of the sphere within which the measured charge of the atom is distributed. For this purpose one can use the equation*

$$r = 1{,}8na_0/\eta \qquad (3)$$

(where a_0 is the Bohr radius) which determines the distance between the nucleus and the maximum of probability for an np electron, i.e., in our case the excited K electron passing to the np state. Actually, in order to determine the effective charge of an atom, just this electron plays the role of a probe charge, and its distance from the center of distribution of the effective charge η will be minimum when it lies on the first energy level with a quantum number n.

Let us consider now the more complicated case of the K absorption spectrum of an atom whose valency electrons participate in chemical bonds so that their distribution differs from the distribution of the external electrons of the free atoms (see, e.g., Fig. 2). Here, as in the case of a free atom, the formation of stationary energy levels of a system consisting of a positive charge in the K shell of the absorbing atom, of a K electron extracted from it, and of the other electrons of the molecule may be expected. Naturally, in this case only the valency electrons will play an essential role because the distribution of the charge in the field shells enjoys a spherical symmetry and the total charge of the shell is compensated by the charge of the nucleus of the atom.

The redistribution of the valency electrons of atoms, due to the formation of a chemical bond, may produce the appearance, in the region of the atom under investigation, of an additional charge, either positive or negative. Its value will be higher, the higher the ionic character of the bonds with other atoms. Consequently, the electron extracted from the K shell of an atom may be in the field of a new charge, in addition to the unit positive charge in the K shell of the absorbing atom, i.e., the quantity η in Eqs. (1) and (2) may become greater or smaller than 1. It is also evident that the effective charge at the periphery of the atom due only to the redistribution of the valency electrons is equal to $\eta' = \eta - 1$. If $\eta' \leq -1$ ($\eta \leq 0$), the Tydberg series does not arise.

We shall not report here the arguments proving that the system under consideration is similar to a hydrogen atom also in this more complex case. Such a proof has been given with sufficient detail [4,5]. We shall consider only one question which has an essential significance for us: whether the K electron at the periphery of an atom introduces a distortion in the distribution of the charge of the electrons of the chemical bond. Such a phenomenon would actually take place if the hole in the K shell of an atom and the external electron produced a strong polarization of the shells of the neighboring atoms. This would lead to replacing the term $\eta^2 Ry/n^2$ of Eq. (1) with $\eta^2 Ry/\epsilon^2 n^2$ (where ϵ is the dielectric constant for high frequencies), i.e., to a sharp contraction of the range of the series of absorption lines. However, as was noted [6], such a phenomenon is not observed experimentally. In fact, the short lifetime of the K states of atoms ($\sim 10^{-15}$ - 10^{-16} sec.) and, consequently, the high inertia of the system with respect to x-ray absorption indicate that the quantity ϵ must be close to 1. In [6] are given experimental proofs of the correctness of this conclusion. The authors of [7] also came to similar conclusions on the basis of a regorous theoretical examination of the problem in the frame of the many-electron theory. It was shown that $\epsilon = 1$ if $r \ll \sqrt{\hbar/2m^*\omega}$, where r is the distance between the hole in the K shell and the extracted electron, m^* is the reduced mass of the electron, ω is the frequency of the vibrations of the crystal lattice, and $\hbar$ is Planck's constant. A numerical evaluation shows that $\epsilon = 1$ if $r \ll 10$A, as happens exactly in the case of K spectra (see [6]). Therefore, unlike the case of optical absorption spectra, in the case of x-ray spectra the system under study does not succeed in reacting to the process of K absorption, and the distribution of the electrons of the chemical bond is disturbed only to a negligible degree.

The process of excitation of x-ray K-absorption spectra examined by us is by no means the only possible process, and x-ray spectra are far from always consisting of one series of absorption lines. Very often also other fine structure details may be observed in them, as happens in the case of the absorption of x-rays by metals or by substances having lattices of a pure coordination type. The "exciton" x-ray absorption mechanism we described must be observed as a rule in the absorption K spectra of gaseous molecules and of crystalline complexes with a roughly central symmetry of the field [1,2]. In this case such a spectrum is susceptible of calculation and

* The numerical coefficient in Eq. (3) depends upon the choice of the wave functions describing the behavior of an np electron. The value 1.8 was chosen in order to ensure the best agreement with the experimental data.

becomes a "tool" for the determination of the effective charge of an atom, and, in the absence of other data, also for an approximate calculation of the effective radius of the atom in the compound under study, according to Eq. (3).

Let us consider now some practical examples of the method of calculation described above.

DETERMINATION OF THE CHARGES OF ATOMS IN MOLECULES AND IN COMPLEXES

1. Comparison with other data. At present a small number of well studied K-absorption spectra of gaseous molecules are available, which can be treated in the way shown above in order to determine the charge of the atoms composing these molecules [2].

Among these well studied spectra, we mention the K spectra of Cl in HCl and Cl_2, Br in Br_2, Ge and Br in $GeBr_4$, Zn and Br in $ZnBr_2$. In addition, the charges of H and Cl in HCl are known from dipole moment measurements (+0.17 and -0.17, respectively), and chlorine and bromine in Cl_2 and Br_2 must evidently have a zero charge. The charge of bromine in IBr was measured by the nuclear quadrupole resonance method (-0.1). For the other two molecules, if the calculation method is correct, one must expect a compensation of the charges measured separately for each of the atoms.

Table 1 reports the effective charges ($\eta' = \eta - 1$) of the atoms in the molecules listed above, and Fig. 2 gives the K-absorption spectrum of Br in Br_2 and its expansion in a Rydberg series and a continuum. The relative error in the determination of the total charge η nowhere exceeds 10%, and is less than 5% in the case of Cl_2 and Br_2. The correctness of the values of the charges for the first three molecules (and also for IBr), and the compensation of the charges in the two remaining molecules show that the effective charges obtained by the method in question for atoms in chemical compounds have a completely real physical significance.

2. Absence of many-charge ions. In crystal field theory the idea is often used that the atoms of chemical compounds carry large positive or negative charges. There are several experimental data which actually contradict this idea and are in satisfactory agreement with Pauling's electronegativity concept, which denies the existence of multiply charged ions. Since the problem of the possibility of existence of multiply charged ions is particularly serious in the case of complexes of metals in high velency states, it is interesting to analyze the data concerning the value of the effective charge of metals in complexes, according to the x-ray method.

Table 2 gives the results of the calculations from the K-absorption spectra of atoms of various complexes, and also of some ions in water solution (see also Table 1). Figure 3 shows the K absorption spectra of Co^{2+} and Cr^{3+} and their expansion in a Tydberg series and a continuum. The spectra are taken from [10, 11, 12].

An examination of Tables 1 and 2 shows that even for the highest possible valency of the central atom in a complex (e.g., Cr^{VI} and Os^{VIII}) its charge never exceeds two. Moreover, an increase of the valency actually produces a tendency to a decrease of the effective charge: this is particularly evident in the series ($CrSO_4 \cdot 7H_2O$, $Cr(NO_3)_3 \cdot xH_2O$, and K_2CrO_4. Chromium, manganese, cobalt, and zinc have similar effective charges also as ions in water solution. The results obtained are in agreement with the idea that, with an increase of the valency of an atom, the covalent character of its chemical bonds increases sharply (in the case of ions in water solution the bonds are formed with the solvate sphere). As regards osmium compounds, a similar conclusion was already arrived to in [12], where it was found that in passing to compounds with osmium in a lower valency state, the increase of the charge and of the ionic character of the bonds is accompanied by a repulsion of the 6sp electrons of osmium towards the ligands.

It is interesting to note that the effective charges of Zn in $Zn(C_6H_5)_2$ and $Zn(C_5H_7O_2)_2$ are sharply different: this is understandable if one takes into account the difference between the electronegativities of oxygen and carbon. It is then evident that in the first case zinc is linked to the C_6H_5 group through a carbon atom, whereas in the second there is a Zn—O bond. Thus, knowing from the data of x-ray spectra the effective charge of an atom, it is possible, in some cases, to solve the problem of deciding through which particular atom is a certain radical linked to the central metal atom.

3. Calculation of the effective radii of atoms and of the lengths of bonds. The results of the analysis of the K-absorption x-ray spectra (determination of the quantities η and n) may be used for calculating, according to Eq. (3), the effective radii of the spheres within which the measured charges of atoms are distributed. Such a calculation, conducted for chlorine and bromine atoms in the Cl_2 and Br_2 molecules, gives radii of 1.1 and 1.2 A,

i.e., values very close to the covalent radii of chlorine and bromine. For Ge, Zn, and Br in the molecules $GeBr_4$ and $ZnBr_2$, the corresponding values (1.0, 1.2, and 1.4) A) have intermediate values between the covalent and ionic radii of these atoms. The bond lengths calculated on their basis are in satisfactory agreement with experimental data. The values of the effective radii of ions and atoms of transitions metals in the compounds shown in Table 2 also occupy intermediate positions between the covalent and ionic (for a doubly charged ion) radii of these elements: for the Cr^{2+}, Mn^{2+}, Co^{2+}, and Zn^{2+} ions (0.75 - 0.85 A) they are close to the radii of doubly charged ions. Thus, with respect to their effective charges and radii, the ions in question behave, in a water solution, as free ions. Only when one passes to ions with a +3 charge does one find that the influence of hydration starts to be important.

Naturally, the evaluation of bond lengths according to the approximate Eq. (3) has a sense only when data obtained by more precise methods are not available. The importance of Eq. (3) consists of the fact that it gives the effective radii of atoms, whose direct determination is often impossible.

4. Aromatic complexes of transition elements. In recent times, many data concerning investigation of the K-absorption spectra of bis-cyclopentadienyl compounds of transitions metals have appeared in the literature. Due to the great interest of this class of compounds (see, e.g., [13, 14]) it has seemed appropriate to apply the method described above to the calculation of the charges of transition element atoms in some aromatic complexes. The results of the calculations are reported in Table 2. Figures 4 and 5 show the K-absorption spectra of bis-cyclopentadienyl compounds of iron and manganese, of cyclopentadienyl carbonyl manganese and of the cobalticinium ion in $(C_5H_5)_2CoNO_3$ and their expansions in Rydberg series and continuous absorptions.

The determination of the effective charge of atoms of transition metals permitted, first of all, to obtain a direct proof of the ionic character of bonds in $(C_5H_5)_2$ Mn(charge of Mn + 1.5) and of the covalent character of bonds in ferrocene (charge of Fe + 0.4). The reason for this "anomalous" behavior of bis-cyclopentadienyl manganese has been examined theoretically [15]. In addition to this, the K spectrum of $(C_5H_5)_2$ Mn shows the "drift" towards the long-wave slide of the spectrum (shaded area) characteristic for the compounds of this class, and which is apparently due to the transition of the K electron to molecular levels of the system. This drift is seen even more clearly in the K spectrum of ferrocene. The large width of the absorption lines in the K spectrum of $(C_5H_5)_2$ Mn is also due to the presence here of the manganese ion.

The type of bond between C_5H_5 and Mn in cyclopentadienyl carbonyl manganese has not been so far sufficiently clear. A calculation of the K-absorption spectra shows that the transition from $(C_5H_5)_2$ Mn to $C_5H_5Mn(CO)_3$ is accompanied by a sharp decrease of the charge of manganese (+0.6). This proves the presence in $C_5H_5Mn(CO)_3$ of a bond to C_5H_5 of the ferrocene type, since the charge of Mn due to its bond with the CO group does not exceed + 0.5. The conclusions descending from this fact are examined in a review by Dyatkina [14].

The determination of the effective charge of cobalt in the cobalticinium cation $(C_5H_5)_2Co^+$ leads to a value + 0.6, i.e., 0.2 higher than in cobalticene. This means that the displacement of the electron takes place mainly from the rings, and consequently in the cobalticinium ion they produce a positive charge of + 0.4.

The data obtained above for the effective charges of transition metal atoms in aromatic complexes may be compared with the theoretical calculations of these charges by the molecular orbital method [16] (+1.5 in $(C_6H_6)_2Cr$, + 0.7 in $(C_5H_5)_2$ Fe, and - 0.1 in $(C_5H_5)_2Co^+$). A comparison with the data of Table 2 shows the general agreement of the results obtained by different methods.

In conclusion, we note that the effective charge of the central atom in complex ions and compounds is practically independent of the aggregation state of the substance [2]. From this point of view, a crystalline complex (ion or molecule) may be considered to a good approximation as a gaseous molecule, since the influence of the crystal lattice is important only on the additional widening of the lines of the K-absorption spectra (see the K spectrum of ferrocene in Fig. 4).

SUMMARY

1. The physical basis of a method for calculating the x-ray K-absorption spectra of atoms in molecules and in complex molecules or ions with an approximate central symmetry of the field around the absorbing atom has been examined.

2. It has been shown that it is possible to determine the effective charge of an atom and to calculate

approximately the radius of the sphere within which this charge is distributed.

3. The method is used for the calculation of the effective charge of the atoms of transition metals in complicated complex ions and molecules. The possibility of determining from the x-ray spectra the effective radii of atoms and the lengths of bonds has been shown.

4. The results of calculation definitely indicate that, in the compounds investigated, there are no multiply charged ions (even for atoms in their highest valency state). The tendency to a sharp decrease of the charge with an increase of the valency of an atom has been noted.

5. The determination of the effective charge of atoms of transition elements in aromatic complexes has shown that the type of bond in this class of compounds is mainly covalent, with the exception of $(C_5H_5)_2$ Mn which has ionic bonds. It has been shown that the bond of Mn to C_5H_5 in C_5H_5 $Mn(CO)_3$ is of the ferrocene type.

LITERATURE CITED

1. E. G. Nadzhakov and R. L. Barinskii, Doklady Akad. Nauk SSSR 129, 6, 1279 (1959).*
2. R. L. Barinskii and E. G. Nadzhakov, Izvest. Akad. Nauk SSSR, Ser. Fiz. 24, 4, 407 (1960).
3. Uspekhi Khim 27, 6,731 (1958).
4. É. E. Vainshtein, R. L. Barinskii, and K. I. Narbutt, Zhur. Éksp., Teoret. Fiz. 23, 5, 593 (1952).
5. R. L. Barinskii, E. E. Vainshtein, and K. I. Narbutt, Izvest. Akad. Nauk SSSR, Ser. Fiz. 21, 10, 1351 (1957).
6. R. L. Barinskii and É. E. Vainshtein, Izvest. Akad. Nauk SSSR, Set. Fiz. 23, 5, 585 (1959).
7. H. Haken and W. Schottky, Z. Phys. Chem. 16, 3, 218 (1958).
8. J. Backovsky, Ceskosl. casop. fys. 4, 118 (1954).
9. C. H. Shaw, Phys. Rev. 57, 877 (1940).
10. K. Böke, Z. Phys. Chem. 11, 5, 326 (1957); 10, 1, 45 (1957).
11. E. O. Fischer, G. Joos, and E. Vogg, Z. Phys. Chem. 18, 1, 80 (1958).
12. E. G. Nadzhakov and R. L. Barinskii, Izvest. Akad. Nauk SSSR, Ser. Fiz. 24, 4, 415 (1960).
13. A. N. Nesmeyanov and É. G. Perevalova, Uspekhi Khimi. 27, 1, 1 (1958).
14. M. E. Dyatkina, Uspekhi Khim 27, 1, 55 (1958).
15. E. M. Shustorovich and M. E. Dyatkina, Zhur. Neorg. Khim. 3, 12, 2721 (1958).
16. E. M. Shustorovich and M. E. Dyatkina, Doklady Akad. Nauk SSSR 128, 6, 1234 (1959).*

*Original Russian pagination. See C. B. translation.

RADII OF THE IONS IN MOLECULES OF GASEOUS INORGANIC COMPOUNDS OF ELEMENTS OF THE PRINCIPAL GROUPS OF THE PERIODIC SYSTEM

K. S. Krasnov

Ivanovsk Chemicotechnological Institute

Translated from Zhurnal Strukturnoi Khimii, Vol. 1, No. 2, pp. 209-216,
July-August, 1960
Original article submitted November 15, 1958

The radii of the ions in molecules of compounds of the elements of the principal groups of the periodic system are calculated on the basis of a method analogous to Pauling's method for crystals. The interatomic distances, calculated for 96 molecular gaseous inorganic compounds on the basis of the additivity of the ionic radii, are in good agreement with the experimental values. Discrepancies from additivity are on the whole reconcilable with concepts of the polarization of the ions.

Hitherto, in calculating the length of the bonds in gaseous inorganic compounds, ionic radii have been used exclusively for diatomic molecules [1, 2]. A more complete system of empirical ionic radii, especially for diatomic molecules, was recently proposed by Gattow [3].

Radii of the Ions of Polyatomic Molecules

In contrast to the empirical approach by Gattow, limited only to diatomic molecules, a semiempirical calculation of the radii of the ions in molecules of polyatomic inorganic gaseous compounds of elements of the principal groups of the periodic system in a state of corresponding higher valence is possible. The partial covalence of the bond in molecules, which according to Büchler and Klemperer has been established even for alkaline earth halides [4], does not interfere with this calculation. The radii of highly-charged ions must in this case be regarded rather as calculation constants, since the existence of such ions in molecules is doubtful. These radii reflect with adequate approximation the effective size of the atoms in a molecule with polar bonds. As in the case of crystalline radii, "the sign of S^{6+} must be regarded as an indication of the valence but not the charge" [5].

Our method of calculation is analogous to that developed by Pauling [6] for crystals.

In quantum chemistry, the following relationship is used for radii of isoelectronic ions having an 8- or 18-electron shell:

$$R = \frac{C_n}{Z - \sigma}, \qquad (1)$$

where C_n is a constant for ions having the same value of the principal quantum number of the outer electrons, Z is the charge of the nucleus, and σ is a screening constant, which can be determined according to Pauling [7], $Z - \sigma = Z_{eff}$ is the effective charge of the nucleus.

It follows from (1) that the radii of isoelectronic ions are inversely proportional to the effective charges on the nuclei. From this, knowing the interatomic distance in a molecule built up of such ions (for example, KCl), we determine the radii of the ions (K^+ and Cl^-).

The radius of a chlorine (or potassium) ion serves as standard in calculating C_n in Eq. (1), and therefore for the calculation according to (1) of the radii of all the ions of the given isoelectronic series. As standard for five series of isoelectric ions, we have selected the distances in the molecules LiH [8], NaF [9]*, KCl, RbBr and CsI [2]. It is also possible to make a start with the distances in the molecules MgF_2, $CaCl_2$, $SrBr_2$ and BaI_2, measured by Akishin and co-workers [11]. The agreement between the calculated values of the ionic radii of the halogens in one case or the other (Table 1, columns 2 and 3), confirms that the formulation of the problem as a whole is correct. For comparison, Table 1 also includes the values of the radii of halogen ions according to Honig and Gattow.

TABLE 1. Radii of Halogen Ions, A

Ion	Semiempirical from the halides		According to Gattow [3]	According to Honig [2]*
	Alkaline	Alkaline Earth		
F^-	1,11	1,11	0,94	1,13
Cl^-	1,53	1,52	1,53	1,53
Br^-	1,67	1,68	1,69	1,67
I^-	1,86	1,88	1,92	1,89

* The Cl^- radius was calculated by Honig, like the radius in the second column. The others were calculated from the interatomic distances by difference.

Table 2 shows the radii of the ions of the elements of the principal groups of the periodic system, calculated according to [1].** In contrast to the radii given by Gattow, particularly applicable for diatomic molecules, these radii are applicable for all molecules where the valence of the positive element is equal to the group number.

Charge of the Ion, Coordination and Radius

In the crystal chemistry of ionic compounds, in accordance with Pauling [6], a distinction is made between univalent (R_1) ionic radii and crystalline (R_Z) ionic radii. The first are obtained by direct calculation according to formula (1); the transition from the first to the second, taking into account the difference of the charge of the ion from unity, is accomplished according to the formula.

$$R_z = R_1 z^{-\frac{2}{n-1}}, \qquad (2)$$

TABLE 2. Univalent Radii (A) of Ions in Molecules of Gaseous Compounds of Elements of the Principal Groups of the Periodic System

Period \ Group	Cations						Anions	
	I*	II	III	IV	V	VI	VII	VI
II	Li^+ 0,36	Be^{2+} 0,26	B^{3+} 0,20	C^{4+} 0,17	N^{5+} 0,15		F^- 1,11	O^{2-} 1,43
III	Na^+ 0,77	Mg^{2+} 0,66	Al^{3+} 0,59	Si^{4+} 0,52	P^{5+} 0,47	S^{6+} 0,43	Cl^- 1,52	S^{2-} 1,85
IV	K^+ 1,12	Ca^{2+} 0,99	Ga^{3+} 0,69	Ge^{4+} 0,64	As^{5+} 0,60	Se^{6+} 0,56	Br^- 1,68	Se^{2-} 1,99
V	Rb^+ 1,28	Sr^{2+} 1,14	In^{3+} 0,90	Sn^{4+} 0,82	Sb^{5+} 0,76	Te^{6+} 0,71	I^- 1,88	Te^{2-} 2,18
VI	Cs^+ 1,47	Ba^{2+} 1,32	Tl^{3+} 0,99	Pb^{4+} 0,92	Bi^{5+} 0,85			

* Honig [2] gives the values: Li^+ 0.48, Na^+ 0.83, K^+ 1.13, Rb^+ 1.25, Cs^+ 1.37 A. They calculated only the potassium radius semiempirically. The others were calculated so as best to satisfy the condition of additivity.

* This value is taken as a mean of those quoted in the papers [2] and [10].

** Based on the radii of the halogen ions from column 3, Table 1. The value of C_n for the crystalline state is different from that for the gaseous state.

where z is the valence of the ion, and n is the Born repulsion coefficient*. The interatomic distance r in crystals is determined as the sum of the univalent radii only for salts of univalent ions. In all other crystals, r is defined as the sum of the crystalline radii:

$$r = R_z^+ + R_z^-. \tag{3}$$

The radii of the ions in the molecules given in Table 2 correspond to univalent ions according to Pauling. For molecules of the type $Me^{z_1+}X_{z_1}^-$ (compound with a single-charge anion), however, in contrast to the crystalline state, the effective radius of a multicharge cation ought not to differ from the univalent radius calculated according to (1), a point which is confirmed by experiment (see Table 3).

TABLE 3. Interatomic Distances (A) in Molecules of Gaseous Compounds

Molecule	Bond	Interatomic distance	Sum of ionic radii		Sum of Gattow radii	
		experiment	$R_+ + R_-$	Δ_{ion}	$R' + R''$	Δ_{cov}
LiF		1,51±0,08[20]	1,47	—0,04	1,63	+0,12
LiCl		(2,02) *	1,88	(—0,14)	2,03	+0,01
LiBr		2,17	2,03	—0,14	2,17	0,00
LiI		2,39	2,24	—0,15	2,39	0,00
NaF		(1,88)	1,88	(0)	1,96	+0,08
NaCl		2,36	2,29	—0,07	2,36	0,00
NaBr		2,50	2,45	—0,05	2,50	0,00
NaI		2,71	2,65	—0,06	2,12	+0,01
KF		(2,14)	2,23	(+0,09)	2,26	+0,12
KCl		2,67	2,64	—0,03		
KBr		2,82	2,80	—0,02		
KI		3,05	3,00	—0,05	3,02	—0,03
RbF		(2,25)	2,38	(+0,13)	2,39	+0,14
RbCl		2,79	2,79	0,00		
RbBr		2,94	2,94	0,00		
RbI		3,17	3,15	—0,02		
CsF		2,35	2,58	+0,23	2,54	+0,19
CsCl		2,91	2,92	+0,01		
CsBr		3,07	3,14	+0,07		
CsI		3,32	3,35	+0,03		
BaF_2	Be — F	1,40±0,03 **	1,37	—0,03		
$BeCl_2$	Be — Cl	1,75±0,02	1,78	+0,03		
$BeBr_2$	Be — Br	1,91±0,02	1,94	+0,03		
BeI_2	Be — I	2,18±0,02	2,14	—0,04		
MgF_2	Mg — F	1,77±0,02	1,77	0,00		
$MgCl_2$	Mg — Cl	2,18±0,02	2,18	0,00		
$MgBr_2$	Mg — Br	2,34±0,03	2,34	0,00		
MgI_2	Mg — I	(2,54)	2,54	(0,00)		
CaF_2	Ca — F	2,10±0,03	2,10	0,00		
$CaCl_2$	Ca — Cl	2,51±0,03	2,51	0,00		
$CaBr_2$	Ca — Br	2,67±0,03	2,67	0,00		
CaI_2	Ca — I	2,88±0,03	2,87	—0,01		
SrF_2	Sr — F	2,20±0,03	2,25	+0,05		
$SrCl_2$	Sr — Cl	2,67±0,03	2,66	—0,01		
$SrBr_2$	Sr — Br	2,82±0,03	2,82	0,00		
SrI_2	Sr — I	3,03±0,03	3,02	—0,01		
BaF_2	Ba — F	2,32±0,03	2,43	+0,11		
$BaCl_2$	Ba — Cl	2,82±0,03	2,84	+0,02		
$BaBr_2$	Ba — Br	2,99±0,03	3,00	+0,01		
BaI_2	Ba — I	3,20±0,03	3,20	0,00		

* For the alkali halides, all the measured distances are according to [2], the calculated distances (in brackets) according to [9].

** Alkaline earth halides, according to [11].

* Formula (2) is approximate. Theory gives the accurate formula

$$r = [R_1^+ + R_1^-]\,(\sqrt{z_+ z_-})^{-\frac{2}{n-1}}. \tag{3'}$$

(2) and (3') give the best agreement with experiment.

TABLE 3 (Continued)

Molecule	Bond	Interatomic distance		Sum of ionic radii		Sum of covalent radii (Pauling)	
		experiment		$R_+ + R_-$	Δ_{ion}	$R'_0 + R''_0$	Δ_{cov}
BF_3	B — F	1,29	C*	1,31	+0,02	1,44	+0,15
BCl_3	B — Cl	1,74	C	1,72	—0,02	1,79	+0,06
BBr_3	B — Br	1,87	C	1,88	+0,01	1,94	+0,07
BI_3	B — I	(2,08) [6]	C	2,08	(0,00)	2,13	(+0,05)
Al_2Cl_6	Al — Cl**	2,06 ± 0,04	L	2,11	+0,05		
Al_2Br_6	Al — Br	2,21 ± 0,04	L	2,27	+0,06		
Al_2I_6	Al — I	2,53 ± 0,04	L	2,47	—0,06		
GaF_3	Ga — F	1,88	A	1,80	—0,08		
Ga_2Cl_6	Ga — Cl	2,09	A	2,21	+0,12		
Ga_2Br_6	Ga — Br	2,25	A	2,37	+0,12		
CF_4	C — F	1,36 ± 0,02		1,28	—0,08	1,41	+0,05
CCl_4	C — Cl	1,76 ± 0,01		1,69	—0,07	1,76	0,00
CBr_4	C — Br	1,94 ± 0,03		1,85	—0,09	1,91	0,03
CI_4	C — I	2,12 ± 0,02		2,05	—0,07	2,10	0,02
SiF_4	Si — F	1,54	C	1,63	+0,09	1,81	+0,27
$SiClF_3$	Si — F	1,55 ± 0,02	L	1,63	+0,08	1,81	+0,26
$SiCl_4$	Si — Cl	2,02 ± 0,02	L	2,04	+0,02	2,16	+0,14
$SiClF_3$	Si — Cl	2,03 ± 0,02	L	2,04	+0,01	2,16	+0,13
$SiBrCl_3$	Si — Cl	2,05	C	2,04	—0,01	2,16	+0,11
$SiCl_6$	Si — Cl	2,00 ± 0,05	L	2,04	+0,04	2,16	+0,16
$SiCCl_6$	Si — Cl	2,02	[23]	2,04	+0,02	2,16	+0,14
$SiBr_4$	Si — Br	2,15 ± 0,03	L	2,20	+0,05	2,31	+0,16
$SiBrCl_3$	Si — Br	2,19	L	2,20	+0,01	2,31	+0,12
SiF_2Br_2	Si — Br	2,16 ± 0,03	L	2,20	+0,04	2,31	+0,15
SiI_4	Si — I	2,43	C	2,40	—0,03	2,50	+0,07
GeF_4	Ge — F	1,67 ± 0,03	[19]	1,75	+0,08	1,86	+0,19
$GeCl_4$	Ge — Cl	2,08 ± 0,02	L	2,16	+0,08	2,22	+0,13
$GeBr_4$	Ge — Br	2,32	L	2,32	0,00	2,36	+0,04
GeI_4	Ge — I	2,50	L	2,52	+0,02	2,55	+0,05
$SnCl_4$	Sn — Cl	2,30 ± 0,02	L	2,34	+0,04	2,39	+0,09
$SnBr_4$	Sn — Br	2,44	L	2,50	+0,06	2,54	+0,10
SnI_4	Sn — I	2,64	L	2,70	+0,06	2,73	+0,09
$PbCl_4$	Pb — Cl	2,43	L	2,44	+0,01	2,45	+0,02
PF_5	P — F	1,57 ± 0,02	L	1,58	+0,01	1,74	+0,17
PF_3Cl_2	P — F	1,59	L	1,58	—0,01	1,74	+0,15
POF_3	P — F	1,52	L	1,58	+0,06	1,74	+0,22
$POFCl_2$	P — F	1,50 ± 0,03	L	1,58	+0,08	1,74	+0,24
POF_2Cl	P — F	1,51	L	1,58	+0,07	1,74	+0,23
PSF_3	P — F	1,51 ± 0,2	L	1,58	+0,07	1,74	+0,23
$PSFBr_2$	P — F	1,50 ± 0,10	L	1,58	+0,08	1,74	+0,24
PCl_5	P — Cl	2,10	L	1,99	—0,11	2,09	—0,01
PF_3Cl_2	P — Cl	2,05	L	1,99	—0,06	2,09	+0,04
$POCl_3$	P — Cl	2,02	L	1,99	—0,03	2,09	+0,07
$POFCl_2$	P — Cl	1,99 ± 0,04	L	1,99	0,00	2,09	+0,10
POF_2Cl	P — Cl	2,01	L	1,99	—0,02	2,09	+0,08
$PSCl_3$	P — Cl	2,01 ± 0,02	L	1,99	—0,02	2,09	+0,08
$POBr_3$	P — Br	2,06 ± 0,03	L	2,15	+0,09	2,24	+0,18
$PSFBr_2$	P — Br	2,18 ± 0,03	L	2,15	—0,03	2,24	+0,06
PSF_2Br	P — Br	2,14 ± 0,04	L	2,15	+0,01	2,24	+0,10
POF_3	P = O	1,56	L	1,51	—0,05	1,55	—0,01
$POCl_3$	P = O	1,58	L	1,51	—0,07	1,55	—0,03
$POFCl_2$	P = O	1,54 ± 0,03	L	1,51	—0,03	1,55	—0,01
POF_2Cl	P = O	1,55	L	1,51	—0,04	1,55	0,00
$POBr_3$	P = O	1,41	L	1,51	+0,10	1,55	+0,14
PSF_3	P = S	1,85 ± 0,02	L	1,84	—0,01	1,94	+0,09
$PSCl_3$	P = S	1,94 ± 0,06	L	1,84	—0,10	1,94	0,00
$PSBr_3$	P = S	1,81 ± 0,06	L	1,84	+0,03	1,94	+0,13
$PSFBr_2$	P = S	1,87 ± 0,05	L	1,84	—0,03	1,94	+0,07
PSF_2Br	P = S	1,87 ± 0,05	L	1,84	—0,03	1,94	+0,07
SbF_5	Sb — F	2,00 [24]	L	1,87	—0,13	2,05	+0,05
SF_6		1,58 ± 0,03	C	1,54	—0,04	1,68	+0,10

*C — according to Cottrell [8], L — according to Landolt [21], A — according to Akishin [22].

** The shortest Me — X distances in dimers are given.

TABLE 3 (Continued)

Molecule	Bond	Interatomic distance		Sum of ionic radii		Sum of covalent radii (Pauling)	
		experiment		$R_+ + R_-$	Δ_{ion}	$R'_0 + R''_0$	Δ_{cov}
SO_2F_2	S — F	1,56 ± 0,03	L	1,54	—0,02	1,68	+0,12
SO_2Cl_2	S — Cl	1,99 ± 0,02	L	1,95	—0,04	2,03	+0,04
SO_2F_2	S = O	1,43 ± 0,02	L	1,47	+0,04	1,70	+0,27
SO_2Cl_2	S = O	1,43 ± 0,02	L	1,47	+0,04	1,70	+0,27
SeF_6	Se — F	1,67	L	1,67	0,00	1,81	+0,14
TeF_6	Te — F	1,82	L	1,82	0,00	2,01	+0,19
BeO	Be = O	1,34	C	1,34	0,00		
MgO	Mg = O	1,753	C	1,73	—0,02		
SrO	Sr = O	1,924	C	2,04	+0,12		
BaO	Ba = O	1,942	C	2,18	+0,22		
SO_3	S = O	1,43	C	1,47	+0,04	1,49	+0,06
CS_2	C = S	1,5545 [25]	C	1,60	+0,05	1,60	+0,05
Li_2O	Li — O	1,82 ± 0,02 [26]		1,79	—0,03	1,89	+0,07

The explanation of this paradox is as follows. To allow for the influence of the charge of the ions on the distance between them, the sum of the univalent radii is multiplied in accordance with (3') by

$$(\sqrt{z_1 z_2})^{-\frac{2}{n-1}} = (\sqrt{z_1})^{-\frac{2}{n-1}} = z_1^{-\frac{1}{n-1}}, \quad \text{since} \quad z_2 = 1.$$

To allow for the transition from the coordination number 1 in the molecule $Me^+ X^-_{z_1}$ to the coordination number z_1 in the molecule $Me^{z_1+} X^-_{z_1}$, it is necessary to multiply by the quantity $(1/z_1)^{\frac{1}{n-1}}$. But $z_1^{-\frac{1}{n-1}} \cdot z_1^{\frac{1}{n-1}} = 1$.

It is for just this reason that the distance in the molecule between the multicharge cation and the single-charge anion is equal to the sum of the univalent radii given in Table 2. Consequently, the radii of corresponding halogens in columns 2 and 3 of Table 1 are equal to each other.

For molecules of the type $Me^{Z+} X^{Z-}$ ($z > 2$), for example BeO, however, the interatomic distance is calculated according to formula (3'). It ought also to be used for calculating the distance in bonds of the type P = O in $POCl_3$, P = S in PSF_3 and so forth. Here z_1 and z_2 are equal to the "multiplicity" of the bond, i.e., in our example, $z_1 = z_2 = 2$*.

The calculation thus postulates that the charge of the central ion in the molecule is as if distributed equally among all the bonds. An approach analogous to this is employed in crystal chemistry where the concept of the ionic bond or electrostatic valence [14] is introduced.

The calculated radii of the ions in molecules may be used for calculating the lengths of the bonds both in purely ionic compounds and in compounds with bonds of intermediate type. The correctness of the approach to intermediate types of bond with the position of the ionic bond between polarized ions is well demonstrated by many examples both in the field of crystal chemistry [14, 15] and in the examination of the form and structure of polar molecules [16].

Comparison of the Calculated Interatomic Distances with the Measured Values. Discussion of the Results

In Table 3, the experimental values of the interatomic distances in molecules are compared with the values calculated as the sum of the radii of the ions. The values in brackets in the column "Experiment" are

* The quantity $(\sqrt{z_1 z_2})^{-\frac{2}{n-1}}$ in formula (3') is dependent on n. For crystals, the mean value of n = 9. For molecules of the alkali halides $n \approx 7$ [13]. We shall also assume for the other molecules a mean value n = 7. The transition factor from the sum of univalent radii to the interatomic distance in formula (3') for a bond of the type Be = 0, P = O ($z_1 = z_2 = 2$) will then be 1.26, for $z_1 = z_2 = 3$, it will be correspondingly 1.44 and so forth.

the interatomic distances, calculated by other reliable methods, for those cases where there are no experimental data. Since the length of the bonds in molecules of compounds of the elements of groups IV-VI is often determined by adding together the covalent radii according to Pauling [17], the corresponding sums of the covalent radii are also given in Table 3 for comparison of the methods. For the alkali halides, the sums of the radii according to Gattow are also given (except for the molecules which he took as starting molecules).

Analysis of the deviations Δ of the calculated values from the experimental values leads to the following:

For the 96 molecules (114 bonds), for which there are experimental data, the deviation Δ_{ion} of the sum of the ionic radii from the interatomic distance has a mean value of 2-3%. Since the model of the molecule with rigid ions appears to be over-idealized for most of the molecules considered, the agreement with experiment is quite satisfactory and much better than when covalent radii are used (except in the case of carbon compounds). The advantages of the ionic radii would be still more obvious if the true covalent radii of fluorine (0.72A) and carbon (0.74 A) were used, as was done by Schomaker and Stevenson [18], instead of the values according to Pauling (0.64 and 0.66 A) used here.

The deviations Δ_{ion} from additivity of the ionic radii may split up into three groups:

1. Δ_{ion} of the order of ± 0.01 - 0.05 A. Such deviations are in the majority (75 out of 114). It is evident that here the polarizing effects are compensated by the repulsion of the anions, and the additive principle is fully satisfactory.

2. Considerable positive deviations ("compression of the ionic radii"). In the case of CsF and BaF_2, it is explained by the polarizing effect of the fluorine on the bulky cations (for details, see [10]). To indicate deviations of this type, the supposed values of Δ_{ion} are given for RbF and KF, for which the values of the interatomic distances have been extrapolated. In the case of the alkali halides, the position values of Δ_{ion} are greater than in the case of the other groups, since in this case, unilateral deformation is not compensated by the repulsion of the anions. The good agreement of the sum of the radii according to Gattow with the interatomic distance for these molecules may be explained by the fact that the radii according to Gattow have mostly been calculated on the basis of the additivity principle. The positive values of Δ_{ion} for compounds of ions having an 18-electron shell and an ionic charge ≤ 4 may be explained by the so-called additional polarization effect, amounting to a deformation of both ions [16]. For germanium compounds, it is found in GeF_4 and $GeCl_4$ but disappears in $GeBr_4$ and GeI_4, since the charge +4 is high enough for the Br^- and I^- ions to be able to produce an appreciable deformation of the Ge^{4+} ion. It will later be necessary to explain the fairly high "compression of ionic radii" in SiF_4 ($\Delta_{ion} = +0.08$ A), but it is still much less than the very high Δ_{cov} in fluorides, for the explanation of which the conceptions of either a double-bond nature or spd hybridization have not been found very apt (see [19]).

3. Considerable negative deviations. In lithium compounds they are due to the fact that the Li^+ radius, determined from LiH, is extremely small in consequence of the high polarizability of the H^- ion. By determining R_{Li^+} by difference from LiI, LiBr and LiCl, and also from LiF according to [10] ($R_{LiF} = 1.584$ A), but not according to [20], where R_F is inaccurately determined, we get $R_{Li^+} = 0.50$ A, which gives values of Δ_{ion} equal to 0.01, 0.01, 0.00 and 0.02 A. As objective characteristics of the Pauling method, we have in fact given the worst alternative.* The deviations in the case of SbF_5, PCl_5 and GaF_3 cannot yet be explained, unless we take into account the possibility of errors in the experimental results.

The proposed system of ionic radii, like any which may be used for calculations on the basis of the additivity concept, is imperfect. It may be improved by a slight variation in the calculated radii by averaging the deviations, as was done by Honig and coworkers for the alkali metals and halides [2], or by taking polarization into account, as has been done for the alkali halides [10]. Its advantage is that it permits the calculation of the radii also of those ions, for the compounds of which there are no experimental data. For compounds of group III elements, it is the only possible way of estimating the length of the bonds, since the covalent radii of these elements in the gaseous state are unknown.

* R_{Li^+} for crystals is calculated by Pauling by difference from the interatomic distance in Li_2O, and not by the method of isoelectronic series. If he had used it, Pauling would have obtained from the data of a crystal of LiH a value much worse than that he accepted (0.46 instead of 0.60 A). He does not, however, discuss this discrepancy anywhere.

The proposed system in its present form does not include compounds of the transition metals (elements with d shells being filled, Sc - Zn) and their analogues, as well as notoriously covalent compounds (compounds of carbon and others).

LITERATURE CITED

1. E. S. Rittner, J. Chem. Phys. 19, 1030 (1951).
2. A. Honig, M. Mandel, M. Stitch, and C. Townes, Phys. Rev. 96, 629 (1954).
3. G. Gattow, Z. anorgan. und allgem. Chemie 294, 205 (1958).
4. A. Büchler and W. Klemperer, J. Chem. Phys. 29, 121 (1958).
5. G. B. Bokii, Introduction to Crystal Chemistry [in Russian] (Izd. MGU, 1954).
6. L. Pauling, The Nature of the Chemical Bond [Russian translation] (Goskhimizdat, Moscow, 1947).
7. L. Pauling, Proc. Roy. Soc. A 114, 181 (1927).
8. T. Cottrell, The Strength of Chemical Bonds [Russian translation] (IL, Moscow, 1956).
9. K. S. Krasnov, Zhur. Neorg. Khim. 2, 1725 (1957).
10. K. S. Krasnov, Zhur. Neorg. Khim. 4, 530 (1959).
11. P. A. Akishin and V. P. Spiridonov, Kristallografiya 2, 475 (1957).
12. L. Pauling, J. Am. Chem. Soc. 49, 765 (1927).
13. J. Varshni, Trans. Faraday Soc. 53, 132 (1957).
14. R. Evans, An Introduction to Crystal Chemistry [Russian translation] (Goskhimizdat, Moscow-Leningrad, 1948).
15. L. H. Ahrens, Nature, 4298, 463 (1952); Geochim. Cosmochim. Acta. 3, 1 (1953).
16. B. V. Nekrasov, A Course of General Chemistry [in Russian] (Goskhimizdat, Moscow, 1954).
17. L. Pauling, J. Amer. Chem. Soc. 69, 542 (1947).
18. V. Schomaker and D. Stevenson, J. Amer. Chem. Soc. 63, 37 (1941).
19. A. Gaunt, H. Mackle, and L. Sutton, Trans. Faraday Soc. 47, 943 (1951).
20. R. Braunstein and J. Trischka, Phys. Rev. 89, 1092 (1955).
21. Landolt-Börnstein, Zahlenwerte (Berlin, 1951), Vol. 6,No. 1, p. 2.
22. P. A. Akishin, V. A. Naumov, and V. M. Tatevskii, Nauchn. Dokl. Vyssh. Shkoly. Khimiya i Khim. Tekhnol. 1, 205 (1958).
23. J. Morino and E. Hirota, J. Chem. Phys. 28, 185 (1958).
24. J. Gaunt and J. Ainscough, Spectrochim. Acta 10, 57 (1958).
25. A. Guenther, T. Wigging, and D. Rank, J. Chem. Phys. 28, 682 (1958).
26. P. A. Akishin and N. G. Rambidi, Doklady Akad. Nauk SSSR 118, 973 (1958).*

* Original Russian pagination. See C. B. translation.

THE DROP MODEL OF ATOMIC STRUCTURE*

A. F. Kapustinskii

D. I. Mendeleev Chemicotechnical Institute, Moscow, USSR
Translated from Zhurnal Strukturnoi Khimii, Vol. 1, No. 2, pp. 217-232,
July-August, 1960
Original article submitted November 27, 1959

A model of the electron structure of atoms is examined in which the electrons approximate drops which circulate around the position of the charged nucleus. With its help, it is possible to explain the sphericity of ions of any type, many dimensions of the electron shells, diagonal relationships in the periodic table, and the constancy and contraction of radii. The theory leads to a simple equation for the effective radii of ions which does not contain empirical parameters, and which agrees with the experimental facts.

Introduction

An understanding of the aggregate state and calculations from macroscopic characteristics are used in a study of the atomic world. The nucleus has been described by models based on solid bodies, on liquid drops and on gases, each of which reveals a particular side of its structure, but the theory does not reduce to any one of these models. According to the type of interaction the nucleus resembles one or other of the macroscopic states. In essence there is a union of different ideas which is interpreted by wave mechanics. This is an amalgamation of ideas on particles and waves. Along with the quantized nature of elementary particles, this is one of the characteristics of the atomic world.

The electron structure of the atom has been modeled on solid globular electrons (Lewis, Kassel, Bohr) or on on a statistical picture of a degenerate electron gas (Fermi, Dirac, Gombash). Like the nuclear structure of the nucleus, it has traits similar to the liquid state and it is with this aspect that the present article is concerned. It is shown that it is possible to place the drop model of the atom on a quantitative basis which permits one to understand many of the features of its structure.

Physical Constants of the Electron and of the Hydrogen Atoms

The basic constants of the electron (1) are its charge and mass.

$$e = 4{,}802 \cdot 10^{-10} CGSE, \tag{1}$$

$$m = 9{,}106 \cdot 10^{-28} \text{ g}. \tag{2}$$

The size of the isolated electron (about 10^{-13} cm) is known with less precision; it depends to a considerable extent on the conditions of the investigation.

It is known [2] that a hydrogen atom consists of a proton and an electron which rotates around the former in the closest quantum orbital, called K, which has principal quantum number, n = 1.

According to the Bohr theory the radius of this orbital is

$$r = \frac{n^2 h^2}{4\pi^2 m e^2}, \tag{3}$$

* This paper is printed as matter for discussion.

where Plank's constant is

$$h = 6.6242 \cdot 10^{-27} \text{ erg} \cdot \text{sec}. \quad (4)$$

By substitution in (3) the latter becomes

$$r_H = 0.53 \cdot 10^{-8} \text{ cm} = 0.53 \text{ A}. \quad (5)$$

Such orbits are seen in the model (Fig. 1) where the point electron rotates in a circle about the point proton. Wave mechanics retained the valuable features of the Bohr theory and eliminated its errors. The categorical prohibition of the presence of the electron outside the quantized orbits is replaced by the possibility of allowing it to be at any point with the electron density slowly diffusing from the nucleus and with a maximum of the distribution function D in the quantized orbitals. Thus, for the electron cloud with n = 1 (Fig. 1), this maximum corresponds exactly with the Bohr orbit [5]. Since r corresponds to the distance between the proton and electron, and the size of the proton in all calculations has no greater accuracy than 0.001 A, the latter can be considered to be zero (the approximate calculations in [3] showed that the proton is about a thousand times smaller than the electron). Then R can be considered to be equal to the effective radius r_0 of the electron cloud in the primitive atom – in the isolated hydrogen atom (Fig. 2): $r_H = r_{proton} + r_0 = 0.53$ A. But because $r_{proton} = 0$,

$$r_0 = 0.53 \text{ Å}. \quad (6)$$

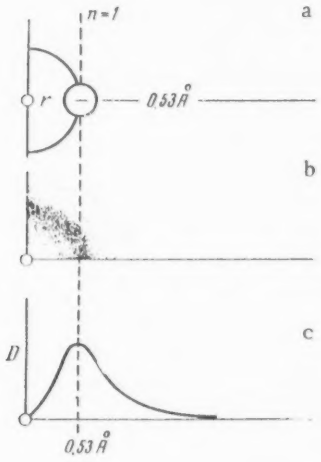

Fig. 1.

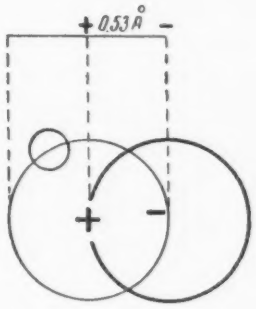

Fig. 2.

Fig. 1. The hydrogen atom: a) Bohr model; b) wave model; c) distribution function.

Fig. 2. Effective radius of an electron in the isolated hydrogen atom.

Structure of the K Shell and the Effective Radius of the Electron

From the Pauli exclusion principle it follows that the K level cannot hold more than two electrons and this should give for sperical electrons, a solid of revolution resembling a torus (Fig. 3). The torus has a greater surface than the sphere of equal volume. Therefore it is natural to assume that the two electrons will fuse together like drops to give a single globule with the same volume but with a reduced surface. In terms of the wave theory, this means that one electron cloud arises around the nucleus instead of two, and this single cloud has a single maximum of the distribution function for the K level. Let us test this assumption. Calling the radius of the electron r_0 and using a simple geometrical construction (Fig. 4), the aim is to find the radius R_0 of the sphere whose volume is equal to that of the two electron volumes:

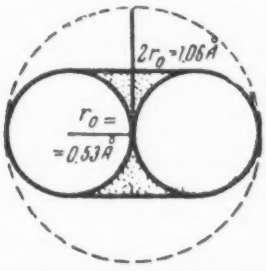

Fig. 3. Rotation of two electrons around the nucleus.

$$\frac{4}{3}\pi r_0^3 + \frac{4}{3}\pi r_0^3 = \frac{4}{3}\pi R_0^3, \quad 2r_0^3 = R_0^3, \quad (6A)$$

$$R_0 = r_0 \sqrt[3]{2} = 1.26 \cdot r_0 = 1.26 \cdot 0.53 = 0.67 \approx 0.7 \text{ Å}. \quad (6B)$$

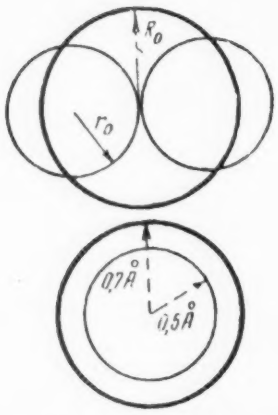

Fig. 4. Fusion of two spheres of radius r_0 into a sphere of radius R_0 and of equal volume.

TABLE 1. Comparison of Different Estimates of the Size of the K Shell.

Author	Radius of K shell (ionic radius of lithium), A	
Goldschmidt	0.78	
Zachariasen	0.68	Approximate
Bokil and Belov	0.68	value
Theoretical calculations	0.67	0.7 ±0.1
Pauling	0.60	

This should be the radius of the first two-electron shell K with principal quantum number 1. But this is also the shell of the basic lithium atom after removal of its valence electron and, consequently, we should compare the estimated radius of the K shell with the ionic radius of lithium. By various methods Goldschmidt, Pauling, Zachariasen, Bokii, and Belov [4] obtained the data shown in Table 4 which confirms our calculation.

Although the isolated electron has dimensions some five orders less than those of the atom, its dimensions in the isolated hydrogen atom are equal to those of the nonexcited (n = 1) hydrogen atom, i.e., 0.53 A. At first sight this seems to contradict our calculated value of the radius of the K shell (0.7 A). But this value of 0.53 A applies to the isolated hydrogen atom. When such an atom is transferred to the strong field of the crystal, its electron is subjected to the influence not only of the central force of the proton but also to the influence of all those around it. Applying the same considerations by which the effective radius of the electron in the isolated hydrogen atom is equal to the radius of the Bohr orbital, the effective radius of the electron in a crystal should be equal to the radius of the hydrogen atom, but in this case the crystallographic radius. In fact [5] the radius of hydrogen in the crystalline state is $\bar{r}_H = 0.78$ A, which incidentally is exactly equal to the value of the radius of an electron in the crystalline lattice, which (earlier) was found by us by three different methods to be $R_0 = 0.78 \pm 0.02$ A.

Both these constants are close to the value of 0.7 A found by our theoretical calculation. Since the latter is lower, although not by much, than the two values quoted above we choose as the definitive value the one which corresponds to the lower limit of the permitted errors (±0.02 A). Thus, the effective radius of the electron is equal to the effective radius of the K shell, and is

$$R_0 = r_K = 0{,}76 \text{ Å}. \tag{7}$$

Structure of the L Shell and Outer Shells

Thus, the K shell really arises as the result of simple deformation of an electron cloud. When the K level is completed the next electron enters a new shell, L. The electron-sphere is not localized in a particular space (Fig. 5) but rotates, and its appearance leads to a larger atom with a new shell. In this shell there is sufficient room for the motion of all the eight electrons permitted by the Pauli principle. The size of the L shell with n = 2 remains constant, no matter how many of the "permitted" number of electrons it contains, because the size of the previous shell did not depend on the number of electrons it contained, i.e., two in the lithium ion or one in the hydrogen atom.

Here, however, the electrons do not complete a layer of elementary spheres, but forms a single solid spherical structure as the result of deformation of the electron clouds without change in the average electron density. The electrons form an equivalent shell, the volume of which is equal to the volume of the spherical electrons, just as in the previous layer. Calling the radii of the electrons of the shells K and L, corresponding to R_0, r_K and r_L we have

$$^4/_3\,\pi r_L^3 - {}^4/_3\,\pi r_K^3 = {}^4/_3\,\pi R_0^3, \tag{7A}$$

or

$$r_L^3 - r_K^3 = R_0^3. \tag{7B}$$

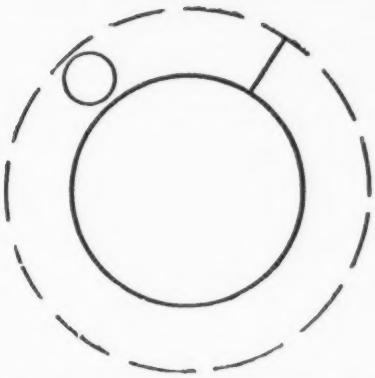

Fig. 5. Appearance of an electron sphere in a new quantum level.

Or, according to (7), we obtain

$$r_L = r_K \sqrt[3]{2}, \tag{8}$$

or

$$r_L = R_0 \sqrt[3]{2} = 0{,}76 \cdot 1{,}26, \tag{8A}$$

and thus r_L = 0.96 A.

The radius of shell L with the principal quantum number n = 2 can be evaluated geometrically since it is the radius of the sodium ion. The estimated value of this parameter agrees well with the value obtained by us.

The general principles developed for the electronic architecture of the atom are simple. While retaining their quantum structure, the electrons are stratified according to their spherical charge clouds. The number of the stratum is given by the principal quantum number n, while its geometry is given by the law governing the stratification.

The size of the shell with quantum number n is linked to R_0 by the geometrical progression $r_n = R_0 \sqrt[3]{n}$. We chose this simple expression to express the quantization of the particle dimensions since it agrees well with the (experimental) facts. Figuratively speaking, "electron drops" spread over the surface of the previous sphere and retain their own volume but decrease their thickness, according to the size of the sphere they flow over, i.e., according to the distance from the nucleus. The variation in the thickness S of the shells is very small so long as one is limited to the structure of the atoms of the first six shells. They can be calculated purely by geometry and fluctuate within the limits of 0.26 to 0.20 A, and this may be rounded off to 0.2 A for approximate calculations.

If one ignores the repulsive forces between electrons in the electron gas (despite the fact that they neutralize the effects of the atomic nucleus) then the formula written above is precisely correct to the end of the Mendeleev table. However, this repulsion for atoms with many electrons has so large an effect that the difference from experimental results reaches 0.1 A. Therefore, a more exact form of expression is a "mixed" progression which more nearly approaches an arithmetic progression the more nearly one approaches the end of the periodic table [7]. It is important to emphasize only that whatever formula is written for our model, it must lead to the recurrent thickness of the orbitals, which is close to the thickness of a single electron.

TABLE 2. Comparison of Values for the Radius of the L Shell

Author	Radius of the L Shell (ionic radius of sodium), A
Goldschmidt (empirical method)	0.98
Our theoretical calculation	0.96
Pauling (semiempirical method).	0.95

The divisibility of atomic radii by this number was discovered earlier [8]. For anions, and also cations, from the beginning of the periodic system one should use the purely geometrical value 0.26 A for the thickness of the shells when carrying out more accurate calculations. Generally speaking, bearing in mind the whole wide range of the periodic system, it is sufficient to use the mean value, S = 0.23 A, so long as its variation does not exceed the limits of the vibration of ionic radii (±0.02 to 0.03 A) found in crystal chemistry.

Divisibility of Ionic Radii by the Bohr Hydrogen Electron Orbital

Thus, each quantum shell has an approximately constant electronic cloud thickness, δ.

Only at the very beginning of the system, in discussing the size of the hydrogen atom in the isolated state and in the crystal lattice, both with principal quantum number n = 1, does one find two spheres which differ by the parameter δ. It will be recalled that the discussion was about the K shell in the isolated hydrogen atom of radius 0.53 A and of the same K shell in a hydrogen in the strong field which has the radius 0.76 A;

$$R_0 = r_0 + \delta = 0{,}53 + 0{,}23 = 0{,}76 \text{ Å}. \tag{9}$$

Summarizing what has been said above, we arrived at an equation giving a mathematical expression for the radii of single-charged ions of any type

$$r = r_0 + n\delta, \tag{10}$$

according to which the radius of an ion is determined by the Bohr orbit (0.53 A) plus n-times the second of these fundamental dimensions. Such a multiplicity is a natural ratio since in the model of the atom discussed δ represents the thickness of the electron cloud surrounding an atom, and this thickness in the isolated form is always a sphere of radius R_0. This simple model, which is represented in Fig. 6, demonstrates distinctly the "equal-thickness" of the electronic shells of the atom. The degree to which this regularity is observed is shown in Fig. 7., in which the straight line is drawn according to Eq. (10), and also in Table 3 where the results of calculations according to (10) are compared with Goldschmidt's empirical data: the latter will be taken as the basis of all comparisons because it agrees with the whole mass of crystal chemical experiments.

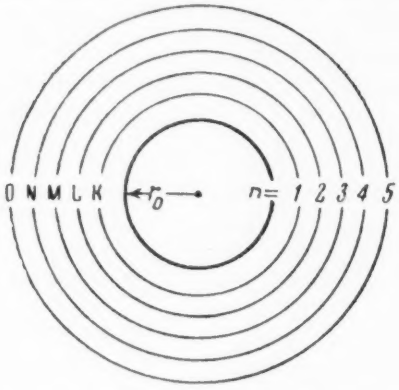

Fig. 6. "Equal thickness" of electron shells.

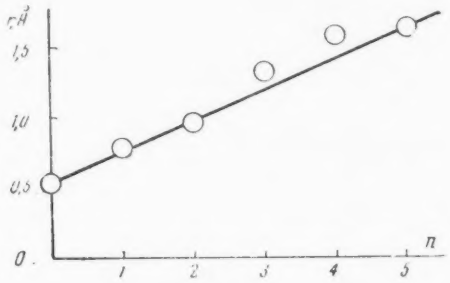

Fig. 7. Test of the law of the multiplicity of ionic radii according to Equation (10).

TABLE 3. Comparison of the Empirical Radii (A) with those Calculated from Equation (10)

Particle	H Atom	Li^+	Na^+	K^+	Rb^+	Cs^+
According to Eq. (10)	0,53	0,76	0,99	1,22	1,45	1,68
Empirical (Goldschmidt)	0,53 *	0,78	0,98	1,33	1,58	1,65
Difference, Δ	0,00	0,02	—0,01	0,11	0,13	—0,03
Precision	Within 0.2 A limits			Within 0.1 A limits		

* Bohr orbit.

From potassium onwards the equation cited above becomes less good: the divergence between experimental and calculated results reaches 0.1 A. For a further statement of (10) it is convenient to rewrite it in the form of an expression containing the effective radius of the electron, R_0. This is done by substituting into (10) the value of r_0 from (9)

$$r = R_0 + \delta(n - 1). \tag{10a}$$

The Drop Model of the Electronic Structure of the Atom

The nuclear structures of Frenkel', Bohr, and Kalkar [9] are based on drops of liquid, the surface tension of which retains its spherical form. The force of interparticle attraction prevails over the repulsion between protons in the nucleus. The model shows that the density of liquid drops and of the nuclear substance is uniform and does not depend on its dimensions. The theory reflects the known complex properties of the nucleus and supplements ideas on the Fermi gas, the layer structure of the nucleus and the solid spherical particle model.

Until now, the drop model has been applied to the nucleus and has not been extended to the atom as a whole. However, as the account given above shows, it is evident that these are sufficient data to carry out this step.

Indeed, the electronic environment of the nucleus consists of quantized accumulations of electrons of constant volume [this arises from (10)], i.e., as in drops, the volume increases without a change in the density. The drop model is given in Fig. 8. The electrons approximate to liquid drops. The first layer from the nucleus, K, is formed by the fusion of two drop electrons into one, which has the combined volume and encircles the central position.

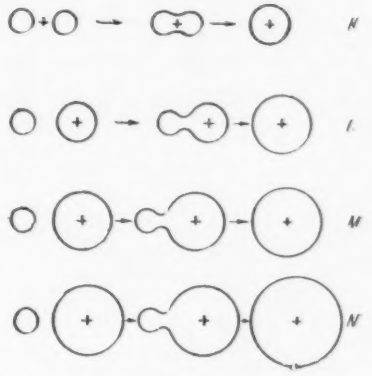

Fig. 8. Drop model of atoms.

The thermodynamics of such a process are completely justified. It is easy to calculate the change in free surface energy which occurs on fusing two drops into one. A 20% decrease in free energy is obtained.

Addition of the third drop-electron leads to a growth in volume equal in size to that of the drop absorbed. Each time we have a spherical drop corresponding to the spherical structure of an ion with any type of (electronic) structure. Such a "swelling" always occurs with the same increase in size which agrees completely with the predictions of the drop theory, a natural consequence of which is the regularity established above, namely that atomic radii are multiples of 0.23 A, which is itself the size of a drop-electron. The stability of such an atomic model is explained no less convincingly than the stability of the corresponding drop model of the atomic nucleus. In both cases repulsion takes place between the particles of like charge-electrons in the shells and protons in the nucleus; but in the case of the whole atom the electrons are attracted together by the central charges.

Each drop possesses contrasting properties—solidity and discreteness which are displayed according to the influences acting on the drops. Thus the electron drops may behave either as solid spheres or as waves or as a degenerate Fermi gas according as they take part in a chemical reaction, or undergo a spectral transition, or take part in diffraction phenomena. The drop model is only an approximation to the truth and, to understand the properties of an atom in toto, it is necessary to use analogies with all three macroscopic states of aggregation. The basic advantages of the drop model lie in the problem of predicting atomic sizes. But here it is necessary to confirm the predictions about the electron gas. Until now we have left aside the problem of the effect of changes in positive charge. In an earlier paper [10] we succeeded in showing that an electron gas filling a volume $\underline{v}$ with some average density behaved according to a simple gas law $\eta v = \text{const}$, where η is the charge on an ion having the same pressure in the kinetic gas theory. Changing from volumes to radii, we have $\eta r^3 = \text{const}$, whence $\eta_1 r_1^3 = \eta_2 r_2^3$ or $r_1 = r_2 \sqrt[3]{\eta_2/\eta_1}$, which for a transition from $\eta_1 = 1$ to any charge η gives $R_0 = r_\eta \sqrt[3]{\eta}$.

Comparing this expression with the formula which connects the radius of an orbit with its quantum number $\underline{n}$, $r_n = R_0 \sqrt[3]{n}$, we are convinced of their similarity and that is why equation (10a), which determines the rate of growth of size with $\underline{n}$, can confirm the equation, which thus reflects the decrease in radius with increase in the charge $\underline{n}$ on the cation: $r = R_0 + \delta(n - 1) - \delta(\eta - 1)$, or

$$r = R_0 + \delta(n - \eta). \tag{11}$$

Test of the General Formula for Ionic Radii Against the Empirical and Semiempirical Data of Chemistry

The basic equation (11) is characterized by the absence of any empirical parameters. Therefore, below we shall call it the theoretical equation.

In comparing results calculated from (11) with those which give an empirical or semiempirical approach to the problem, we shall for the present restrict ourselves to the structure of cations of any type since these correspond most closely to the elementary requirements of a spherical model.

Among the works the results of which we shall discuss, the first is that of Wasastjerna whose estimates of radii became the basis of the Goldschmidt system of radii. To this are added the cited works of Pauling, Zachariasen, Bokii, and Belov, and also of Stockar, Jensen, Meyer-Gossler, Rohde, Ahrens, Spiro, Kordes [11] and some other investigators.

In the comparison below the first figure is the ionic radius in A calculated from (10), and the second is the Goldschmidt radius. Finally confirmatory information is given.

Lithium	0.76	0.78	From a study of the chloride – 0.76.
Sodium	0.99	0.98	
Potassium	1.22	1.33	Agrees with Stockar's 1.22. Povarennykh suggests 1.29 as a lower limit.
Rubidium	1.45	1.49	Jensen, Meyer-Gossler, and Rohde suggest 1.44.
Caesium	1.68	1.65	Zachariasen, Spiro, and Ahrens calculated 1.68.
Beryllium	0.53	0.34	The only case of sharp and inexplicable divergence.
Magnesium	0.76	0.78	
Calcium	0.99	1.06	According to Pauling, Stockar, Kordes, and Ahrens 0.99.
Strontium	1.22	1.27	Wasastjerna postulated 1.20.
Barium	1.45	1.43	
Boron	0.3		Experimental material is unreliable. Goldschmidt did not calculate it. Bokii gave 0.2 approximately.
Aluminum	0.53	0.57	Kordes gives 0.52.
Scandium	0.76	0.83	Zachariasen gives 0.78.
Yttrium	0.99	1.06	Kordes gives 0.96.
Lanthanum	1.22	1.22	
Carbon	0.07	~0.2	
Silicon	0.30	0.39	
Titanium	0.53	0.64	Povarennykh suggests 0.49.
Zirconium	0.76	0.87	Agrees with Zachariasen's 0.79.
Cerium	0.99	1.02	

With the exception of boron the correspondence can be considered satisfactory.

The Diagonal Relationship Theorem. Heterovalent Isomorphism

The Mendeleev system has the function of connecting the properties of atoms. If these connections could be expressed quantitatively a mathematical approach to them would be permissible as for example in the theory of spectra, in equations of motion and in the analysis of the structure of systems [13], etc.

The characteristics of the atoms of elements change in the direction in which the table is written according to a periodic law in the cartesian planar system both horizontally and vertically. These give rise to the diagonal relationship.

Let point A (Fig. 9) represent the position of an element in the system. Let us represent the direction of change of any property of the element horizontally by the vector $\vec{AB}$ and vertically by the vector $\vec{AD}$. Then the properties of the element X represented by the point X on the diagonal of the vector analysis parallelogram are determined by the vector $\vec{AK}$ as the geometric mean (of $\vec{AB}$ and $\vec{AD}$).

It is true that Mendeleev in 1872 noticed this in a purely qualitative way.

This general theorem is applied with particular success to properties whose quantitative expression falls by unity horizontally and increases by unity vertically. In this case the vector $\vec{AB}$ will be equal and opposite to $\vec{AD}$, the geometric sum changes into an algebraic difference, and the resultant vector $\vec{AX}$ gives no change in this property.

From the above it follows that the size of an ion falls by δ in passing one place to the right and rises by δ in going down one place. This is naturally so because according to the drop model of the atom the parameter δ

is the unit of the quantized size of the atom. Consequently the effects of a diagonal move should be zero, and so ions of any type separated by one diagonal unit in the Mendeleev system should possess equal radii. This in fact occurs.

Since isomorphism means primarily geometrical interchangeability then, on the basis of this theorem, we arrive at the recognition of heterovalent isomorphism[14], i.e., the interchangeability of differently charged ions which are diagonally distributed in the periodic system. Such isomorphism is the result of equal radii. It is well known chemically and mineralogically, the following series serving as examples:

$$Li^{\cdot} - Mg^{\cdot\cdot} - Sc^{\cdot\cdot\cdot} - Zr^{\cdot\cdot\cdot\cdot} \; ; \; Na^{\cdot} - Ca^{\cdot\cdot} - Y^{\cdot\cdot\cdot} - Ce^{\cdot\cdot\cdot\cdot}.$$

We shall come to a detailed consideration of the theory of polymorphism and isomorphism in a subsequent communication. The exact formulation of the conditions for equality of ionic radii will be given in the following section.

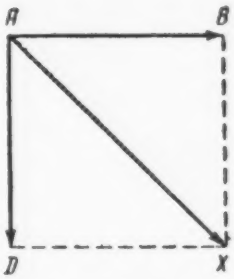

Fig. 9. Diagram of the diagonal relationship theorem.

Three Rules for Change in Size of Ions of Any Type in the Mendeleev System

The general rule (11) derived theoretically above is used in a detailed investigation to derive the three rules of change in ionic radius.

1. The rule of radius increase in groups (in the vertical direction in the periodic system). Within a group the valency is constant, i.e., η = const.

Therefore, for the radii of the first and any other element in the group, we have

$$r_1 = R_0 + \delta n_1 - \delta\eta_1, \quad r_x = R_0 + \delta n_x - \delta\eta \quad \text{or} \quad r_x - r_1 = \delta\,(n_x - n_1).$$

Thence,

$$r_x = r_1 + \delta\,(n_x - n_1), \tag{12}$$

i.e., within a group, the radii increase directly in proportion to the principal quantum numbers.

2. The rule of radius decrease in periods (in the horizontal direction).

In a series of horizontally placed isoelectronic ions the charge increases but the principal quantum number remains constant, n = const.

Therefore, on going from the first element to any other element we have $r_1 = R_0 + \delta n - \delta\eta_1$, $r_X = R_0 + \delta n - \delta\eta_X$, and $r_X - r_1 = \delta(\eta_1 - \eta_X) = -\delta\,(\eta_X - \eta_1)$.

Thence
$$r_x = r_1 - \delta\,(\eta_x - \eta_1), \tag{13}$$

i.e., within a period the radii decrease directly in proportion to the charge on the ions.

3. The rule of constant ionic radii (in the diagonal direction). According to (11) we have for the radii of two elements 1 and $\underline{x}$: $r_1 = R_0 + \delta(n_1 - \eta_1)$, $r_X = R_0 + \delta(n_X - \eta_X)$.

The required equality of the radii $r_1 = r_X$ leads to the condition $n_1 - \eta_1 = n_X - \eta_X$, or

$$n_1 - n_x = \eta_1 - \eta_x, \tag{14}$$

i.e., ions possess equal radii if their difference in charge equals their difference in (principal) quantum numbers. From this last rule it follows that no types of ions with equal volumes can occur either within a group or within a period because the requirement described above is met only by elements disposed diagonally to one another in the periodic system.

Dependence of Ion Size on Valency

In discussing the drop model it was mentioned that the electron gas obeyed a simple gas law. Since (see previous section) $r_1 = r_2\sqrt[3]{\eta_2/\eta_1}$ it is possible, knowing the radius for charge η_1, to calculate the radius for another charge η_2.

For example, the radius of Ti^{4+} is 0.64 A. Thence for Ti^{3+} we obtain a value 0.70 A, whereas the empirical value is 0.69 A. Starting from $r_{Ti^{4+}} = 1.05$ A we obtain r = 1.51 A for Ti^{3+} which is in close agreement with the Goldschmidt radius of 1.49 A.

Similar calculations for Cu, Ce, Pr, and some other elements which occur in different oxidation states showed that the divergencies lay within the limits 0.02 to 0.05 A. Thus although one can consider that the problem of the dependence of radii on charge has been elucidated in principle, the results obtained are not always sufficiently good, especially when we change to ions which have symmetry which is far from spherical and when we turn to anions.

Eighteen Electron Anions

Thus, the ionic radii depend directly on the number of quantum layers which are formed in the same way as the rare gas structure. Such shells are structurally complete, ideally symmetrical, spherical and form the framework which dictates the size of particles.

On the other hand loose and noncompact shells (for example those with eighteen electrons) are easily deformed and play a small part in the structure of the atom. Examples are the elements of the sub group copper, zinc, and gallium. Let us consider zinc. Its atom which is in the 4th period has K, L, M, and N shells and its ion has K, L, and M shells. The M shell has 18 electrons and its role is practically nil. Therefore Zn^{2+} has only two shells with the rare gas configuration and its dimensions are determined therefore by the principal quantum number two. Thence r = 0.76 + 0.23 (2-2) = 0.76 A whereas the Goldschmidt and Pauling values are respectively 0.83 and 0.74 A. For Cd^{2+} for which in this sense n = 3, we obtain r = 0.99 A which differs little from the value established by Goldschmidt and coincides with that of Bokii and Belov (0.99 A). Our calculated radii for eighteen electron ions are cited in Table 4.

TABLE 4. Radii of Eighteen Electron Ions

Ion	Cu^{+}	Ag^{+}	Au^{+}	Zn^{++}	Cd^{++}	Hg^{++}	Ga^{+++}	In^{+++}	Tl^{+++}
Theoretical	0,99	1,22	1,45	0,76	0,99	1,22	0,53	0,76	0,99
Empirical (Goldschmidt)	—	1,13	—	0,83	1,03	1,12	0,62	0,92	1,05
Semiempirical (Pauling)	0,96	1,26	1,37	0,74	0,97	1,10	0,62	0,81	0,95

With the exception of mercury, gallium and indium our results are much closer to Goldschmidt's results than are Pauling's semiempirical estimates.

The Completion of Electron Shells

Pauli's principle permits 18 electrons in the third shell from the nucleus, M. The completion of level M begins at scandium and in all divalent ions starting from Ti^{2+} the 3rd group of this level is being filled.

Here, as in the previous section, we are concerned with "formless shells" whose properties are very different from the solid spherical rare gas carcase. It is easily seen that the filling up of such a formless and labile external layer with electrons (which is shown roughly in Fig. 10) does not alter the radius of the ion. An examination of (11) leads to this conclusion. The number of shells of rare gas type is two, namely K and L. Consequently, n = 2, and for a doubly charged ion, for which $\eta = 2$, we obtain $n - \eta = 0$, i.e.,

$$r = 0{,}76 \approx 0{,}8 \text{ Å}. \tag{15}$$

However the filling up process has one peculiarity. In agreement with Hund's rule [15] the state with the maximum number of electrons with parallel spins with the limits of the given quantum subgroup is energetically favored, and, hence, single (unpaired) electrons are found in the divalent ions which posess five d-orbitals; manganese is the only example in which this is achieved. The special properties of the manganese ion were shown by Yatsimirskii [16], and their similarity to the sp-elements was discussed by Ormont [5]. The thirteen-electron ion of manganese ought to be spherical in form and hence it ought to have a radius of 0.99 A, in agreement with (11).

The prediction has been borne out. In the series of divalent ions of the iron group (i.e., titanium, vanadium, chromium, manganese, iron, cobalt, nickel, copper, and zinc) the ionic radii remain almost constant, varying within ± 0.03 A, but with manganese we have a jump to 0.91 A; for all these ions $r_M \approx 0.80 \pm 0.03$ A, in good agreement with (15), only the V^{2+} ion falling outside these limits. The results are shown in Fig. 11 where the radius of the circles is 0.03 A.

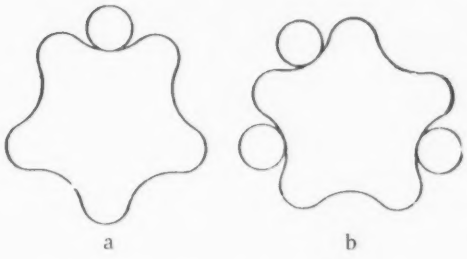

Fig. 10. Diagram of the filling of a non-spherical layer.

However one must not go to extremes and suggest that the eighteen electron shell does not in general take its place in the volume of the atom. It appears amorphous and labile only when it is an external layer. When it is "hidden" under other shells, it also takes part in making up the atomic volume, Fig. 12.

Contraction Caused by Filling Inner Energy Levels

In the sixth period on going from cesium to barium and then to lanthanum we encounter exactly the same regular drop in size, but the transition from the La^{3+} ion to the Hf^{4+} ion is, as expected, connected with the same regular decrease of the ionic radius (see Bokii [4]) $\delta = r_{La^{3+}} - r_{Hf^{4+}} = 1.04 - 0.82 = 0.22$ A.

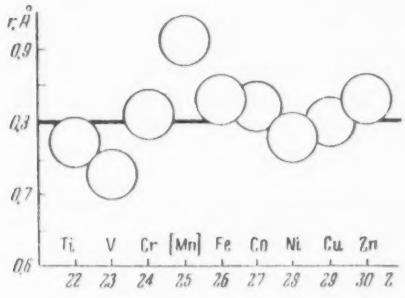

Fig. 11. Divalent ionic radii of the iron series.

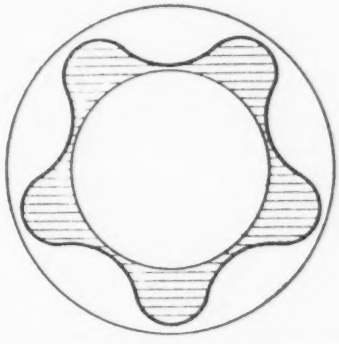

Fig. 12. Diagram of the eighteen electron shell within the atom.

But this transition does not happen all at once but in stages because between lanthanum and hafnium occur fourteen rare-earth elements, the lanthanides, and the well-known "lanthanide contraction" is observed. This is a decrease in size caused by an increase in the charge on the nucleus which goes on at the same time as the 4f level is filled, the outer electron structure remaining the same, i.e., the valency is the same (M^{3+}). The attraction of the nucleus for the surrounding electrons increases stepwise until we reach the end of this group of elements, i.e., up to hafnium. Consequently this decrease should be stepwise and we rightly expect to find a constant unit of decrease which is obtained by dividing the value for the width of the electron layer (found above by theoretical means)by fourteen, which corresponds to the fourteen lanthanide elements; $\delta' = \delta/14 = 0.23/14 = 0.016$ A. This can be used for the ionic radii of stable three valent ions from lanthanum with atomic number z = 57 to hafnium with z = 72.

$$r = r_{La^{\cdots}} + \delta' (Z_{La^{\cdots}} - Z_X), \tag{16}$$

i.e.,

$$r = 1{,}22 + 0{,}016\,(57 - Z_X). \tag{16a}$$

Equation (16) contains only theoretically justified parameters. Comparison with Goldschmidt's empirical values [17] shows (Table 5) that it agrees in general with the facts (with an accuracy of up to 0.02 A, i.e., to the same accuracy as the ionic radii are known).

One can discuss the actinides in the same way. It is not expected that the established value for the unit of contraction should have any different value. Therefore, starting with the ionic radius of actinium $r_{Ac^{3+}} = 1.11$ A, we should have

TABLE 5. The Lanthanide Contraction. Comparison of the Theoretical Values r_{theor} with the Empirical Values r_{emp} for the M^{3+} Ions for Lanthanum to Hafnium

Element	La	Ce	Pr	Nd	Pm	Sm	Eu	Gd	Tb	Dy	Ho	Er	Tm	Yb	Lu
Z	57	58	59	60	61	62	63	64	65	66	67	68	69	70	71
r_{Theor}	1,22	1,20	1,18	1,17	1,16	1,14	1,12	1,11	1,09	1,08	1,06	1,04	1,03	1,01	1,00
r_{Emp}	1,22	1,18	1,16	1,15	—	1,13	1,13	1,11	1,09	1,07	1,05	1,04	1,04	1,00	0,99

TABLE 6. The Actinide Contraction Comparison of the Theoretical Values with the Empirical Values for M^{3+} Ions from Actinium to the Elements with Z = 103.

Element	Ac	Th	Pa	U	Np	Pu	Am	Cm	Bk	Cf	En	Fm	Mv	No	103
Z	89	90	91	92	93	94	95	96	97	98	99	100	101	102	103
r_{Theor}	1,11	1,09	1,08	1,06	1,05	1,03	1,01	1,00	0,98	0,97	0,95	0,93	0,92	(0,90)	(0,89)
r_{Emp}	1,11	(1,08)	1,07	1,03	1,02	1,01	0,99	0,97	0,95	0,95	0,92	0,90	0,89	—	—

$$r = r_{Ac^{\cdots}} + \delta' (Z_{Ac^{\cdots}} - Z_X), \tag{17}$$

$$r = 1{,}11 + 0{,}016 (89 - Z_X). \tag{17a}$$

To test (17) the values of the ionic radii found by Zachariasen [4] and Kapustinskii [18] are included as the last line in Table 6. Here also the differences are not greater than 0.03 A which is good confirmation of the model under discussion.

The Size of Anions

The same (11) can be used for anions but since the discussion begins with elements at the beginning of the system one must use the direct geometric value $\delta = 0.26$ A in place of the mean value 0.23 A.

$$r = 0{,}76 + 0{,}26 (n - \eta). \tag{18}$$

We encounter here a new circumstance namely that the charges in (18) are negative. While the positive charge of the cation behaves as a positive pressure, it is possible that, by analogy, the negative charge behaves as a negative pressure [19]. Here we meet the dangerous extrapolation from positive pressures to negative ones. An analogous situation arises for anions so we use it only for small negative charges in calculating strictly quantitative values. The ions H^-, F^-, Cl^-, Br^- and I^- are simple systems of this type. The calculated values are compared with the Goldschmidt and Pauling radii in Table 7. The difference from the empirical values for

TABLE 7. Radii of Univalent Anions (in A)

Anion	H^-	F^-	Cl^-	Br^-	I^-
Theoretical, Eq. (11)	1,28	1,54	1,80	2,06	2,32
Empirical, Goldschmidt	1,54	1,33	1,81	1,96	2,20
Semiempirical, Pauling	2,08	1,36	1,81	1,95	2,16

H^- and F^- is striking and is especially marked for H^-. However the literature data for the anion are contradictory. By comparison with our difference, the difference between the Pauling and Goldschmidt values is twice as large, whereas Bokii and Belov's [4] recently improved value (1.36 A) differs from ours by only 0.08 A.

As expected, the results obtained for divalent anions are much more crude. The order of the values for O^{2-}, Se^{2-}, Te^{2-} is in general correct but they are all about 0.4 A higher than the Goldschmidt radii. Our formula gives the correct direction of the radius changes in a group and, in contradistinction to the Goldschmidt system, the right radius change for the transition from F^- to O^{2-}. Indeed Ahrens [11] and Bokii and Belov [4]

have shown that the size of the O^{2-} ion should be greater than that of the F^- ion, in contrast to Goldschmidt's suggestion; recently Povarennykh [12] has also come to the same conclusion.

Theoretical Forecasting of X-Ray Data

One of the problems of a structural theory is the theoretical forecasting of the parameters which determine the structure of a solid body. It is still not possible to do this with the necessary completeness. However in principle the necessary calculation is practicable for the best studied simple systems using the drop model of the atom. It is sufficient for this to use either direct addition of the ionic radii obtained theoretically from the equations derived below.

By definition effective radii are parameters whose sum is equal to the shortest distance between the particle-components in the crystal lattice $d = r_K + r_A$.

Combining (11) and (18) we obtain

$$d = 2R_0 + \delta(n_K + n_A) - \delta(\eta_{i_K} + \eta_{i_A}). \tag{19}$$

This expression is simplified still further for crystals in which the charges on the cation and anion are the same.

$$\eta_{i_K} = -\eta_{i_A},$$
$$d = 2R_0 + \delta(n_K + n_A). \tag{20}$$

The use of this formula is demonstrated by two examples.

Lithium hydride is formed from the very light cation Li^+ and the equally light anion H^-. For this compound $n_{Li^+} = n_{H^-} = 1$ and $d = 2 \times 0.76 + 2 \times 0.26 = 2.04$ A. This coincides completely with x-ray results [5].

Another interesting example is sodium chloride, the structure of which is used as a standard form in crystal chemistry, and which plays a part in crystal chemistry as important as that of hydrogen in spectroscopy. Sodium chloride can be obtained very pure and its crystals have been studied experimentally with considerable accuracy. According to x-ray data $d = 2.81356 \pm 0.00002$ A. In agreement with this our theoretical calculation gives ($n_{Na^+} = 2$ and $n_{Cl^-} = 3$), $d = 2 \times 0.76 + 5 \times 0.26 = 2.82$ A. Such ideal agreements are certainly rather fortuitous and exceptional. A broader comparison is therefore needed. The simplest and most accurately studied salts are the alkali halides (Table 8).

TABLE 8. Comparison of the Theoretically Calculated and Experimentally Determined Interatomic Distances d in Crytalline Chlorides (in A).

Salt	LiCl	NaCl	KCl	RbCl	CsCl
Theoretical (Eq. 20)	2,56	2,82	3,08	3,34	3,60
X-ray data	2,56	2,81	3,14	3,27	3,51
Difference	0,00	0,01	—0,06	0,07	0,09

Analogous results are obtained for hydrides, fluorides, bromides and iodides but the accuracy is less, being of the order 0.1 - 0.2 A.

Thus for the most thoroughly studied simple components the experimental values of d (obtained by x-ray investigations) agree to an accuracy of some hundredths of an Angstrom unit with those obtained using the simple, theoretically-based formulae. These theoretical formulae only require values for the Bohr orbit of an electron, and the principal quantum numbers and charges of the ions.

Only rational geometrical structures arising logically from the drop model for atomic structure were used to reach this conclusion. This supports the model proposed and unity is attained in discussing the nucleus and the electronic orbitals of the atom in the light of the drop theory.

SUMMARY

1. In making models of the microstructure ideas from all three states of matter are applied equally and simultaneously. Depending on the type of interactions involved traits are displayed which are characteristic of one or other of the states, and these are united through wave mechanics and statistics and subjected to quantum limitations.

2. By approximating the electrons to drops flowing around the centrally placed nucleus, it is possible to explain logically the sphericity of any type of ion, the formation of electron levels with constant width, and this suggestion combines harmoniously with the drop theory of the atomic nucleus (Frenkel, Bohr, and Kal'kar) to give a unified model of the atom.

3. The change in size of atoms with increasing charge is discussed as the effects of pressure on the degenerate gas in the electron orbitals of the atom.

4. The drop model is used to obtain the equation $r = R_0 + \delta(n - \eta)$ which links the size of an ion, r, with the radius of the Bohr orbital, R_0, the principal quantum number, n, and the ionic charge, η. This expression explains the regularity of the changes in radius sizes, the diagonal relationship in the Mendeleev system, the constant size of radii during the filling of orbitals, and the lanthanide and actinide contractions. The correctness of the model is confirmed by comparing calculations based on it with empirical data of chemistry.

LITERATURE CITED

1. H. Taylor and S. Glasstone, A Treatise on Physical Chemistry (New York, 1942), Vol. 1.
2. N. Bohr, Three Papers on Spectra and the Structure of the Atom [Russian translation] (GIZ, Moscow, 1923).
3. O. Blackwood, et al., Essays on the Physics of the Atom [Russian translation] (ONTI, Moscow-Leningrad, 1937).
4. V. M. Goldschmidt, Crystal Chemistry [Russian translation] (GIZ, Moscow, 1941); L. Pauling, Nature of the Chemical Bond [Russian translation] (Goskhimizdat, Moscow, 1947); W. Zachariasen, Phys. Rev., 73, 1104 (1948); G. B. Bokii, Introduction to Crystal Chemistry [in Russian] (Izd. Mau, 1954).
5. B. F. Ormont, Structure of Inorganic Compounds [in Russian] (GITTL, Moscow-Leningrad, 1950).
6. A. F. Kapustinskii, Doklady Akad. Nauk. SSSR 124, 1265 (1959).*
7. J. Wasastjerna, Soc. Sci. Fenn. Comm. Phys. Math. 38, 1 (1923).
8. A. F. Kapustinskii, Krystallografiya 1, 90 (1956).
9. Ya. I. Frenkel', Principles of the Theory of the Atomic Nucleus [in Russian] (Izd. AN SSSR, Moscow-Leningrad, 1950); S. Devons, Energy Levels of the Nucleus [Russian translation] (IL, Moscow, 1950); G. Bethe and F. Morrison, Elementary Theory of the Nucleus [Russian translation] (IL, Moscow, 1958).
10. A. K. Kapustinskii, Zhur. Neorg. Khim. 1, 82 (1956); A. Kapustinskii, Z. Phys. Chem. 209, 352 (1958).
11. K. Stockar, Helv. Chim. Acta. 33, 1409 (1950); H. Jensen, G. Meyer-Gossler, and H. Rohde, Z. Phys. 110, 277 (1938); L. Ahrens, Geochim. et Cosmochim. Acta. 2, 3, 155 (1952); N. Spiro, Tr. Ingf. Galurgii, 21, 262 (1949); E. Kordes, Z. Elektrochem. 47, 2, 152 (1941).
12. A. S. Povarennykh, Doklady Akad. Nauk SSSR 109, 1167 (1956).*
13. A. F. Kapustinskii, Izvest. Akad. Nauk SSSR, Otdel. Khim. Nauk, 3 (1953).*
14. A. E. Fersman, Doklady Akad. Nauk SSSR 1, 10, 115 (1936). See also A. A. Saukov, Geochemistry [in Russian] (GIGL, Moscow, 1951).
15. Ya. K. Syrkin and M. E. Dyatkina, Chemical Bonds and the Structure of Molecules [in Russian] (Goskhimizdat, Moscow, 1946).
16. K. B. Yatsimirskii, Zhur. Neorg. Khim. 1, 96 (1956).
17. T. Moeller, Inorganic Chemistry (New York, 1952).
18. A. F. Kapustinskii, Krystallografiya 1, 382 (1956).
19. J. Partington, An Advanced Treatise on Physical Chemistry (London, 1949), Vol. 1.

* Original Russian translation. See C. B. translation.

DETERMINATION OF THE MINIMUM EFFECTIVE RADII OF THE ATOMS

MINIMUM EFFECTIVE RADII OF THE ATOMS OF ELEMENTS OF THE FIRST THREE PRINCIPAL GROUPS OF THE PERIODIC SYSTEM*

G. Dimov and Ml. Genchev

Faculty of Chemistry and Physics, Higher Medical Institute, Sofia

Translated from Zhumal Strukturnoi Khimii, Vol. 1, No. 2, pp. 233-237,
July-August, 1960
Original article submitted June 20, 1959

Starting from two analytical forms of Einstein's coefficient A_{21} for spontaneous electron transitions, the authors have established a connection between the matrix element D_{21} of the electric moment D of an optical electron, and the force f of the corresponding oscillator of the atom. The relationship obtained is employed as a new method of determining the minimum effective radii of the atoms of the elements. For this purpose, use is made of the resonance spectral lines of the elements, and the values of the absolute force of the resonance oscillators are determined experimentally. This method may also be used for simple ions.

A linear relationship exists between the force of the resonance oscillators and the order numbers of the elements in the first, second, and third principal groups of the periodic system.

From the relationship between Einstein's coefficient A_{21} for the probability of spontaneous electron transitions, and the force f_{12} of a dipole oscillator [1] between two spectral terms 1 and 2,

$$A_{21} = 3f_{12}\gamma g_1/g_2, \tag{1}$$

where $\gamma = 8\pi^2e^2/3mc\lambda^2$ is the classical damping constant and $A_{21} = 4(2\pi)^4D_{21}^2/3h\lambda^3$, it follows that

$$\frac{D_{21}^2}{\lambda} = \frac{g_1}{g_2} \cdot \frac{3e\mu_0}{2\pi} f_{12}. \tag{2}$$

D_{21} is the matrix element of the electric moment $D = \vec{er}$ of an optical electron of the atom, $\underline{r}$ is the distance between the nucleus of the atom and the electron, $\mu_0 = eh/4\pi mc = 0.927 \cdot 10^{-20}$ erg/gauss, the Bohr magneton, and g_1 and g_2 are the statistical weights of the quantum levels 1 and 2.

It is here necessary to point out that the relationship (1) has significance only for isotropic atomic systems, for which

$$|(D_{21})_x|^2 = |(D_{21})_y|^2 = |(D_{21})_z|^2.$$

The statistical weight of a spectral term is determined by the degree of degeneration of the quantum level, i.e., the number of values which the magnetic quantum number can assume. This number is equal to $(2j + 1)$, where $\underline{j}$ is the quantum number of the total moment of the quantity of movements of the atom. The statistical weight $\underline{g}$ of the term $3^2P_{3/2}$ of sodium, for example, is equal to $g = 2j + 1 = 2 \times {}^3/_2 + 1 = 4$ and the term $3^2P_{1/2}$ is equal to 2.

* This article is printed as a discussion.

The oscillator force f as measure of the intensity of the spontaneous quantum transitions of the electrons may be calculated for different quantum transitions if the characteristic wave functions of the atomic system considered are known. It can, however, also be determined experimentally. Several methods of varying degrees of accuracy are known for determining f. In the first place, there is the interferometer method of D. S. Rozhdestvenskii, then comes the method of the total absorption of light, and so forth.

The matrix element D_{21} of the electric moment of an optical electron expresses its dipole moment on transition from one quantum state (2) to another (1). It is known that the mean values of the dipole moments of an electron in its stationary states 1 and 2 having the respective characteristic functions ψ_1^0 and ψ_2^0 are equal to

$$D_{11} = er_{11} = e\int \psi_1^{0*} r\psi_1^0 d\tau \text{ and } D_{22} = er_{22} = e\int \psi_2^{0*} r\psi_2^0 d\tau.$$

The expression

$$D_{21} = er_{21} = e\int \psi_2^{0*} r\psi_1^0 d\tau$$

is therefore called by some authors the mean dipole moment of the electron for the $2 \rightarrow 1$ transition. The quantity r_{21} may be called the mean effective radius of the atom in this transition. When the quantum state 1 is the normal state of the neutral atom, and the quantum state 2 is the closest excited state of the atom, the effective radius r_{21} has a minimum value. In this sense, the relationship (2) affords the possibility of obtaining values which express the minimum effective radii of the atoms of the elements, provided we know the absolute values of f for their resonance spectral lines, which appear in the participation of the normal (ground) term of the atom. It is known that the resonance spectral lines are the most intense lines in the atomic emission spectra of the elements.

In the same way, it is also possible to determine the minimum effective radii in simple ions.

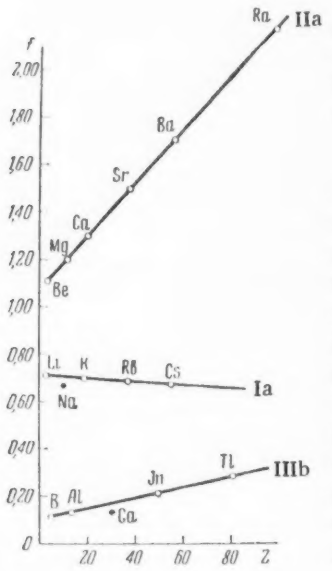

Dependence of the force of the resonance oscillator on the number of an element in the periodic system.

The resonance spectral lines of the atoms of the elements of the first group of the periodic system are produced by the transition $n^2S_{1/2} - n^2P_{3/2}$, for elements of the second group $n^1S_0 - n^1P_1$, and for elements of the third group $n^2P_{3/2} - (n+1)^2S_{1/2}$, where n is the principal quantum number of the fundamental term of the atom.

On the basis of published experimental values and in some cases also calculated values relative to the absolute magnitude of the force f of the oscillator for resonance spectral lines of the elements [2, 3, 4, 5, 6], we determined the minimum effective radii of the atoms of hydrogen, lithium, sodium, potassium, cesium, magnesium, calcium, strontium, barium, aluminum, gallium, indium, and thallium. The effective radii of atoms of rubidium, beryllium, radium, and boron were calculated with values of f extrapolated on the basis of the linear dependence of f on the atomic number Z of the elements, which was first found by Ostrovskii, Penkin and Shabanova [2] for four elements of the second principal group—magnesium, calcium, strontium and barium and confirmed by us for elements of the first and third principal groups (figure). It should be pointed out that the oscillator force for the resonance spectral line 1215.68 A of hydrogen does not follow the linear dependence shown in the group of the alkali metals.

The minimum effective radius of a hydrogen atom may be calculated either from the relationship (2) or from the characteristic functions of its 1 s and 2 p states:

$$\psi_{1s}^0 = \frac{1}{\sqrt{\pi}}\left(\frac{Z}{a_1}\right)^{3/2} e^{-\frac{Z}{a_1}r}$$

$$\psi_{2p_x}^0 = \frac{1}{4\sqrt{2\pi}}\left(\frac{Z}{a_1}\right)^{5/2}\left(\frac{Z}{a_1}r\right) e^{-\frac{Z}{2a_1}r} \sin\theta\cos\varphi \quad (\text{or } m = +1)$$

$$\psi_{2p_y}^0 = \frac{1}{4\sqrt{2\pi}}\left(\frac{Z}{a_1}\right)^{5/2}\left(\frac{Z}{a_1}r\right) e^{-\frac{Z}{2a_1}r} \sin\theta\cos\varphi \quad (\text{or } m = -1)$$

TABLE 1. Resonance Lines and Minimum Effective Radii of Atoms of the Elements of the First Three Groups of the Periodic System (λ and r are given in A).

$n^2S_{1/2} - n^2P_{3/2}$	$n^1S_0 - n^1P_1$	$n^2P_{3/2} - (n+1)\,{}^2S_{1/2}$
I	II	III
1. H λ = 1215,68 f = 0,4162 r = 0,558		
3. Li λ = 6707,84 f = 0,71 r = 1,50	4. Be λ = 2348,61 f = 1,1 r = 0,90	5. B λ = 2497,73 f = 0,11 r = 0,72
11. Na λ = 5890 f = 0,67 r = 1,36	12. Mg λ = 2852,13 f = 1,2 r = 1,03	13. Al λ = 3961,5 f = 0,13 r = 0,98
19. K λ = 7664,91 f = 0,70 r = 1,59	20. Ca λ = 4226,73 f = 1,3 r = 1,31	
		31. Ga λ = 4172,06 f = 0,135 r = 1,02
37. Rb λ = 7800,23 f = 0,69 r = 1,59	38. Sr λ = 4607,33 f = 1,5 r = 1,47	
		49. In λ = 4511,32 f = 0,218 r = 1,35
55. Cs λ = 8521,10 f = 0,67 r = 1,64	56. Ba λ = 5535,55 f = 1,7 r = 1,71	
		81. Tl λ = 5350,46 f = 0,28 r = 1,68
	88. Ra λ = 4825,91 f = 2,05 r = 1,75	

TABLE 2. Comparison of Minimum Effective Radii (in A) with Published Data

Element	Minimum effective radius	Radius according to Laves and Vitskov	Standard radii for the covalent bond (Pauling)
1. Hydrogen	0.558	0.78	–
3. Lithium	1.50	1.56	–
4. Beryllium	0.90	1.13	1.07
5. Boron	0.72	0.95	0.89
11. Sodium	1.36	1.91	–
12. Magnesium	1.03	1.60	1.40
13. Aluminum	0.98	1.43	1.26
19. Potassium	1.59	2.36	–
20. Calcium	1.31	1.96	–
31. Gallium	1.02	1.22	1.26
37. Rubidium	1.59	2.53	–
38. Strontium	1.47	2.13	–
49. Indium	1.35	1.62	1.44
55. Cesium	1.64	2.74	–
56. Barium	1.71	2.25	–
81. Thallium	1.68	1.70	1.47
88. Radium	1.75	1.67	

$$\psi^0_{2p_z} = \frac{1}{4\sqrt{2\pi}}\left(\frac{Z}{a_1}\right)^{3/2}\left(\frac{Z}{a_1}r\right)e^{-\frac{Z}{2a_1}r}\cos\theta \qquad (\text{or} \quad m=0). \tag{3}$$

The components of this radius on the coordinate axes x, y, z are expressed by the integrals

$$x_{21} = \int_0^{\infty}\int_0^{\pi}\int_0^{2\pi} r\cos\varphi\sin\theta\psi^0_{1}\psi^{0*}_{2}r^2\sin\theta\,dr d\theta\,d\varphi$$

$$y_{21} = \int_0^{\infty}\int_0^{\pi}\int_0^{2\pi} r\sin\varphi\sin\theta\psi^0_{1}\psi^{0*}_{2}r^2\sin\theta\,dr\,d\theta\,d\varphi$$

$$z_{21} = \int_0^{\infty}\int_0^{\pi}\int_0^{2\pi} r\cos\theta\psi^0_{1}\psi^{0*}_{2}r^2\sin\theta\,dr\,d\theta\,d\varphi$$

by substitution in them of the functions ψ by the expressions (3). We find that

$$x_{21} = z_{21} = 0{,}748\,a_1; \quad y_{21} = 0,$$

where $a_1 = 0.529 \cdot 10^{-8}$ cm is the radius of the first Bohr orbit.

Thus, the minimum effective radius of the hydrogen atom $r_{21} = z_{21}\sqrt{2} = 1.058 \cdot a_1 = 0.560$ A. In accordance with the relationship (2) for f = 0.4162 and for the resonance line 1215.68 A and $g_1 = g_2$, and taking into account that $D^2_{21}/\lambda = e\mu_0 f/\pi$, we get for the same radius $r_{21} = 0.558$ A, by virtue of $y_{21} = 0$.

The effective radius of the aluminum atom was calculated by us from its resonance spectral line 3961.53 A, since this corresponds precisely to the transition $^2P_{3/2}-{}^2S_{1/2}$, which is common to all the elements of the third principal group of the periodic system. The oscillator force for this wavelength is also equal to 0.13, as well as for λ = 3944.03 A, corresponding to the transition $^2P_{1/2}-{}^2S_{1/2}$.

It must be mentioned that for thallium several absolute values of the force of the oscillator of the resonance spectral line 5350.46 A have been published [3]. We consider the most suitable value to be that obtained by E. Khinov and Kh. Koon and quoted in the monograph by Gurvich [3], since it follows the linear dependence f(z) found for the values of f for aluminum, gallium and indium. A slight discrepancy of ~0.03 is found for gallium.

Table 1 gives the values of the minimum effective radii of atoms of the elements of only the first three principal groups of the periodic system, since as yet the most complete data are available for the force of their oscillators only. For the elements of the other groups, it is possible to find in the literature only isolated determinations of f, and for some groups they are missing altogether. It is evident that the calculation of the minimum effective radii of the atoms of the other elements of the periodic system by the method we have indicated ought to be carried out in parallel with an experimental or theoretical determination of the force of the oscillator of their resonance lines.

In Table 2, the values we have obtained for the minimum effective radii are compared with the values of the atomic radii obtained by other methods [6].

In conclusion, we would point out that the accuracy of calculating the effective radii of the atoms depends mainly on the accuracy of the determination of the absolute values of the force of their resonance oscillators.

LITERATURE CITED

1. Basic Formulas of Physics, Edited by D. Menzel [in Russian] (1957), p. 566.
2. Yu. I. Ostrovskii, P. N. Penkin and L. N. Shabanova, Izvest. AN SSSR, Ser. Fiz. 22, 6, 725 (1958).
3. L. V. Gurvich, Optika i Spektroskopiya 5, 2, 205 (1958).
4. V. F. Kitaeva and N. N. Sobolev, Optika i Spektroskopiya 1, 3, 311 (1956).
5. Yu. I. Ostrovskii and P. N. Penkin, Optika i Spektroskopiya 4, 6, 719 (1958).
6. Landolt–Bornstein's Physikalische-chemische Tabellen 1, 260 (1955).

SOME RESULTS FROM ELECTRON-DIFFRACTION STUDIES OF THE STRUCTURES OF SEMICONDUCTORS

Z. G. Pinsker

Institute of Crystallography, Academy of Sciences of the USSR
Translated from Zhurnal Strukturnoi Khimii, Vol. 1, No. 2, pp. 238-251,
July-August, 1960
Original article submitted December 12, 1959

Results are presented from electron-diffraction studies of the compositions and structures of films of Sb, Se, Te, and Ge, as well as of semiconductors containing two or more components; the results derive mainly from work done in the electron-diffraction laboratory of the Institute of Crystallography, Academy of Sciences of the USSR.

Advanced methods of examining and testing solids are required in modern solid-state physics (semiconductors, ferroelectrics, ferrites, etc.). Electron diffraction has been used as a valuable supplement to x-ray analysis in structure studies.

We know little about the relations between the structures of these new materials and the optical, electrical, and other properties they display. Knowledge of the structures is all the more important in view of Ioffe's [1] theory of short-range order as the controlling factor, since new materials are being produced continually.

Electron diffraction as applied in studies of structures is the most powerful and valuable use of electron diffraction; it has solved many scientific and practical problems relating to solids [2, 3]. The films of material must be very thin, because electrons are scattered very readily; alternatively, thin surface layers can be examined, an application that is important in connection with various uses of thin films. Another point here is that often a material (e.g., a semiconductor containing several components) can be obtained in large sizes and in equilibrium states only with great difficulty, whereas a thin film will crystallize readily at moderate temperatures. Such films are often found to contain unstable phases and transition structures, which are also of some considerable interest.

Electron diffraction is of great value in controlling vacuum-evaporation processes; the method is of great value in establishing the structure (and sometimes the composition) of an evaporated film, and may sometimes be the sole method usable.

Systematic studies have been made on semiconducting alloys for many years in the electron-diffraction laboratory at the Institute of Crystallography; special methods have been developed for depositing films under vacuum, for causing them to crystallize, to take up defined orientations, and so on. A film containing more than one component may be made by distilling the components simultaneously or in sequence, the product being subsequently annealed or homogenized. Alternatively, an alloy may be distilled. It is to be expected that a stable compound will distill unchanged, but many compounds decompose in part, so the condensate gradually changes in composition (the more volatile components appear first, followed by the less volatile ones). The product may be a solid solution, a phase of variable composition, or a eutectic mixture. Methods of controlling the deposition of individual components have not yet been worked out fully.

The condensate is often amorphous or in extremely finely divided form; Sb, Se, As, and compounds thereof show a great tendency to produce amorphous films, the tendency increasing from Sb to As. Crystalline materials (especially monocrystals) are more likely to cause the films deposited on them to crystallize; the films are also more likely to be crystalline if the material is hot, but this technique is of rather limited use, because the condensate may be volatile or the incident molecules may be reflected by the hot surface. The volatility also limits the annealing temperatures that can be used.

Films are annealed for the following purposes.

1. To homogenize films produced by sequential deposition of two or more components.

2. If the product from the above is amorphous, further annealing may be needed to cause the film to crystallize. Sometimes the resulting particles are so small that the diffraction patterns are not well resolved; in that case the next process is applied.

3. Annealing is prolonged until the crystals are large enough (linear size 3-5 × 10^{-6} cm) to give the sharp patterns required; even so, such patterns are often inadequate for a full structural study, so still further annealing is needed.

4. Continued recrystallization may result in a preferred orientation being taken up; the resulting texture (often of platelet type) gives the best patterns.

The annealing temperature seldom exceeds 200-300°C, and cannot exceed 100-120°C if collodion is used as the backing, so the times needed for annealing may range from 2-3 hr to 10 hr or more.

The above is a brief outline of the methods of preparing films of semiconductors for use in electron-diffraction studies.

Structures of One-Component Films.

Important features to be examined here are the nature of the structure (amorphous or crystalline), the processes of crystallization, and the preferred orientation (if any) of the crystals.

Several studies have been made [2, 4-6] of films of Sb; it has been found that Sb condenses on backings of collodion and other amorphous materials at room temperature as films that are initially amorphous. The patterns usually show a few diffuse rings only; such patterns have been used [4] to examine the short-range order by means of integral analysis. The rings are examined carefully with a microphotometer (standard blackening curves are used) in order to compile an experimental intensity curve, from which is deduced the radial distribution, i.e., the quantity $4\pi r^2 \rho(r)$ as a function of r (Figs. 1 and 2). The experimental curve is normalized by means of a curve for $|f(\sin\vartheta/\lambda)|^2$ for antimony, so the areas under the peaks indicate the numbers of nearest neighbors of each kind.

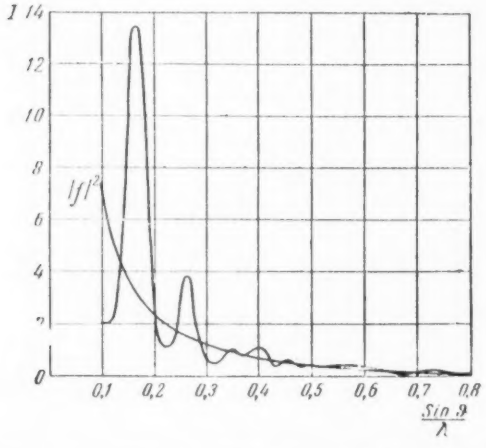

Fig. 1. Experimental intensity curve for a film of amorphous antimony; $|f|^2$ is the atomic scattering factor for Sb.

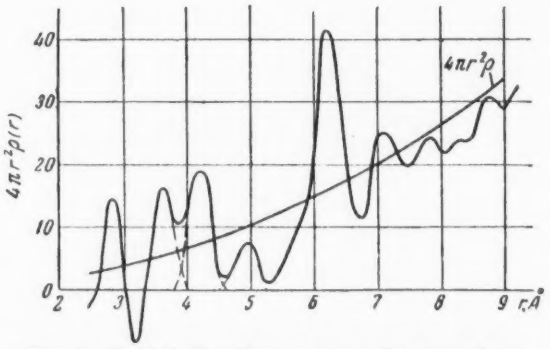

Fig. 2. Radial-distribution curve for amorphous Sb.

The distance and numbers of nearest neighbors have been found also by Hendus [7] by means of x-rays; comparison shows that electron diffraction gives resolution. Amorphous Sb has a coordination number higher than that for crystalline Sb, a result that is in agreement with the general finding that the coordination number increases when a substance having wholly or partly homopolar bonds is melted.

An important point here is that the scattering angles (repeat distances) for the crystalline material are not the same as those for the amorphous material, so the transition from a diffuse pattern to a sharp one is not caused by an increase in the size of the crystals. It has been claimed [8] that dark-field electron microscopy reveals crystalline regions or particles in films of Sb that give diffuse diffraction patterns.

Detailed studies have been made of the factors that cause amorphous films of Sb to crystallize, in particular temperature and the nature of the backing [6]; these films of Sb were formed on polycrystalline salts and metals. A metal free from any trace of oxide film causes antimony to crystallize; amorphous deposits are not found. (Crystallization of Sb in mixed films is dealt with later.)

Rapid deposition, or subsequent heating, causes a film of Sb to produce crystals whose (0001) planes are parallel to the backing, the azimuthal positions being random (Fig. 3). It is found [9] that cube faces of rocksalt produce a rarer form of orientation, in which the $[11\bar{2}1]$ axis is normal to the face and there are two equally probable azimuthal positions, namely

$$[0001]_{Sb} \parallel [100]_{NaCl} \text{ and } [0001]_{Sb} \parallel [010]_{NaCl}.$$

The transition from the amorphous state to the crystalline state is [5] accompanied by a 200-fold change in the electrical conductivity of a very thin film; the nature of the carriers also changes from electrons for amorphous films to holes for crystalline ones. Further, the coefficient of the thermoelectric e.m.f. changes from 100-200 μv/deg (positive) at the same time.

A thin film of Se produced by vacuum evaporation is amorphous [2, 10]; heating under vacuum results first in the monoclinic form, which soon goes over to the hexagonal form at 80-90°C, although the amorphous form can pass directly to the hexagonal form under some circumstances.

Vacuum-evaporated tellurium deposits directly in crystalline form [10]; the films usually are textured, the crystals having their prism faces $\{10\bar{1}0\}$ parallel to the backing and having random azimuthal positions. Figure 4 illustrates the pattern obtained when the film is inclined to the electron beam.

The structures of Sb and Te are responsible for the above features of the orientation; Sb has a layered structure (the layers are parallel to the basal plane), so the element tends to grow as platelets. On the other hand, Te is built up from spiral chains running parallel to c, which are held together by weak residual forces. This structure is responsible for the prismatic habit of Te; the texture is that of a random array of hexagonal rods.

Hot crystalline backings and high-temperature annealing produce Te crystals ordered also in azimuth; for example, on a cube of rocksalt we find the orientations

$$\{10\bar{1}0\}_{Te} \parallel \{100\}_{NaCl} \text{ and } [0001]_{Te} \parallel [100]_{NaCl} \text{ or } [010]_{NaCl}$$

and on mica

$$\{10\bar{1}0\}_{Te} \parallel \{0001\}_{m} \text{ and } [0001]_{Te} \parallel [11\bar{2}0]_{m}.$$

Cd and Bi behave as Sb does (basal planes parallel to the backing).

Disordered solid solutions having the structure of the components are always found when films of composition Bi_nSb_m are subjected to prolonged annealing [11]. The lattice constants of these solutions vary smoothly between the values for the components. A film of Sb oxidized in air gives rise to cubic senarmontite Sb_4O_7, whose crystals have their [111] axes normal to the backing or to the basal plane of Sb. Films of Bi give the cubic oxides I and II, whose lattice repeat periods are 4.65 and 5.49 A respectively. The crystals usually have their cube faces parallel to the backing.

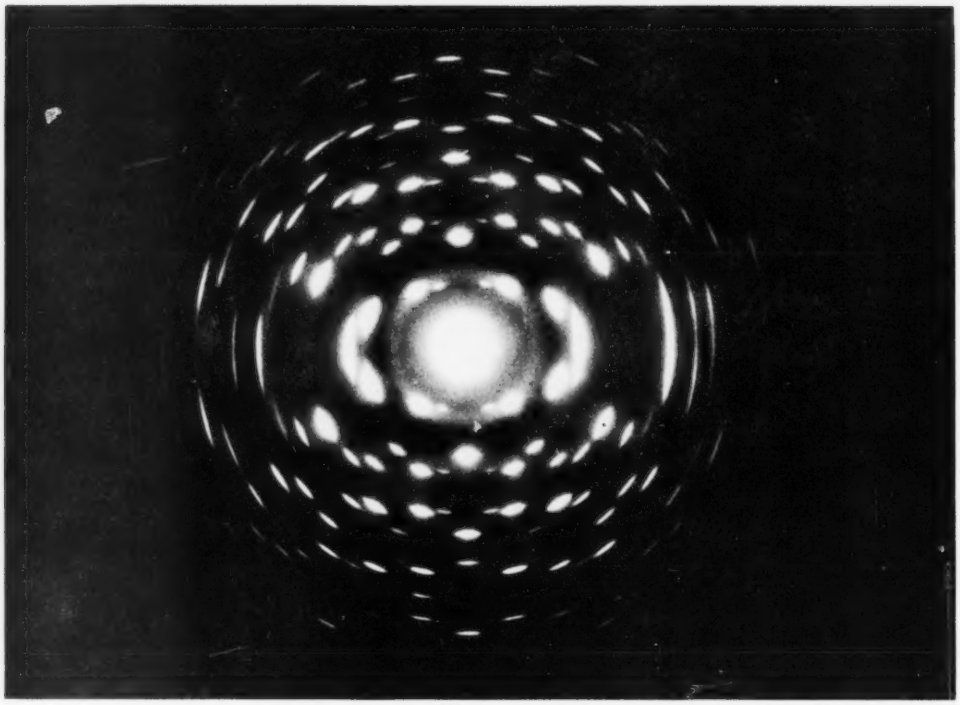

Fig. 3. Oblique-texture pattern from crystalline Sb

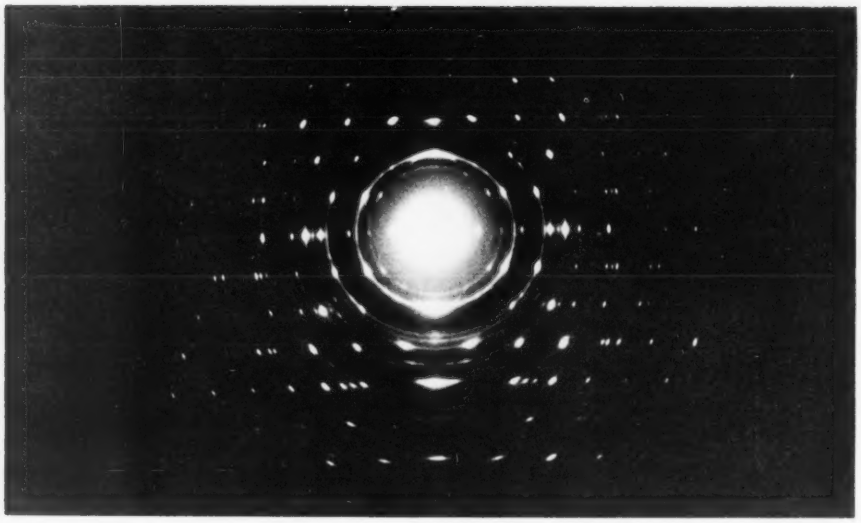

Fig. 4. Oblique-texture pattern from Te.

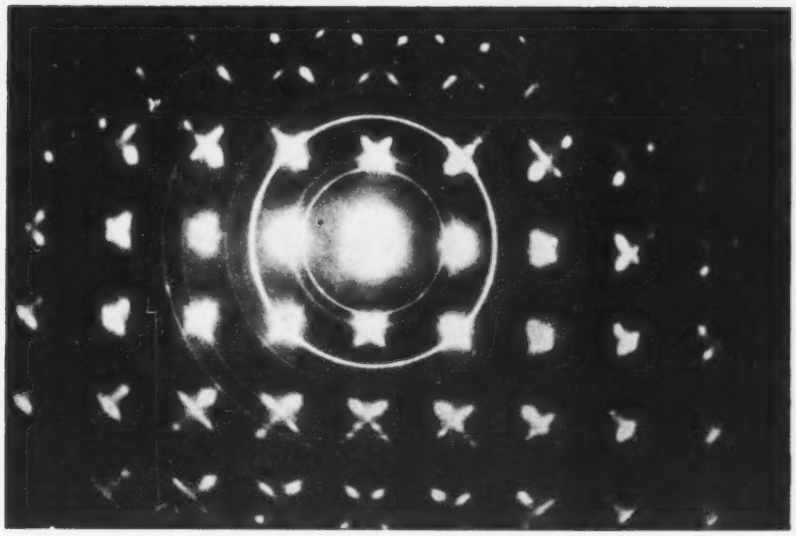

Fig. 7. Diffraction pattern of a film containing BiSe and Bi_3Se_4 (both crystalline). The crosses are caused by the regular pyramidal form of the crystals of BiSe.

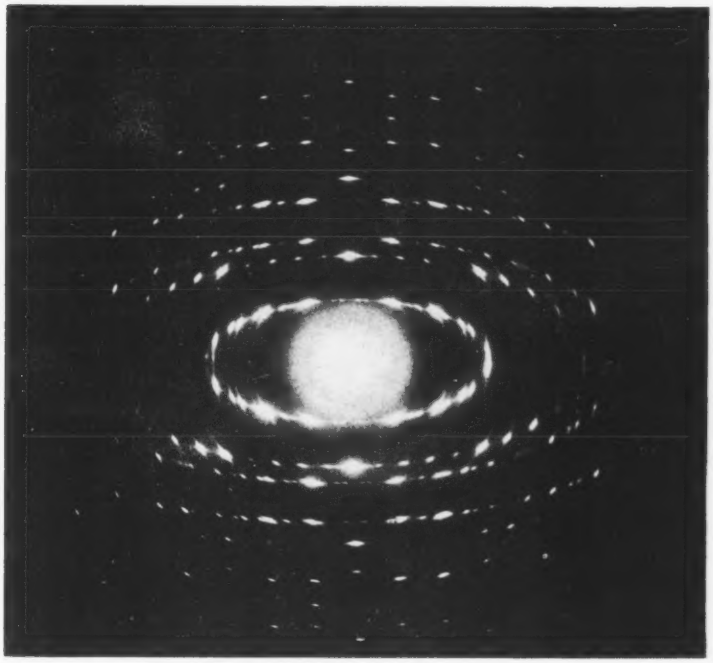

Fig. 8. Oblique-texture pattern from Bi_2Te_3.

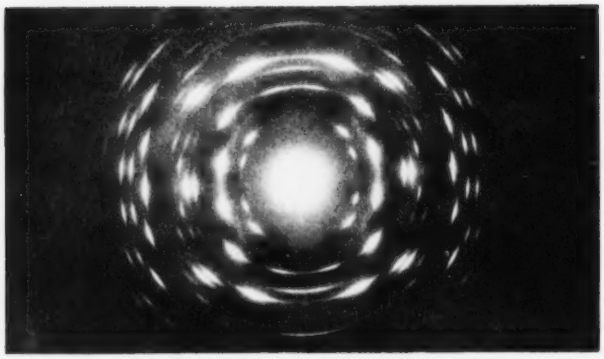

Fig. 9. Oblique-texture pattern from $Tl_2Sb_2Se_4$

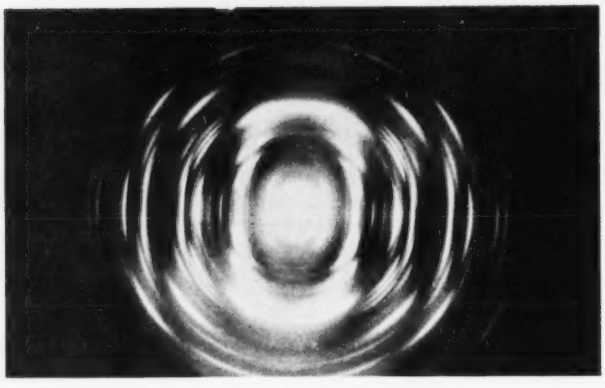

Fig. 13. Oblique-texture pattern from InSe.

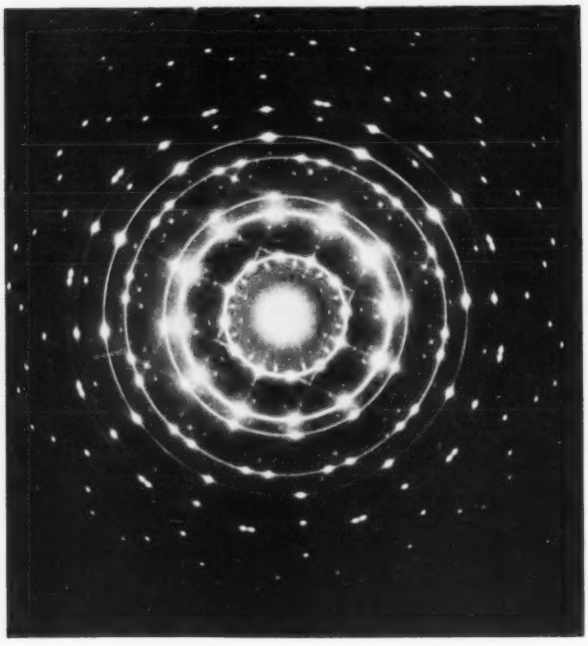

Fig. 14. Diffraction pattern of a highly oriented film of InSe; the pattern contains secondary dynamic reflections and diffraction lines resulting from deformation of the film.

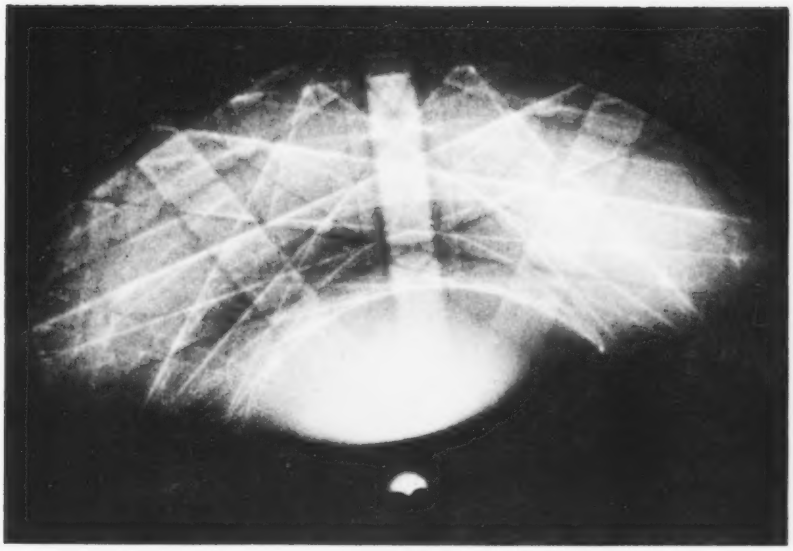

Fig. 15. Diffraction pattern with bands and lines produced by a fresh cleavage surface of a monocrystal of Ge (Z = 250 mm)

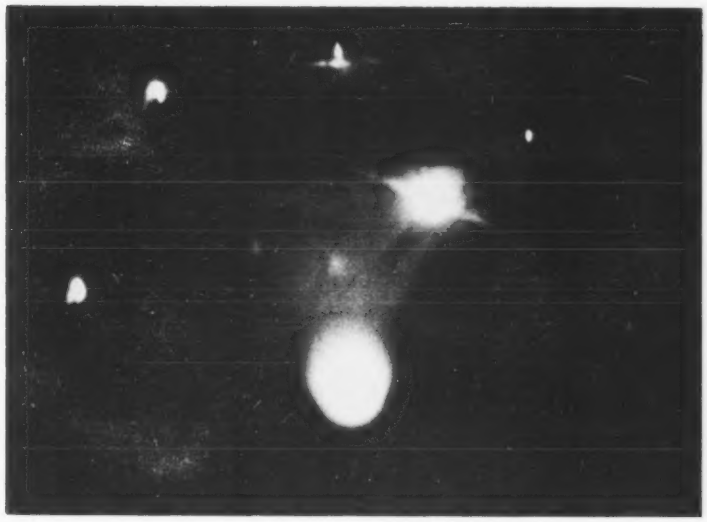

Fig. 16. Diffraction pattern given by the surface of a monocrystal of Ge after polishing and vigorous etching (Z = 700 mm)

Substances with the Zinc Blende Structure

Crystalline materials having structures of ZnS type (sphalerite type) occupy an important place among semiconductors; ZnS, CdS, and AgI exist in sphalerite and wurtzite forms, but most materials with the ZnS structure occur only in one of these forms.

Films of CdTe may be made by distilling the alloy or by distilling the components simultaneously [12].

Only the sphalerite structure is known to exist for CdTe on the basis of x-ray results, but both types of structure have been detected from the electron-diffraction patterns of evaporated films. The transition from the cubic (sphalerite) form to the hexagonal (wurtzite) form is accompanied by a rearrangement of the atoms of the nonmetal [17, 18], so we would expect to find polymorphism; relations that are obeyed more or less exactly are

$$a_h = a_c / \sqrt{2} \;\&\; c_h = 2a_c / \sqrt{3}.$$

The c/a for CdTe is 1.636, which is very close to the 1.633 for ideally close-packed spheres.

The wurzite structure has only one parameter, e.g. the coordinate of Te if the origin is taken on the Cd. The experimental structure amplitudes have been used in F^2 series to give z = 0.368, which is close to the theoretical value (0.375). A full examination of the hexagonal form was possible only on the basis of oblique-texture patterns.

Semiletov [12] has examined the phase compositions of films of CdS, CdTe, and CdSe; he concludes that the proportion of the hexagonal form increases with temperature for the first two compounds, whereas CdSe shows an increasing proportion of the cubic form. The orientations of the crystals are also of interest; cubic crystals of CdTe formed on cleaved mica have the following orientations:

$$\{111\}_{CdTe} \parallel \{0001\}_m \text{ and } [110]_{CdTe} \parallel [11\bar{2}0]_m.$$

An analogous pattern has been reported for Ag condensed on the faces of crystals of silicon carbide [13], mica, and molybdenite.

Semiletov and Rozsival [14] have studied InSb, which is a semiconductor [15], and which is also a compound of ZnS type. A layer of variable composition is formed when the components are evaporated simultaneously, the composition being dependent on the relation to the positions of the sources. An In:Sb ratio of 1:1 gives InSb having the zinc-blende structure; InSb + In and InSb + Sb are formed on either side of that composition. The lattice constants so found agree with those known for the components; solid solutions are not formed.

If InSb is distilled, the material first deposited is Sb, followed later by InSb + Sb, then by pure InSb, and finally by InSb + In. These results are of great importance, because they show that errors can result from any attempt to prepare films in this without direct checks at every stage.

Patterns given by polycrystalline films of InSb have been found to contain reflections corresponding to a hexagonal phase of that composition, whose constants are a 4.56 and c 7.46 A. These are related to the 6.45 A of the cubic form by the relations that apply to CdTe.

Kurov and I [15] have studied InSb as a semiconductor; we made a series of films by evaporating the components simultaneously onto glass, the In and Sb contents of the films varying from 0 to 100%. We measured the thermoelectric power and the resistance as functions of composition for annealed and unannealed films. Fig. 5 shows the thermoelectric power as a function of position (i.e., as a function of the ratio of the components) for an unannealed film; there is one deep minimum (amorphous Sb) and two maxima. This film, annealed, gave only one peak (corresponding to InSb). The electrical resistance (Fig. 6) shows a similar pattern, namely two peaks before annealing and only one afterwards. Here again, we found that amorphous antimony is stable in the form of fairly thick films, on account of the disperse structure of regions consisting of InSb + Sb.

Systems Bi-Se and Bi-Te

The x-ray studies on these interesting systems are rather inadequate, and the data on Bi_2Se_3 and Bi_2Te_3 stand in need of checking.

Semiletov [16] has studied these systems systematically in my laboratory; he used thin evaporated films. The various phases were produced either by distilling the components simultaneously or by distilling a suitable alloy or by combining these two methods.

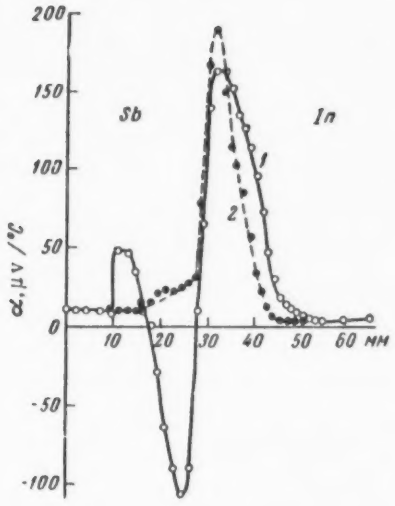

Fig. 5. Thermoelectric power as a function of position for a specimen of In-Sb.

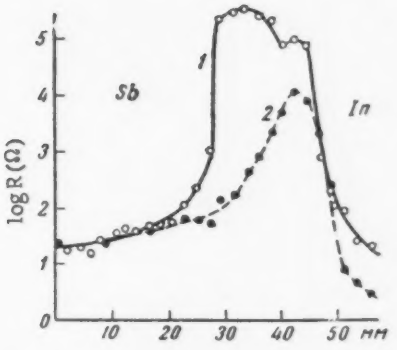

Fig. 6. Electrical resistance as a function of position for a specimen of In-Sb.

In most cases the films were condensed on cleaved surfaces of mica or rocksalt; very often the sharpness of the reflections from the hki0 faces was very much better than the sharpness for other hkil faces, on account of the platelet shape of the crystals, which were very thin. Particles of this shape are favorable to the production of an ordered array. Sometimes mosaic monocrystals were formed (see Fig. 7).

The following phases have been detected in the Bi-Se system.

An alloy composition $BiSe_3$ was distilled to give films producing sharp oblique-texture patterns and good reflection patterns. The lattice constants for this phase (in hexagonal axes) are

$$a = 4{,}12 \div 4{,}17\ (\pm 0{,}01)\ \text{Å};\quad c = 28{,}6 \div 29{,}2\ (\pm 0{,}2)\ \text{Å}$$

which corresponds to the a (4.14 A) found from x-ray analysis for Bi_2Se_3 (Z = 3), but which give a c five times the latter one (5.71 A). Further, the absences indicate that the structure is orthorhombic. The structure was established from F^2 and F syntheses in conjunction with geometrical considerations; it was found to be a close-packed nine-layer array of Se atoms (i.e., one with the c repeat period covering nine layers of Se atoms) in which the Bi atoms lie in the octahedral holes (they fill those in two layers out of every three). Let A, B, C denote successive layers of Se atoms, and let the corresponding small letters denote the layers of Bi atoms; then the layers are arranged as in

$$b \mid AcBAcBaCBaCbACb \mid A,$$

in which the vertical strokes denote one c period. The space group is $R\bar{3}m$; the Se atoms lie at positions 3(a) and 6(a), with z 0.196, and the Bi atoms at positions 6(c) with z 0.395.

Other types of pattern were found as well; these point to the presence of a phase Bi_3Se_4, whose structure was established as before, the lattice constants being a = 4.22 ± 0.01 A; c = 40.4 ± 0.3 A. The unit cell contains three Bi_3Se_4 units, and the space group is $R\bar{3}m$. The Bi atoms are in positions 3(a) and 6(c), with z 0.428; the Se atoms are in positions 6(c) with z_1 0.139 and 6(c) with z_2 0.286. The structure is a 12-layer orthorhombic array of Se atoms, the Bi atoms filling the octahedral holes in $^3/_4$ of the layers.

Finally, a third phase BiSe was detected, whose structure is of NaCl type with a = 5.85 - 5.98 (± 0.02 A).

The more important interatomic distances are

	Bi_2Se_3	Bi_3Se_4	BiSe
Se — Se	3,30	3,30	—
Bi — Se	2,99—3,07	3,00—3,10	2,99
	Bi_2Te_3	BiTe	
Te — Te	3,72	—	—
Bi — Te	3,04—3,24	3,23	—

We found that the lattice constants of these phases tended to vary greatly from one specimen to another; the nature of the solid solutions was examined by distilling an appropriate alloy and one of the components simultaneously to form a film on a common backing. We found that solid solutions formed by the phases with the components are responsible for the tendency of the lattice constants to vary. Solid solutions containing excess Bi have the extra atoms located in the otherwise unused octahedral holes (hence the increase in the lattice constants). Only $BiSe_3$ and Bi_3Se_4 can form such solid solutions, because only those compounds contain such holes; this cannot occur for BiSe, so the maximum lattice constant (a 5.98 A) must correspond to the stoichiometric composition.

Conversely, solid solutions containing excess Se (lacking Bi) are ones (as it were) formed by loss of Bi atoms, so the lattice constants are smaller than those for the ideal structures. All three phases show this type of solid solution.

Similar results were obtained for Bi-Te (Fig. 8); here Bi_2Te_3 and BiTe are entirely analogous to the corresponding compounds for Bi-Se. For Bi_2Te_3 we have a = 4.35 - 4.42 (± 0.01) A; c = 30.2 - 31.00 (± 0.2) A; z_{Bi} = = 0.400; Z_{Te} = 0.212.

For BiTe we have a 6.46 A (see above for interatomic distances).

The system resembles Bi-Se in that these two phases can dissolve either component; excess Bi causes the lattice constants to increase, whereas excess Te in Bi_2Te_3 as before causes the lattice constants to decrease.

The use of semiconductor films frequently involves heating in air or in oxygen at reduced pressures, so we [19] examined the effects of heating evaporated films of Bi_2Se_3 and Bi_2Te_3 in air (the films were examined in diffraction at every stage). The initial effect is that Se(Te) is replaced by oxygen, the subsequent effect being that the lattice was reconstructed to correspond to an oxide of probable composition BiO and having an NaCl structure whose lattice constant decreased gradually from 5.65 to 5.50 A (see above, also [11]). The electrical parameters of the films changed greatly during these processes.

Systems Containing Two or More of the Elements Tl, Sb, As, Se

Kolomiets and Goryunova initiated work on these materials, which they have studied systematically [20-22].

This section of the work was concerned with the pseudobinary section of the Tl-Sb-Se system and with a section of the pseudoternary system Tl_2Se-Sb_2Se_3-As_2Se_3. The phase diagram for the Tl_2Se-Sb_2Se_3 system contains a special point corresponding to $Tl_2Sb_2Se_4$; our electron-diffraction study [24] confirmed that this is so, for a phase with that composition was present as well as Tl_2Se and Sb_2Se_3. The structure of that phase has been worked out fully.

The parent compounds were prepared as thin films by evaporating alloys onto collodion, the products being annealed at a temperature slightly above 100°C. We found that Sb_2Se_3 has a structure analogous to the structure of Sb_2S_3, which is in full agreement with the x-ray evidence [23].

Stasova and Vainshtein [25] have used polycrystals and oblique-texture patterns in a special study of Tl_2Se; the constants of the tetragonal cell (a = 8.52 ± 0.02 A and c = 12.6 ± 0.03 A) are exactly those found from x-ray studies, which provided a means of checking the composition of the films. The unit cell contains the Tl_2Se units. The absences correspond to space group $P4/ncc - D_{4h}^8$.

The analysis was based on 107 reflections, whose intensities were estimated in part on the microphotometer and in part visually by reference to a series of exposures. First, projections and two-dimensional sections of the F^2 series were constructed in order to obtain a general picture of the structure; further projections and sections of the potential were constructed to get a more exact picture. Alternating planes parallel to xy0 are built up from the 16 Tl atoms and 8 Se atoms in the unit cell. In each layer the Tl (Se) atoms lie at the corners of rhombs elongated along one diagonal or the other. Let a and b denote layers with these two modes of elongation; then the sequence of layers along c is Tl(a)Se(b)Tl(a)Tl(b)Se(a)Tl(b)...The residual four Tl atoms and two Se atoms in each cell form linear groups along the fourfold axes at $0\,^1/_2\,z$ and $^1/_2\,0\,z$; in these groups the Se atoms are arranged at random with weight $^1/_2$, so the phase could vary in composition as regards increase in the Se content. The positions obtained for space group P4/ncc are Tl at 16(g) with x 0.140, y 0.148, z 0.081; Se at 8(f) with x 0.34; Tl at 4(c) with z 0.25; and Se at 4(c) with z 0. The main interatomic distances are Tl-Tl 3.24 to 4.71 A, Se-Se 3.85 to 4.50 A, and Tl-Se 2.80 to 3.28 A.

The phase $Tl_2Sb_2Se_4$ or $TlSbSe_2$ is formed [24] when alloys containing Tl_2Se and Sb_2Se_3 in various ratios are are distilled; it is produced in pure form when the ratio is 1:1. The pattern of Fig. 9 gives a = 4.18 A, b = 4.50 A, c = 12.00 A, V = 225.7 A^3 (orthorhombic). The density of the original alloy was 6.988 g/cc, which corresponds fairly exactly to one $Tl_2Sb_2Se_4$ unit per unit cell. The data for Tl_2Se and Sb_2Se_3 indicate that the volumes of those formula units are Tl_2Se-92 A^3; Sb_2Se_3-133.7 A; 92 + 133.7 = 225.7A, which agrees exactly with the volume assigned to one $Tl_2Sb_2Se_4$ unit.

The x-ray pattern of a specimen of the original alloy contained about 10 lines superimposed on a strong background. The d_{hkl} for those lines agree well with the d_{hkl} found from the strongest reflections on the oblique-texture electron-diffraction patterns.

The absence on the latter patterns could correspond to group Pmna D_{2h}^7 or to group Pna – C_{2v}^9; the first was selected for further study. The positions selected initially on the basis of geometry are

$$Tl \text{ in } 2(c) - {}^1/_2\,{}^1/_2\,0 \text{ and } 0\,{}^1/_2\,{}^1/_2;\ Se \text{ in } 2(a) - 000 \text{ and } {}^1/_2\,0\,{}^1/_2.$$

Together these form a side-centered lattice. The Se atoms were assigned to the fourfold positions (h) having two parameters. The F^2 series were used in most of the subsequent work; projections on the 001 plane were constructed, as were sections of the three-dimensional series, which were found to confirm the above choice of positions for Tl and Sb (y ≈ 0.5 and z ≈ 0.26 for Se). The parameters were found more exactly by computing a section of the F series for the plane y = $^1/_2$ (Fig. 10) and minimizing R. The final z is 0.272; if we neglect certain weak spots of hkl type with h + l ≠ 2n, we can take y to be 0.5, in which case the structure can be described in group Cmmm – D_{2h}^{19}. The structure is built up from centered grids of Tl and Sb atoms alternating along c, there being zigzag chains of Se atoms extending along a (Fig. 11). The Se-Se distance in these chains (2.15A)

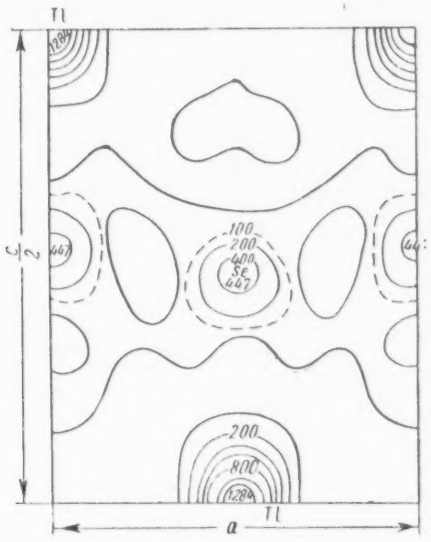

Fig. 10. The structure of $Tl_2Sb_2Se_4$. Section of the three-dimensional potential in the plane y = $^1/_2$.

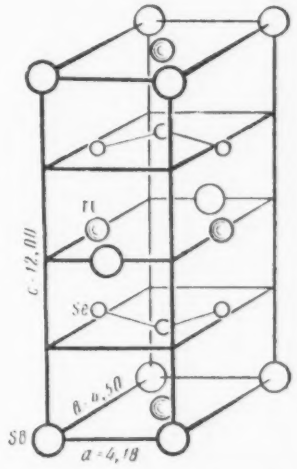

Fig. 11. The structure of $Tl_2Sb_2Se_4$.

is somewhat less than that distance in selenium (2.32 A), which points to the presence of strong homopolar bonds in the chains. The Tl-Sb distance (3.07 A) in the grids falls between the sum of the ionic radii and the sum of the homopolar radii. The Tl-Se distance (2.74 A) between the Se chains and the grids is equivalent to a fairly weak interaction.

Khitrova and I [26] have examined a phase that differs from the above in having some of the Sb replaced by As. We found that the composition could be established from the electron-diffraction results. Films of the four-component material were prepared by distilling specimens made under vacuum in quartz tubes [20-22].

Two alloys made in this way gave two series of films differing somewhat in structure (or composition). Cool collodion was used as the backing in order to avoid any loss of volatile components; the films were largely amorphous or disordered and would crystallize only on prolonged annealing. The arsenic favored the production of amorphous films that were slow to crystallize. It is likely that a macroscopic specimen could never become fully ordered, because even these thin films were difficult to crystallize fully. The patterns given by the four-component films showed an unusually strong background and a rather rapid fall in intensity with increase in $\sin\theta/\lambda$. However, the contrast was quite good, and the number of spots was sufficient to establish the structure. In general the patterns were very similar to those given by $Tl_2Sb_2Se_4$.

The patterns given by the two sets of films were worked up to give two slightly different orthorhombic cells, namely I. a = 4.15, b = 2.48, c = 11.85 A; II. a = 3.99, b = 4.43, c = 11.55 A.

Comparison with $Tl_2Sb_2Se_4$ shows that the As atoms in part replace the Sb atoms (As has the smaller atomic radius) and that the As content of I is less than that of II. These conclusions disagree with those drawn from large specimens, namely that the arsenic forms only an amorphous component $Tl_2As_2Se_4$ and does not form a crystalline phase.

The F^2 series were used in most of the work on I, which we found to resemble $Tl_2Sb_2Se_4$, with z_{Se} 0.266. The heights of the peaks on a section of the potential indicate that As replaces Sb at random.

Similar results were obtained for II; the compositions of the two phases were established by minimization, the best fit being obtained for 20% arsenic in I and 75% in II. These results may relate only to the crystalline component; the rest of the As may form an amorphous component of the composition quoted above, which would give rise to the diffuse background.

The number of reflections was rather smaller than is usual, which may have been caused by some random disorder in the structures. In part that disorder is caused by replacement of the Sb, so it is surprising that there is no continuous change in the lattice constants; instead, two phases with distinct lattice constants occur.

These results are important in relation to the discovery of an extensive class of amorphous semiconductors [22]. We still lack good methods of determining the short-range order for an amorphous solid containing several kinds of atoms. Ternary systems of general formula $A^{I}B^{V}X^{VI}$ (in which the roman numerals denote the groups of the periodic system) can have Tl for A^{I}, in which case disordered phases with the structure of NaCl are produced. It is not clear whether these phases are stable above some temperature or are merely metastable. The NaCl structure has been reported [44] for disordered phases $TlSbS_2$ and $TlBiSe_2$; annealing produces an ordered phase of low symmetry in the second case. The same paper gives a review of published work on compounds with that general formula and the NaCl structure.

Phases with Structures of GaS type.

The structure of GaS has the following parameters [27]: a 3.57, c 15.47 A, Z = 4; space group $P6_3/mmc - D_{6h}^4$. Positions of Ga and S 4(f), z_{Ga} 0.17, z_S 0.60. Hexagonal layers of Ga and S alternate along c; if we de-

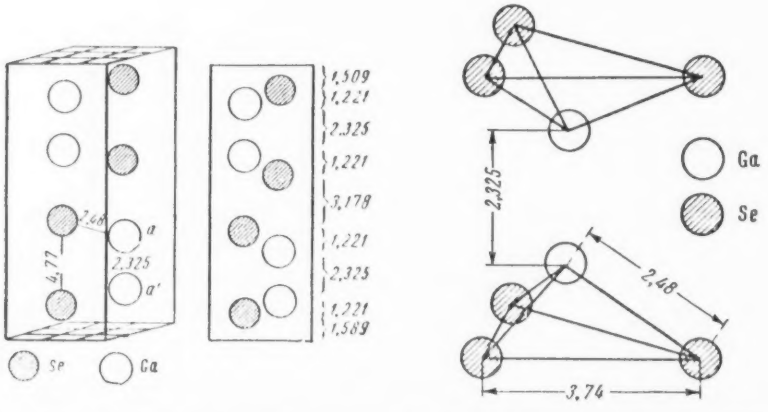

Fig. 12. The GaS structure type (GaSe, InSe): general view of the structure and coordination of the Ga(In) atoms.

note the layers by A and B for sulfur and by a and b for gallium [each atom of layer A(a) lies opposite the center of a hole formed between three atoms in layer B(b)], then the sequence of layers (Fig. 12) is

$$\ldots B \mid AbbA \mid BaaB \mid AbbA \mid BaaB \mid A \ldots$$

Thus the structure consists of layers, sets of which (those separated by vertical lines) are only weakly bound together. The distance between adjacent S atoms in adjacent layers A and B is 3.73 A, as against a sum of about 2.10 A for the atomic radii. Each Ga atom lies at the corner of a three-faced pyramid having S atoms at its base; the S-S distance in a layer is 3.09 A, the Ga-S 2.34 A (sum of the atomic radii 2.37 A, sum of the ionic radii 2.36 A). The shortest Ga-Ga distance along a vertical line is 2.46 A (diameter of the atom 2.52 A), so each Ga atom has fourfold coordination (as in ZnS).

The structure of GaSe has been reported [28], but the results are not reliable; two forms were reported, one hexagonal with a 3.735, c 15.887 A and the other orthorhombic with a 3.74, c 23.862 A.

A characteristic feature is that long times are needed for ordering and crystallization, as in phases containing arsenic. The electron-diffraction results are of value here. We have found [29] that specimens can be prepared by subliming GaSe or by allowing the very fine particles in an aqueous suspension to settle out on collodion. The hexagonal lattice has a 3.74 and c 15.89 A (very nearly the values for GaS); the orthorhombic phase was not detected in thin films.

Every pattern had two types of spot (sharp and diffuse), the latter corresponding to $h - k \neq 3n$ with $l \neq 0$. A distinctive feature was the large number of absences (far more than would be expected for any hexagonal space group), namely any hkil, 000l for $l = 2n$ only, hh2hl only for $l = 2n$, and khil with $h - k = 3n$ only for $l = 2n$. These absences are possible in groups $P6_3/mmc$, which was the one we chose.

The intensities of the sharp spots were estimated visually; those of the diffuse, by means of a microphotometer (the readings were corrected for the large half-width). The F^2 and F series were used to check that the structure is of GaS type, but Ga and Se are almost equal in scattering power, so the heights of the peaks could not be used to assign the positions to Ga and Se. This assignment was made in a later paper [30] concerned with InSe. The Ga atoms in GaSe occupy the same positions as in GaS, and the Se those of S; here $z_{Ga} = -0.10$ and $z_{Se} = 0.117$ (the latter is slightly different from the values for S). The probable error of the z cannot be estimated reliably, but it is not likely to exceed 0.03-0.05 A.

Semiletov has obtained interesting results for In-Se, which gives rise to a GaS structure. He distilled an alloy having the composition InSe onto NaCl, and obtained films which, when annealed, had a hexagonal structure with a 4.03 and c 16.90 A (Figs. 13 and 14).

However, x-ray studies in In-Se alloys indicate an orthorhombic symmetry for InSe a = 4.05, c = 25.00 A $\approx {}^3/_2 \cdot 16.90$ A.

The electron-diffraction patterns given by InSe and GaSe are extremely similar; they show the same absences and diffuseness (Figs. 13 and 14). If we assume that there are four InSe units in the cell and that the space group is $P6_3/mmc - D_{6h}^4$, we can test the coordinates found for GaS and GaSe and then use the F^2 series to test the result. A section along z clearly revealed differences in the heights of the peaks, and it was possible to assign the In to the center of the pyramid having Se atoms at the base and In at the vertex. The parameters found from the F^2 series were revised by minimizing R; they are $z_{In} = 0.157$ and $z_{Se} = 0.102$. Then the In-In distance within the pyramid is 3.16 A (diameter of In 2.88 A), while the In-Se distance is 2.50 A (sum of the tetrahedral covalent radii 2.58 A).

The tetrahedral coordination characteristic of ZnS structures has a bearing on the position of the atom at the center of the pyramid. Semiletov supposes that the pair of In atoms in the pyramid in InSe are to be considered as an ion In_2^{4+}, whence it follows that the formula should be put as In_2Se_2.

It may be that structures of GaS type resemble those of ZnS type in having bonds of intermediate character; in the second case the insertion of a heavier atom makes the bonds more nearly metallic, whereas in the first it makes them more ionic.

Other Semiconductors

Oxidation processes in alloys are of interest in connection with certain processes used in electronics and semiconductor technology.

It has been found [31] that unoxidized Ag-Mg (I) and Cu-Mg (II) alloys have slightly high lattice constants $a_I = 4.14$ A and $a_{II} = 3.69$ A, because the atomic radius of Mg exceeds the radii of copper and silver. These values do not change when the outer layers are removed by etching or polishing.

The Mg diffuses to the surface and is oxidized to MgO when these alloys are annealed at high temperatures; the process can continue until no magnesium metal remains in the alloy.

A similar process has been observed [32] for Mg-Bi, Mg-Sb, and Mg-Sn alloys; these systems contain respectively the compounds Mg_3Bi_2, Mg_3Sb_2, and Mg_2Sn, of which the first two have structures of La_2O_3 type, while the third is antiisomorphous to CaF_2. But these compounds are unstable; they decompose when they react with oxygen. The components of any of these compounds may be evaporated onto glass to give a film that varies in composition along its length; the central area rapidly becomes transparent when atmospheric oxygen acts on it, and the resistance meanwhile rises by 7-10 orders of magnitude. Electron-diffraction results show that the process is associated with the diffusion of Mg atoms to the edges of the crystals of those compounds; MgO is formed and insulates the residual particles of metal. Here Mg behaves as in Mg-Ag and Mg-Cu alloys, which is very surprising, because in the one case we have definite compounds whereas in the other we have solid solutions. In Mg-Sb films the Mg_3Sb_2 breaks up to yield amorphous Sb, even though the thickness of the film may exceed greatly the limiting thickness for amorphous antimony. Here the insulating films of MgO stabilize the dispersed particles of Sb.

This conclusion is confirmed by results for thin films of Sb with Al, Be, and Cr [6]. The latter three metals oxidize rapidly and stabilize the grains of amorphous Sb.

PbS, PbSe, and PbTe are also oxidized in certain processes; PbS has been examined in most detail [33, 34]. The oxides of lead are very labile (they form various phases, often containing water or hydroxyl); moreover, little is known about the oxygen-sulfur compounds of lead, so a detailed and precise study is very difficult. There is little doubt as to the existence of phases $PbO \cdot PbSO_4$, $4PbO \cdot PbSO_4$, and PbO; PbO and $Pb(OH)_2 \cdot PbCO_3$ are also possible. Wilman [33] supposes that small deviations from the stoichiometric composition are important (these deviations are not detectable in terms of the lattice constants), as well as the distribution taken up in the PbS by the $PbO \cdot PbSO_4$. Vertsner [34] considers that the heating conditions are most important, because these produce various phases containing oxygen and having various distributions. He has detected lines that cannot be assigned to any known phase.

Boettcher et al [35] have studied phase transitions in the systems Ag-S, Ag-Se, and Cu-Se for the compounds Ag_2S, Ag_2Se, and CuSe, which have typical defect structures. The room-temperature orthorhombic phases become cubic at higher temperatures; intermediate (often tetragonal) structures are observed near the transition temperatures. The following phases have been demonstrated by means of x-ray methods for Ag_2S. Near 180°C there exists a cubic phase with $\underline{a}$ 4.88 A; below that temperature there is an orthorhombic one with $\underline{a}$ 4.77, $\underline{b}$ 6.92, and $\underline{c}$ 6.99 A (or $\underline{c}$ 6.88 A in another paper). The cubic phase has Z = 2 (four Ag and two S in the unit cell); the S atoms are in fixed positions, but the four Ag atoms are randomly distributed over 42 possible positions. The same may be true for the orthorhombic phase. Results have also been given [36] for the structure of the monoclinic β phase.

Electron-diffraction studies have confirmed that the transition temperature is 180°C and have provided the parameters of the tetragonal intermediate structure formed near 180°C. They are $\underline{a}$ 4.77 A and $\underline{c}$ 6.90 ($= 4.88\sqrt{2}$) A, and they show that this structure is closely related to those of the stable phases.

Two phases have been established for Ag_2Se (transition point 133°C) by x-ray methods. The cubic (high-temperature) form with $\underline{a}$ 4.98 A has a structure similar to that of Ag_2S, but the distribution of the Ag atoms is not entirely random. No x-ray results are available for the low-temperature form. The electron-diffraction results are as follows. A cubic phase and several tetragonal phases have been reported from kinetic studies for the Ag-Se system [36]; the transition point (cubic to tetragonal) is about 133°C, and the cubic form has $\underline{a}$ 4.98 A. Hysteresis occurs when the specimens are run through heating cycles. The tetragonal cells are as follows I. a = 7.06 and c = 4.98 A; II. a = 4.98, c = 4.78 A; III. a = 7.06 and c = 4.67 A; IV. a = 4.98 and c = 4.85 A.

Now $4.38 = 7.06/\sqrt{2}$, which implies that the cubic phase is closely related to the tetragonal phase. The low-temperature orthorhombic form was not detected.

On the other hand, ordinary methods have been applied to Ag-Se films [37] to demonstrate that a cubic phase is formed above 140°C (a 4.978 A); diffusion of Se into Ag at room temperature over an extended period gives an orthorhombic form whose oblique-texture pattern corresponds to a = 4.978 A. No detailed study was made of this phase.

A point here is that kinetic methods cannot be applied to equilibrium states and stable phases when those states or phases are produced only as the result of prolonged diffusion, ordering, or recrystallization.

Ag-Te films made in the same way have been examined [38]; the results agree with x-ray data in indicating that cubic Ag_2Te (a 6.58 ± 0.03 A) occurs above 150°C, the phase existing below that temperature being of low symmetry (no results are available).

The CuSe system has been examined by Boettcher et al [35]. Several phases very similar in structure to Ag_2Se and Ag_2S are formed between the compositions Cu_2Se and $Cu_{1.8}Se$. The work is as yet unfinished, so I present only certain results without detailed discussion. At room temperature Cu_2Se has a complex structure so far unexamined, which goes over to a cubic side-centered form with a 5.84 A above 110°C. The structure consists of a rigid framework of Se atoms, the Cu atoms being randomly distributed over a large number of possible positions. A tetragonal phase appears at room temperature (a = 11.43, c = 11.72 A) if the copper content is reduced to $Cu_{1.96}Se$; a cubic one (composition Cu_xSe, $x < 1.19$, a 5.80 A) replaces it.

The electron-diffraction results indicate that there are several different tetragonal and cubic structures that differ in the distribution of the Cu atoms (which is not always random). The various possible positions in the Se framework have different volumes, so the lattice parameters vary with the distribution.

Thin Films and Surfaces of Monocrystals of Ge

Several studies have been made on monocrystals and thin evaporated films of germanium in the last five to eight years. These studies have two important aspects. On the one hand they represent a method of testing the structure of an important semiconductor, and on the other they form a method of solving some general problems of the structures of real crystals (e.g., the nature and distribution of the defects or dislocations).

The diffraction pattern obtained in reflection from a face of a monocrystal is controlled by the actual structure of that face. For example, a diamond gives patterns showing many sharp-edged lines and bands, as well as bands at certain azimuths. A simple theory is used as the basis from which to judge the degree of perfection of the face, by which is meant mainly the absence of block structures in the surface layers. However, some results obtained with thin films and monocrystals of Ge indicate that our ideas need modification.

We [39] have studied the effects of polishing and etching on the structure of the surface of a monocrystal of Ge. A freshly cleaved surface gives a reflection pattern such as that seen in Fig. 15; the pattern resembles that given by a diamond. The lines are much weaker, and a point-network of reflections is seen, when the surface has been formed by cutting. This is evidence for plastic deformation in the surface layer; the individual blocks show a scatter in orientation of 2-3°. Rings characteristic of a polycrystal appear when the surface is ground (fine detritus on the surface is responsible). The original structure is gradually restored when various etching agents are allowed to act for long times at fairly high temperatures. At first we get again the point-network, which degenerates to separate bright spots and finally reverts to the system of lines and bands (Fig. 16).

Vacuum-evaporated films of Ge have been examined [40, 41]; the vapor condenses to amorphous films when various backings are used at temperatures below 370°C. Polycrystalline films are formed above that temperature. Rapid deposition on materials heated to 500-900°C produces textured films; an important feature here is the direction of incidence of the molecular beam. The crystals of Ge present their {110} and {100} faces to surfaces of silicon carbide and polished graphite, their {111} and {100} faces to glass, and their {100} faces to polished corundum at 700-800°C.

Mosaic monocrystals giving point patterns are formed on cleavage surfaces of calcite and mica. The orientations are

$$\{111\}_{Ge} \parallel \{10\bar{1}1\}_{CaCO_3} \;\&\; \{111\}_{Ge} \quad \text{or} \quad \{110\}_{Ge} \parallel \{0001\}\ \text{m}\,.$$

An oriented film is formed when Ge is distilled onto a polished and etched surface of a Ge monocrystal. Mosaic-monocrystal structures are formed at temperatures slightly exceeding 500°C; the structures are more perfect (to judge from the reflection patterns) if the crystal is at 700-800°C. Films of this kind up to 20μ thick have been found [42] to deviate very considerably in properties from the original highly pure material (resistivity about 0.02 ohm-cm, Hall constant about 3 cm^3/coulomb, carrier (hole) mobility 150 cm^2/sec). In every case the films show hole conduction, as has been reported elsewhere [43] (in the latter work the effects were ascribed to surface levels present in the small crystals).

Etch figures have been examined with electron and optical microscopes and have revealed that films of Ge contain symmetrically arranged defects. The transition from point patterns to line patterns is accompanied by a great increase in the size of the blocks (perhaps by $1\text{-}1^1/_2$ orders of magnitude) and by the adoption of a fairly highly ordered array.

Electron-diffraction methods may prove very useful in establishing the real structure and the degree of perfection of monocrystals of Ge and Si.

I wish to thank B. K. Vainshtein and S. A. Semiletov for valuable comments made on the draft of this paper.

LITERATURE CITED

1. A. F. Ioffe, Physics of Semiconductors [in Russian] (Izd. AN SSSR, Moscow, 1957).
2. Z. G. Pinsker, Electron Diffraction [in Russian] (Izd. AN SSSR, Moscow, 1949).
3. B. K. Vainshtein, Structural Electron Diffraction [in Russian] (Izd. AN SSSR, Moscow, 1955).
4. L. I. Tatarinova and Z. G. Pinsker, Doklady Akad. Nauk SSSR 95, 265 (1954); L. I. Tatarinova, Trudy Inst. Kristall. Akad. Nauk SSSR 11, 104 (1955).
5. G. A. Kurov and Z. G. Pinsker, Kristallografiya 1, 407 (1956).
6. L. S. Palatnik and V. M. Kosevich, Doklady Akad. Nauk SSSR 121, 97 (1958); Kristallografiya 3, 709 (1958); 4, 42, 673 (1959).
7. H. Hendus, Z. Phys. 119, 265 (1942).
8. I. G. Stoyanova and A. I. Frimer, Zavodskaya Lab. 18, 1472 (1952).
9. L. I. Tatarinova, Trudy Inst. Kristall. Akad. Nauk SSSR 11, 101 (1955).
10. S. A. Semiletov, Trudy Inst. Kristall. Akad. Nauk SSSR 11, 115 (1955).
11. Z. G. Pinsker, O. S. Orekho, and A. I. Miller, Kristallografiya 1, 239 (1956).
12. S. A. Semiletov, Kristallografiya 1, 306 (1956).
13. B. K. Vainshtein and G. G. Lemmlein, Trudy Inst. Kristall. Akad. Nauk SSSR 6, 203 (1951).
14. S. A. Semiletov and M. Rozsival, Kristallografiya 2, 287 (1957).
15. G. A. Kurov and Z. G. Pinsker, Zh. Tekh. Fiz. 28, 29 (1958).
16. S. A. Semiletov, Trudy Inst. Kristall. Akad. Nauk SSSR 10, 181 (1950).
17. L. Pauling, Nature of the Chemical Bond [Russian translation] (Goskhimizdat, Moscow, 1947).
18. N. V. Belov, Doklady Akad. Nauk SSSR 23, 171 (1938).
19. S. A. Semiletov and Z. G. Pinsker, Zhur. Tekh. Fiz. 25, 2336 (1955).
20. B. T. Kolomiets and N. A. Goryunova, Zhur. Tekh. Fiz. 25, 984 (1955).
21. N. A. Goryunova and B. T. Kolomiets, Zhur. Tekh. Fiz. 25, 2069 (1955).
22. N. A. Goryunova, B. T. Kolomiets, and V. P. Shilo, Zhur. Tekh. Fiz. 28, 982 (1958).
23. N. W. Tideswell, F. H. Kruse, and J. O. McCullough, Acta Cryst. 10, 99 (1957).
24. Z. G. Pinsker, S. A. Semiletov, and E. N. Belova, Doklady Akad. Nauk. SSSR 106, 1003 (1956).
25. M. M. Stasova and B. K. Vainshtein, Kristallografiya 3, 141 (1958).
26. Z. G. Pinsker and V. I. Khitrova, Kristollografiya 1, 300 (1956).
27. H. Hahn and G. Frank, Z. Anorgan. Allgem. Chem. 278, 340 (1955).
28. K. Schubert, E. Dorre, and M. Kluge, Z. Metallkunde 46, 216 (1955).
29. L. I. Tatarinova, Yu. K. Auleitner, and Z. G. Pinsker, Kristallografiya 1, 537 (1956).
30. S. A. Semiletov, Kristallografiya 3, 288 (1958).
31. B. S. Kul'varskaya and B. K. Vainshtein, Trudy Inst. Kristall. Akad. Nauk SSSR 11, 97 (1955).
32. G. A. Kurov, Doklady Akad. Nauk SSSR 94, 207 (1954); G. A. Kurov and Z. G. Pinsker, Doklady Akad. SSSR 94, 439 (1954).

33. H. Wilman, Proc. Phys. Soc. 60, 117 (1948).
34. V. N. Vertsner, Kristallografiya 2, 497 (1957).
35. A. Boettcher, G. Haase, and H. Treupel, Z. Angew. Phys. 7, 478 (1955).
36. A. J. Fruen, Z. Krist. 110, 136 (1958).
37. U. Zorll, Ann. Phys. 16, 7 (1955).
38. U. Zorll, Ann. Phys. 14, 385 (1954).
39. S. A. Semiletov and Z. G. Pinsker, Kristallografiya 1, 209 (1956).
40. G. Haas, Phys. Rev. 72, 174 (1947); J. Thornhill and K. Lark-Horowitz, Phys. Rev. 82, 762 (1952).
41. S. A. Semiletov, Kristallografiya 1, 542 (1956).
42. G. A. Kurov, S. A. Semiletov, and Z. G. Pinsker, Kristallografiya 2, 59 (1957).
43. S. A. Semiletov and L. I. Mann, Kristallografiya 4, 414 (1959).

USE OF NUCLEAR QUADRUPOLE RESONANCE IN CHEMICAL CRYSTALLOGRAPHY

G. K. Semin and É. I. Fedin

Institute of Organoelement Compounds, Academy of Sciences of the USSR
Translated from Zhurnal Strukturnoi Khimii, Vol. 1, No. 2, pp. 252-267,
July-August, 1960
Original paper submitted December 14, 1959

This review deals with applications to molecular structure and crystal structure. The first part is concerned with the main features of the effects responsible for nuclear quadrupole resonance spectra; relationships needed in practical work are presented. The second part* gives a survey of the results so far obtained and brief descriptions of apparatus.

I. NATURE OF THE EFFECT

1. Energy Levels

Dehmelt and Kruger [1] made the first observations of nuclear quadrupole resonance (NQR) in 1949; it is one of the more recently discovered forms of magnetic resonance [2, 3]. It forms a division of spectroscopy and is concerned with the energy levels of solids; those levels have spacings corresponding to electromagnetic frequencies in the range from 1 to 1000 Mcps. First we must consider the nature of these levels.

Very often a nuclide has nuclei whose form differs from spherical; the electric quadrupole moment of the nucleus is a measure of the deviation from spherical form:

$$Q = \frac{1}{e}\int \rho\,(3z_m^2 - r^2)\,dx\,dy\,dz \qquad (1)$$

in which e is the electronic charge, ρ is the density distribution of the charge in the nucleus, $r^2 = x^2 + y^2 + z^2$, and z_m is an axis coincident in direction with the nuclear spin vector I.

We see that Q is positive if the nucleus is elongated along the spin vector and is negative if the nucleus is foreshortened in that direction (Fig. 1).

Nuclear theory [4] shows that this moment is related to I; Q = 0 if I is 0 or $^1/_2$, and Q differs from zero only if $I \geq 1$. Table 1 gives the values at present known; those nuclides with M < 40 not appearing in Table 1 are known for certain to have Q = 0.

Suppose we have an atom having a finite moment present in a molecule forming part of a crystal. In Fig. 2 that atom is A; it is bound to atom A_1 by a covalent bond. Along the direction of that bond 0z there is a strong and inhomogeneous electric field specified by the field gradient $q_{zz} = \partial^2 V/\partial z^2$, in which V is the electrostatic potential produced by nearby charges. Strictly speaking, q is a tensor quantity having nine components in

* Part II appears in No. 4 of this journal for 1960.

TABLE 1.

Atomic No.	Element	Mass No.	Natural abundance, %	Spin	Magnetic moment in magnetons		Gyromagnetic ratio	Quadrupole moment, 10^{-24} cm^2		Ratio of quadrupole moments
					[43]	[44]		[43]	[44]	
1	H(D)	2	0,015	1	+0,857348 ± 3	+0,857392	653,5	+0,00274	+0,002738	
3	Li	6	7,2	1	+0,82189 ± 4	+0,82193	626,7	+0,0005 ± 5	—	$Q_6/Q_7 = 1,9 \cdot 10^{-2}$
»	»	7	92,7	3/2	+3,2559 ± 1	+3,25598	1655,0	−0,012	—	
4	Be	9	100	3/2	−1,1774 ± 8	−1,1772	598,7	+0,02	+0,02	
5	B	10	18,83	3	+1,8004 ± 7	+1,8004	457,6	+0,06	+0,086	$Q_{10}/Q_{11} = 2,084$
»	»	11	81,17	3/2	+2,6886 ± 3	+2,68798	1367,0	+0,036	+0,042	
7	Na	14	99,62	1	+0,40365 ± 3	+0,4036	307,7	+0,02	+0,02	
8	O	17	0,4	5/2	−1,8929 ± 2	−1,89295	577,2	−0,004	−0,005	
11	Na	23	100,0	3/2	+2,2171 ± 2	+2,2161	1126,7	+0,11	+0,10	
13	Al	27	100,0	5/2	+3,6408 ± 4	+3,63853	1110,0	+0,156	+0,150	
16	S	33	0,74	3/2	+0,6429 ± 1	+0,6427	326,7	−0,065	−0,067	
17	Cl	35	75,4	3/2	+0,8219 ± 2	+0,82086	417,3	−0,0789	−0,085	
»	»	37	24,6	3/2	+0,6841 ± 2	+0,68330	347,4	−0,0621	−0,067	$Q_{35}/Q_{37} = 1,2688$
19	K	39	93,2	3/2	+0,391 ± 1	+0,39094	198,7	+0,14	—	$Q_{39}/Q_{41} = 1,220$
»	»	41	6,8	3/2	+0,215 ± 1	+0,21506	109,2	—	—	
21	Sc	45	100,0	7/2	+4,749			−0,22 *		
23	V	51	100,0	7/2	+5,1478 ± 5	+5,138	1121,0	—	+0,3	
25	Mn	55	100,0	5/2	+3,4677 ± 4	+3,4611	1056,0	0,5	+0,4	
27	Co	59	100,0	7/2	+4,6482 ± 6	+4,6389	1011,0	—	+0,5	
29	Cu	63	68,9	3/2	+2,2262 ± 4	+2,2213	1131,0	−0,16	−0,16	$Q_{63}/Q_{65} = 1,0806$
»	»	65	31,1	3/2	+2,3845 ± 4	+2,3790	1213,0	−0,15	−0,14	
31	Ga	69	60,1	3/2	+2,017 ± 1	+2,0108	1023,0	+0,18	+0,24	$Q_{69}/Q_{71} = 1,5867$
»	»	71	39,9	3/2	+2,561 ± 1	+2,5549	1299,0	+0,11	+0,15	
32	Ge	73	7,8	9/2	−0,8767 ± 1	−0,87680	148,8	−0,21	−0,22	
33	As	75	100,0	3/2	+1,4347 ± 3	+1,43491	729,3	+0,3	−0,3	
35	Br	79	50,6	3/2	+2,1058 ± 4	+2,0990	1070,0	+0,36	+0,33	$Q_{79}/Q_{81} = 1,19707$
»	»	81	49,4	3/2	+2,2696 ± 5	+2,2626	1153,0	+0,28	+0,28	
36	Kr	83	11,5	9/2	−0,9704	−0,966	164,0	+0,15	+0,16	
37	Rb	85	72,8	5/2	+1,3532 ± 4	+1,3482	411,3	+0,3	+2,8	$Q_{87}/Q_{85} = 2,07$
»	»	87	27,2	3/2	+2,7501 ± 5	+2,7414	1397,0	+0,14	+1,4	

* From [62]

TABLE 1 (continued)

Atomic No.	Element	Mass. No.	Natural abundance, %	Spin	Magnetic moment in magnetons		Gyromagnetic ratio	Quadrupole moment, 10^{-24} cm^2		Ratio of quadrupole moments
					[43]	[44]		[43]	[44]	
41	Nb	93	100,0	9/2	+6,166 ± 3	+6,1435	1045,0	—	—	
49	In	113	4,5	9/2	+5,486 ± 3	+5,4962	931,1	+0,75	+1,18	Q_{115}/Q_{113}= 1,0146
»	»	115	95,5	9/2	+5,500 ± 3	+5,5074	933,1	+0,76	+1,20	
51	Sb	121	57,25	5/2	+3,3591 ± 5	+3,3416	1019,0	−0,5 −1,2	−1,3	Q_{123}/Q_{125}=1,27475
»	»	123	42,75	7/2	+2,5465 ± 5	+2,5334	551,9	−0,7 −1,5	−1,8	
53	I	127	100,0	5/2	+2,8086 ± 8	+2,7938	856,5	−0,6 ± 2	−0,61	
54	Xe	131	21,18	3/2	+0,70	+0,704	410,0	−0,12	−0,12	
55	Cs	133	100,0	7/2	+2,5771 ± 9	+2,5642	561,7	−0,003	−0,03	
57	La	138	0,089	5	−2,776 ± 3	+3,68	605,0	—	+3,0	
»	»	139	100,0	7/2		+2,7615	—	+0,3	+0,9	Q_{138}/Q_{139}=3,0
59	Pr	141	100,0	5/2	+3,9	+3,8	1160,0	−0,05	−0,054	
60	Nd	143	12,2	7/2	−1,0 ± 2	−1,0	220,0	1,2	—	
»	»	145	8,3	7/2	−0,65 ± 9	−0,62	140,0	1,2	—	
62	Sm	147	17,0	7/2	−0,68 ± 8	−0,68	147,0	0,72	—	
»	»	149	15,0	7/2	−0,55 ± 6	−0,55	119,0	0,72	—	
63	Eu	151	47,8	5/2	+3,4	+3,4	1000,0	+1,2	+1,2	
»	»	153	52,2	5/2	+1,5	+1,5	460,0	+2,5	+2,6	
68	Er	167	22,94	7/2	—	—	—	—	+10,0	
70	Yb	173	17,02	5/2	−0,65	−0,66	198,0	+3,9	+0,4	
71	Lu	175	97,5	7/2	+2,9 ± 5	+2,9	570,0	+5,9	+6,5	
»	»	176	2,60	7	—	+4,2	—	—	+8,0	
73	Ta	181	100,0	7/2	+2,1	+2,1	460,0	+6,0	+7,0	
75	Re	185	31,7	5/2	+3,1433 ± 6	+3,1438	958,4	+2,8	+2,9	Q_{185}/Q_{187}= 1,06
»	»	187	62,9	5/2	+3,1755 ± 6	+3,1760	968,1	+2,6	+2,7	
76	Os	189	16,1	3/2	+0,65	+0,65066	360,0	2,0	+2,0	
77	Ir	191	38,5	3/2	+0,17	+0,17	81,0	+1,5	+1,5	
»	»	193	61,5	3/2	+0,17	+0,17	86,0	+1,5	+1,5	
79	Au	197	100,0	3/2	+0,20	+0,14	69,1	+0,6	—	
80	Hg	201	13,18	3/2	−0,5590 ± 1	−0,607	308,0	+0,65	+0,5	
83	Bi	209	100,0	9/2	+4,0801 ± 5	+4,388	684,3	−0,4	−0,4	
92	U	235	0,715	(5/2)	—	—	—	—	—	

cartesian coordinates x, y, z; an exact mathematical description of the interaction between that inhomogeneous field and the aspheric nucleus is extremely complicated. The usual approach is to assume that q is axially symmetric with respect to z; i.e., that $\partial^2 V/\partial x^2 = \partial^2 V/\partial y^2$, and to select axes such that the tensor for q takes a diagonal form. Then quantum mechanics [5] may be used to show that the energy arising from Q in the field of q takes the form

$$E_m = \frac{eq_{zz}Q\,[3m^2 - I\,(I+1)]}{4I\,(2I-1)} \tag{2}$$

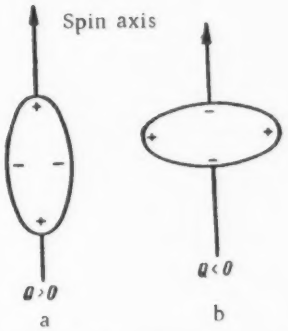

Fig. 1. Quadrupole configurations.

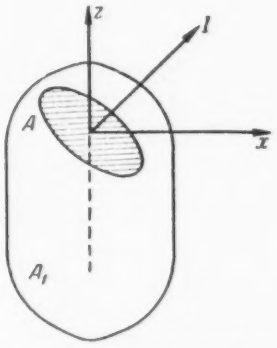

Fig. 2. Asymmetric nucleus in the inhomogeneous electric field of a molecule; z is the bond direction.

Here m is the magnetic quantum number, which takes 2I + 1 values between I and -I. We see from (2) that the energy levels are doubly degenerate with respect to m, because E_m depends only on |m|. For example, Table 1 and (2) show that N and Cl have only two energy levels each; transitions between those levels can produce only one emission or absorption line. Those transitions can be stimulated by an electromagnetic field whose quanta have the energy

$$h\nu = E_{(m)} - E_{(m-1)}. \tag{3}$$

The Boltzmann distribution implies $E_{(m-1)}$ level will be the more densely populated one; the difference in the population densities will be $E_{(m)}$, i.e., will be extremely small at room temperature. That difference is responsible for the absorption; the tendency for a field in accordance with (3) to produce transitions upwards will be greater than the tendency for the upper level to produce emission. Although the energy levels of (2) are electrical in origin, the transitions are caused by the interaction between the magnetic component of the field and the magnetic moment of the nucleus. The absorption line is usually very narrow, $\Delta\nu$ being such that $\nu/\Delta\nu \geq 10^4$. (The factors that influence the line width are dealt with below.)

From (2) and (3) we have the resonance frequency as

$$\nu_r = \frac{3eQq_{zz}}{4hI\,(2I-1)}\,(2|m_I| - 1) \tag{4}$$

in which m_I is the larger of the two magnetic quantum numbers for the transition. The quantity eQq/h is usually called the quadrupole coupling constant and is expressed in Mcps (Planck's constant is omitted in writing the quantity). Then we have $\nu_r = 3eQq/4$ for I = 1, eQq/2 for I = 3/2, and so on.

Very often q is not axially symmetric; then we use the asymmetry parameter $\eta = (q_{xx} - q_{yy})/q_{zz}$. In this case the formula for the energy levels is a function of I and is more complicated than (2). Table 2 gives equations that have been derived [5-7].

Formulas have been derived [2] for the resonance frequencies from the equations of Table 2; they are

TABLE 2.

I	Equation	Units of E
3/2	$E^2 - 3\eta^2 - 9 = 0$	$A = \frac{eQq_{zz}}{4I(2I-1)}$
5/2	$E^3 - 7(3+\eta^2)\,E^2 - 20(1-\eta^2) = 0$	$2A$
7/2	$E^4 - 42\left(1+\frac{\eta^2}{3}\right)E^2 - 64\,(1-\eta^2)\,E + 105\left(1+\frac{\eta^2}{3}\right)^2 = 0$	$3A$
9/2	$E^5 - 11(3+\eta^2)E^3 - 44(1-\eta^2)E^2 + \frac{44}{3}\,(3+\eta^2)^2 E + 48(3+\eta^2)\,(1-\eta^2) = 0$	$6A$

$$I = 1;\ \nu = \frac{3eQ\,(q_{zz})}{4} \cdot \left(1 \pm \frac{\eta}{3}\right)$$

$$I = {}^3/_2;\ \nu = \frac{eQ\,|\,q_{zz}\,|}{2} \cdot \left(1 + \frac{\eta^2}{3}\right)^{\frac{1}{2}}$$

$$I = {}^5/_2;\ \nu_1 = \frac{3eQ\,|\,q_{zz}\,|}{20} \cdot (1 + 1{,}09259)\,\eta^2 - 0{,}63403\,\eta^4)$$

$$\nu_2 = \frac{3eQ\,|\,q_{zz}\,|}{10} \cdot (1 - 0{,}20370\,\eta^2 + 0{,}16215\,\eta^4)$$

$$I = {}^7/_2;\ \nu_1 = \frac{eQ\,|\,q_{zz}\,|}{14} \cdot (1 + 3{,}63333\,\eta^2 - 7{,}26070\,\eta^4) \qquad (5)$$

$$\nu_2 = \frac{2eQ\,|\,q_{zz}\,|}{14} \cdot (1 - 0{,}56667\,\eta^2 + 1{,}85952\,\eta^4)$$

$$\nu_3 = \frac{3eQ\,|\,q_{zz}\,|}{14} \cdot (1 - 0{,}1000\,\eta^2 - 0{,}01804\,\eta^4)$$

$$I = {}^9/_2;\ \nu_1 = \frac{eQ\,|\,q_{zz}\,|}{24} \cdot (1 + 9{,}03333\,\eta^2 - 45{,}69070\,\eta^4)$$

$$\nu_2 = \frac{2eQ\,|\,q_{zz}\,|}{24} \cdot (1 - 1{,}338095\,\eta^2 + 11{,}72240\,\eta^4)$$

$$\nu_3 = \frac{3eQ\,|\,q_{zz}\,|}{24} \cdot (1 - 0{,}18571\,\eta^2 - 0{,}12329\,\eta^4)$$

$$\nu_4 = \frac{4eQ\,|\,q_{zz}\,|}{24} \cdot (1 - 0{,}08095\,\eta^2 - 0{,}004258\,\eta^4)$$

We see that the spectrum becomes more complicated as the spin increases. We cannot determine eQq and η from the resonance frequency of an unknown compound if $I = {}^3/_2$, but those quantities can be deduced (from the Zeeman effect) if a monocrystal of that compound is available. In all other cases the number of lines is sufficient to establish those quantities. We shall see below that both of those quantities give us valuable information about the molecule. Cohen [7] gives a table of energy levels for $0 \leq \eta \leq 1$.

Experiment gives us eQq_{zz} and η, which may appear at first sight very abstract quantities of little value to those concerned with molecular structure. However, even the early experiments demonstrated that eQq_{zz} and η are very sensitive to details of the structures of the molecule and crystal. We shall see in section 7 that q_{zz} is very sensitive to the structure of the electron shells and that eQq_{zz} gives us unique information about the degree of ionic character and (sometimes) the hybridization of covalent bonds. In many cases η enables us to estimate the π-electron concentration near the atom.

The most important feature is that these effects on eQq_{zz} and η are not small. For example, the frequencies for Cl^{35} in trichloromethane and dichloromethane respectively are 38.2809 and 35.9912 Mcps, whereas the frequencies themselves can be measured to six or seven significant figures. The η are found to vary from 0.05 to 0.8.

Nonequivalent positions in the unit cell give rise to well resolved distinct lines. For example, $CHCl_3$ gives resonances at 38.3081 and 38.2537 Mcps, which implies that the crystal contains molecules in two distinct sets of positions. These splittings exceed the line widths by one to two orders of magnitude. Phase transitions and other effects can be detected.

The results obtained in this way are dealt with systematically in the second part of this review.

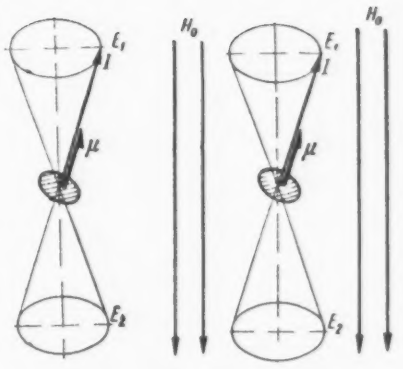

Fig. 3. Nuclear precession in the absence and in the presence of an external constant magnetic field H_0. On the left $E_1 = E_2$, on the right $E_1 > E_2$.

2. Zeeman Effect in NQR

The above description of quadrupole resonance may be illustrated by considering the precession of the nuclear spin about the bond direction 0z. Then the various E_m correspond to various angles between I and the axis of precession (Fig. 2). This model illustrates the degeneracy implied by (2), because, for a given m, the energy of the state in which I makes an angle θ with the axis does not differ from the energy for the state in which the angle is $180-\theta$.

However, an external fixed magnetic field H_0 produces a change in the picture; if H_0 is oriented as in Fig. 3, the angle θ corresponds to an energy higher than the energy corresponding to $180 - \theta$. Now the energy difference $\Delta E \ll kT$ for these two positions of $\vec{\mu}_I$, so the two levels will be populated and the degeneracy with respect to m has been removed. Thus the NQR line is split into two components by the external field (Fig. 3).

The ultimate effect of this splitting takes one form for a monocrystal and another for a polycrystalline material; in the first case the signals from all nuclei combine to give a resolved spectrum, whereas the random arrangement in a polycrystalline material merely causes the line to broaden, with the result that the peak strength of the signal is reduced. This behavior is used to identify the signal; a NQR line is broadened by a weak magnetic field, so the absence of broadening indicates that the line has another origin.

In the simplest case the field H_0 produces [7] a splitting

$$\Delta E = \pm m\mu_I H_0 \cos\theta / I, \tag{6}$$

in which θ is the angle between H_0 and the axis of q, and μ_I/I is the gyromagnetic ratio (417.214 cps/gauss for Cl^{35}). We see that the splitting is zero if H_0 lies at 90° to the axis of q. A more complicated case is that in which H_0 removes the degeneracy of an $E_{1/2}$ level; the states with $m = +\frac{1}{2}$ and $m = -\frac{1}{2}$ have $\Delta m = 1$ and both interact with H_0. Then H_0 produces mixed levels described by

$$E_{\pm} = \frac{eQq_{zz}}{4I(2I-1)}\left[\frac{3}{4} - I(I+1)\right] \pm \left[\cos^2\theta + \left(I+\frac{1}{2}\right)^2 \sin^2\theta\right]\frac{\mu_I}{2_I} H_0. \tag{7}$$

Now (7) implies that zero splitting cannot occur for any θ. Fig. 4 shows that the splitting produces four observed lines when $I = \frac{3}{2}$; the $E_+ \rightarrow E-$ transitions are not observed at ordinary H_0, because the corresponding frequency is less than ν_L by some two orders of magnitude. Fig. 4, with (6) and (7), gives us that the internal lines have a frequency separation

$$\nu_{\alpha\alpha'} = 3\frac{\mu_I}{I} H_0 \cos\theta + \frac{\mu_I}{I} H_0 \sqrt{\cos^2\theta + \left(I+\frac{1}{2}\right)^2 \sin^2\theta}. \tag{8}$$

Again, (8) implies that these two lines (the strongest) become one lying at ν_L for a certain θ; for $I = \frac{3}{2}$ that angle is given by (8) as $\theta = \sqrt{2}$, i.e., $\theta = 54°44'$. This feature is used in structure studies on monocrystals; the crystal is rotated to find the directions for H_0 that give no splitting, and those directions form a cone whose axis is the direction of the bond.

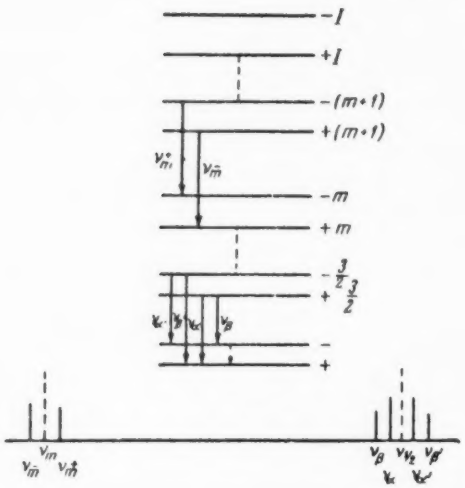

Fig. 4. Zeeman splitting of quadrupole levels.

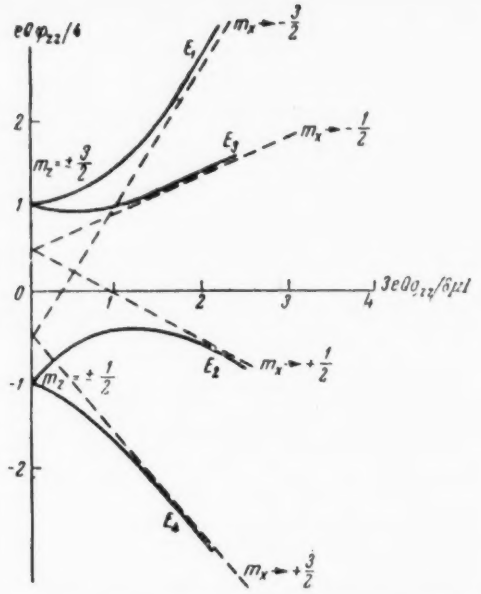

Fig. 5. Nonlinear variation of splitting with H_0 in strong fields.

Formulas (6), (7), and (8) are correct for H_0 small. Fig. 5 (from [10]) shows results for $I = {}^3/_2$, $\eta = 0$ and $\theta = 90°$. Here the abscissa is H_0 in relative units. This orientation of the field is such that the energy levels can be calculated [11-13] by means of a second approximation in perturbation theory. We see that the splitting varies very nonlinearly with field for $H_0 \to 3eQq_{ZZ}/8\mu_I$. This field is $H_0 = \frac{3 \cdot 108 \cdot 10^6 \cdot 6{,}6 \cdot 10^{-27}}{8 \cdot 0{,}82 \cdot 0{,}5 \cdot 10^{-23}} = 65400$ gauss for Cl^{35}; by strong fields are meant those with $H_0 = (5 - 15) \cdot 10^3$ gauss in practical work, so formulas (6), (7), and (8) are quite adequate in all cases.

3. Line Width

The difference in population density corresponding to (2) is extremely small, but the resonance is very often detectable at or above 300°K, so we must conclude that $\Delta\nu$ is very small ($\nu_I/\Delta\nu \geq 10^5$) for an isolated molecule. If the width were unchanged in the crystal, it would always be possible (though perhaps troublesome) to detect the resonance, and the sensitivity would not need to be any higher than the value commonly found in NMR spectrometers, which have been commercially available for some years.

However, things are not always so favorable; the line is often much broadened, with the result that the peak height is reduced (that the sensitivity must be much higher). The problem of line width is that of detecting the resonance at all; it requires the most careful attention. The main factors affecting the line width are dealt with in the next section.

4. Static Factors Affecting the Line Width

Magnetic interactions are the most important; the nuclei surrounding the species of interest may have magnetic moments as well, so the local magnetic fields have to be considered. Those fields produce an internal Zeeman effect, which may appear either as a splitting or (more often) as a mere broadening (the strength and directions of the fields are decisive here). We may differentiate between direct magnetic dipole-dipole interactions and indirect interactions via the electrons in the bonds (the I bond effect).

The dipole-dipole interaction occurs between immediately adjacent nuclei, in which case a fine-structure is seen, as in the case of HIO_3 [14]. Here the effects of the fields of more distant nuclei are suppressed by the field H of the nucleus and cause only a certain broadening of the fine-structure components.

Alternatively, no dipole-dipole interaction may be possible between nearest neighbors, in which case the other nuclei having dipole moments produce only broadening. Koe et al [15] have discussed the natural line widths (those controlled by the lifetimes of the quadrupole states) and the broadening produced by dipole-dipole

interactions. If the line width found for some elements is that caused by the lifetime, then the ratio of the line widths for two isotopes of that element equals the ratio of the squares of the quadrupole moments. This principle has been extended [16, 17] in careful theoretical and experimental studies on $NaClO_3$ and NaBrO. Exact line-width calculations based on the work of Abragam et al [18] have shown that dipole-dipole interactions are responsible for the major part of the line width in each case, although the actual width is not very much larger than the natural width for $NaBrO_3$.

The indirect interaction can affect the line shape only via interactions confined within the molecule; the splitting is appreciable for Br_2, I_2, and ICl [19, 20]. Kozima et al [21] have discussed the splitting found for Br_2; theory predicts a spectrum with 18 lines (nine produced by Br^{79} Br^{79} and Br^{81} Br^{81}, and nine others produced by Br^{79} Br^{81}). The width of each line exceeds 10 kcps, so the spectrum cannot be resolved; experiment reveals a broad line on which can be seen three weak peaks, the shape of the line corresponding roughly with the calculated one. The interaction constant J is about 3 kcps.

It is stated [14, 15] that terrestrial fields can affect the line width in some cases; Koi has observed that the Earth's field broadens the very narrow line of $NaBrO_3$ (the line becomes narrower when that field is eliminated). Livingston and Zeldes report a similar effect for $KClO_3$, whose line is exceptionally narrow (width about 290 cps).

The third static factor is associated with defects and stresses in the crystal. Defects cause a random variation in q, and so the line is broadened. Stresses (e.g., produced by rapid growth, etc.) have the same effect, as Allen and Dean [22, 23, 26] were the first to observe. Wang [24] has found that the lines of Sb and Cl in $SbCl_3$ become broader when the temperature is reduced; he explains the effect in terms of stresses induced in the crystal. Fuke and Koi [16] have confirmed the effect, though they find that Wang's values for the line widths are wrong. We also find that those [24] results for the line width of Sb at room temperature are too small. Koi et al [25] have compared the measured line width for $KBrO_3$ with the one calculated on the basis of dipole-dipole interactions; they concluded that imperfections in the crystal account for a great deal of the broadening. [The systematic work of Duchesne and Monfils (on the effects of impurities) is dealt with below.] Das and Hahn [5] point out that an exact theory of this effect cannot be produced unless we know the law of the molecular interaction and the effects of that interaction on the electric field gradient. This interesting problem has not yet been solved.

5. Dynamic Factors Influencing the Line Width

The motion of the molecule in the crystal can affect the line width; thermal oscillations restrict the lifetime and control the natural line width. The effects are much smaller than those of the static factors, although such oscillations may also have effects resembling those of defects, namely may cause an extra spread in q and so broaden the line.

The spin-lattice relaxation time T_1 is used to estimate these effects. Quanta of energy satisfying (3) act on the set of levels and make the population densities on the states equal.

When the radiofrequency field is turned off, the difference in population density Δn produced by that field tends to return to the original difference Δn_0 (which is determined by the temperature) in accordance with the law

$$\Delta n = \Delta n_0 (1 - e^{-t/T_1}), \tag{9}$$

in which t is time elapsed.

The excited state has a long lifetime if T_1 is large; in that case the thermal processes may be unable to maintain any appreciable difference in population density, with the result that, after a certain time, the number of quanta absorbed in unit time equals the number emitted in that time, so the specimen ceases to produce a signal. This power-saturation effect is avoided in NMR by keeping the radiofrequency power as small as possible. It is very much more difficult to produce saturation in quadrupole resonance. (Gutowsky et al. [27] give T_1 for p-dichlorobenzene as 20 msec, for example.) All the same, although the signal may not vanish, the line width may be increased. See Wang [24] for details.

The spin-spin relaxation time T_2^* is used to specify the line shape more directly. Let the function $g(\nu)$ describe the distribution of resonance frequencies produced by all factors acting together. That function is nor-

malized via the condition $\int_{-\infty}^{\infty} g(\nu)d\nu = 1$. Then we have

$$T_2^* = 2g(\nu_r). \tag{10}$$

The line shape gives us information about the relaxation processes. Spin-echo methods (see part II) provide the most accurate means of measuring T_1 and T_2^*. Stresses in the crystal affect the line width via the spin-spin relaxation, i.e., via T_2^* for p-dichlorobenzene to vary from 0.5 msec to 70 μsec, although T_1 is not affected [27].

Livingston [28] has observed (on BCl_3) an interesting effect of the molecular vibrations. The line for Cl is a doublet showing a small splitting (2.8 kcps), although the crystal structure is such as to exclude the possibility that there are two positions for the molecule in the unit cell; again, the dipole-dipole interactions are too weak to explain the effect. Douglas [5] explains the effect in terms of the internal vibrations of the molecule; the B^{10} vibrates more rapidly, so the resonance frequency for $B^{10}Cl_3$ should be lower (see section 6). The $B^{10}Cl_3$ and $B^{11}Cl_3$ molecules differ in the motion of their B atoms. This difference is found to give an effect on q_{zz} equivalent to 2 kcps. The rest of the splitting is caused by dipole-dipole interactions. Douglas's view is confirmed by the fact that it predicts the intensity ratio of the doublet correctly. Now B^{10} is the less abundant isotope, so the low-frequency component of the doublet should be the weaker one, as is actually the case. The effect is best observed on molecules in which D replaces H. Duchesne et al.[29] have used CH_3Br^{79}, CD_3Br^{79}, and so on for this purpose, but they found that the large splittings are the reverse of those predicted on the basis of Douglas's explanation. Douglas [30] has calculated the structure of the resonance line of Cl_2, which Crane et al.[31] have examined. The results are used to explain the isotope effects (of Cl^{35} and Cl^{37}) on q_{zz} in terms of rotary oscillations about the center of gravity of the molecule.

Several studies have been made of the effects of inhibiting molecular rotation [32-34].

6. Dynamic Effects that Affect the Resonance Frequency

Bayer [35] has considered the effects of rotary oscillations on q_{zz}, i.e., on the frequency; Raman and infrared spectra indicate that the lowest frequencies for such oscillations are at least two orders of magnitude higher than the highest possible frequencies for quadrupole resonance. Bayer deduces from this the important result that the nucleus is in an electric field whose $\underline{q}$ differs from that for a molecule at rest (the effective $\underline{q}$ is a function of temperature). His calculation for $I = {}^3/_2$ gives the resonance frequency as a function of temperature in the form

$$\frac{1}{\nu_r}\cdot\frac{d\nu}{dT} = -\frac{3h^2}{8\pi^2kT^2}\left[\frac{e^{h\nu_x/kT}}{A_x(e^{h\nu_x/kT}-1)^2}+\frac{e^{h\nu_y/kT}}{A_y(e^{h\nu_y/kT}-1)^2}\right] \tag{11}$$

in which ν_{pr} is the frequency for $\eta = 0$, ν' is the same corrected for η, T is temperature, ν_x and ν_y are the frequencies of the oscillations about the $\underline{x}$ and $\underline{y}$ axes of the tensor for $\underline{q}$, and A_x and A_y are the corresponding moments of inertia. Oscillations on $\underline{z}$ do not contribute to $\underline{q}$ (they affect only η), and (5) with $I = {}^3/_2$, may be used to demonstrate that this effect may be neglected in (11). Fig. 6 shows a curve calculated from (11); we see that the frequency rises as the temperature falls. The temperature coefficient for p-dibromobenzene is 18.7 kcps/deg; that for p-dichlorobenzene is 2.7 kcps/deg. These values are such that the specimen must be kept at a fixed temperature; even a difference of 2-3°C between parts of a specimen can broaden the line very considerably.

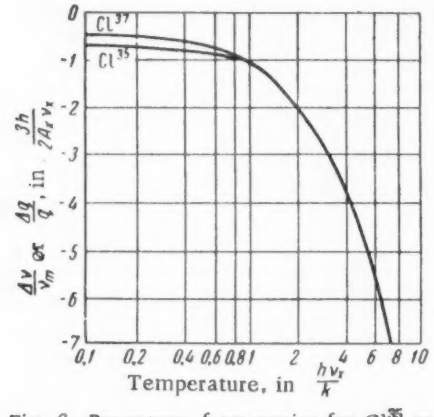

Fig. 6. Resonance frequencies for Cl^{35} and Cl^{37} as functions of temperature on Bayer's theory.

Bayer's predicted result is found to agree with the results for most compounds, although anomalous behavior is not unknown. Barnes and Engardt [36] have found that $TiBr_4$ gives a frequency that increases between room temperature and -50°C but thereafter decreases. This anomaly cannot be explained on Bayer's theory, but Kushida et al [37] and Gutowsky et al.[38] have interpreted it by means of a theory in which allowance is made for the pressure produced within the lattice when the temperature is lowered. If

$$\left|-\frac{\alpha}{\varkappa}\left(\frac{\partial\nu}{\partial P}\right)_T\right| > \left|\left(\frac{\partial\nu}{\partial T}\right)_V\right|$$

(in which α is the thermal-expansion coefficient and $\varkappa$ is compressibility), then the temperature coefficient is positive; the Bayer mech-

anism is then a minor one, as occurs at low temperatures, for Fig. 6 shows that $(\partial \nu / \partial T)_V$ falls as $T \to 0$. This can occur only if $(\partial \nu / \partial P)_T < 0$. The sign of this derivative has been examined for $TiBr_4$ [36]; it actually is negative, so any detailed consideration of the frequency as a function of temperature must take account of dynamic and static factors.

7. The Quadrupole Interaction Constant

No exact theory is available to relate q to the electron-density distribution. Townes and Dailey's semiempirical formulas [5, 42, 44] are nearly always used in interpreting results, although they give only a rough general estimate of the bond type. However, the terminology they introduced has become so widely used that we have adhered to it in what follows.

We follow Das and Hahn [5] and consider Townes and Dailey's theory in relation to ICl. The external electrons have the configuration $5s^2 5p^5$ in the I atom and $3s^2 3p^5$ in the Cl atom, i.e., one p electron is needed to complete a shell. A closed shell would have spherical symmetry, so the electric field gradient at the nucleus would be zero. Therefore Townes and Dailey assume that the actual q in the free atoms are caused by lack of a 5p or 3p electron respectively, i.e., equal the q caused by one p electron, apart from sign. The electron orbitals overlap when ICl is formed; for simplicity it is assumed that the main overlap occurs in the p_z orbital forming a σ-bond. (The possible effects of π bonds formed from p_x and p_y orbitals are considered in section 8.)

The electrons forming the σ bond have an orbital ψ that is a linear combination [47, 49] of the atomic orbitals ψ_{Cl} and ψ_I:

$$\psi = a\psi_{Cl} + b\psi_I . \tag{12}$$

Here a and b are normalized in accordance with the condition $a^2 + b^2 + 2abS = 1$, in which $S = \int \psi_{Cl} \psi_I d\tau$ is the overlap integral. We have a = b for a purely covalent bond, as occurs in Cl_2, I_2, etc., but $a \neq b$ if the atoms are different. Pauling [54] states that in the latter case the bond is partly ionic, a measure of the proportion of ionic character being

$$i = |a^2 - b^2| . \tag{13}$$

The bond is fully ionic if b = 0; in that case we would have Cl^- (with a closed shell) and I^+ (lacking two p electrons). This does not in fact occur, and the I-Cl bond is intermediate in type; the p_z orbital of Cl contains (1+i) electrons, and that of I contains (1 - i) electrons.

Then (12) may be used to find the field gradient at the center of the Cl atom. By definition we have

$$q_{zz} = \frac{\partial^2}{\partial z^2}\left(\frac{e}{r}\right) = \frac{e(3z^2 - r^2)}{r^5} = \frac{e(3\cos^2\theta - 1)}{r^3} , \tag{14}$$

in which r is the distance from the charge e to the nucleus, and θ is the angle between r and z axis. The exact q_{zz} is to be found by averaging (14) with respect to (12):

$$\begin{aligned} q_{zz} &= e\int (a\psi_{Cl} + b\psi_I)\frac{3\cos^2\theta - 1}{r^3}(a\psi^*_{Cl} + b\psi^*_I)\,d\tau = \\ &= a^2 e\int \psi_{Cl}\frac{3\cos^2\theta - 1}{r^3}\psi^*_{Cl}\,d\tau + 2abe\int \psi_{Cl}\frac{3\cos^2\theta - 1}{r^3}\psi^*_I\,d\tau + \\ &\quad + b^2 e\int \psi_I \frac{3\cos^2\theta - 1}{r^3}\psi^*_I\,d\tau . \end{aligned} \tag{15}$$

The first term on the right in (15) is a^2 times the gradient q_0 produced by one electron in the orbital ψ_{Cl} so that the magnetic quantum number of that electron is $m_l = 0$; the second is the gradient produced by the electron density in the overlap region, and the third is the contribution from ψ_I. Now the gradient varies as $1/r^3$, so we can neglect the third term, and even the second at the expense of some loss of accuracy. Then

$$q_{zz} \approx a^2 q_0 . \tag{16}$$

From (13) and the normalization condition we have

$$a^2 = \frac{1+i}{2(1+S)}. \tag{17}$$

Experiment and general arguments show that S can be neglected in (17); although the overlap governs the bond energy, it has little effect on the nuclear interaction. Then

$$2q_{zz} = (1+i)\,q_0. \tag{18}$$

In addition to the two σ-electrons, which make a contribution to q_{zz}, there are many other electrons that may make a certain contribution (to $q_{zz\,Cl}$, for example) in ICl. Those electrons are a) two pairs of $3p_x$ and $3p_y$ electrons (π electrons) of Cl, b) the $3s^2$ electrons, c) the inner ($1s^2 2s^2 2p^6$) electrons of Cl, and d) the joint action of all the charges in I, which supplies one 5p electron to the σ-bond (this last Townes and Daily allow for by means of one elementary positive charge placed at the center of the nucleus). Now q is calculated for the nucleus, which contains no electrons, so Laplace's equation applies, i.e.

$$q_{zz} + q_{xx} + q_{yy} = 0. \tag{19}$$

Now $q_{xx} = q_{yy}$ on account of the axial symmetry, so

$$q_{p_x} = -\frac{1}{2}\,q_0, \tag{20}$$

and each π electron produces a gradient

$$q_{p_x} = -\frac{1}{2}\,q_{p_z} = q_{p_y} \tag{21}$$

while all the π electrons of the Cl atom together produce a gradient at the center of the Cl nucleus of

$$q_\pi = -2q_0. \tag{22}$$

The contributions under b) and c) above are smaller, but they ought to be incorporated, strictly speaking. Townes and Daily neglected them.

The contribution to q under d) is of the order of $1/r^3$ (r is the distance between the nuclei); this correction is usually negligible.

Thus the p electrons are found to produce the main contribution to q. Let N_x, N_y, N_z denote the populations of the $3p_x$, $3p_y$, and $3p_z$ states of the Cl atom; then (21) and (22) imply that the p electrons make a contribution to q_{zz} of

$$q_{zz} = \left(\frac{N_x + N_y}{2} - N_z\right) \cdot q_0 = U_p q_0, \tag{23}$$

in which q_0 is as defined above for (16) for the p_z electron of Cl.

Here U_p is the number of unbalanced p electrons; its sign is taken as positive when there is a deficit of p electrons along the z axis.

Free atoms are encountered in molecular beams and show their effects in atomic spectra; here the projection of the orbital moment on the special direction is maximal ($m_l = \pm 1$). Experiments of this kind give the standard data for quadrupole interactions in atoms, so it would be best to derive q_{zz} in terms of such states. Then (21) and (23) give us that

$$eQq_{zz} = eQU_p q_0 = -2\,eQq_{\pm 1}U_p = -2U_p\,(eQq)_{\text{atom}}. \tag{24}$$

Then, with (18) on the assumption that the σ-bond is ionic, and with $N_x = N_y = 2$ in (23), we have

$$eQq_{zz} = -(1-i)\,(eQq)_{\text{atom}}. \tag{25}$$

In section 1 we stated that NQR experiments give us the quadrupole interaction constant for a molecule in a crystal. Now (25) shows that the eQq_{zz} found in this way can be used to calculate the proportion of ionic character. For ICl we have $eQq_{zz} = -82.50$ Mcps [47], and $(eQq)_{\text{atom}} = 109.74$ Mcps. Then (25) gives i = 0.25,

a value that agrees with Gordy's view [45, 47] that sp hybridization need not be considered in relation to the bonding orbitals of Cl (in which he differs from Townes and Dailey). The long discussion of this topic [45-49] has not yet produced any clear-cut results. Let us consider how sp hybridization for I-Cl would affect the above results. Let the degree of s character of the above bonding orbital of Cl be s. Here the number of effective p_z electrons in this orbital is reduced from (1 + i) to (1 + i)(1 - s), but the s orbital has now become a hybrid sp orbital of degree of hybridization s, so it contains 2s effective p_z electrons. The total number of p_z electrons is then (1 + i)(1 - s) + 2s, so a change occurs in the number of unbalanced p electrons:

$$U_p = 2 - ((1 + i)(1 - s) + 2s] = (1 - i)(1 - s). \quad (26)$$

We see that (26) shows that sp hybridization produces the same effect as ionic character (it reduces the quadrupole interaction). Experiment gives only $|eQq_{zz}|$, so it is very difficult to choose between one form (in which all of the reduction in eQq is caused by the ionic character) and the other (in which hybridization makes a contribution as well); the problem can be resolved only by resort to information obtained in other ways.

Townes and Daily differ from Gordy in not concluding that the above eQq_{zz} and $(eQq)_{atom}$ for I-Cl imply that the I-Cl bond is rather ionic. They use Pauling's value i = 0.08 for that bond, and use (26) to find that the p_z orbital has 18% s hybridization. They survey a large number of bonds to formulate their hybridization rule "If a halogen atom is bound to an atom B such that the difference of the electronegativities is $(x_A - x_B) \geq$ ≥ 0.25, then the A-B bond has s = 0.15 for its degree of s character; s hybridization is absent if $(x = x_B) > 0.25$".

Figure 7 illustrates the difference between the two approaches (ionic character as a function of the difference in the electronegativities). Gordy's curve predicts a greater degree of ionic character, but both run far above the curves compiled earlier on the basis of dipole moments. Quite apart from the difficulty about the exact proportion of s hybridization, it is clear that the quadrupole-interaction results imply that the bonds formed by the halogens are much more ionic that had been supposed previously [47].

An interesting feature of Fig. 7 is that the quadrupole results predict that the bond will be 100% ionic if $(x_A - x_B) \geq 2$. Wilmhurst [50] has proposed a relation

$$i = \frac{|x_A - x_B|}{x_A + x_B} \quad (27)$$

which implies that universal curves $i = f(x_A - x_B)$ cannot be constructed; all we can do is to construct curves relating i to x_B or $x_A - x_B$ for each kind of atom A. Wilmhurst has used the quadrupole results to estimate the s character of carbon-halogen bonds; his s come out much larger even than Townes and Dailey's, which means that the i given in [47] are to be reduced correspondingly.

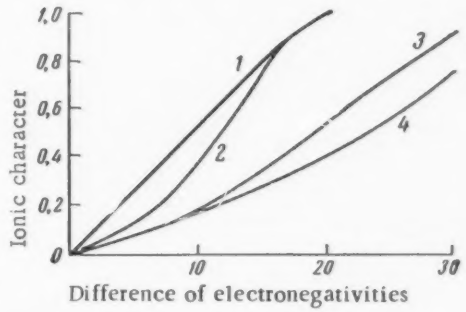

Fig. 7. Degree of ionic character of a bond A-B as a function of $x_A - x_B$. 1) Gordy; 2) Townes and Daily; 3) Pauling (from dipole moments); 4) Hannay and Smith [53] (from dipole moments) a) Ionic character; b) difference of electronegativities.

Further work is required to establish the true position and to resolve this conflict of views.

We much point out that Townes and Dailey's semiempirical treatment can give no rigorous basis for choosing between the various ways of separating the contributions to eQq from ionic character and hybridization (the more so as regards determining the type of hybridization). Experiment gives only |eQq|, and results on hybridization and ionic character so obtained will remain somewhat undefined while we lack a proper theory of quadrupole interactions. Both difficulties can be obviated if we proceed purely empirically by measuring the eQq for extensive series of related compounds; on that basis conclusions can be drawn about the nature of the bonds from the trend in the values.

More rigorous treatments have been attempted; Bassompiere [55-57] has performed an exceptionally laborious rigorous calculation of the eQq for nitrogen in HCN and has obtained satisfactory agreement with experiment. The volume of calculation is such that no similar calculation has yet been attempted for a more complicated molecule. Benderskii and Blyumenfel'd [58, 59] have found that the contribution to the $(eQq)_{atom}$ from polariza-

tion of the filled shells by the unbalanced electron may be as much as 20-30% for elements in the fourth and subsequent groups. (This implies that we are justified in neglecting polarization for Cl but not for I in the example above.) They have also proposed a new method of computing the wave functions for diatomic molecules in terms of measured eQq and dipole moments; in this way the degree of ionic character and the s character can be estimated directly without resort to further assumptions. Calculations for HCl and HBr show that the method is usable, but serious difficulties are encountered in applying it to more complex molecules.

Schatz [60, 61] has adopted the entirely opposite approach (that of calculating eQq from the parameters of the molecular orbital), but his results cannot be compared with experiment, for those parameters are unknown.

We conclude that there is at present no sound theoretical basis for calculating the parameters of bonds from measured quadrupole interaction constants. The importance of NQR to chemistry is not that it enables one to estimate those parameters but that eQq is exceptionally sensitive to small changes in the character of a bond. In the second part we give some examples which demonstrate that the changes in eQq are additive for chloroalkanes, that eQq is proportional to Hamett's constant σ, etc. Much of value is to be expected from empirical laws of this kind derived from NQR studies.

8. Asymmetry in the Field Gradient

Formulas (25) and (26) relate to the case $\eta = 0$, although this is not so in most cases; then the interaction constant varies not only with the bond type but also on account of the fact that $N_x + N_y$ in (23) deviates from the value four proper to a σ bond. But the change in the p_x and p_y orbitals is equivalent to the production of a π bond, so two bond types are involved.

Let us consider ICl again; it is the degree to which the second type of bond is present in π, in which π may be defined as the difference between p_x (or p_y) for the free Cl (or I) atom and the same quantity for the bound Cl (or I) atom.

Then the contribution to q_{zz} from the π electrons is reduced by πq_{atom} relative to the contribution for the case in which only a single bond type is involved [that case corresponds to (22)]. Then (26) is replaced by

$$U_d = (1 - i)(1 - s) - \pi . \tag{28}$$

Now we consider the relation of π to η, for which purpose we introduce in (23) the symbol $(U_p)_z$ for the number of unbalanced p electrons; then

$$\begin{aligned} (U_p)_x &= N_x - \frac{N_y + N_z}{2} , \\ (U_p)_y &= N_y - \frac{N_x + N_z}{2} . \end{aligned} \tag{29}$$

Hence $q_{xx} = (U_p)_x \cdot q_0$, $q_{yy} = (U_p)_y \cdot q_0$, so the asymmetry parameter is

$$\eta = \frac{q_{xx} - q_{yy}}{q_{zz}} = \frac{\frac{3}{2}(N_x - N_y)}{N_z - \frac{N_x + N_y}{2}} . \tag{30}$$

If η is not too large, we can neglect η^2 above and in (5), in which case we have

$$\begin{aligned} I = {}^3/_2; \quad \eta &= \frac{3(N_x - N_y)(eQq)_{atom}}{4\nu} , \\ I = {}^5/_2; \quad \eta &= \frac{3(N_x - N_y)(eQq)_{atom}}{2\nu} . \end{aligned} \tag{31}$$

In (31) we have ν as the frequency of the $E_{1/2} \leftrightarrows E_{3/2}$ transition, so the asymmetry parameter is a direct measure of the difference in the populations of the $3p_x$ and $3p_y$ states. That difference is a direct measure of the degree of duality in the bond for a planar molecule; recent studies [51, 52] of substituted benzenes and heterocyclic compounds have given some interesting results, which we shall consider in the second part of this review.

There are some compounds whose molecules are axially symmetric about a double bond, in which case duality in the bond type causes no appreciable difference in the $3p_x$ and $3p_y$ orbitals [5]; the asymmetry parameter is zero. It is more difficult to examine the bond type for such a molecule by means of NQR.

LITERATURE CITED

1. H. Dehmelt and H. Krüger, Naturwissenschaften 37, 11 (1950).
2. D. J. E. Ingram, Spectroscopy at Radio and Microwave Frequencies [Russian translation] (IL, Moscow, 1959).
3. E. R. Andrew, Nuclear Magnetic Resonance, [Russian translation] (IL, Moscow, 1958).
4. V. V. Malyarov, Theory of the Nucleus [in Russian] (Fizmatgiz, Moscow, 1959).
5. T. P. Das and E. L. Hahn, Nuclear Quadrupole Resonance Spectrocopy (New York, 1958).
6. R. Bersohn, J. Chem. Phys. 20, 1505 (1952).
7. M. Cohen, Phys. Rev. 96, 5, 1278 (1954).
8. R. Livingston, J. Chem. Phys. 26, 1102 (1957).
9. H. Meal, J. Chem. Phys. 24, 1011 (1956).
10. H. Krüger, Z. Phys. 130, 371 (1951).
11. Whitmer, Weidner, Hsiang and Weiss, Phys. Rev. 74, 1478 (1948).
12. R. V. Pound, Phys. Rev. 79, 685 (1950).
13. G. Becker and H. Krüger, Naturwissenschaften 38, 121 (1951).
14. R. Livingston and H. Zeldes, J. Chem. Phys. 26, 351 (1957).
15. V. Koi, A. Tsujimura and T. Fuke, J. Chem. Phys. 23, 1346 (1955).
16. T. Fuke and V. Koi, J. Chem. Phys. 29, 973 (1958).
17. K. Kano, J. Phys. Soc. Japan 13, 975 (1958).
18. A. Abragam and K. Kambe, Phys. Rev. 91, 1184 (1953).
19. S. Kojima and K. Tsukada, J. Phys. Soc. Japan 10, 591 (1955).
20. G. D. Watkins and R. Walker, Bull. Amer. Phys. Soc., (II) 1, 11 (1956).
21. S. Kojima, et al., J Phys. Soc. Japan 12, 1225 (1957).
22. H. Allen, J. Amer. Chem. Soc. 74, 6074 (1952).
23. C. Dean, J. Chem. Phys. 23, 1734 (1955).
24. T. C. Wang, Phys. Rev. 99, 566 (1955).
25. V. Koi, A. Tsujimura, and V. Imaeda, J. Chem. Phys. 27, 603 (1957).
26. C. Dean, Phys. Rev. 96, 1053 (1954).
27. H. Gutowsky and D. Woessner, J. Chem. Phys. 27, 1072 (1957).
28. R. Livingston, J. Phys. Chem. 57, 496 (1953).
29. J. Duchesne, A. Monfils, and J. Garson, Physica 22, 817 (1956).
30. D. C. Douglas, J. Chem. Phys. 28, 504 (1959).
31. L. Crane, R. Anderson and H. Robinson, Bull. Am. Phys. Soc., (II) 4, 11 (1959).
32. M. Buyle-Bodin, Ann. Phys. 10, 533 (1955).
33. H. Dodgen and I. Ragle, J. Chem. Phys. 25, 376 (1956).
34. E. Lassetre and C. Dean, J. Chem. Phys. 17, 31 (1949).
35. H. Bayer, Z. Phys. 130, 227 (1951).
36. R. G. Barnes and R. Engardt, J. Chem. Phys. 28, 731 (1958).
37. T. Kushida, G. Benedeck, and N. Bloemberger, Phys. Rev. 104, 1364 (1956).
38. H. Gutowsky and G. Williams, Phys. Rev. 105, 464 (1957).
39. R. Barnes and W. Smith, Phys. Rev. 93, 95 (1954).
40. R. Bacher and S. Goudsmith, Atomic Energy States (New York, 1932); C. E. Moore, Atomic Energy Levels, Nat. Bur. Standards. Circ. 467 (Washington, 1949).
41. H. Bethe and R. Bacher, Rev. Mod. Phys. 8, 226 (1936).
42. C. Townes and B. Dailey, J. Chem. Phys. 17, 782 (1949).
43. A. Lösche, Kerninduction (Berlin, 1957).
44. C. Townes and A. Schawlow, Microwave Spectroscopy (New York, 1955).
45. W. Gordy, J. Chem. Phys. 19, 792 (1951).
46. W. Gordy, Disc. Faraday Soc., 18 (1955).
47. Spectroscopy in Chemistry [in Russian] (IL, Moscow, 1959), Chap. II.
48. B. Dailey, Disc. Faraday Soc., 18 (1955).

49. W. J. Orville-Thomas, Quart. Rev., XI, 162 (1957).
50. J. Wilmshurst, J. Chem. Phys. 30, 561 (1959).
51. F. Adrian, J. Chem. Phys. 29, 1381 (1958).
52. M. Dewar and E. Lucken, J. Chem. Soc. (London), 2653 (1958).
53. N. Hannay and C. Smith, J. Amer. Chem. Soc. 68, 171 (1946).
54. L. Pauling, Nature of the Chemical Bond [Russian translation] (Goshkimizdat, Moscow, 1947).
55. L. Bassompiere, Disc. Faraday Soc., 18 (1955).
56. L. Bassompiere, J. Chem. Phys. 21, 614 (1954).
57. L. Bassompiere, Compt. read. Acad. Sci. 240, 285 (1955).
58. V. A. Benderskii and L. A. Blyumenfel'd, Optika i Spektroskopiya 3, 402 (1957).
59. V. A. Benderskii, Diploma work [in Russian] (Izd. MGU, 1959).
60. P. Schatz, J. Chem. Phys. 21, 730 (1954).
61. P. Schatz, J. Chem. Phys. 22, 695 (1954).
62. G. Fricke, et al., Phys. Verhandl. 10, 13 (1959).

PROTON RELAXATION IN AQUEOUS SOLUTIONS OF DIAMAGNETIC SALTS

III. EFFECTS OF POLARIZATION PARAMAGNETISM

V. M. Vdovenko and V. A. Shcherbakov

Khlopin Radium Institute, Academy of Sciences of the USSR, Leningrad
Translated from Zhurnal Strukturnoi Khimii Vol. 1, No. 2, pp. 268-269, July-August, 1960
Original article submitted January 7, 1960

In the first paper in this series [1] we explained the anomalous effects of ions from the zinc subgroup in terms of covalent bonds occurring in hydrated ions of the type $Me(H_2O)_x^{2+}$. The electron density is distributed between the ion and the water molecules, with the result that the hydrated ion is weakly paramagnetic and so is more effective in producing an effect on T_1, the proton relaxation time. An important point here is the effects on T_1 of ions whose polarization paramagnetism parameters [2] have been found by means of static measurements of the magnetic susceptibility. The results are of interest in that they may serve as a direct test of the above supposition; they are also of interest in relation to the theory of nuclear relaxation.

We present here the main results for UO_2^{2+}, which does not have any unpaired electrons but which has a positive and temperature-independent susceptibility (+56 x 10^{-6} cgs units), i.e., which shows polarization paramagnetism [2, 3]. This behavior is caused, as Eisenstein and Pryce have shown, by the hybrid bonds formed by the 5*f* and 6d electrons between the uranium and the oxygen [3]. The equatorial bonds are largely covalent [4]. The large ionic radius (1.91 A [4]) makes the ion-dipole interaction with the water not very important [1], so the ion is very suitable for use in establishing the role of polarization paramagnetism in shortening the proton relaxation time.

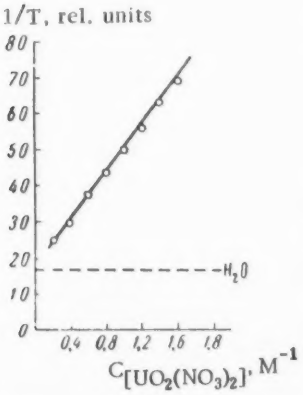

Proton relaxation time for uranyl nitrate solution. (The value given by a solution $4.02 \cdot 10^{-4}$ M in Mn^{2+} is taken as 100.)

Two conclusions can be drawn from the results of part I.

1. An ion showing polarization paramagnetism should decrease the relaxation time in accordance with its effective magnetic moment μ_N. Therefore we may predict the relaxation time relative to T_1 (the time for pure water). The μ_N calculated in this way from the effect on $1/T_1$ is between 1.0 and 1.4 $\cdot 10^{-2}$ Bohr magneton; this calculation is confirmed by the relation of $1/T_1$ to uranyl nitrate concentration (see figure)*. The molar relaxation shift Δ_M [1] comes out as 40 units (relative)**.

2. The paramagnetism must be increased as a result of hydration, because the ground state is further perturbed. Our results, used in the usual way [5], give

* The methods used in no way differ from those of part I. The uranyl nitrate was purified by extraction into diethyl ether; the solutions were prepared by dissolving weighted amounts of UO_4 or uranyl nitrate hexahydrate in nitric acid (pH about 0) to prevent hydrolysis. Permanganate and gravimetric methods were used to check the UO_2^{2+} concentration.

** O. B. Stebunov did some of the measurements.

the effective magnetic moment of the uranyl ion in these solutions as $(7.2 \pm 0.9) \cdot 10^{-2}$ Bohr magneton, which is far larger than the values indicated by the static susceptibility. The reason is that the total contribution from the excited states (from the inherent paramagnetism and from the paramagnetism resulting from the interaction with the water) is equivalent to a change in the electron density, which increases with the transfer of proton energy. The susceptibility of the uranyl ion is nearly constant at 0.4×10^{-2} Bohr magneton in solids and in solutions [3], although the effect on the relaxation time would appear to point to a much larger μ_N. Rivkind [6] has shown for the 3d elements that the covalent bonds between the addends and the central ion by the d electrons cannot be detected from static susceptibility measurements, because the total magnetic moment is almost unaffected. The reason is that the energy of the field surrounding the ion is inadequate to overcome the coulomb repulsion between the electrons in the central ion if the covalent bonds are weak; the magnetic moment does not differ appreciably from the value found for the free ion. Much the same is true for the uranyl ion; in fact, the μ_N corresponds exactly to the expected covalent character of the equatorial bonds [4].

LITERATURE CITED

1. V. M. Vdovenko and V. A. Shcherbakov, Zhur. Strukt. Khim. 1, 1, 28 (1960).*
2. H. Van Vleck, Electric and Magnetic Susceptibilities (Oxford, 1932).
3. J. C. Eisenstein and M. H. L. Pryce, Proc. Roy. Soc. A229, 20 (1955).
4. I. I. Lipilina, Uranyl and its Compounds [in Russian] (Izd. AN SSSR, Moscow, 1959).
5. B. M. Kozyrev and A. I. Rivkind, Zhur. Éksp. Teoret. Fiz. 27, 69 (1954).
6. A. I. Rivkind, Zhur. Neorg. Khim. 4, 1291 (1959).

*Original Russian pagination. See C. B. translation.

LIST OF PAPERS ON RADIOFREQUENCY AND MICROWAVE SPECTROSCOPY PUBLISHED OR ACCEPTED FOR PUBLICATION DURING 1959-1960

Translated from Zhurnal Strukturnoi Khimii, Vol. 1, No. 2, pp. 270-272, July-August, 1960

The rapid development of radiofrequency and microwave spectroscopy (especially as applied to chemistry) has led the Commission on Radio Spectroscopy of the Division of Chemical Sciences, Academy of Sciences of the USSR, to start a regular compilation of papers published or accepted for publication; this has been done on account of the great importance of this field to many Soviet scientists.

The list of papers will be published as an appendix to the Journal of Structural Chemistry from time to time. The Commission requests anyone working in this field to send to it a copy of any paper accepted for publication with a statement of the data of publication and of the name of the journal; the address is Moscow V 133, Institute of Chemical Physics, Academy of Sciences of the USSR, Commission on Radio Frequency Spectroscopy of the Division of Chemical Sciences, Academy of Sciences of the USSR.

I. GENERAL*

1. Yu. S. Konstantinov, "A parametrically excited circuit as a means of observing paramagnetic resonance," Pribor i Tekh., 6, 134 (1959) [Moscow State University, Physics Faculty].
2. A. A. Manenkov, "Superheterodyne spectrometer for use in paramagnetic-resonance studies," Col.: Transactions of the All-Union Conference on Paramagnetic Resonance, June 1959 [PI].
3. A. G. Semenov and V. M. Chibrikin, "Maximum possible sensitivity of a superheterodyne ESR spectrometer," Coll. [ICP].
4. L. L. Dekabrun, A. U. Stepanyants, E. Z. Utyanskaya, and Yu. E. Bukolov, "Permanent magnets for use in high-resolution NMR," Coll. [ICP].
5. N. M. Ievskaya and R. M. Umarkhodzhaev, "Apparatus for use in finestructure studies on proton NMR," Coll. [Moscow State University, Physics Faculty].
6. Yu. N. Molin, N. Ya. Buben, A. T. Koritskii, A. G. Semenov, and V. N. Shamshev, "Apparatus for observing ESR spectra of solids exposed to fast electrons," Pribor. i Tekh. Eksp., 6, 73-77 (1960) [ICP].
7. E. Z. Utyanskaya, V. F. Bystrov, L. L. Dekabrun, Yu. N. Kil'yanov, and A. U. Stepanyants, "High-resolution NMR apparatus," Pribori i Tekh. Eksp., 1 (1960) [ICP].
8. G. M. Zverev and L. S. Kornienko, "Cavity for use at low temperatures in 3.2 cm spectrometer," Pribor. i Tekh. Eksp., 2 (1960)[NPI].

---

* The names of the Institutes are abbreviated as follows:
IOEC - Institute of Organoelement Compounds, Academy of Sciences of the USSR.
ICP - Institute of Chemical Physics, Academy of Sciences of the USSR.
NPI - Nuclear Physics Institute, Moscow State University.
RI - Radium Institute, Academy of Sciences of the USSR.
PI - Physics Institute, Academy of Sciences of the USSR.

9. N. M. Ievskaya and R. M. Umarkhodzhaev, "Conditions for observing fine-structure in NMR signals," Vest. Mosk. Univ., Feb., 1960 [Moscow State University, Physics Faculty].

II. Electron-Spin Resonance

10. L. A. Blyumenfel'd, "Substituents in DNA," Doklady Akad. Nauk SSSR 130, 887 (1960) [ICP].
11. Yu. Sh. Moshkovskii, "ESR spectra on cyanin dyes," Doklady Akad. Nauk SSSR 130, 1277 (1960)* [ICP].
12. A. K. Piskunov, "ESR spectra of some chelate compounds of copper," Doklady Akad. Nauk SSSR 130, 1284 (1960)* [Karpov Institute of Physical Chemistry].
13. I. I. Chkheidze, et al., "ESR spectra and kinetics of the accumulation of radicals in the radiolysis of aromatic compounds," Doklady Akad. Nauk SSSR 130, 1291 (1960)* [ICP].
14. Yu. N. Molin, et al., "ESR studies of energy transfer in the radiolysis of some frozen hydrocarbons," Doklady Akad. Nauk SSSR 131, 125 (1960)* [ICP].
15. V. M. Kazakova and Ya. K. Syrkin, "Hyperfine structure of the ESR spectrum of benzophenone-K-ketyl," Doklady Akad. Nauk SSSR 131, 346, (1960)* [Lomonosov Institute of Fine-Chemical Technology, Moscow].
16. N. N. Bubnov, "ESR spectra observed for illuminated plant leaves and in photoreductions of pigments," Biofizika 5, 121 (1960)* [Bakh Institute of Biochemistry, Academy of Sciences of the USSR].
17. G. K. Morozova and L. A. Blyumenfel'd, "Effects of oxygen on the ESR spectra of freeze-dried tissues," Biofizika 5, 235 (1960)* [ICP].
18. N. V. Afanas'eva, "Ground states of bound paramagnetic rare-earth ions in external magnetic fields," Optika i Spektroskopiya 8, 8 (1960).
19. S. I Vetchinkin, S. P. Solodovnikov, and V. M. Chibrikin, "Spin-density distribution in the cation of chromium dibenzyl," Optika i Spektroskopiya 8, 137 (1960) [ICP].
20. U. K. Kopvillen, "Second moment of a paramagnetic-resonance absorption line, with allowance for the fine and hyperfine structures," Zhur. Eksp. i Teoret. Fiz. 38, 151 (1960) [Kazan State University].
21. V. B. Kazanskii and Yu. I. Pechevskaya, "ESR in irradiated aluminum oxide," Zhur. Eksp. i. Teoret. Fiz. 38, 477 (1960) [ICP].
22. S. D. Kaitmazov and A. M. Prokhorov, "ESR of the radicals OH and HO_2," Coll. [PI].
23. A. A. Manekov and A. M. Prokhorov, "Spin-lattice relaxation in corundum containing chromium," Col. [PI].
24. A. A. Manenkov and V. B. Federov, "Line width and shape for the ESR of Cr^{3+} in corundum monocrystals," Coll. [PI].
25. V. M. Chibrikin, S. P. Solodovnikov, and S. I. Vetchinkin, "ESR studies of derivatives of the cation of chromium dibenzyl," Coll. [ICP].
26. V. M. Chibrikin, S. P. Solodovnikov, and V. V. Voevodskii, "ESR spectra of the negative ion-radicals of some aromatic compounds," Coll. [ICP].
27. V. B. Kazanskii, Yu. I. Pechevskaya, and V. V. Voevodskii, "ESR studies of the chemical crystallography of a chromium catalyst," Kinetika i Kataliz 1, 257 (1960) [ICP].*
28. Yu. D. Tsvetkov, Ya. S. Lebedev, and V. V. Voevodskii, "The free radicals in irradiated teflon (PTFE)," Transactions of the Tashkent Conference on the Peaceful Uses of Atomic Energy, September, 1960 (in Russian) [ICP].
29. Ya. S. Lebedev, Yu. D. Tsvetkov, and V. V. Voevodskii, "ESR spectrum of the fluoroalkyl radical in irradiated teflon," Optika i Spektroskopiya, September, 1959 [ICP].
30. N. N. Tikhomirova, I. V. Nikolaeva, and V. V. Voevosdkii, "ESR studies of the molecular structure of coal," Zhur. Strukt. Khim. 1, 1, 99 (1960)* [ICP].
31. L. A. Blyumenfel'd, L. A. Berlin, A. A. Shinkin, and A. E. Kalmanson, "New magnetic parameters of macromolecular compounds having conjugated double bonds," Zhur. Struct. Khim. 1, 1, 103 (1960)* [ICP].
32. V. V. Voevodskii, "Uses of ESR in chemistry," Kinetika i Kataliz 1, 1, 45 (1960)* [ICP].
33. G. M. Zverev and A. M. Prokhorov, "ESR and spin-lattice relaxation of Co^{2+} in corundum," Zhur. Eksp. i Teoret. Fiz., Feb., 1960 [NPI].
34. A. K. Zelirova, N. N. Tikhomirova, and A. E. Shilov, "Structures of some compounds formed in reaction between aluminum alkyls and titanium halides," Doklady Akad. Nauk. SSSR 132, 5 (1960)* [ICP].
35. Z. S. Egerova, Yu. M. Malinskii, V. L. Karpov, A. E. Kalmanson, and L. A. Blyumenfel'd, "Chemical changes caused in PVC by ionizing radiation," Vysokomol. Soed. 2, 6, 891 (1960) [Karpov Institute of Physical Chemistry and ICP].

*Original Russian pagination. See C. B. translation.

36. S. P. Solodovnikov, "ESR spectra of the negative ion-radicals of some aromatic compounds," Zhur. Strukt. Khim. 1, 4 (1960).*
37. L. S. Kornienko and A. M. Prokhorov, "ESR of Ti^{3+} in corundum," Zhur. Eksp. i Teoret. Fiz., March, 1960, [NPI].
38. E. A. Yakovleva, et al., "Effects of metal and solvent on the formation of aromatic ion-radicals (polymerization initiators)," Doklady Akad. Nauk SSSR 133, 3 (1960)* [Karpov Institute of Physical Chemistry and ICP].
39. V. M. Kazakova and Ya. K. Syrkin, "ESR spectra of solutions of some aromatic and aliphatic metal ketyls," Doklady Akad. Nauk SSSR 133, 112 (1960)* [Lomonosov Institute of Fine-Chemical Technology, Moscow].
40. V. M. Kazakova and Ya. K. Syrkin, ESR spectra of some aromatic and aliphatic metal ketyls," Doklady Akad. Nauk SSSR, Feb., 1960 [Lomonosov Institute of Fine-Chemical Technology, Moscow].
41. L. V. Vozvysheva and L. A. Blyumenfel'd, "Effects of ionizing radiation on the magnetic parameters of RNA," Biofizika 5, 5 (1960)* [ICP].

III. Nuclear Magnetic Resonance

42. I. V. Aleksandrov, N. N. Korst, and N. D. Sokolov, "Effects of proton exchange on the line widths of NMR spectra for crystals," Coll. [ICP].
43. I. V. Aleksandrov, N. N. Korst, and N. D. Sokolov, "Effects of proton mobility on the line widths of NMR spectra," Optika i Spektroskopiya, Oct., 1959 [ICP].
44. B. N. Provorotov, "NMR spectra of solids," Zhur. Eksp. i Teoret. Fiz., March, 1960 [ICP].
45. I. V. Aleksandrov, "Effects of tunneling on the line widths of NMR spectra for crystals," Doklady Akad. Nauk SSSR 133, 1057 (1960) [ICP].
46. V. M. Vdovenko and V. A. Shcherbakov, "Proton relaxation in aqueous solutions of diamagnetic salts. I. Solutions of nitrates of elements in the second group of the periodic system," Zhur. Strukt. Khim. 1, 1, 28 (1960)* [RI].
47. V. M. Vdovenko and V. A. Shcherbakov, "Proton relaxation in aqueous solutions of diamagnetic salts. II. Alkali-metal cations and halide anions," Zhur. Struk. Khim. 1, 122 (1960)* [RI].
48. V. M. Vdovenko and V. A. Shcherbakov, "Proton relaxation in aqueous solutions of diamagnetic salts. III. Effects of polarization paramagnetism," Zhur. Strukt. Khim. 1, 2, 268 (1960)* [RI].
49. V. M. Vdovenko and V. A. Shcherbakov, "Proton relaxation in aqueous solutions of diamagnetic salts. IV. Role of ion structure," Zhur. Strukt. Khim. 1, 4 (1960)* [RI].
50. V. M. Vdovenko, V. A. Shcherbakov, and O. B. Stebunov, "Proton relaxation in aqueous solutions of diamagnetic salts. V. Solutions of uranyl salts," Zhur. Strukt. Khim. 1, 4 (1960)* [RI].

IV. Nuclear Quadrupole Resonance

51. A. I. Kitaigorodskii and E. I. Fedin, "Changes in the strength of the nuclear quadrupole resonance signal given by a molecular crystal irradiated by fast electrons," Doklady Akad. Nauk SSSR 130, 1005 (1960).
52. K. A. Valiev, "Theory of quadrupole relaxation of nuclear spins in liquids," Zhur. Eksp. i Teoret. Fiz. [Kazan State University].
53. G. K. Semin, "Nuclear quadrupole resonance of isotopes of bromine and iodine," Coll. [IOEC].
54. E. I. Fedin, "Nuclear quadrupole resonance of isotopes of chlorine," Col. [IOEC].
55. E. I. Fedin, "Nuclear quadrupole resonance spectrum of 1, 2, 3-trichlorobenzene," Zhur. Strukt. Khim. 1, 1, 124 (1960).*
56. G. K. Semin and E. I. Fedin, "Use of nuclear quadrupole resonance of isotopes in chemical crystallography," Zhur. Strukt. Khim. 1, 2, 252 (1960)* [IOEC].
57. S. V. Tyablikov, "Theory of ferromagnetic resonance," Fiz. Tverd. Tela 2, 361 (1960).

* Original Russian pagination. See C. B. translation.

SIGNIFICANCE OF ABBREVIATIONS MOST FREQUENTLY ENCOUNTERED IN SOVIET PERIODICALS

FIAN	Phys. Inst. Acad. Sci. USSR.
GDI	Water Power Inst.
GITI	State Sci.-Tech. Press
GITTL	State Tech. and Theor. Lit. Press
GONTI	State United Sci.-Tech. Press
Gosenergoizdat	State Power Press
Goskhimizdat	State Chem. Press
GOST	All-Union State Standard
GTTI	State Tech. and Theor. Lit. Press
IL	Foreign Lit. Press
ISN (Izd. Sov. Nauk)	Soviet Science Press
Izd. AN SSSR	Acad. Sci. USSR Press
Izd. MGU	Moscow State Univ. Press
LEIIZhT	Leningrad Power Inst. of Railroad Engineering
LET	Leningrad Elec. Engr. School
LETI	Leningrad Electrotechnical Inst.
LETIIZhT	Leningrad Electrical Engineering Research Inst. of Railroad Engr.
Mashgiz	State Sci.-Tech. Press for Machine Construction Lit.
MEP	Ministry of Electrical Industry
MES	Ministry of Electrical Power Plants
MESEP	Ministry of Electrical Power Plants and the Electrical Industry
MGU	Moscow State Univ.
MKhTI	Moscow Inst. Chem. Tech.
MOPI	Moscow Regional Pedagogical Inst.
MSP	Ministry of Industrial Construction
NII ZVUKSZAPIOI	Scientific Research Inst. of Sound Recording
NIKFI	Sci. Inst. of Modern Motion Picture Photography
ONTI	United Sci.-Tech. Press
OTI	Division of Technical Information
OTN	Div. Tech. Sci.
Stroiizdat	Construction Press
TOE	Association of Power Engineers
TsKTI	Central Research Inst. for Boilers and Turbines
TsNIEL	Central Scientific Research Elec. Engr. Lab.
TsNIEL-MES	Central Scientific Research Elec. Engr. Lab.– Ministry of Electric Power Plants
TsVTI	Central Office of Economic Information
UF	Ural Branch
VIESKh	All-Union Inst. of Rural Elec. Power Stations
VNIIM	All-Union Scientific Research Inst. of Metrology
VNIIZhDT	All-Union Scientific Research Inst. of Railroad Engineering
VTI	All-Union Thermotech. Inst.
VZEI	All-Union Power Correspondence Inst.

Note: Abbreviations not on this list and not explained in the translation have been transliterated, no further information about their significance being available to us. – Publisher.

SOVIET

research in

ANALYTICAL CHEMISTRY

OF URANIUM

A collection of ten papers from the Consultants Bureau translations of the Soviet Journal of Analytical Chemistry and the famous "Doklady" of the Academy of Sciences (1949-58)... This collection will acquaint the analytical chemist working in this field with Soviet techniques for the determination of uranium in solutions, in ores and the products of their treatments, and in accessory minerals, plus methods for the determination of impurities in uranium.

heavy paper covers illustrated $10.00

CONTENTS

- Extraction of Uranyl α-Nitroso-β-naphtholate and Separation of Uranium from Vanadium and Iron.
- The Composition of Uranyl Selenite. A Volumetric Method of Determining Uranium.
- The Composition of the Luminescence Center of Sodium Fluoride Beads Activated by Uranium.
- Rapid Luminescent Determination of Uranium in Solutions.
- Preparation of Slightly Soluble Compounds of Quadrivalent Uranium Using Rongalite.
- Investigation of Complex Compounds of the Uranyl Ion Which are of Importance in Analytical Chemistry.
- Uranyl and Thorium Selenites.
- The Evaporation Method and Its Use for the Determination of Boron and Other Impurities in Uranium.
- Spectrographic Determination of Uranium in Ores and the Products Obtained by Treatment of These Ores.
- Determination of Uranium in Accessory Minerals.

c/b CONSULTANTS BUREAU

227 WEST 17TH STREET, NEW YORK 11, N. Y.

RESEARCH BY SOVIET EXPERTS

Translated by Western Scientists

INSTABILITY CONSTANTS OF COMPLEX COMPOUNDS

by K. B. Yatsimirskii and V. P. Vasil'ev

Instability constants quantitatively characterize the equilibrium in solutions of complex compounds and, in this connection, are very widely used by chemists in different fields (analytical chemistry, electrochemistry, technology of nonferrous and rare metals, etc.) for appropriate calculations.

The instability constants of 1381 complex compounds are given. The authors have prefaced the summary of instability constants with an introductory section which examines methods of calculating instability constants from experimental data, the effect of external conditions (temperature and ionic strength) on the stability of complexes and the main factors determining the stability of complex compounds in aqueous solutions.

Cloth **200 pages** **$6.75**

SOVIET RESEARCH ON COMPLEXES AND CO-ORDINATION CHEMISTRY

This collection consists of 372 articles by Russian scientists in the general area of the chemistry of complexes. These reports have been complied from the Consultants Bureau translations of the following Soviet journals:

Journal of General Chemistry
Journal of Analytical Chemistry
Bulletin of the Academy of Sciences
Division of Chemical Sciences
Proceedings of the Academy of Sciences
Journal of Applied Chemistry
Soviet Journal of Atomic Energy

The articles have been grouped into five volumes, each of which may be purchased separately.

I. Inorganic Complexes—103 articles	..	**$65.00**
II. Metal-Organic Complexes—86 articles	..	**$45.00**
III. Thermodynamic and Kinetic Studies—57 articles	..	**$37.50**
IV. Complexes in Analytical Chemistry—57 articles	..	**$37.50**
V. Condensed Inorganic Systems; Miscellaneous —38 articles —31 articles	..	**$45.00**
Complete collection	..	**$200.000**

Tables of contents on request

Payment in sterling may be made to Barclays Bank in London, England

CONSULTANTS BUREAU

227 West 17th Street · New York 11, N. Y.